Aus dem Institute of Experimental Pneumology der

Ludwig-Maximilians-Universität München

Direktor: Dr. Ali Önder Yildirim

Dissertation
zum Erwerb des Doctor of Philosophy (Ph.D.)
an der Medizinischen Fakultät der
Ludwig-Maximilians-Universität zu München

Role of PRMT7 in the recruitment of monocyte-derived macrophages into lung tissue and COPD pathogenesis

vorgelegt von:

Gizem Günes Günsel

aus:

Nazilli, Türkei

Jahr:

2021

First supervisor: *PD. Dr. med. Anne Hilgendorff*

Second supervisor*:* *Dr. Ali Önder Yildirim*

Third supervisor: *Dr. rer. nat. Alexander Wolf*

Dean: Prof. Dr. med. dent. Reinhard Hickel

Datum der Verteidigung:

_30.06.2021_

To my family...

Table of Contents

ABBREVIATIONS

Abbreviation	*Full name*
Ab	Antibody
ADMA	Asymmetric dimethylarginine
AdoMet	S-adenosyl-L-methionine
APC	Antigen-presenting cell
APS	Ammonium persulfate
ATI	Alveolar epithelial type I
ATII	Alveolar epithelial type I
%	Percent
BAL	Bronchoalveolar lavage
BALF	The broncho-alveolar lavage fluid
BCA assay	Bicinchoninic acid assay
BSA	Bovine serum albumin
BMDM	Bone marrow derived macrophages
CARM1	Co-activator associated arginine methyltransferase
CAST	Computer assisted stereological toolbox
CCL	Chemokine (C-C motif) ligand
CCR	C-C chemokine receptor
CDS	Coding sequence
cDNA	Complementary DNA
Cdyn	Dynamic compliance
CO	Carbon monoxide
COPD	Chronic Obstructive Pulmonary Disease
CS	Cigarette smoke
CSE	Cigarette smoke extract
CXCL	Chemokine (C-X-C motif) ligand
CXCR	C-X-C chemokine receptor
CT	Computer tomography
DC	Dendritic cell
DMSO	Dimethyl sulfoxide
DMEM	Dulbecco's Modified Eagle Medium
DNA	Deoxyribonucleic acid
dNTP	Deoxyribonucleoside triphosphate
E.coli	Escherichia coli
EAE	Experimental Autoimmune Encephalomyelitis
ECL	Enhanced chemiluminescence
EDTA	Ethylenediaminetetraacetic acid
EtOH	Ethanol
ERK	Extracellular signal-regulated kinase
FA	Filtered air
FACS	Fluorescence-activated cell sorting

FBS	Fetal Bovine Serum
FSC	Forward scatter
FDC	Follicular dendritic cell
FEV	Forced expiratory volume
FITC	Fluorescein isothiocyanate
FVC	Forced vital capacity
FRC	Functional residual capacity
Gal-3	Galectin-3
GM-CSF	Granulocyte-macrophage colony-stimulating factor
GOLD	Global initiative for chronic obstructive lung disease
GSEA	Gene set enrichment analysis
h	Hour
HIER	Heat Induced Epitope Retrieval
Het	Heterozygous
HEV	High endothelial venule
H&E	Hematoxylin and eosin
HRP	Horseradish peroxidase
iBALT	Inducible bronchus-associated lymphoid tissue
ICAM	Intercellular adhesion molecule
ICS	Inhaled corticosteroids
IFN	Interferon
Ig	Immunoglobulin
IL	Interleukin
iNOS	Inducible nitric oxide synthase
ITGAL	Integrin subunit alpha L
ITGAM	Integrin subunit alpha M
IP	Immunoprecipitation
kDa	Kilo Dalton
LABA	Long acting β adrenergic receptor (B_2) agonist
LAMA	Long acting muscarinic antagonists
LF	Lymphoid follicle
Lm	Mean linear intercept
LPS	Lipopolysaccharide
MACS	Magnetic-activated cell sorting
MAPK	Mitogen-activated protein kinase
M1	Classically activated macrophage
M2	Alternatively activated macrophage

MCL	Mean Chord Length
MCP	Monocyte chemoattractant protein
MHC	Major histocompatibility complex
MHS	Murine alveolar macrophage
mg	Milligram
MMA	Monomethylated arginine
MMP	Matrix metalloproteinase
µMT	B cell deficient
µl	Microliter
µm	Micrometer
mRNA	Messenger RNA
ml	Millilitre
NF-κB	Nuclear factor 'kappa-light chain-enhancer' of activated B cells
NE	Neutrophil elastase
ng	Nanogram
NK cells	Natural killer cells
NO	Nitric oxide
NOS	Nitric oxide synthase
PBMC	Peripheral blood mononuclear cells
PBS	Phosphate buffered saline
PCR	Polymerase chain reaction
PFA	Paraformaldehyde
PPE	Porcine pancreatic elastase
PRMT	Protein arginine methyltransferase
PVDF	Polyvinylidene fluoride
RIPA	Radioimmunoprecipitation assay
RNA	Ribonucleic acid
ROS	Reactive oxygen species
RPMI	Roswell park memorial institute
RT	Room temperature
SDS PAGE	Sodium dodecyl sulphate polyacrylamide gel electrophoresis
siRNA	Small interfering RNA
SDMA	Symmetric ω-NG, N'G-dimethylarginine
SSC	Side scatter
STAT	Signal transducer and activator of transcription
TEMED	Tetramethylethylenediamine
TGF-β	Transforming growth factor β

Th	T helper cells
TIMP1	TIMP metallopeptidase inhibitor
TLC	Total lung capacity
TLO	Tertiary lymphoid organ
TLR	Toll-like-receptor
TNF-α	Tumor necrosis factor α
Treg	Regulatory T cell
VCAM	Vascular cell adhesion molecule
VEGF	Vascular endothelial growth factor
VFR	Vulcan fast red
WT	Wild type
WHO	World health organization

SUMMARY

Chronic obstructive pulmonary disease (COPD) is the third leading cause of death worldwide with limited therapeutic options. While cigarette smoke is the main reason of tissue inflammation and destruction in COPD, the regulatory mechanisms underlying the immunological processes still remain unclear. There are multiple factors contributing to the progression of COPD; such as genetics, gender, age, infections and last but not least epigenetics. In recent years, the importance of epigenetics to the pathogenesis of the disease has emerged. Methylation of protein arginine residues is a post-translational modification performing as an epigenetic modulator of many cellular mechanisms including cell signaling, transcription and mRNA processing. More importantly, it has been implicated in immune system dysfunction and inflammation.

In this study, it is reported that the expression of one member of the protein arginine methyltransferase (PRMT) enzyme family, PRMT7, is enriched in the lungs of COPD patients and that this correlates with disease severity. Interestingly, the major cell type in the lung, which predominantly expressed PRMT7, is found to be macrophages. The expression of PRMT7 in monocytes and macrophages increases with inflammatory insult through NF-κB/RelA signaling. In parallel, PRMT7 is demonstrated to be essential for monocyte-driven macrophage accumulation in the development of COPD and fibrosis. Under inflammatory conditions, the extravasation of monocytes into tissues is a fundamental immunological process, crucially dependent upon trans-endothelial migration from blood vessels into inflamed tissues with the subsequent differentiation into macrophages initiating and perpetuating disease pathogenesis. In COPD, fibrosis and skin injury mouse models, mice with reduced expression of PRMT7 are protected against disease development as recruitment of monocyte derived-pro-inflammatory macrophages to the site of injury is impaired. Additionally, CRISPR/Cas9-targeted knockout of PRMT7 reveals a mechanism whereby mono-methylation of histone proteins regulate RAP1 mediated MAPK signaling and subsequent migration and adhesion ability. Thus, targeted inhibition of PRMT7 induced mono-

methylation offers novel therapeutic potential against COPD and other monocyte driven chronic inflammatory conditions.

ZUSAMMENFASSUNG

Die chronisch obstruktive Lungenerkrankung (COPD) ist weltweit die dritthäufigste Todesursache mit begrenzten therapeutischen Möglichkeiten. Obwohl Zigarettenrauch die Hauptursache für Gewebeentzündung und -zerstörung bei COPD ist, sind die regulatorischen Mechanismen, die den immunologischen Prozessen zugrunde liegen, noch immer unklar. Es gibt mehrere Faktoren, die zur Entstehung von COPD beitragen; dazu gehören Genetik, Geschlecht, Alter, Infektionen und nicht zuletzt die Epigenetik. In den letzten Jahren hat sich die Bedeutung der Epigenetik für die Pathogenese der Krankheit herauskristallisiert. Die Methylierung von Protein-Arginin-Resten ist eine posttranslationale Modifikation, die als epigenetischer Modulator vieler zellulärer Mechanismen einschließlich der Zellsignalisierung, Transkription und mRNA-Verarbeitung fungiert. Noch wichtiger ist, dass sie an Funktionsstörungen des Immunsystems und Entzündungen beteiligt ist.

In dieser Studie wird berichtet, dass die Expression eines Mitglieds der Protein-Arginin-Methyltransferase (PRMT)-Enzymfamilie, PRMT7, in den Lungen von COPD-Patienten angereichert ist und dass dies mit dem Schweregrad der Krankheit korreliert. Interessanterweise stellte sich heraus, dass der wichtigste Zelltyp in der Lunge, der PRMT7 vorwiegend exprimiert, Makrophagen sind. Die Expression von PRMT7 in Monozyten und Makrophagen nahm bei entzündlichem Befund durch NF-κB/RelA-Signalisierung zu. Parallel dazu wurde nachgewiesen, dass PRMT7 für die monozytengesteuerte Makrophagenakkumulation bei der Entwicklung von COPD und Fibrose wesentlich ist. Unter entzündlichen Bedingungen ist die Extravasation von Monozyten in Gewebe ein grundlegender immunologischer Prozess, der entscheidend von der trans-endothelialen Migration von Blutgefäßen in entzündetes Gewebe abhängt. In COPD-, Fibrose- und Hautverletzungs-Mausmodellen waren Mäuse mit reduzierter Expression von PRMT7 vor der Krankheitsentstehung geschützt, da die Rekrutierung von pro-inflammatorischen Makrophagen an der Verletzungsstelle beeinträchtigt war. Darüber hinaus zeigte der CRISPR/Cas9-gerichtete Knock-out von PRMT7 einen Mechanismus, bei dem die Monomethylierung von Histonproteinen, die RAP1 regulierten, das MAPK-Signal und die

nachfolgende Migrations- und Adhäsionsfähigkeit vermittelte. Somit bietet die gezielte Hemmung der durch PRMT7 induzierten Monomethylierung ein neues therapeutisches Potenzial gegen COPD und andere monozytengesteuerte chronische Entzündungszustände.

1. INTRODUCTION

1.1 Chronic Obstructive Pulmonary Disease (COPD)

Chronic obstructive pulmonary disease (COPD) is a deadly lung disorder currently being the third common cause of death worldwide (Disease et al., 2018). The morbidity and mortality rate of COPD increases proportional to the rapidly growing elderly population of the world (Feenstra et al., 2001). It is a chronic inflammatory disease characterized by airflow limitation (Brusselle et al., 2009b). A recent meta-analysis study revealed that the prevalence of COPD is more than 12% of the general population, 88% of these patients had mild and moderate COPD, the rest had severe (Varmaghani et al., 2019). The most known and defined risk factor for COPD is cigarette smoke exposure however there are other causes including exposure to particles, dusts and chemicals, air pollution, genetic predisposition, age, socio-economic status or infections (Mannino and Kiriz, 2006). Unfortunately amongst heavy smokers the prevalence of COPD approaches 50% (Cosio et al., 2009).

COPD is unfortunately a deadly disorder when diagnosed late on and does not currently receive sufficient attention and funding for developing effective treatments (Quaderi and Hurst, 2018). Cigarette smoking plays a key role in COPD progression with sufficient evidence that earlier diagnosis of the disease would be critical for smoking cessation to decrease COPD symptoms (Tinkelman et al., 2007). Tobacco smoke contains various cancer causing chemicals and carcinogens such as nicotine, benzene, aromatic amines and 1,3-butadiene and exposing cells and tissues to these damaging oxidants and free radicals leads to inflammatory processes and damages to the airways and lung tissue (Saetta, 1999). The inflammatory response gives rise to mucus hypersecretion (chronic bronchitis) (Tian and Wen, 2015), tissue destruction (emphysema) (Turato et al., 2002), small airway remodelling (Grzela et al., 2016) and deterioration of the repair mechanisms in the lung (Bagdonas et al., 2015).

1.1.1 Classification and diagnosis of COPD

Clinical symptoms and medical history are important indications of COPD but for an accurate diagnosis and classification, the Global Initiative for Chronic Obstructive Lung Disease (GOLD)

committee defined the spirometric criteria (Hernández et al., 2018). Spirometric measurements are essential for diagnosis as well as classifying disease severity and monitoring pathological changes (Welte et al., 2015). Spirometry is known to be the best-established method in order to understand and measure the severity of airflow limitation, the main characteristic of COPD induced by emphysema and obstructive bronchiolitis (Johannessen et al., 2006). According to the GOLD criteria, the ratio of forced expiratory volume measuring how much air can be exhaled over 1s (FEV1) to forced vital capacity (FVC) is considered as a main indicator of airflow limitation (airway obstruction) (Vaz Fragoso et al., 2010). Calculation of these parameters is a robust and reliable tool since both are affected by emphysema and airway obstruction (Pellegrino et al., 2005). Based on GOLD committee recommendations, if the ratio of FEV1 to FVC (FEV1/FVC) is less than 0.7, it is indicative of COPD. COPD has four stages in terms of its severity based on airflow limitation calculated by FEV1/FVC ratio (Mannino et al., 2006). The GOLD stages and their correlations with spirometry analysis are encapsulated in (Table 1.1).

Table 1.1: COPD classification based on spirometric anaylsis with post-bronchodilator FEV1

GOLD Stage	**Severity**	**Spirometry**
Stage I	Mild	FEV1/FVC < 0.70 FEV1 ≥ 80% predicted
Stage II	Moderate	FEV1/FVC < 0.70 50% ≤ FEV1 < 80% predicted
Stage III	Severe	FEV1/FVC < 0.70 30% ≤ FEV1 < 50% predicted
Stage IV	Very Severe	FEV1/FVC < 0.70 FEV1 < 30% predicted or FEV1 < 50% predicted plus chronic respiratory failure

FEV1: forced expiratory volume in one second; FVC: forced vital capacity; respiratory failure: arterial partial pressure of oxygen (PaO2) less than 8.0 kPa (60 mm Hg) with or without arterial partial pressure of CO2 (PaCO2) greater than 6.7 kPa (50 mm Hg) while breathing air at sea level. (Adapted from: GOLD, 2006)

Even though the most common way to measure lung function is spirometry, there are cases where spirometry may not be sufficient and sensitive enough to evaluate and define the severity of COPD. During COPD assessment, it is important to take into consideration other lung parameters such as changes in lung parenchymal structure leading to air trapping or abnormalities in gas exchange (Feenstra et al., 2001; Tang et al., 2016). Whole body plethysmography measures residual volume (RV) and total lung capacity (TLC) to evaluate the

changes in lung hyperinflation (Hartman et al., 2012). Whole-body plethysmography measurements are more precise since they provide the total volume of gas in the thorax instead of the volume of gas that can be exhaled only (Sue, 2013). Diffusion capacity for carbon monoxide (DLCO) is defined as another powerful tool to diagnose the disease (Viegi et al., 1990). In principle, it measures the amount of carbon monoxide (CO) which is transferred from alveoli to red blood cells in the capillaries in one minute (Johnson, 2000). In obstructive cases like COPD, DLCO decreases, correlating with emphysema severity (Balasubramanian et al., 2019; Weinreich et al., 2015). Other methods to diagnose morphological changes in the lung are X-ray-based as well as computer tomography (CT) scans of the chest (Kolodziej et al., 2017).

1.1.2 Hallmarks of COPD

The main pathological and distictive characteristics of COPD are destruction of lung parenchyma (emphysema), chronic bronchitis, abnormal inflammatory response in the airways, and airway obstruction (fibrosis in small airways) (Barnes, 2008). When these abnormalities appear together, chronic and progressive airflow limitation occurs in the lung (Cosio et al., 2009). Emphysema is described as damage occurring in the alveolar structures leading to loss of lung elasticity and collapsed airways (Rennard et al., 2006). Mainly, emphysema causes the alveoli to rupture therefore resulting in less and larger alveoli with reduced surface area available for gas exchange (Saetta, 1999). To date, cigarette smoke is shown to be the most common cause of emphysema formation in the lung (Cosio Piqueras and Cosio, 2001). However, genetic factors also play a crucial role in the development of emphysema such as α-antitrypsin (AAT) deficiency. It is a serine protease inhibitor that protects lung tissue from damage via inhibiting elastase enzymes (Craig and Henao, 2018). Another hallmark of COPD is chronic bronchitis caused by an excessive mucus production, progressively increased inflammation of the airways and small airway obstruction (Kim and Criner, 2015). The definition of chronic bronchitis is having chronic cough and sputum production frequently in a year (Kim and Criner, 2015). The primary reason responsible for excessive mucus causing chronic bronchitis is overproduction of mucus by goblet cells as well as impaired elimination because of poor ciliary clearance (Kim and Criner, 2013). Similar to

emphysema development, mucus hypersecretion arises predominantly from exposure to cigarette smoke (Ebert and Terracio, 1975) but also viral infections (Holtzman et al., 2005) or mucin gene alterations (Burgel and Nadel, 2004) can contribute to mucus hypersecretion. Small airway remodelling in COPD is defined as a mixture of structural changes in epithelial cells, thickening of the airway walls, deposition of collagen and smooth muscle cell hyperplasia (Wang et al., 2018b). These changes have a functional consequence of airway obstruction leading to airflow restriction in COPD patients (Hogg et al., 2004). Abnormalities in small airways such as cellular infiltration by immune cells including innate and adaptive ones, thickening of the airway wall followed by decreasing the airway diameter, destruction of alveoli and enlargement of air spaces associated with COPD (Barnes, 2008).

1.1.3 Pathogenesis of COPD

As introduced above, the main hallmarks of COPD pathogenesis including chronic bronchitis, small airway remodelling and importantly emphysema characterize the disease pathogenesis (MacNee, 2005). Emphysema is defined by the destruction of alveolar structures and walls which causes permanent enlargement of airspaces therefore leading to reduced surface area (Tuder and Petrache, 2012). The contributing factors to the development of emphysema include cigarette smoke, biomass particles, air pollution, genetic factors (e.g. alpha1-antitrypsin deficiency), gender, age, infections, socio-economic situation and epigenetic factors (Hikichi et al., 2019). Although the pathogenesis of emphysema is complex, there are key processes that are highly associated with the development of emphysema such as inflammation, oxidative stress, cellular senescence and apoptosis, protease– anti-protease imbalance and as well as impairment in lung repair mechanisms (MacNee and Tuder, 2009).

Inhalation of toxic particles – mainly cigarette smoke, induced inflammatory reactions, including recruitment of innate and adaptive immune cells to the lung parenchyma and airways, have been attributed to be a central cause in the development of COPD (Curtis et al., 2007). As a first line of defence, cigarette smoke triggers and activates innate immune cells which provides a rapid but nonspecific response (Brusselle et al., 2011). Activated innate immune cells such as macrophages, dendritic cells, neutrophils and lung epithelial cells

secrete several chemotactic factors leading to the recruitment and accumulation of other inflammatory cells into the lungs (Barnes, 2008; Caramori et al., 2016). Importantly, one of the recruited inflammatory cell type is monocytes. When they are activated, monocytes extravasate into tissue from blood upon activation and they undergo differentiation into macrophages either pro-inflammatory or anti-inflammatory type and they contribute to the tissue damage or repair depending on their phenotype and function (Auffray et al., 2007; Gerhardt and Ley, 2015). Recruited T and B lymphocytes as well as neutrophils and macrophages secrete a milieu of cytokines and proteases eventually resulting in emphysema, mucus hypersecretion, small airway remodelling as well as chronic bronchitis and contribute to the development of the disease (Figure 1.1) (Barnes, 2011). The detailed definition of cell types and the components involved in disease development is explained in section 1.2.

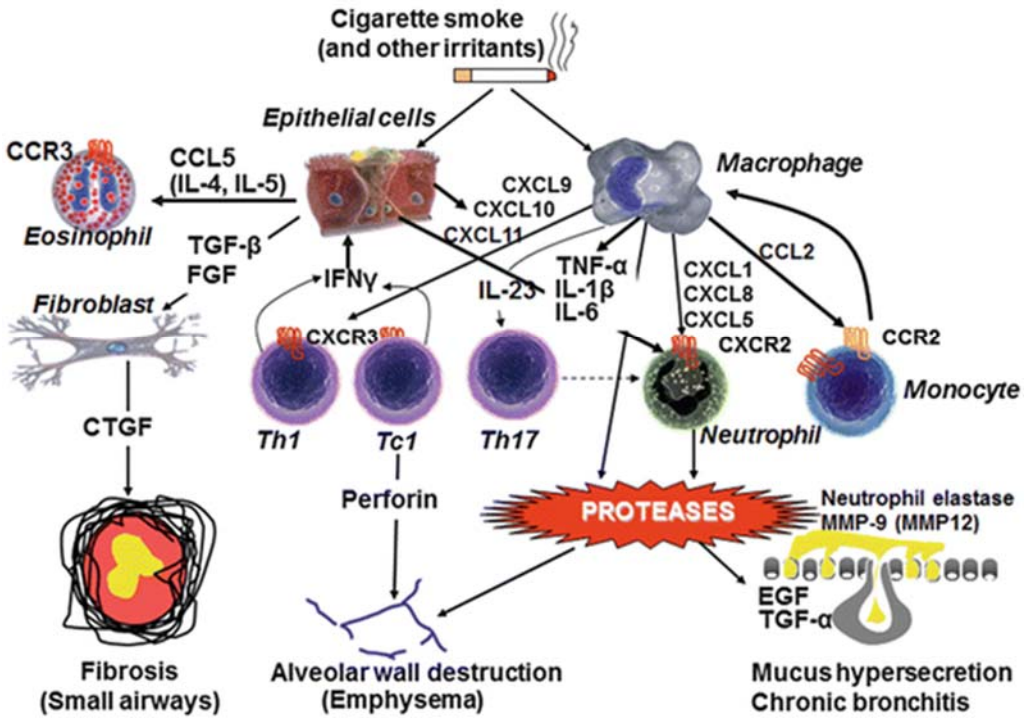

Figure 1.1 Inflammatory components in COPD. Cigarette smoke or other inhaled irritants activate macrophages and epithelial cells as a first line defence mechanism. Activated cells secrete chemotactic factors which recruit inflammatory cells to the site of injury. CCL2 acts on CCR2 on monocytes to attract them, CXCL1 and CXCL8 bind to CXCR2 to recruit neutrophils and monocytes whereas CXCL9, CXCL10 and CXCL11 bind to CXCR3 for recruitment of T cells. These inflammatory cells accumulate in the lung and cause emphysema by secreting proteases. Neutrophils cause mucus hypersecretion and chronic bronchitis. As a result of TGF-β release by epithelial cells and macrophages, fibrosis in small airways occurs (Barnes, 2011).

Oxidative stress plays a pivotal role in the pathogenesis of COPD (Rahman and MacNee, 1996). Maintenance of normal pulmonary cellular functions requires the balance between oxidants and anti-oxidants, and either increase in oxidants or reduction in anti-oxidants destroys the balance in the lung and results in oxidative stress (Bowler et al., 2004). Accumulation of free radicals like reactive oxygen species (ROS), which includes mainly superoxide anion ($O_2.^-$) and hydroxyl radical (.OH), initiates oxidative stress and might result in lung injury and cellular responses (Zinellu et al., 2016). So far, oxidants are highly associated with production of more ROS by activated resident macrophages as well as epithelial cells, which may cause the recruitment of inflammatory cells contributing to lung damage (Rahman and Adcock, 2006). The contribution of cigarette smoke to oxidative stress is undeniable, since a single respiration of cigarette smoke allows around $1x10^{15}$ oxidant molecules entering to the lungs (McGuinness and Sapey, 2017). These reactive oxygen species also are demonstrated to contribute to inflammatory responses via activating several key transcription factors as well as triggering important pathways like MAPK and PI-3K (Rahman and MacNee, 1998; Saetta, 1999). This chain reaction results in increased gene expression of pro-inflammatory mediators including IL-8, IL-6, TNF-α as well as IL-1β (Kamata et al., 2005). Moreover, nitric oxide (NO) levels are also elevated as a result of these reactions (Vleeming et al., 2002). Besides the increased oxidants, reduction in anti-oxidant defence by cigarette smoke has an adverse effect on the development of the disease. Nuclear factor erythroid 2-related factor 2 (Nrf2) is one of the key transcriptional factors regulating the production of antioxidant and cytoprotective molecules (Ishii et al., 2000) and is found being attenuated in the lungs of COPD patients (Goven et al., 2008).

There is increasing evidence that apoptosis plus cellular senescence are considered as important driving mechanisms of COPD pathogenesis as well (Barnes et al., 2019). Cellular senescence is described as an irreversible and permanent growth arrest. Both cell-intrinsic factors like telomere shortening and DNA damage or external stress factors like oxidative stress or radiation might lead to cell cycle arrest and senescence (Antony and Thannickal, 2018). In lung tissue of COPD patients, alveolar epithelial cells which are highly associated with tissue repair and regeneration and endothelial cells, have increased senescence markers

such as β-galactosidase, p21 and p16 resulting from cigarette smoke exposure (Rashid et al., 2018). Accelerated lung cellular senescence deregulates lung tissue repair, regeneration and remodelling, thus contributing to the pathogenesis of COPD (Mercado et al., 2015). Moreover, even though these cells lose their ability to divide they still remain metabolically active and may affect neighbouring cells by secreting several mediators – the so called senescence-associated secretory phenotype (SASP), including inflammatory cytokines, growth factors and reactive gaseous molecules that result in an adverse impact to the surrounding tissue (Barnes, 2017b). Related to senescence, the balance between proliferation and apoptosis has a critical role in the emphysema development (Plataki et al., 2006). Apoptosis is described as a programmed cell death which results in elimination of damaged or infected cells (Gogebakan et al., 2014). Although apoptosis might be beneficial to reduce the excessive amount of activated inflammatory cells, a disrupted balance has been linked to disease pathogenesis via impaired homeostasis (Henson et al., 2006). It has been reported that emphysematous lung tissue has increased levels of apoptosis in airway epithelial and endothelial lung cells as well as lymphocytes specifically T cells and neutrophils resulting in enhanced tissue destruction and diminished host defence respectively (Hodge et al., 2005; Tuder et al., 2003).

Last but not least, protease – anti-protease imbalance has been linked to the progression of emphysema and mucus hypersecretion in the lungs of smokers (Abboud and Vimalanathan, 2008). Proteases are enzymes which lead to cleavage of the components of lung connective tissue, specifically elastin and collagen, whereas anti-proteases are known to inhibit these proteases (Fischer et al., 2011). As mentioned above, cigarette smoke activates macrophages and triggers neutrophil recruitment into the lungs and these activated macrophages and neutrophils secrete several proteases. Neutrophil elastase, proteinase 3, the matrix metalloproteinases (MMPs) as well as cathepsins are known to be main proteases. Proteolytic degradation of elastin fibers occurs from accumulation of neutrophils and secretion of neutrophil elastase (Lomas, 2016; Stockley, 1999). Alpha-1-antitrypsin is known to be the main inhibitor of neutrophil elastase and mutations of alpha-1-antitrypsin or lack of it indicates the development of emphysema (Pandey et al., 2017). Moreover, MMPs are

implicated in the pathogenesis of the disease since they are involved in tissue remodeling and driving inflammation. MMPs are secreted as inactive pro-enzyme forms which are required to be activated by other types of proteases such as plasmin and other serine proteinases (Churg et al., 2012; Ra and Parks, 2007). So far, mainly MMP-1, -2, -7, -9 and -12 (Belvisi and Bottomley, 2003) are highly associated with progression of emphysema in COPD animal models. MMPs will be mentioned more in detail in section 1.2.1. Besides the contribution of increased activity of MMPs to emphysema, their tissue inhibitor of metalloproteinases (TIMPs) have a protective effect against emphysema development (Gomis-Rüth et al., 1997) suggesting that balance between MMPs and TIMPs is a contributing factor to COPD pathogenesis (Gharib et al., 2018).

1.1.4 Current Treatment Strategies for COPD

COPD is considered a very complex disease affecting around 200 million people worldwide (Ferkol and Schraufnagel, 2014) and so far, current treatments are only able to relieve the symptoms, prevent further development of disease and decrease the possibility of complications (Lakshmi et al., 2017). Effective COPD therapies do not reverse disease progression completely but they help patients to improve their quality of life (Vogelmeier et al., 2017). The most significant improvement could be achieved by smoking cessation since greater emphysema development and further lung damage can be prevented (Halpin et al., 2017). Today, there are nicotine replacement products including e-cigarettes, pharmacological products including varenicline and bupropion that helps to quit plus smoking cessation programs with professional help (Vogelmeier et al., 2017). Besides smoking cessation, pharmacological therapies including bronchodilators, corticosteroids, antibiotics, and ventilatory support are recommended treatment strategies for severe COPD exacerbations (Welte, 2009). Moreover, regular physical activity and exercise, vaccination, pulmonary rehabilitation, having a proper diet as well as oxygen therapy are considered as beneficial non-pharmacological interventions for patients (Clini and Ambrosino, 2008). Surgery for lung transplantation might also be considered in some COPD patients with severe progressive disease (Siddiqui and Diamond, 2018).

Concerning pharmacological intervention, inhaled bronchodilators are used mainly to manage symptoms in mild and moderate GOLD stage COPD patients by increasing FEV1 (Vogelmeier et al., 2017) and opening the air passages in the lungs to help the patients to relieve symptoms (Diaz et al., 2008). Beta2-agonists such as short acting (SABA) and long acting (LABA) (Lakshmi et al., 2017), antimuscarinic drugs including ipratropium and methylxanthines like throphylline are used as current bronchodilators (Vogelmeier et al., 2017). They can be used as a treatment separately but combining therapy of several bronchodilators with different mechanisms is considered as a more efficient way to treat patients (Ernst et al., 2015). It has been also suggested that inhaled corticosteroids improve the exacerbations and help shortness of breath (Shafazand, 2013; Tashkin and Strange, 2018). Although corticosteroid treatment does not reverse the loss of lung function (Walters et al., 2005), it improves survival of the patients especially when they are combined with bronchodilators (Falk et al., 2008; Shafazand, 2013). Moreover, the use of systemic corticosteroids is suggested to decrease inflammation and therefore may be beneficial to COPD patients (Barnes, 2006). Since one of the hallmarks of COPD is an abnormally elevated inflammatory immune response in the lungs, anti-inflammatory treatment strategies to suppress the inflammatory response are critical to prevent disease progression (Barnes, 2013). Inhibitors of inflammatory mediators directly like TNF-α, NF-κB and p38 MAPK (Cazzola et al., 2012) and drugs having anti-inflammatory properties like protease inhibitors and antioxidant drugs become potential targets for anti-inflammatory therapy in COPD (Loukides et al., 2013).

Antibiotics are widely used for the treatment of acute exacerbations however their benefits and harms are still under debate (Siddiqi and Sethi, 2008). Antibiotic selection is quite crucial in this aspect (Siddiqi and Sethi, 2008). Some of the antibiotics such as erythromycin are considered to be beneficial against respiratory infections such as pneumonia (Zhou et al., 2012). Oxygen therapy is recommended for patients who are hypoxic because of impairment in normal ventilation leading to reduced oxygenated blood and systemic hypoxia (Brill and Wedzicha, 2014). As a further treatment option, lung transplantation which is a surgical procedure to replace the lung of patients partially or totally with a donor lung is well-used

strategy for the patients with end-stage lung disorder (Aziz et al., 2010). However, alternatively removing small regions of damaged lung tissue by surgery is considered a better treatment option for COPD patients to decrease total lung volume (Decramer et al., 2012; Lahzami et al., 2010).

1.2 Inflammatory and immune cell mechanisms in COPD

1.2.1 The key immune cells involved in COPD

COPD is predominantly characterized by recruitment, activation and accumulation of inflammatory cells in the lungs, particularly in the small airways (Nurwidya et al., 2016). Immune responses in COPD are divided into two arms, innate and adaptive immunity with specific cell types and functions of these cells contributing uniquely to the disease outcome (Craig et al., 2017). Innate immune cells which consist of mainly monocytes, macrophages, dendritic cells (DCs), neutrophils and natural killer (NK) cells are responsible for the first line of immune defence in combination with the epithelial barrier and mucuciliary clearance (Bhat et al., 2015). In response to cigarette smoke or toxic particles, the function of innate immune cells have been found to be impaired and contributes to disease development (Ni and Dong, 2018). Moreover, a crucial role of innate cells is to trigger the adaptive immune response which is more specific and targeted. Chronic exposure to particles including cigarette smoke causes activation of B lymphocytes and various T lymphocyte subtypes which are components of the adaptive immune system (Rovina et al., 2013).

Neutrophils are a key component of the innate immune system and are highly correlated with disease severity (Walton et al., 2016). Activated neutrophils are found to be increased in the sputum and bronchoalveolar lavage and this increase is correlated with increased airflow limitation as well as impaired lung function (Saetta et al., 1997). The ratio of neutrophils to lymphocytes in the peripheral blood is considered as an indicator of COPD exacerbation and this ratio is also used as a biomarker for the disease diagnosis (Lee et al., 2016). Recruitment of neutrophils to the airways through endothelial cells requires interaction with E-selectin, and in COPD patients, E-selectin is significantly increased in the airway lumen resulting in increased migration toward chemotactic mediators such as cytokines or bacterial peptides

released by infected tissue (Di Stefano et al., 1994). In the lung, enhanced levels of chemoattractants including CXCL8, IL-8, CXCL1, CXCL5 and LTB4 are responsible for neutrophil migration to the site of inflammation (Traves et al., 2002). Recruited neutrophils to the airways of COPD patients release proteinases such as neutrophil elastase (NE), cathepsin G and metalloproteinases (MMPs) with collagenase activity, particularly MMP8 and MMP9, which might promote alveolar destruction (Hibbs et al., 1985; Tsai and Hwang, 2015). NEs and MMPs have the ability to degrade matrix proteins resulting in emphysema as well as to trigger mucin secretion (Martin et al., 2014) causing enhanced mucus production leading to impaired mucociliary clearance in COPD patients (Fahy and Dickey, 2010). Consistent with these findings, neutrophil elastase-deficient mice are significantly protected from the development of emphysema in comparison to wild type control mice when both groups exposed to cigarette smoke for 6 months indicating the role of neutrophil elastase in pulmonary disease (Shapiro et al., 2003).

DCs are professional antigen presenting cells (APCs) functioning as a bridge between innate and adaptive immunity and playing a central role in the defence mechanism of the lung (Banchereau et al., 2000; Upham and Xi, 2017). DCs capture antigens in the peripheral tissue particularly at mucosal surfaces where they present them to T lymphocytes in local lymph nodes. DCs have pattern recognition receptors against stimuli resulting from tissue damage, infection and necrosis and through these receptors, they are highly sensitive in detecting foreign molecules (Lambrecht et al., 2001; Vermaelen and Pauwels, 2005). After recognition of antigen by DCs, it is internalized and processed to be presented on major histocompatibility complex (MHC) class I and class II molecules to the T cell receptor (TCR) of T lymphocytes (Janeway and Bottomly, 1994). Cigarette smoke or other irritants induce activation and accumulation of DCs releasing pro-inflammatory cytokines including IFNα, IL-6 and IL-12 (Qiu et al., 2018). The increased number of activated DCs expressing CD80, CD83 and CD86 has been detected in the small airways of COPD patients, positively correlating with disease severity and impaired lung function (Brusselle et al., 2011; Wang et al., 2015). CC chemokine ligand (CCL) 20, the main chemoattractant for DC recruitment, was found to be significantly upregulated in the lung of COPD patients (Rogers et al., 2008). Another important role for

DCs in the pathogenesis of the disease is associated with the development of tertiary lymphoid follicles (Brusselle et al., 2011), by promoting adaptive immune responses including T helper, CD4+, CD8+ T lymphocytes and B lymphocytes in response to chronic inflammation.

Mast cells are secretory immune cells that are mainly localized to mucosal and epithelial tissues in the body (da Silva et al., 2014). Mast cells are associated with disease pathology since they have the ability to induce collagen production and fibroblast proliferation (Garbuzenko et al., 2002), as well as to release several proteases (Abe et al., 2000), including tryptase and chymase which might mediate tissue destruction (Siddiqui et al., 2007). Although mast cells are essential players in the pathogenesis of allergic disorders, recently it has been shown that their numbers are significantly upregulated in COPD airways (Grashoff et al., 1997), as well as in the sputum of smokers in comparison to ex-smokers (O'Donnell et al., 2006). Moreover, in a recent study, it was demonstrated that cigarette smoke extract induced the production of several chemokines, including TNFα and IL-8, from mast cells and these chemokines may recruit neutrophils to the lung (Mortaz et al., 2011). However, the involvement of mast cells in the development of emphysema still remains to be investigated and more research is essential to support the role of mast cells in the pathogenesis of COPD.

NK cells are one of the innate immune cell types which demonstrate cytotoxic effect against cells under stress and mediates anti-tumour and anti-viral responses by killing these cells directly (Paul and Lal, 2017). Once they become active, NK cells release various cytokines like other innate immune cells to regulate further innate and adaptive immune cells (Abel et al., 2018). Mainly, they secrete IFNγ, TNFα, GM-CSF, CCL1, CCL2, CCL3, CCL4, CCL5 and CXCL8. NK cells release perforin to generate pores in the membrane and induce apoptosis of target cells by triggering caspase cleavage via granzyme proteases (Thiery et al., 2011). If there is an abnormal activation of NK cells, it may result in tissue damage by continuous inflammation (Osterburg et al., 2020). In a disease context, COPD patients have increased numbers of NK cells in the peripheral blood indicating a potential role for NK cells in disease pathogenesis (Wang et al., 2013). Moreover, the ratio of activated NK cells is found to be noticeably higher in smokers when compared to non-smokers or ex-smokers (Wang et al., 2013). It is also positively correlated with the amount of cigarettes currently consumed (Wang et al., 2013).

A recent study also demonstrated that CS-exposed mice have pre-activated NK cells producing an increased amount of IFN-γ triggering chronic inflammation (Motz et al., 2010).

Long term exposure to toxic particles including cigarette smoke results in inflammation in the airways activating adaptive immune cells such as T and B lymphocytes. These play a central role in disease pathogenesis through antigen specificity, clonal expansion and immunological memory (Ni and Dong, 2018). Elevated levels of T cells mainly CD8+ T cells and B cells have been observed in both large and small airways of COPD patients and in the lung parenchyma (Tetley, 2005). The number of T cells (Chen et al., 2016) and B cells (Seys et al., 2015) is positively correlated with alveolar destruction and inversely correlated with lung function. T cell subsets including Th1 and Th17 which are a major source of IFN-γ are also increased in the airways of smokers (Nurwidya et al., 2016). Antigen-driven specific immune responses generated by B cells contribute to inflammatory processes leading to COPD development (Brandsma et al., 2009). Moreover, there is increasing evidence for the crucial role of tertiary lymphoid follicles in the development of COPD. In the lungs, exposure to chronic cigarette smoke induces inflammatory responses causing the accumulation of B and T cells which organize into structures named inducible bronchus-associated lymphoid tissue (iBALT) (Elliot et al., 2004). The chemoattractant molecules CCL19 and CXCL13 mediate T and B cell migration to the lungs, respectively (Brusselle et al., 2009a). iBALT can develop during infections, autoimmunity and chronic inflammation in the lungs and predominantly forms on bronchial epithelium (Hwang et al., 2016). They consist of mainly memory and naïve B cells, germinal center like B cells, T follicular helper cells, follicular dendritic cells and high endothelial venules (HEVs) (Hwang et al., 2016). Presence of iBALT formations in the lung has a beneficial role against viral infections, maintaining memory cells and generating primary immune responses (Tan et al., 2019). However, it could be also detrimental to the host by producing autoantibodies, enhancing ongoing inflammatory responses as well as producing degradation products of the extracellular matrix (Brusselle et al., 2009a). The presence of iBALT structures in the lung is strongly linked to disease severity (Jia et al., 2018; Polverino et al., 2015) and this indicates the importance of B and T cells in the pathogenesis of COPD. Supporting this finding, our laboratory demonstrated that B cell deficient mice were

protected against the development of emphysema after chronic cigarette smoke exposure as they were not able to form iBALT structures (John-Schuster et al., 2014a). In the follow-up work, our laboratory also reported that inhibiting the action of oxysterol enzymes, that are crucial for secondary lymphoid tissue organization (Cyster et al., 2014; Hannedouche et al., 2011), prevented iBALT formation and protected against emphysema development when mice were exposed to chronic cigarette smoke for four months (Jia et al., 2018).

Last but not least, macrophages play a central role in the pathogenesis of COPD (Tetley, 2002). Their pivotal functions include the production of reactive oxygen species (ROS), growth factors, MMPs as well as pro-inflammatory cytokines and chemokines which have a dramatic impact upon the recruitment of other innate and adaptive immune cells and tissue destruction (Barnes, 2004). Not surprisingly, macrophage number is significantly elevated in the airways, BAL fluid, lung parenchyma as well as in the sputum of COPD patients and this increase is positively correlated with disease development (Di Stefano et al., 1998; Traves et al., 2004). A detailed explanation about their specific role in the disease is provided in section 1.2.2.

1.2.2 The role of macrophages in the pathogenesis of COPD

As introduced above, macrophage contribution to the pathogenesis of COPD is well established. Macrophages are mononuclear phagocytic cells locating throughout the respiratory tract to function as a gateway to eliminating potentially harmful inhaled substances (Hodge et al., 2003). Besides their phagocytic role, they produce various mediators in response to inflammatory insult to promote the required immune response to clear these harmful substances (Vlahos and Bozinovski, 2014). They are found to be localized in the airways, alveolar tissues as well as lung parenchyma tissues. Macrophages are divided into two subsets in terms of their origin as a tissue resident population and a monocyte-derived population (Figure 1.2) (Yamasaki and Eeden, 2018). The main difference between tissue resident lung macrophages and monocyte-derived lung macrophages is their ability to proliferate. Compared to tissue resident macrophages, monocyte derived macrophages have limited capability of proliferation (van Furth et al., 1972). Furthermore, lung resident

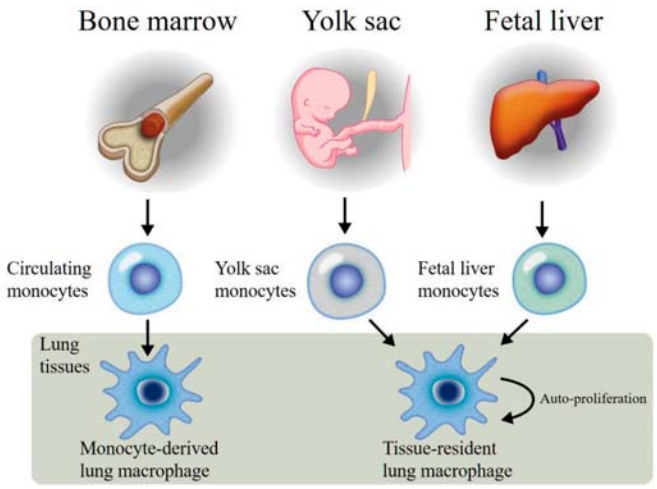

Figure 1.2 The origin of two distinct macrophage population in the lung. Monocyte derived lung macrophages originate from bone marrow, release into the peripheral blood and migrate into lung tissue whereas tissue resident lung macrophages are developed from yolk sac or fetal liver and migrate to the lungs and stay in the lung permanently called resident macrophages (Yamasaki and Eeden, 2018).

macrophages have distinct areas in the tissue where they reside such as alveolar macrophages (AMs) located in alveolar spaces and interstitial macrophages (IMs) locating between the alveoli and blood vessels. Overall the lung macrophage population is composed of 90% AMs (van oud Alblas and van Furth, 1979). AMs are specialized mainly for phagocytosing inhaled particles and metabolizing lung surfactant, while IMs take part in tissue repair and antigen presentation (Yamasaki and Eeden, 2018). These populations can be separated from each other by specific surface markers CD45, CD11b, F4/80 as well as CD11c (Zaynagetdinov et al., 2013), with AMs being $F4/80^{hi}$ $CD11c^{hi}$ $CD11b^{-}$ and IMs being $F4/80^{low}$ $CD11c^{low}$ $CD11b^{+}$ (Zaynagetdinov et al., 2013).

Independent of their origin and localization, lung macrophages are heterogeneous in terms of their distinct phenotypes and were historically classified as M1 or M2 macrophages depending upon their inflammatory profile (Morales-Nebreda et al., 2015). According to many studies, some macrophages are more prone to possess a pro-inflammatory phenotype which is referred to as M1 while the rest have a tendency to have an anti-inflammatory profile and are referred to as M2 (Liu et al., 2014). M1 macrophages known as classically activated, produce high levels of pro-inflammatory cytokines following IFNγ stimulation including IL-1β, TNF, IL-12, CXCL1, CXCL8, CCL2 and reactive oxygen species that attract monocytes, neutrophils and promote a Th1 response (Culpitt et al., 2003). Moreover, they also express

MHC II, CD68, CD80, CD86 on their surface and iNOS intracellularly (Trombetta et al., 2018). However, M2 macrophages known as alternatively activated, have a more immunomodulatory function such as promoting tissue repair, remodeling and phagocytosis. M2 macrophages are induced mainly by IL-4 and IL-13 and secrete CCL22, IL-10, CCL18 and TGF-β (Mantovani et al., 2004; Saqib et al., 2018). Unlike M1 macrophages, they are characterized by having CD206 and CD163 on their surface (Kaku et al., 2014). Despite having distinct phenotypes and functions, both M1 and M2 macrophages contribute to the development of COPD (Eapen et al., 2017). Upon chronic inflammation, lung resident macrophage levels are highly elevated since blood monocytes are recruited to the lung tissue following several key cytokines and chemokines such as CCL2, CCL3, CCL7 and CXCL12 (Shi and Pamer, 2011; Traves et al., 2002). There are studies claiming that recruited macrophages to the lung in response to stimuli have a tendency to become pro-inflammatory (M1 like) whereas resident macrophages are more likely to become anti-inflammatory (M2 like) (Yamasaki and Eeden, 2018; Yona et al., 2013). However, distinct macrophage subpopulations and their precise contribution to disease pathogenesis are still under discussion. Further investigation is required to comprehend the dynamics of macrophages and the alterations between subpopulations when exposed to environmental insult.

In the case of COPD, many studies demonstrated that M1 and M2 populations are both elevated, but their abilities to migrate, phagocytose and secrete mediators are impaired (Culpitt et al., 2003). In a recent study, it was also demonstrated that macrophages from COPD patients released higher amounts of inflammatory cytokines like TNF-α, IL-6, IL-1β, and chemokines including CXCL1, CXCL8 and CCL2 as well as ROS products that might give rise to more tissue damage (Barnes, 2017a). Moreover, as mentioned above, proteolytic enzymes including elastases, MMPs and cathepsins released by macrophages have a detrimental role in the development of emphysema. The excessive production of MMPs specifically MMP2, MMP9, MMP12 and cathepsins like cathepsin K, L, S by macrophages from COPD patients have been demonstrated in response to foreign particulate exposure (Nakajima et al., 2016; Russell et al., 2002). Importantly, mice deficient in MMP12 were protected against cigarette smoke induced emphysema (Shapiro et al., 2003). In addition, COPD macrophages including

alveolar and monocyte derived ones have reduced capacity for phagocytic uptake of bacteria, which results in enhanced acute reactions to infection (Taylor et al., 2010) and impaired clearance of apoptotic cells termed efferocytosis causing a defect in resolving existing inflammation (Hodge et al., 2003). Considering that lung macrophages serve as the gate keeper for the lungs, their numbers, functions and interactions with other cells are critical for lung tissue inflammation and COPD pathogenesis (Vlahos and Bozinovski, 2014).

There are many studies investigating the role of resident lung macrophages including AMs, however monocyte derived macrophages also play a critical role in the presence of exposure to environmental stimuli in the development of the disease (Desch et al., 2016). Monocytes are recruited from the blood stream to the site of injury via specific chemokines, mainly CCL2 (Deshmane et al., 2009). Elevated levels of CCL2, known as also MCP-1 (Monocyte chemoattractant protein 1), has been observed in BAL fluid from smokers and in the sputum of COPD patients (Culpitt et al., 2003). When monocytes migrate from blood to lung tissue, they differentiate into macrophages. The vast majority of studies suggest that monocyte derived macrophages have a tendency to differentiate into a pro-inflammatory phenotype and contribute to disease development by promoting inflammation (Yamasaki and Eeden, 2018). However, this topic is still under debate since monocyte derived macrophages also have anti-inflammatory properties in several diseases and may also contribute to tissue repair and recovery by resolving inflammation (Ginhoux and Jung, 2014). Due to the undeniable role of monocyte-derived macrophages in disease pathogenesis, their migration dynamics toward inflamed tissue is important to comprehend.

Recruitment of monocytes from blood to the tissue requires a tightly regulated, multistep process, including adhesive interactions between monocytes and endothelial cells and intracellular signaling pathways (Mestas and Ley, 2008). Chemokines released by immune cells upon chronic inflammation and adhesion molecules on monocytes and on endothelial cells are the key components of migration (Rosseau et al., 2000). Critical molecules and migration steps for monocytes are summarized in Figure 1.3 (Gerhardt and Ley, 2015).

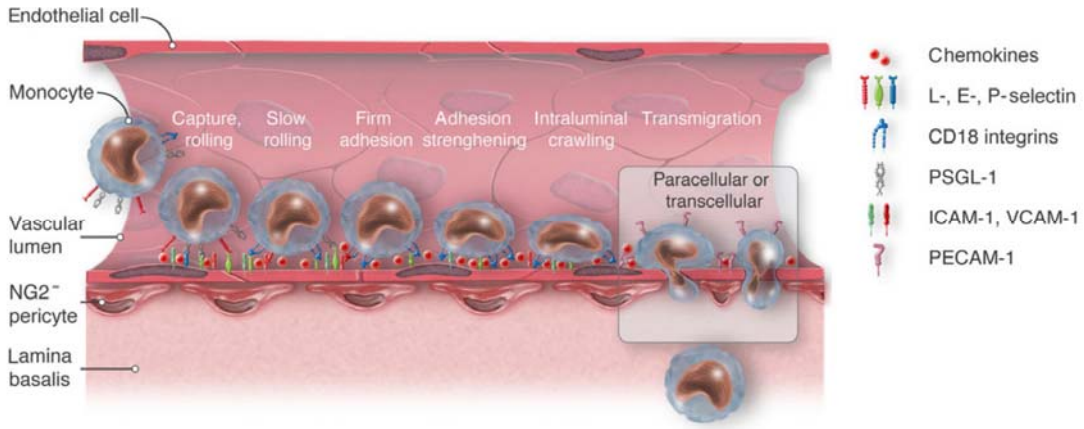

Figure 1.3 Schematic view of the monocyte migration from blood to the tissue. Monocyte migration is a multistep process starting with capturing and rolling upon chemokine release. During slow rolling, adhesion of monocytes to endothelial cells is initiated via adhesion molecules including selectins, CD18 integrins, PSGL-1, ICAM-1, VCAM-1 and PECAM-1. With the help of the adhesion molecules, transendothelial migration occurs either paracellularly or transcellularly (Gerhardt and Ley, 2015).

Firstly, endothelial cells are activated through cytokines like TNF-α or IL-1β released from inflamed tissue macrophages which triggers the expression of adhesion molecules mainly VCAM-1 and ICAM-1 on the surface of endothelial cells (Min et al., 2005). At the same time, monocytes sense cytokines such as CCL2 (MCP-1) following inflammation and start rolling and adhering to endothelial cells with the help of integrins, specifically LFA-1 (CD11a, Itgal), Mac-1 (CD11b, Itgam) and VLA-4 (CD49d, Itga4) (Shi and Pamer, 2011). Monocyte adhesion to endothelial cells is a key step of transendothelial migration. Several studies have shown that disability of these adhesion molecules and integrins inhibit monocyte migration into the tissue (Hsu et al., 2011; Schenkel et al., 2004; Wong et al., 2010).

Monocyte-derived macrophages are not only crucial for COPD but are associated with the severity of other inflammatory diseases like asthma, fibrosis, atherosclerosis, diabetes, obesity, skin injury, cancer and even in multiple sclerosis (Ponzoni et al., 2018). Considering the pivotal role of monocyte-derived macrophages in various diseases, targeting macrophages by manipulating their migration into tissue or altering their function might be beneficial in improving disease pathogenesis. In mouse models, relevant therapeutic approaches targeting macrophages through nanotechnology-based systems or complete depletion produced already positive results against the development of disease (Ahsan et al., 2002; Lee et al., 2015). Consistently, alendronate treatment of alveolar macrophages

prevented alveolar airspace enlargement in an elastase-induced as well as cigarette smoke-induced emphysema mouse models (Ueno et al., 2015b). However, some points are still controversial about the involvement of monocytes in disease development. Therefore, further investigation will provide us more detailed information to fully understand the recruitment, differentiation and function of monocytes and their contribution to progression of various diseases including COPD.

1.3 Post-translational modification of arginine

Post translational modifications (PTMs) are described as chemical modifications of a polypeptide chain that occurs after RNA is translated into protein in eukaryotic cells to diversify the proteome in terms of protein stability, localization, interactions and function (Wang et al., 2014b). PTMs range from proteolytic cleavage of peptide bonds or addition of modifying chemical groups to the polypeptide chain including phosphorylation, glycosylation, acetylation and methylation, and they are highly associated with initiating or amplifying the signal in signalling cascades (Fulton et al., 2019). PTMs, particularly acetylation and methylation of histone proteins, are also crucial mediators of epigenetic regulation (Blanc and Richard, 2017).

Protein methylation is a crucial PTM involved in multiple cellular mechanisms mainly signalling pathways, transcriptional gene regulation, translation, translocation, DNA repair, protein-protein interactions and protein stability (Bedford and Richard, 2005; Deribe et al., 2010). Protein methylation has been identified primarily on lysine and arginine residues. There is growing interest in arginine methylation currently considering the identification of the family of protein arginine methyltransferase enzymes responsible for the PTM and the role of these enzymes playing in physiology and their potential contribution to disease pathogenesis (Greenblatt et al., 2016).

1.3.1 Protein arginine methylation

Arginine methylation is a very prevalent and ubiquitous PTM which potentially takes place on both nuclear and cytoplasmic proteins and is conserved across all eukaryotic organisms (Bedford and Clarke, 2009). Arginine methylation is the chemical modification in which the

guanidine nitrogen atoms of arginine residues can be modified to contain methyl groups from the donor S-adenosylmethionine (AdoMet) resulting in monomethylarginine (MMA), asymmetrical dimethylarginine (ADMA) or symmetrical dimethylarginine (SDMA) (Bedford and Richard, 2005). Arginine methylation plays a central role in transcriptional regulation through the methylation of histones, resulting in activating histone marks like H4R3me2a, H3R2me2s, H3R17me2a and H3R26me2a or repressive histone marks including H3R2me2a, H3R8me2a and H4R3me2s (Blanc and Richard, 2017). Besides its role in gene regulation, arginine methylation is associated with many biological processes including translation, DNA repair, mRNA splicing and a variety of signalling cascades (Guccione and Richard, 2019). Dysregulated arginine methylation is significantly linked to the development of several human diseases, particularly cancer (Poulard et al., 2016), even though only 0.5-1% of total arginine residues are exposed to methylation (Lamberth, 2016). Arginine methylation is catalysed by a family of protein arginine methyltransferases (PRMTs) consisting of 9 family members (Di Lorenzo and Bedford, 2011). Detailed information about PRMTs and their function is summarized in section 1.3.2.

1.3.2 Protein arginine methyl transferases (PRMTs) in mammals

As described above, arginine methylation is mediated by PRMT enzymes in mammalian cells catalysing the transfer of a methyl group from the methyl donor – AdoMet to the nitrogen atom of arginine residues (Katz et al., 2003). Final products of this reaction are methylated arginine and S-adenosylhomocysteine (AdoHcy). PRMT enzymes are branched into three categories based on their catalytic function; type I, type II and type III PRMTs. Type I PRMTs including PRMT1, PRMT2, PRMT3, PRMT4 (also referred to as coactivator-associated arginine methyltransferase 1 – CARM1), PRMT6 and PRMT8 catalyse the addition of two methyl groups onto the same nitrogen atom of arginine forming asymmetrical di-methylarginine (ADMA, Rme2a) (Lin et al., 1996). Type II PRMTs like PRMT5 and PRMT9 carry out the addition of two methyl groups onto different nitrogen atoms of the arginine residue generating symmetrical di-methylation (SDMA, Rme2s) (Yang et al., 2015). Type III PRMTs, including only PRMT7, is unique in its function as it only generates mono-methylation (MMA) of the arginine

residue (Feng et al., 2013). Figure 1.4 illustrates the different types of PRMTs involved in arginine methylation (Auclair and Richard, 2013).

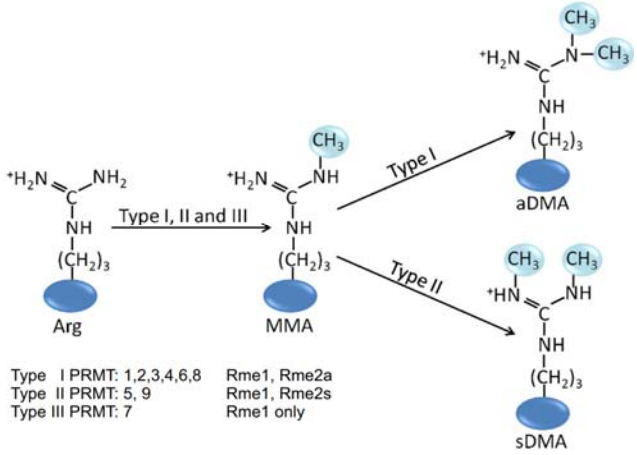

Figure 1.4 Protein arginine methylation by PRMTs. Specific types of PRMT enzymes catalize either mono-methylation or dimethylation of arginine residues. The type I enzymes (PRMT1, PRMT2, PRMT3, PRMT4, PRMT6 and PRMT8) catalyze asymmetrical dimethylation (aDMA) reaction whereas Type II enzymes (PRMT5 and PRMT9) form symmetrically dimethylation (sDMA). Type III enzyme (PRMT7) only generates mono-methylation (MMA) (Auclair and Richard, 2013).

PRMTs potentially target histones, predominantly H2AR3, H2BR29, H3R2-R8-R17, and H4R3-R17-R19 (Fuhrmann and Thompson, 2016), or proteins with glycine and arginine rich (GAR) motifs known as RGG boxes/motifs (Najbauer et al., 1993). All PRMTs possess a pair of highly preserved glutamate residues (Double-E-loop) that is negatively charged, in the active site pocket to orientate the guanidino group of the arginine residue on the substrate, which is positively charged. The characteristics and size of the active pocket are considered to play a key role in substrate specificity and recognition (Morales et al., 2016). PRMTs also contain conserved threonine-histidine-tryptophan (THW) loops that are specific only to the PRMT family (Hasegawa et al., 2014). It has been suggested that the THW loops are important for the formation of the AdoMet-binding pocket in a collaboration with double E loop and αY helix (Zhang et al., 2000). Moreover, in terms of structure, all PRMTs contain Rossman fold domains and β-barrel sheets which are parts of the conserved catalytic core where the cofactor and substrate binds respectively (Cheng et al., 2005). Certain protein-protein interaction regions including a SH3 domain, a zinc finger, pleckstrin homology domain, a TIM barrel and myristoylation motifs are unique to PRMT2, PRMT3, CARM1, PRMT5 and PRMT8, respectively, which are located predominantly at the N-terminus of the core domain and

contribute to substrate recruitment and binding (Cheng et al., 2005; Wolf, 2009). Figure 1.5 summarizes the structure of PRMTs.

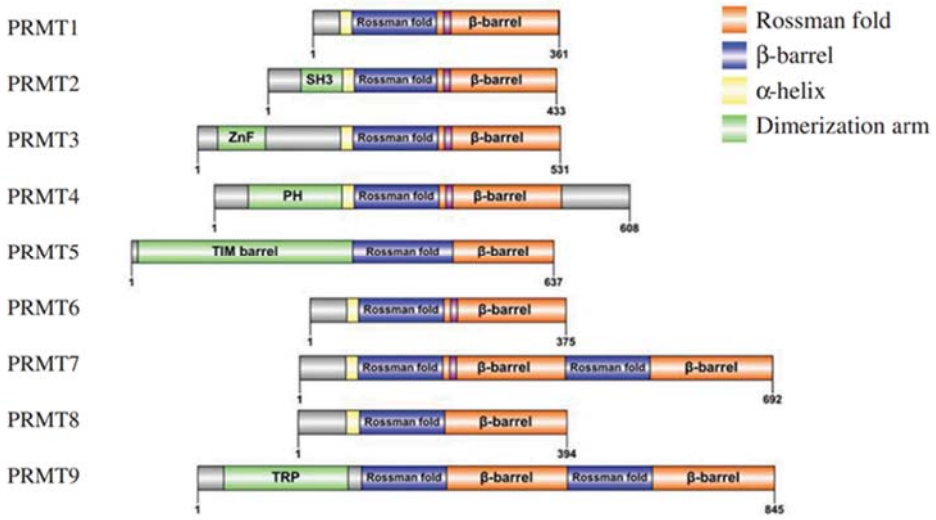

Figure 1.5 Structures of PRMTs in mammalian cells. Rossman fold is conserved core region shown in blue and β- barrel is shown in orange. α-helix domain located at N-terminus of Rossman domain is shown in yellow. The number indicates the amino acid for each PRMT. SH3, SH3 domain; ZnF, zing finger motif; PH, pleckstrin homology domain; TPR, tetratricopeptide repeat (Smith et al., 2018).

1.3.3 Biological Roles of PRMTs

PRMTs are involved in diverse cellular processes and systems mainly including transcriptional regulation, RNA processing, the DNA damage response, cell proliferation, and signal transduction (Blanc and Richard, 2017; Guccione and Richard, 2019).

Transcription

Transcriptional activation and repression can be regulated by the activity of PRMTs (Yang and Bedford, 2013). PRMT1, a type I enzyme, is responsible for the methylation of histone 4 at arginine 3 resulting in H4R3me2a which recruits other transcriptional regulators like p300 acetyltransferase to the chromatin and functions as a transcriptional activator mark inducing gene expression (Huang et al., 2005). Other type I enzymes including PRMT2 and PRMT4 are also co-activators of transcription by generating predominantly H3R17me2a, H3R26me2a and H3R42me2a modifications at the promoters of several genes (Yang and Bedford, 2013). Conversely, some PRMTs predominantly PRMT5 and PRMT6, function as co-repressors to mediate transcriptional repression via the formation of H4R3me2s and H3R8me2s by PRMT5

(Zhu and Rui, 2019) and H3R2me2a by PRMT6 (Bouchard et al., 2018). Recruitment of PRMTs to gene promoters can be induced by several transcriptional factors such as p53, NF-KB and YY1 (Bedford and Richard, 2005; Covic et al., 2005). Additionally, the impact of PRMTs on transcriptional regulation can also be independent of histone methylation. For example, PRMT1 directly methylates Ash2L which subsequently induces H3K4 triggering transcription (Butler et al., 2011) whereas CARM1 mediates NF-κB recruitment to the nucleus by forming a complex with p300 resulting in transcriptional activity (Covic et al., 2005).

RNA Processing

RNA binding proteins (RBPs), including splicing factors, are crucial for proper RNA folding, RNA localization, RNA stabilization as well as mRNA translation (Herrmann et al., 2004). They include GAR motifs, making them a potential target for PRMTs to methylate and regulate their function (Liu and Dreyfuss, 1995). To date, PRMT1, CARM1, PRMT5 and PRMT9 are highly associated with RNA splicing by regulating localization, maturation and function of RBPs (Guccione and Richard, 2019). PRMT1 has been found to modify RNA transport via methylation of substrate proteins such as hnRNPs, fibrillarin, nucleolin and poly(A)-binding protein II (Gary and Clarke, 1998; Smith et al., 1999). PRMT5 is also one of the main PRMTs that plays a key role in maintaining splicing integrity via assuring the maturation of small nuclear ribonucleoproteins (snRNPs) (Meister et al., 2001). Sm proteins, which are rich in RGG motifs, are major targets for methylation and after being methylated are recognized by Tudor domains, resulting in snRNP maturation (Meister and Fischer, 2002). PRMT9 has a similar function to PRMT5 but their substrates are different and not interchangeable (Yang et al., 2015). Lastly, CARM1 has been identified to be involved in alternative splicing by promoting exon skipping. Specifically, CARM1 di-methylates splicing factors including SAP49 and U1C, and the transcription elongation repressor CA150 to enable them to bind to SMN Tudor domains and process splicing (Cheng et al., 2007).

DNA Damage Response

Following the exposure of DNA to genotoxic agents, pivotal functions of DNA are impaired, including transcription and replication (Ciccia and Elledge, 2010). Arginine methylation by PRMTs are involved in the DNA damage response (DDR) by regulating the checkpoints of cell

cycle process or DNA repair proteins (Auclair and Richard, 2013). PRMT1, PRMT5 and PRMT7 enzymes are found to be the key regulators of DDR since deficiency of these enzymes causes hypersensitivity to DNA damage (Guccione and Richard, 2019; Raposo and Piller, 2018). PRMT1 methylates several proteins such as MRE11 (Boisvert et al., 2005), 53BP1 (Vadnais et al., 2018) and BRCA1 (Guendel et al., 2010) which are key players in DNA damage response needed for repair of double-strand breaks. Therefore, in the absence of PRMT1 cells are more prone to spontaneous DNA damage, dysregulated chromatin stability and checkpoint defects (Yu et al., 2009). Besides PRMT1, the loss of PRMT5 gives rise to cell cycle arrest, spontaneous DNA damage and dysregulated p53 activation (Hamard et al., 2018), by modifying proteins including p53 (Jansson et al., 2008), FEN1 (Guo et al., 2010) and Rad9a (He et al., 2011). Additionally, the involvement of PRMT7 in DNA damage response is dependent upon its activity to methylate histone 2A Arg-3 (H2AR3) and histone 4 Arg-3 (H4R3) (Karkhanis et al., 2012). PRMT7 has been reported to negatively regulate the transcription of DNA repair genes such as *ALKBH5*, *APEX2*, *POLD1* and *POLD2* via these histone modifications. Reduced PRMT7 expression improves the ability of cells to resist DNA damage and promotes expression of the DNA repair genes (Karkhanis et al., 2012).

Cell Proliferation

Cell proliferation is required for cellular growth, tissue repair and regeneration and thus tightly regulated (Norbury and Nurse, 1992). Arginine methylation via the action of several PRMTs has a critical role in the orchestration of controlled cell division and cell cycle phases (Kim et al., 2010). Among PRMTs, PRMT1, PRMT2, CARM1, PRMT5 and PRMT6 have been implicated in modifying key regulatory proteins of the cell cycle (Raposo and Piller, 2018). PRMT1 has been found to interact with BGT2, a tumour suppressor protein and together induce differentiation of pre-B cells by ceasing cell cycle progression (Dolezal et al., 2017). PRMT1 and PRMT5 work in opposite directions in terms of proliferation and apoptosis by methylating the same transcription factor, E2F-1 (Zheng et al., 2013). PRMT5 methylation of E2F-1 triggers proliferation whereas PRMT1 favours apoptosis (Cho et al., 2012). Supporting this finding, many other studies also demonstrated that PRMT5 is needed for cellular proliferation (Pal et al., 2004). Overexpression of PRMT5 is involved in cancer development

by promoting tumour cell growth and PRMT5 deficiency contributes to apoptosis in different cell types (Bao et al., 2013). PRMT6 also has pro-proliferative and pro-oncogenic functions, as the methylation of p16 and p21 by PRMT6 elevates cellular proliferation (Wang et al., 2012). However, it is not a straight forward classification, as the activities of each PRMT upon the regulation of cellular proliferation has been found to be not only organism specific but also cell type specific.

Signal Transduction

Although arginine methylation via PRMTs has an important impact upon transcriptional regulation and RNA splicing in the nucleus, further investigations are still underway to fully elucidate their role in the cytoplasm and effect on signalling pathways. In this section, outstanding studies about major PRMTs including PRMT1, CARM1, PRMT5 and PRMT7 and their involvements in signalling pathways via methylation are discussed.

Starting with PRMT1, it regulates proliferation and metastasis of hepatocellular carcinoma cells by switching on the STAT3 signalling pathway (Zhang et al., 2018). It is also involved in epidermal growth factor receptor methylation where causes reduced proliferation and sphere formation in breast cancer cells (Nakai et al., 2018). Moreover, PRMT1 is a critical regulator of TGF-β signalling, which controls the epithelial-to-mesenchymal trans-differentiation and stemness of epithelial cells, via the methylation of SMAD7 (Katsuno et al., 2018). PRMT1 has been also associated with podocyte apoptosis and glomerular fibrosis by angiotensin II induced activation of ERK1/2 (Zhu, 2018).

CARM1 controls pulmonary cell growth and differentiation of epithelial cells by mediating glucocorticoid-mediated signalling (O'Brien et al., 2010). Wnt/β-catenin signalling in colorectal cancer cells is also regulated by CARM1, via direct methylation of β-catenin, supporting its function in cell growth and survival (Ou et al., 2011). Additionally, CARM1 directly methylates malate dehydrogenase 1 and regulates cellular redox homeostasis by suppressing glutamine metabolism in pancreatic cancer cells (Wang et al., 2016). Recently, another study showed that CARM1 interacts with NF-κB subunit p65 and increases methylation of p65 resulting in neural differentiation via NF-κB signalling (Niu et al., 2020).

PRMT5 is so far the most studied PRMT enzyme regarding signal transduction. PRMT5 promotes proliferation and glycolysis in pancreatic cancer cells by silencing the tumour suppressor FBW7, resulting in enhanced cMyc levels (Qin et al., 2019). In the same direction, PRMT5 directly interacts with Akt causing an increase in its phosphorylation levels, which promotes proliferation of lung cancer cells (Zhang et al., 2019). Moreover, PRMT5 activates PI3K-AKT signalling axis to enhance cell survival and proliferation of lymphoma cells (Zhu et al., 2019). Besides AKT signalling, PRMT5 is shown to be associated with proliferation of hepatocellular carcinoma cells as a result of downregulating BTG2 expression via ERK signalling (Jiang et al., 2018). PRMT5 stimulates Wnt/β-catenin signalling and promotes pro-survival genes in lymphoma cells (Chung et al., 2019). On the other hand, PRMT5 has been reported to enhance hypoxia and ischemia-induced apoptosis through p38 MAPK and JNK signalling pathways in human lung epithelial cells (Lim et al., 2013). The molecular and cellular functions of PRMT7 are discussed in detail in section 1.3.5.

1.3.4 Protein arginine methyltransferase 7 (PRMT7)

PRMT7 is a unique member of the protein arginine methyltransferase family, the only member that displays type III enzyme activity, shown in Figure 1.6A, that is it can only undertake mono-methylation of arginine substrates (Miranda et al., 2004; Zurita-Lopez et al., 2012). Crucially, analysis of publically available transcriptomics data (Morrow et al., 2017) revealed it to be the most enhanced PRMT in the lungs of COPD patients compared to healthy smokers. Recent studies investigating the restrictive activity of PRMT7 to only undertake mono-methylation, suggested that the active site volume of PRMT7 does not allow it to form di-methylated products. Crystal structure analysis described that the guanidine binding pocket of PRMT7 is quite small and narrow while other PRMTs which can form di-methylation have larger cavities as shown in Figure 1.6B (Caceres et al., 2018). Moreover, PRMT7 differs from other PRMTs regarding substrate specificity, as it preferentially targets RXR motifs in arginine and lysine rich regions, accounting for the narrow substrate selectivity of PRMT7 (Feng et al., 2013).

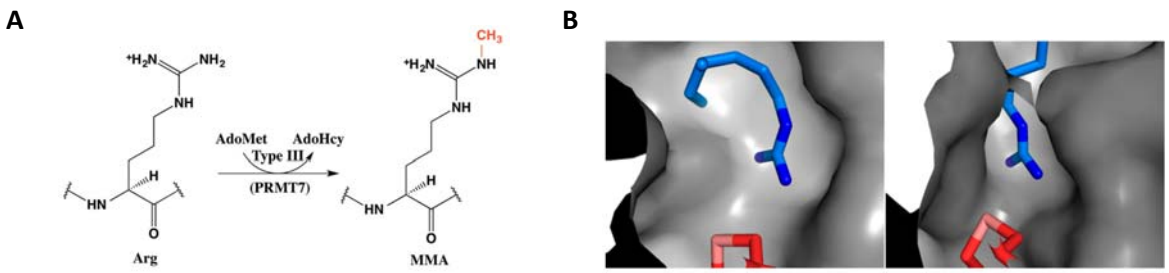

Figure 1.6 PRMT7 is a type III enzyme which only monomethylates its substrates. A) PRMT7 adds CH_3 group to the N atom of the arginine using AdoMet and producing AdoHcy. It is referred as type III enzyme activity. **B)** The comparison of substrate arginine in the binding pockets of ratPRMT1 (left) and TbPRMT7 (right). PRMT1 crystal structure shows larger binding site pocket while PRMT7 has more congested active site. Blue and red colours represent substrate arginine and S-adenosylhomocysteine, respectively (Caceres et al., 2018; Feng et al., 2013).

PRMT7 is a 692-amino acid protein in humans and mice and is predominantly localized in the cytoplasm (Herrmann et al., 2009). However, there are studies confirming that PRMT7 shuttles between the cytoplasm and nucleus since it is crucial for histone methylation (Jain and Clarke, 2019). Structurally, it contains two tandem repeated core domains, as shown in Figure 1.7, where N-terminal core domain is conserved between other PRMTs and maintains catalytic activity (Hasegawa et al., 2014). The C-terminal core domain is not evolutionary well conserved, and is not associated with the catalytic activity of PRMT7 (Hasegawa et al., 2014; Miranda et al., 2004).

PRMT7 targets histone proteins as well as non-histone proteins for catalysing arginine mono-methylation (Zurita-Lopez et al., 2012). The best-characterized histone substrates for PRMT7 are histone 3 Arg-2, histone 4 Arg-3/17/19, histone 2B Arg-29/31/33 and histone 2A (Feng et al., 2013; Szewczyk et al., 2019). PRMT7 regulates the transcriptional expression of various genes associated with various cellular events including RNA splicing and DNA repair through histone methylation (Blanc and Richard, 2017). Interestingly, PRMT7 mono-methylation on

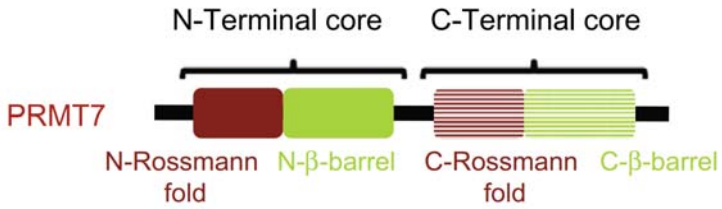

Figure 1.7 Schematic representation of the domain structure of PRMT7. PRMT7 includes two core domains, N-terminal and C-terminal. Conserved Rosmann fold domains shown in red and β-barrel domains shown in green (Hasegawa et al., 2014).

specific histones may regulate the activity of other PRMTs. For example; histone 4 Arg-17 mono-methylation by PRMT7 allosterically triggers the activity of PRMT5 on histone 4 Arg-3 suggesting that PRMT7 mono-methylation may interplay with di-methylation (Jain et al., 2017). Recent studies also demonstrated that PRMT7 not only methylates histones but also methylates directly non-histone proteins. To date, DVL3 (Bikkavilli et al., 2012), G3BP2 (Bikkavilli and Malbon, 2012), eIF2α (Haghandish et al., 2019) and HSP70 (Szewczyk et al., 2020) have been described as PRMT7 substrates. The specific roles of these substrates and involvement of PRMT7 in several cellular processes and signalling pathways are explained detailly in section 1.3.5.

1.3.5 Molecular and cellular functions of PRMT7

The physiological roles of PRMT7 through the targeting of both histone and non-histone proteins have been associated with many cellular mechanisms, including regulation of the transcriptional activity of genes involved in DNA repair (Karkhanis et al., 2012), methylation of Sm proteins and biogenesis of small nuclear ribonucleoprotein (Gonsalvez et al., 2007b), maintenance of pluripotent state of undifferentiated embryonic stem cells and germ cells (Buhr et al., 2008; Chen et al., 2018), regulation of the function and regenerative capacity of skeletal muscles (Blanc et al., 2016; Jang et al., 2017) and immune cells (Ying et al., 2015). Additionally, various studies elegantly demonstrated that the function of PRMT7 is critical in the promotion of breast cancer metastasis (Thomassen et al., 2009; Yao et al., 2014), mediating cellular stress response pathways (Haghandish et al., 2019), maintaining muscle oxidative metabolism (Jeong et al., 2016), germinal center formation (Ying et al., 2015), Wnt signalling (Bikkavilli et al., 2012; Bikkavilli and Malbon, 2012) and cellular differentiation (Dhar et al., 2012). To date, it is currently implicated to play a role in several diseases including cancer (Baldwin et al., 2015; Cheng et al., 2018; Geng et al., 2017; Liu et al., 2020; Yao et al., 2014), obesity (Leem et al., 2019), DNA damage (Auclair and Richard, 2013; Karkhanis et al., 2012) and short stature, brachdactyly, intellectual development disability, and seizures (SBIDDS) syndrome (Agolini et al., 2018; Birnbaum et al., 2019; Kernohan et al., 2017; Valenzuela et al., 2019).

PRMT7 contributes to the DNA damage response by specifically mono-methylating H2A Arg-3 (H2AR3) and H4 Arg-3 (H4R3) resulting in reduced transcriptional expression of genes including *ALKBH5*, *APEX2*, *POLD1* and *POLD2* which play a key role in the DNA repair process. In the absence of PRMT7 expression, the repression of DNA repair genes is removed and resistance to DNA damage is enhanced in the cell (Karkhanis et al., 2012). Moreover, the involvement of PRMT7 in Wnt-β-catenin signalling depends on the methylation of dishevelled 3 (Dvl3), a central component in Wnt signalling pathways. Arginine mono-methylation of Dvl3 protein by PRMT7 mediates the translocation of Dvl3 protein to the cell membrane therefore regulating Wnt signalling activation (Bikkavilli et al., 2012). PRMT7 has been associated with stress granule formation, which promotes cell survival in tumours via direct methylation of the eukaryotic translation initiation factor 2α (eIF2α). Methylation of eIF2α promotes phosphorylation, which is required for eIF2α-dependent stress granule formation (Haghandish et al., 2019). Additionally, with the help of PRMT5, PRMT7 prevents HIV-1 accessory protein viral protein R (Vpr) from proteasomal degradation and mediate its stability. Thus, together with PRMT5, they promote HIV-1 virus replication in macrophages via stabilization of Vpr (Murakami et al., 2020). So far, the function of PRMT7 in various tumour cells is well investigated. There are many studies showing that PRMT7 is overexpressed in cancer cells behaving as an oncogene and promoting the growth of tumour cells contributing to the malignancy of tumours (Cheng et al., 2018; Geng et al., 2017). A recent study implicated PRMT7 in the regulation of the β-catenin/C-MYC axis, by inhibiting ubiquitination of β-catenin via direct methylation, and that this supported the proliferation of renal cell carcinomas (Liu et al., 2020). There is also evidence that PRMT7 regulates epithelium to mesenchymal transition via inhibition of the E-cadherin expression with the help of histone modifications in breast cancer and promotes metastasis (Yao et al., 2014). Another critical target of PRMT7 is PGC-1α, which is known as a transcriptional coactivator of the genes of energy metabolism. It is a master mediator of oxidative muscle metabolism and mitochondrial biogenesis. PRMT7 induced the expression of PGC-1α through the methylation of p38 MAPK which activates phosphorylation of ATF2 and recruits p-ATF2 to the promoter of PGC-1α, inducing its expression (Jeong et al., 2016). In keeping, a further study demonstrated that muscle stem cell self-renewal and regeneration was dependent upon

PRMT7 activity (Blanc et al., 2016). In this study, it was suggested that PRMT7 is involved in controlling the expression of DNMT3b and p21, which are responsible for satellite cell function maintenance and muscle regeneration (Blanc et al., 2016). Last but not least, today, the function of PRMT7 in immune cells is gaining appreciation. PRMT7 has been found to be an important player in B cells by controlling germinal center formation and plasma cell differentiation via the inhibition of *Bcl6* gene transcription following H4R3 methylation on its promoter site. BCL6 is a master regulator of germinal center formation and, when PRMT7 is deficient, late B cell differentiation is impaired whereas germinal center B cell differentiation is promoted (Ying et al., 2015).

Considering the above findings, that PRMT7 implements important roles in mammalian cells, it is still not characterized as much as the other members of the PRMT family regarding its specific substrates, catalytic activity, inhibition and particularly its involvement in disease pathogenesis. Earlier studies already demonstrated that several PRMTs are expressed in the mouse lung suggesting a possible involvement in lung development (Zakrzewicz et al., 2012) or disease pathogenesis (Yildirim et al., 2006). It was recently demonstrated by our laboratory that CARM1 is critical in lung injury and repair by regulating cellular senescence, in both alveolar epithelial type II cells (Sarker et al., 2015) and the airway epithelium (Sarker et al., 2019). However, the function of PRMT7 is only well described for cancer progression, therefore further investigation is needed to fully comprehend the link between PRMT7 and its potential pathogenic role in chronic disease, particularly inflammatory lung diseases such as COPD.

1.4 Aim of the study

COPD is defined as a chronic obstructive pulmonary disorder and is characterized by alveolar destruction and tissue damage known as emphysema, resulting in airflow obstruction and progressive reduction in lung function. COPD is the third leading cause of death worldwide and currently has no curative therapies. Substantial evidence demonstrates that inflammatory processes play a central role in the development of emphysema and the pathogenesis of COPD. Even though cigarette smoke is so far identified to be the major cause of COPD, only 20% of smokers develop the disease implying that there are other factors involved affecting the development such as genetics, gender, age, infections and crucially epigenetics. This complexity, and the need for new therapeutic strategies to impair and reverse disease progression, dictates further investigation that is required to identify the main protagonists and develop target-oriented strategies for novel therapies. This study aimed at identifying the intrinsic factors underlying cigarette smoke induced COPD pathogenesis and elucidating the precise molecular mechanisms driving progression of the disease in COPD patients. By analysing already existing gene set enrichment analysis (GSEA) data between smokers and COPD patients, protein arginine methyltransferase 7 (PRMT7) has been suggested to be involved in the pathogenesis of COPD.

Therefore, more specifically, the aims of the project are:

- To identify in which cells PRMT7 is predominantly expressed in the lungs of COPD patients and how it contributes to inflammation process in disease pathogenesis
- To investigate the upstream regulation of PRMT7 in inflammatory conditions
- To elucidate the role of PRMT7 in animal models of COPD
- To comprehend the involvement of PRMT7 and its function in additional inflammatory disease models

In the light of the aims, this study has demonstrated that the epigenetic regulation of RAP1A via PRMT7 mediated histone methylation controls monocyte transendothelial migration and subsequent inflammation and disease development. These findings could help establishing

novel therapeutic options to prevent disease development where chronic inflammation is an underlying cause like in COPD.

2. MATERIALS AND METHODS

2.1 Materials

2.1.1 Mice

C57BL/6N-Tyr$^{c\text{-}Brd}$ *Prmt7*$^{tm1a(EUCOMM)Wtsi}$/WtsiCnbc mice were purchased from The Wellcome Trust Sanger Institute, Cambridge, UK. Heterozygous, *Prmt7*$^{+/-}$, mice carrying a single copy of the insertion were mated with wild-type (WT) mice to maintain the production of new generation of mice. 8 to 10 week old *Prmt7*$^{+/-}$ mice and their wild-type littermate controls were used in all experiments. The gender of mice used in the experiments were female and male according to experiment type. Moreover, conditional knockout mice of Prmt7 in myeloid cell lineage, *Lyz2-Cre Prmt7*$^{flox/flox}$, were also used in some part of this study to understand the role of Prmt7 in distinct cell types. Targeting procedure of transgenic mice was demonstrated in Figure 2.1.

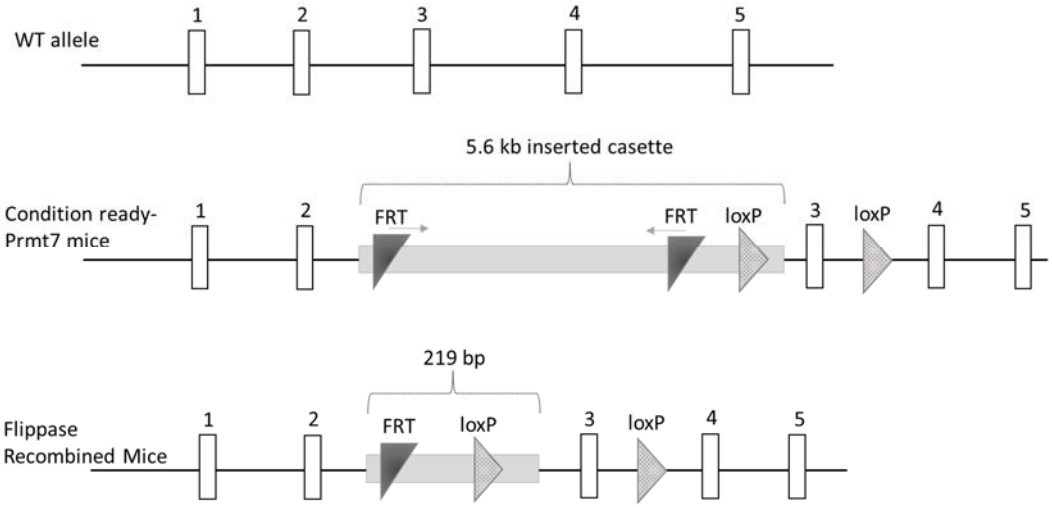

Figure 2.1 Targetting strategy of the *Prmt7* allele. Schematic representative picture of genetically modified alleles applied in this study.

All mice were bred on C57BL/6 genetic background and maintained under specific pathogen-free facility. They were kept under specific conditions with a constant temperature and humidity with a 12-hour light cycle in accordance with Helmholtz Zentrum Muenchen institutional, state and federal guidelines.

2.1.2 Reagents and chemicals

Table 2.1: Solutions, reagents and chemicals used in the study

Product	*Company*
Absolute ethanol	Sigma-Aldrich
Agar	AppliChem
0.25% Trypsin-EDTA solution	Sigma-Aldrich
87% Glycerol	AppliChem
0.4% (w/v) Trypan Blue	Thermo Fisher Scientific
Acrylamide: N,N-Methylene–Bisacrylamide 40% (29:1)	Carl Roth
Ammoniumsulfate(APS)	ZYTOMED Systems
Antibody diluent	ZYTOMED Systems
Amersham ECL Prime	Sigma-Aldrich
B-Mercaptoethanol	Sigma-Aldrich
Bovine serum albumin (BSA)	Sigma-Aldrich
Collagen G from bovine calf skin	Merck Millipore
Pierce Protein A Agarose beads	Thermo Fisher
Protein A and Protein G magnetic beads	Thermo Fisher 10003A/D
Glycine	Carl Roth
HIER Citrate Buffer, pH 6	ZYTOMED Systems
EDTA Buffer, pH 9	Roche Diagnostics
Hematoxylin	Sigma-Aldrich
Entellan	Merck Millipore
Hydrogen peroxide (H_2O_2)	Sigma-Aldrich
4x Laemmli sample buffer	Bio-Rad
Complete® Mini without EDTA (Protease-inhibitor)	Roche Diagnostics
DAPI (4', 6-diamino-2-phenylindole)	Sigma-Aldrich
DNase/RNase free water	Promega
$MgCl_2$ (25mM)	Life Technologies
Blot Stripping Buffer	Thermo Fisher
Distilled water	ZYTOMED Systems
dNTP Mix 10mM 1000µl	Carl Roth
Methanol	Merck Millipore
Fetal Bovine Serum (FBS)	Bio and Sell
T-PER lysis buffer	Thermo Fisher
Fluorescent Mounting Medium	Dako
Isopropanol	Carl Roth
MuLV Reverse Transcriptase 5000U (Reverse Transcriptase)	Carl Roth
Phosphatase Inhibitor (Vanadate)	Life Technologies
PCR Buffer II + $MgCl_2$	New England Biolabs
Non-fat dried milk powder	AppliChem
Paraformaldehyde (PFA)	AppliChem
Penicillin-Streptomycin (100 U/ml)	Gibco, Life Technologies

Dakopen	Dako
Protein Standards	Bio-Rad
Dimethyl sulfoxide (DMSO)	Carl Roth
PBS	Life Technologies
Temed	Bio-Rad
Random Hexamers 50µM	Thermo Fisher Scientific
SensiFAST syber green	Bioline
SDS	AppliChem
Rodent block M	Biocare Medical
Tween 20	Sigma-Aldrich
Xylol	Sigma-Aldrich
RNase Inhibitor 20 U/µl, 2000U	Bela-pharm
Non-essential amino acids (NEA)	Biochrom
Polyvinylidene difluoride (PVDF) membrane	Bio-Rad
Rabbit on rodent Alkaline phosphatase (AP)-Polymer	Biocare Medical
Formaldehyde	Thermo Fisher Scientific
3R4F research cigarette	Lexington,KY,USA
Sodium chloride (NaCl)	Braun
PowerUp SYBR Green Master Mix-50 mL	Thermo Fisher Scientific
Tris	Carl Roth
Vulcan fast red (VFR)	Biocare Medical
Xylene	Carl Roth
Nonident P40	Sigma-Aldrich
Xfect™ Transfection Reagent	Clontech
Bleomycin	Sigma-Aldrich
Roti-Quick	Carl Roth

2.1.3 Buffers and stock solutions

Table 2.2: Composition of buffers and stock solutions

Buffer Name	***Composition***
FACS-MACS	0.5% FBS and 2mM EDTA in PBS
2% Agar	2g of Agar, 100 ml of Tap water
Fixative solution	Formaldehyde- 2% and Glutaraldehyde- 0.2% in PBS
Paraformaldehyde (PFA) 4%	4g of PFA and 100 ml of PBS
10x PBS	25.6 g -Na_2HPO_4 2g- KH_2PO_4 80g- NaCl 2g- KCl 900ml- dH_2O
1.8% of H_2O_2 solution	30% H_2O_2 in 6 ml, dH_2O in 14 ml, Methanol of 80 ml
Laemmli sample buffer 1x	10 µl of β-mercaptoethanol and 90µl of 4X Laemmli buffer

Paraformaldehyde (PFA) 6%	6g of PFA and 100ml of PBS
PBS-T / Washing Buffer	1x PBS 1% Tween
Running buffer	15.1g of Tris, 50 ml of 10% SDS, 94g of Glycine, 900 ml of dH_2O
RT buffer mix for qPCR	dNTPs, Random octamers, and oligo dT-16
RIPA lysis buffer	NaCl 150 mM Tris pH7,2 10 mM SDS 0.1% Triton x100 1% Deoxycholate 1% EDTA 5mM
Transfer/blotting buffer	150mM Glycine 20mM Tris 20% Methanol
Ponceau S solution	0.1% of Ponceau S, 5% of acetic acid
TBS buffer 1x	20X TBS- 50 ml, dH_2O-950 ml
Vulcan fast red	2.5 ml of VFR buffer and 1 drop of VFR
Saponin buffer	PBS 1 % BSA 0.5% Saponin
SDS PAGE buffer	25 mM Tris 250mM glycine 0.1% SDS
Ketamine- xylazine solution	Ketamine-14%, Xylazine-3% and NaCl-83%
TE wash buffer	10 mM Tris-HCl, 1 mM EDTA, pH 8.0
Elution buffer	1% SDS and 0.1 M $NaHCO_3$

2.1.4 Consumables

Table 2.3: Consumables

Product Name	***Supplier***
1.5 ml, 2 ml ependorf tubes	Eppendorf
15 ml, 50 ml falcons	Falcon
Cell culture plates	Greiner Bio-One, Cellstar
96-well imaging plates, Falcon®	Corning, Thermo Fisher Scientific
White 96-well microplates	Berthold Technologies
Cell culture dishes	Corning, Thermo Fisher Scientific
Cell scraper	Corning, Thermo Fisher Scientific
Combitips advanced®	Eppendorf
Cryovials 1.5 ml	Greiner Bio- One
70 µm Nylon filters	BD Bioscience
3 mm of Filter paper Whatman	Bio-Rad
Gloves	Kimtech Sterling Nitrile Gloves
FACS tubes	BD Bioscience
Trucount tubes for FACS	BD Bioscience

Disposable pipetting reservoirs	Greiner Bio-One
Glas Pasteur pipettes	VWR International
Sterile Measuring pipettes	VWR International
Microscope slides	Thermo Fisher Scientific
PVDF membrane	Merck Millipore
LS columns	Miltenyi Biotec
C tubes	Miltenyi Biotec
96-well PCR plates	Bio-Rad
Sealing foils for PCR plates	Lager
Tips	Eppendorf
30µM and 70µM filters	Miltenyi Biotec
Transwells 24 well inserts with 5µm pore size	Corning, Thermo Fisher Scientific
Syringes and needles	B.Braun
Cell culture flasks 25	Greiner Bio-One
100µm, 20µm and 10 µm nylon meshes	Sefar

2.1.5 Antibodies

Table 2.4: Primary antibodies used for western blotting

Antibody name	*Host*	*Dilution*	*Company*
PRMT7 (NBP2-26135)	Goat	1:1000	Novus Biologicals, Bio-Techne
PRMT7 (sc-98882)	Rabbit	1:400	Santa Cruz Biotechnology
Mono-Methyl Arginine[mme-R](8015)	Rabbit	1:1000	Cell signalling Technology
ICAM-1 (1A29)	Mouse	1:250	Thermo Fisher Scientific
VCAM-1 (ab134047)	Rabbit	1:10000	Abcam
T1-alpha (AF3244)	Goat	1:1000	R&D Systems
H3R2me1 (NB21-1001)	Rabbit	1:500	Novus Biologicals, Bio-Techne
B actin (A3854)	HRP-conjugated	1:40000	Sigma-Aldrich
H3 (ab1791)	Rabbit	1:1000	Abcam
P-p44/42 MAPK (T202-Y204)(4370S)	Rabbit	1:2000	Cell signalling Technology
P-p38 MAPK (4631S)	Rabbit	1:1000	Cell signalling Technology
H4R3me1 (NB21-2011)	Rabbit	1:1000	Novus Biologicals, Bio-Techne
H4R3me2 (ab5823)	Rabbit	1:1000	Abcam
H3R2me2 (04-808)	Rabbit	1:500	Merck Milipore
RAP1A/B (ab187659)	Rabbit	1:10000	Abcam
P44/42 MAPK (4695S)(Erk1/2)	rabbit	1:1000	Cell signalling Technology
P38 MAPK (8690S)	Rabbit	1:1000	Cell signalling Technology
H3R2me1 (ab15584)	Rabbit	1:500	Abcam

Table 2.5: Secondary antibodies used for western blotting

Antibody Name	*Host*	*Dilution*	*Company*
Anti-rabbit IgG (7074S)	HRP-conjugated	1:3000	Cell signalling Technology
Anti-goat IgG (sc2768)	HRP-conjugated	1:4000	Santa Cruz
Anti-mouse IgG (NA931VS)	HRP-conjugated	1:3000	Amersham,GE healthcare Life Sciences

Table 2.6: Antibodies for flow cytometry analysis

Antibody Name	*Host*	*Dilution*	*Company*
Anti CD16/CD32	mouse	1:100	eBioscience,ThermoFisher
Anti-CD45-Viogreen	mouse	1:10	Miltenyi Biotec
Anti-Ly6G-Vioblue	mouse	1:10	Miltenyi Biotec
Anti-MHCII-FITC	mouse	1:10	Miltenyi Biotec
Anti-F480-PerCP-Vio700	mouse	1:10	Miltenyi Biotec
Anti-CD11b-PE	mouse	1:10	Miltenyi Biotec
Anti-CD11c-APC	mouse	1:10	Miltenyi Biotec
Anti-CD11a-Amcyan	mouse	1:10	Miltenyi Biotec
Anti-CD49d-PE-CYP7	mouse	1:10	Miltenyi Biotec
Anti-CD80-PE	mouse	1:10	Miltenyi Biotec
Anti-CD86-APC-Vio 770	mouse	1:10	Miltenyi Biotec
Anti-IgG-FITC	mouse	1:100	eBioscience,ThermoFisher
Anti-CD19-APC	mouse	1:10	Miltenyi Biotec
Anti-MHCII-Percp-CY5	mouse	1:10	Miltenyi Biotec
Anti-CD80-PE	mouse	1:10	Miltenyi Biotec
Anti-CD69-Amcyan	mouse	1:10	Miltenyi Biotec
Anti-CD3e-APC-CY7	mouse	1:10	Miltenyi Biotec
Anti-CD22-PE-CY7	mouse	1:10	Miltenyi Biotec
Anti-GL7-Pacific Blue	mouse	1:100	eBioscience,ThermoFisher
Anti-CCR2-PE	mouse	1:100	eBioscience,ThermoFisher
Anti-Siglec-F	mouse	1:10	Miltenyi Biotec
Anti-CD31	mouse	1:10	Miltenyi Biotec

Table 2.7: Primary antibodies used for immunofluorescence and immunohistochemistry staining

Antibody Name	*Host*	*Dilution*	*Company*
Anti-galectin (sc-20157)	Rabbit	1:100	Santa Cruz
Anti-Prmt7 (sc-98882)	Rabbit	1:50	Santa Cruz
Anti-CC10 (sc-365992)	Mouse	1:200	Santa Cruz
Anti-Pro SPC (AB3786)	Rabbit	1:50	Merck Milipore

Table 2.8: Secondary antibodies for immunofluorescence staining

Antibody Name	*Host*	*Dilution*	*Company*
DAPI	Rabbit	1:2000	Sigma-Aldrich
Anti- rabbit with AlexaFluor 488 conjugate	Goat	1:250	Life Technologies

Anti- mouse with AlexaFluor 555 conjugate	Rabbit	1:250	Life Technologies
Anti-goat IgG Alexa Fluor 568 conjugate	Rabbit	1:250	Life Technologies
Alkaline phosphatase-conjugated	-	-	Biocare Medical
Anti-mouse with Alexa Fluor 488	Goat	1:250	Life Technologies
Anti-rabbit with Alexa Fluor 555	Goat	1:250	Life Technologies

Table 2.9: Antibodies for immunoprecipitation and CHIP

Antibody Name	*Host*	*Dilution*	*Company*
Anti-mono-methylated arginine antibody-(8015)	Rabbit	4µg	Cell signalling Technology
Anti-PRMT7-(NBP2-19939)	Rabbit	5µg	Novus Biologicals, Bio-Techne

2.1.6 Commercially available Kits

Table 2.10: List of commercial kits

Kits	*Company*
Mouse Monocyte isolation kit (BM)	Miltenyi Biotec
OneStep RT-PCR Kit	Qiagen
Human monocyte isolation kit	Miltenyi Biotec
DNeasy Blood and Tissue kit	Qiagen
PeqGOLD Total RNA kit	PEQLAB Biotechnology
Vulcan fast red chromogen kit	ZYTOMED Systems
PowerUp SYBR Green Master Mix-50 mL	Thermo Fisher Scientific
Lung dissociation kit	Miltenyi Biotec
ELISA kit	EBioscience,ThermoFisher Scientific
Pierce BCA Protein Assay kit	Thermo Fisher Scientific
PCR purification kit	Qiagen

2.1.7 Enzymes

Table 2.11: Enzymes

Enzyme	*Company*
Proteinase K	Roche
DNAse 1	Peqlab
Dispase	BD Bioscience
MuLV Reverse transcriptase	Applied Biosystems, Thermofisher Tech
Porcine pancreatic elastase (PPE)	Sigma-Aldrich

2.1.8 Cytokines and inhibitors

Table 2.12: Cytokines and inhibitors used in cell culture

Name	*Company*
CCL2	PeproTech and R&D System
PMA	Calbiochem
LPS- (*E. coli* O55:B5)	Sigma-Aldrich
CSE	In-house production
Murine recombinant M-CSF	ImmunoTools
TNF-α	PeproTech
BAY11-7082 (B5556)	Sigma-Aldrich
JSH23-(J4455)	Sigma-Aldrich
SGC3027 (HY-112445-1)	Hycultec GmbH
GGTI 298 trifluoroacetate salt hydrate (G5169)	Sigma-Aldrich
Murine recombinant GM-CSF	ImmunoTools
IL-4	ImmunoTools
IFNγ	ImmunoTools

2.1.9 Cell lines and cell culture

Table 2.13: List of cell lines

Cell Lines	*Company*
SVEC4-10 endothelial cells	ATCC CRL-2181
MHS macrophage cells	CRL-2019, ATCC
MHS Prmt7^{null} cells	In-house production
MLE12 ATII cells	CRL-2110, ATCC

Table 2.14: Cell culture components and mediums

Component	*Company*
Dulbecco's Modified Eagle Medium (DMEM)	Gibco, Life Technologies
RPMI medium	Biochrom
Non-essential amino acids (NEAA) 100x	Thermo Fisher Scientific
HEPES pH 7.4 (1M)	Thermo Fisher Scientific
L-Glutamine 200mM	Thermo Fisher Scientific
Penicillin-streptomycin (10,000 U/ml)	Thermo Fisher Scientific
Sodium pyruvate (100mM)	Lonza
β-mercaptoethanol	Sigma-Aldrich
Fetal bovine serum (FBS)	Gibco, Life Technologies
DMEM/ F12 (1:1)	Gibco, Life Technologies

2.1.10 Transfection reagents

Table 2.15: siRNA and transfection reagents

Reagent	*Company*
HiPerFect Transfection Reagent	Qiagen
Prmt7-specific siRNA	Qiagen
Xfect™ Transfection Reagent	Clontech
pX335.guide RNA A	Clontech
pX335.guide RNA B	Clontech
pARv-RFP	Clontech
AllStars negative control siRNA	Qiagen

2.1.11 Oligodeoxynucleotides/primers for mouse and human

Primer-BLAST software (http://www.ncbi.nlm.nih.gov/tools/primer-blast/) was used to design primers.

Table 2.16: Sequences of primers for mouse genes

Target gene	*Sequence 5`-3`*
Prmt7	TAC TGC AGG GGC TGA CTT CT TCA CCT CAG TGG AGT GCT TG
Itgam	GTT TGT TGA AGG CAT TTC CC ATT CGG TGA TCC CTT GGA TT
Itgal	CCA GAC TTT TGC TAC TGG GAC GCT TGT TCG GCA GTG ATA GAG
Ccr2	ATC CAC GGC ATA CTA TCA ACA TC TCG TAG TCA TAC GGT GTG GTG
Mmp23	AGG GAA ATG TAG ATG CGC CAA CGG GTT ACC GAC ATG GTC AAC
Prkcb	AAC GTG ACG AAC TCA TGG C CAC TGC ACC GAC TTC ATC TG
Plcg2	CTC CAT GAT GTC CAG GAA GC GAG CGG AGG ACA GTA CAG ATG
Timp3	CAA CTC CGA CAT CGT GAT CC CAC GTG GGG CAT CTT ACT GA
Acta2	GTT CAG TGG TGC CTC TGT CA ACT GGG ACG ACA TGG AAA AG
Prkca	AAC GAA CTC ATG GCA CCT CT CAC TGC ACC GAC TTC ATC TG
Prkcd	TCA TGG AGA AGC TAT TCG AGA G GTT GCT GTA GTC TGA AGG GGA T
Vcam-1	CAA TGG GGT TGG AAT G CAC CTG GGT TTT TCC A
Icam-1	ACC CAA CTG GTG TTT G

	CAC ACT CTC CAC GAA T
Tnfα	TGC CTC AGC CTC TTC TCA TT CCC ATT TGG GAA CTT CTC CT
IL6	GTT CTC TGG GAA ATC GTG GA TGT ACT CCA GGT AGC TAT GG
IL1b	AGT TGA CGG ACC CCA AAA GAT GGA CAG CCC AGG TCA AAG G
IL10	CCA AGC CTT ATC GGA AAT CA TCA CTC TTC ACC TGC TCC
Hprt1	CCT AAG ATG AGC GCA AGT TGA A CCA CAG GAC TAG AAC ACC TGC TAA
Prmt1	CGA ACT GCA TCA TGG AGA AT AGC GTT GGG CTT CTC CAC TAC
Carm1	GTG GGC AGA CAG TCC TTC AT GTC CGC TCA CTG AAC ACA GA
Prmt5	TGA CCA ACC ACA TCC ACA CT GTG TGT AGT CGG GGC ATT CT
Inos	CGG CAA ACA TGA CTT CAG GC GCA CAT CAA AGC GGC CAT AG
Fizz1	TGC CAA TCC AGC TAA CTA TCC C ACG AGT AAG CAC AGG CAG TT
Arg1	GGA ACC CAG AGA GAG CAT GA TTT TTC CAG CAG ACC AGC TT
Il12p35	ACT AGA GAG ACT TCT TCC ACA ACA AGA G GCA CAG GGT CAT CAT CAA AGA C
Cd86	CTG GAC TCT ACG ACT TCA CAA TG AGT TGG CGA TCACTG ACA GTT
Rap1a	ATG CGT GAG TAC AAG CTA GTA GT AAT CTA CCT CGA CTT GCT TTC TG
Rap1b	GCT CGT CGT GCT TGG ATC AG ATT GCT CCG TTC CTG CAG TGT
Gapdh-CHIP	CTC TGC TCC TCC CTG TTC C TCC CTA GAC CCG TAC AGT GC
Rap1a (1)-CHIP	AAA GTT CCG GTG CAG AGA CA ACC GTG CTA GGA CTT GTT GC
Rap1a (2)-CHIP	GGT GGT TAA GGC CAA CAT TGA ACT AAC AGC TGT CCC ATG GTT G
Acta2	TCC CTG GAG AAG AGC TAC GAA CT GAT GCC CGC TGA CTC CAT
Ccl2	CTT CTG GGC CTG CTG TTC A CCA GCC TAC TCA TTG GGA TCA
Cxcl1	GCT GGG ATT CAC CTC AAG AA TCT CCG TTA CTT GGG GAC AC
Cxcl12	TGC ATC AGT GAC GGT AAA CCA TTC TTC AGC CGT GCA ACA ATC
Itga4	TCC AAA CCA GAC CTG CGA AC TGT GCC CAC AAG TCA CGA TAG

Mmp13	CTT TGG CTT AGA GGT GAC TGG AGG CAC TCC ACA TCT TGG TTT
Timp3	CAA CTC CGA CAT CGT GAT CC CAC GTG GGG CAT CTT ACT GA

Table 2.17: Sequences of primers for human genes

Target gene	***Sequence 5`-3`***
PRMT1	GCT GAG GAC ATG ACA TCC AA GAA GAG GTG CCG GTT ATG AA
PRMT7	GCT GCT GTG AAG ATT GTG GA CCG ATC AGC TCT GTG TCA AA
CARM1	ACA GCG TCC TCA ATC CAG TTC GCT GGG ACA GGT AGG CAT AA
PRMT5	GGC CAT CAC TCT TCC ATG TT CCA CAT CCA CGT TTT CTC CT
CCL2	TTC CCC TAG CTT TCC CCA GA TCC CAG GGG TAG AAC TGT GG
TNFα	GCC TCT TCT CCT TCC TGA TCG AGC TTG AGG GTT TGC TAC AAC A
IL-8	GCA GAG CAC ACA AGC TTC TAG GA CCA GCT TGG AAG TCA TGT TTA CAC
IL-6	CCT GAA CCT TCC AAA GAT GGC TTC ACC AGG CAA GTC TCC TCA
CXCL1	CTT CCT CCT CCC TTC TGG TC CCA AAC CGA AGT CAT AGC CA
HPRT1	AGG AAA GCA AAG TCT GCA TTG TT GGT GGA GAT GAT CTC TCA ACT TTA A

2.1.12 Laboratory Instruments and softwares

Table 2.18: Laboratory equipments

Laboratory equipments/Devices	***Supplier***
Agarose gel chambers	Peqlab
Balances-Precisa XT 6200C-FR	Pesa Waagen AG
Racks for 1.5 ml tubes	Stratagene
Cell freezing container	CoolCell (Biocision)
Chamber for SDS PAGE	Bio-Rad
CO_2 incubator- MCO-18AC	SANYO Component Europe
Microscope	Carl Zeiss Microscopy
Microwave	SHARP
pH meter	pH-Meter inoLab pH 720 (W TW)
Pipetboy	INTEGRA Biosciences
Spectrophotometer	NanoDropTM 1000 Spectrophotometer (ThermoFisher Scientific)
Vacuum pump	BVC basic, Vacuumbrand

Vortex	Ingenieurbüro CAT M. Zipperer
GentleMACS Dissociator	Miltenyi Biotec
Sub Aqua Pro Waterbath	Grant
Centrifuge 5430	Eppendorf AG
Centrifuge Galaxy 16 DH	VWR International
Cool centrifuge, Mikro 220R	Andreas Hettich
Cool centrifuge, Rotina 35R	Andreas Hettich
FACS Canto II flow cytometer	BD Biosciences
Heat block HBT 130	DITABIS, Digital Biomedical Imaging Systems AG
Heat block thermomixer compact	Eppendorf AG
Haemocytometer Neubauer	Karl Knecht Assistent
Magnetic Steerer IKAMAG REO	IKA Werke
Microtome Hyrax m55	Carl Zeiss Microscopy
Multiplate Reader Infinite 200 Pro	Tecan Trading AG
PCR Master cycler (Nexus Eco, Nexus Gradient)	Eppendorf AG
Pipettes	Eppendorf AG
qRT-PCR Thermocycler StepOne™	Applied Biosystems
Scanner Mirax Desk	Carl Zeiss Microscopy
Voltage device	Bio-Rad Laboratories
Vortexer, Vortex Genie 2	Scientific Industries
Tissue processor TP 1020	Leica
Axio Observer.Z1 microscope	Carl Zeiss Microscopy
Electronic stirrer	IKA
Embedding apparatus Histostar	Thermo Scientific
FlexiVent system	SCIREQ Inc
Heating-blocks	Haep Labor Consult
Rotary microtome Hyrax M55	Carl Zeiss Microscopy
Shandon Cytospin 2 centrifuge	Thermo Scientific
Thermal Cycler PTC 200	Bio-Rad
Thermomixer	Eppendorf AG
-80°C freezer U725	Innova, Vacuum insulation Panel Tech
-20°C freezer MediLine LGex 410	Liebherr, GNP
Decloaking chamber	Biocare Medical
Autoclave	WTC, binder
Corning LSE™ Mini Microcentrifuge, 120V	Corning
Gel imagine system ChemiDoc XRS+	Bio-Rad
Liquid nitrogen cell tank BioSafe 420SC	Cryotherm
Roll mixer	VWR International
Micro GC Gas Analyzer	Infinicon
Forced pulmonary maneuver system	Buxco Research Company, Data Sciences International
Axioimager with an M2 microscope	Zeiss

Table 2.19: Softwares

Product	*Company*
BD FACSDIVA	BD Biosciences
FlowJo Software, Version 9.6.4	TreeStart Inc
GraphPad Prism-6	GraphPad Software
Light Cycler 480 software release 1.5.1	Roche Diagnostics
Image Lab Software, Version 5.2.1	Bio-Rad
Magelan Software	Tecan
ZEN 2010-Digital Imaging for Lightmicroscopy Software	Zeiss
Axiovision 4.8 software	Zeiss
Computer Assisted Stereological Toolbox(newCAST) software	Visiopharm
FlexiVent system	SCIREQ Inc
ImageLab 5.0 software	Bio-Rad
StepOnePlus 96 well Real-Time PCR System	Applied Biosystems
Max Quant software package	University of Minnesota,USA
InCroMAP software Version 1.7.0	University of Tübingen, Germany

2.2 Methods

2.2.1 *In vivo* animal experiments

2.2.1.1 Cigarette smoke (CS) exposure

8 to 10 weeks old C57BL/6N and *Prmt7*$^{+/-}$ mice were whole body subjected to active 100% mainstream of 500 mg/m^3 cigarette smoke (CS) to be close to human smoking. 3R4F research cigarettes without filters were utilized for CS from Tobacco Research Institute in Lexington. A membrane pump was used to distribute the cigarette smoke into smoking chamber where mice were put. The time of exposure to CS was for 50 mins, two times in a day for either 3 following days or 4 months as an acute and chronic cigarette smoke mouse models respectively. Total particulate matter (TPM) concentration levels was measured using a quartz fibre filter from the air in the chamber. Gravimetric analysis of the quartz fiber filters demonstrates the TPM mass concentration as a result of total air volume measurements before and after sampling air from the chamber. Another important criterion is the concentrations of CO in the chamber and it was kept steady in each exposure with the help

of GCO 100 CO Meter from Greisinger Electronic. Control mice were exposed to filtered air (FA) instead of CS. After 3 days and 4 months, mice were sacrificed and analysed next day for several experimental purposes.

2.2.1.2 Elastase application

As an another COPD animal model, emphysema was generated in WT and *Prmt7*$^{+/-}$ mice by one-time application of porcine pancreatic elastase (PPE) via oropharyngeal manner. 80µl of PPE was given calculated as 40U per kg to each mouse as previously described (Yildirim et al., 2010). Control mice obtained 80 µl of sterile PBS instead of PPE in the same manner. Mice were analyzed 24h or 28 days following instillation as an acute model and chronic model respectively.

2.2.1.3 Bleomycin treatment

As a fibrosis animal model, lung fibrosis was generated in WT and *Lyz2-Cre Prmt7*$^{flox/flox}$ mice by instillation of a single dose of bleomycin. The volume given to mice was same as elastase. 80µl of bleomycin was given calculated as 2U per kg to each mouse. Control mice obtained 80 µl of sterile PBS instead of bleomycin. Treated mice were sacrificed and analyzed 14 days after instillation.

2.2.1.4 Skin-injury model

0.5 mm silicone plaque was utilized for preparation of splinting rings having 12 mm of outer diameter and 6 mm of inner diameter. Firstly, the splints were washed using detergent followed by rinsing with distilled water and 70% of ethanol was used to sterilize during 30 minutes followed by drying under the hood. The splints were stored in a sterile box for further usage.

To anesthetize 100 µl of MMF was given to each mouse and dorsal hair is cut by the machine. Then, biopsy punch with a 5 mm diameter is used to generate two full-thickness excisional wounds. One face of a splint with glue was kept around the wound region. The splint is fixed with 6 sutures of 6.0 nylon and Tegaderm transparent dressing (3M) is applied into the wound region. At the end of the surgery, mice were woken up with injecting MMF antagonist and

Metamizol was given to the mice as postoperative analgesia in a ratio of 500mg Metamizol in 250ml drinking water. On day 3 post-wounding, mice are sacrificed by cervical dislocation. The full-thickness wound tissues are harvested by cutting 2 mm away from the wound edge. The adjacent normal full-thickness skin is harvested with biopsy punch, which serves as control. The harvested wound and skin tissues are fixed in 2% paraformaldehyde (PFA) for further analysis.

2.2.1.5 Orthotopic lung transplantation

Left lungs from wild-type mice were orthotopically transplanted into wild-type or *Prmt7*$^{+/-}$ recipients as previously described (Smirnova et al., 2019). These are syngeneic transplants, that macroscopically and histologically appear normal (Smirnova et al., 2019), however they were left for 3 weeks to recover from surgery before being exposed to a single dose of PPE calculated as 40U per kg to each mouse oropharyngeally, described as in section 2.2.1.2, and analyzed 28 days later.

2.2.2 Lung function measurements

To measure lung function in mice, firstly mice were put into sleep using ketamine-xylazine mixture as an anesthetic reagent. The working solution was combined with 3% xylazine, 14% Ketamine and 83% NaCl. This solution was applied into mice intraperitoneally at a dosage of 100µl per 10g of mice. The volume is proportional to body weight. When the mice are calm, 18-gauge cannula was used for tracheostomy and mice were connected to the flexiVent system (Scireq, Montréal, Canada). Lung parameters were measured with the help of a flexiVent software and results were analysed for pulmonary function. During lung function measurements, mice were mechanically insufflated at a frequency of 150 breaths per minute with a tidal volume of 10ml per kg of mice to mimic spontaneous breathing. The lung parameters that measured during flexiVent system were the diffusion capacity for carbon monoxide (DFCO), Total Lung Capacity (TLC), Forced Expiratory Volume (FEV), Forced vital capacity (FVC), the ratio of FEV1/FVC which is called tiffeneau-index, Dynamic compliance, Functional Residual Capacity (FRC) as well as tissue elastance. These parameters were quantified during the analysis with the flexiVent system as decribed before (Bonnardel et al.,

2019). Respiratory function of mice was detailly examined with a forced pulmonary maneuver system from Buxco Research Company together with FinePointe Software (version 6, Data Sciences International) (Vanoirbeek et al., 2010). Measurements were repeated at least 3 times per animal and the mean value was taken into account.

2.2.3 Single cell RNA-sequencing

As a first step of this experiment, murine lung lobes were taken, minced, and digested with enzymatic mixture. The enyzmes used in this mixture were dispase (50 caseinolytic U/ml), collagenase (2 mg/ml), elastase (1 mg/ml), and DNase (30 µg/ml). The lungs were digested in this enzymatic mixture for 30 minutes at 37°C. Upcoming mixture was filtered using a strainer with 70 µm to obtain single cells. Next step was to centrifugate for 5 minutes at 300 x g and the pellet was dissolved in 1 ml of PBS with 10% FBS. The cells were counted and separated in PBS containing 0.04% BSA in a way that there was around 100 cells per each µl.

Next step was to perform Dropseq experiments as decribed in (Macosko et al., 2015). First of all, single cells as previously generated in aliquots were enveloped in droplets with beads which were barcoded at rates of 4000µl per hour. Droplets were broken using perfluorooctanol after collecting droplet emulsions around 20 minutes. To reverse transcribe mRNA transcripts, beads were collected and exonuclease I was added to get rid of unused primers. The procedure was followed by washing the beads and counting them. 2000 beads per each reaction were separated for pre-amplification step with 12 PCR cycles. As a result, pre-amplified cDNA with a concentration of 1ng was tagmented with Nextera XT from Illumina. For this step, P5 primer was used as well. As a last step, sequencing was performed on single cell libraries using the Illumina HiSeq4000 with 0.2nM sample.

Analysis of single cell seq data was done using the Drop-seq core computational pipeline following sequencing the generation of count matrices. The evaluation of next generation sequencing reads was performed according to the protocol described as (Macosko et al., 2015) in a collaboration with Herbert Schiller´s lab group.

2.2.4 Bronchoalveolar lavage (BAL) harvesting and quantification

In our study, BAL fluid was collected to define the numbers of neutrophils, macrophages and lymphocytes. For this purpose, after intubation of mice via tracheostomy, the lungs were flushed with sterile PBS containing protease inhibitor cocktail from Roche, 3 times with 500µl and fluid was collected into eppendorf tubes. BAL fluid was centrifuged at 400 x g to obtain the cells and the pellet was dissolved in 500µl of medium with 10% FBS. In our case the medium was RPMI-1640. Afterwards, the cell numbers were defined using a haemocytometer in a same principle as decribed in (Absher, 1973). The next step was to apply cytospin using 30.000 of cells. The volume containing 30.000 cells was replaced into cytofunnel and it was centrifuged for 6 minutes at a rate of 400 rpm. To be able to count different cell types, cell counts were done based on morphology following May-Grünwald-Giemsa staining. Briefly, cells already undergone cytospin were exposed to May Gruenwald's eosin-methylene blue solution, where blue defines nucleus and pink defines cytoplasm, for 10 mins period. Staining was followed by washing step to get rid of excess dye for 2 mins with tap water. To differentiate the cellular structures better in each cell type, the slides were stained with Giemsa solution for 15 minutes followed by washing step for 2 mins. Moreover, BAL fluid without cells was kept to measure cytokine secretion, in our case it was CCL2 and CXCL1 concentration measurement using a ELISA kit (eBioscience, ThermoFisher Scientific).

2.2.5 Mouse lung processing

During dissection of mice lung lobes were collected depending on the purpose of the experiment. In this study, two lung lobes in the right side were collected and snap frozen with liquid nitrogen in order to isolate protein and RNA from these lungs. After homogenization, total RNA and total protein were isolated using peqGOLD Total RNA Kit and protein isolation protocol described in section 2.2.22, respectively. For analysis of macrophage infiltration by flow cytometry, single-cell suspensions of the other right lung lobes were harvested and digested enzymatically in MACS buffer with the help of lung dissociation kit from Miltenyl using a gentleMACS dissociator machine.

After collecting all right lung lobes for RNA, protein as well as FACS analysis, the left lung was reserved for histological analysis. Therefore, the first step was fixation of the lungs via instillation of 6% of paraformaldehyde intratracheally for around 10 mins at a constant pressure not to harm the tissue. This step was followed by the incubation of left lungs in a falcon filled with paraformaldehyde, PFA, at 4°C for 24 hours. Next day, the PFA solution was replaced by PBS and the lungs were kept in the fridge until they were embedded.

After fixation, the left lungs were embedded into paraffin and the sections were cut and stained for different purposes. The first step of paraffin embedding protocol was replacement of the lung into tissue processor for 24h to dehydrate the tissue with sequencial ethanol exposure. The dehydration step was followed by removal of ethonal using Roticlear which is defined as a less harmful xylene product to clear the tissue. Next day, the lung tissues were put into liquid paraffin wax or agar solution and they were incubated in the fridge until the wax got frozen. In this way, the tissue structures including cavities and cells were preserved. This step was followed by sectioning the tissue in 2 mm thickness. These cut agar pieces with tissue were replaced into special embedding casettes carefully with 4% formalin and the casettes were kept until they were solidified. Sectioning of the lung tissue was performed for further staining purposes including hematoxylin and eosin (H&E) staining, immunofluorescence and immunohistochemistry stainings as well as Masson's Trichrome staining.

2.2.5.1 Lung tissue sectioning

Tissue sectioning is a prior step of staining. After embedding the tissue into casettes, the excessive agar was removed to smooth the surface of cassette for better sectioning. The cassettes were kept in the freezer for one hour before sectioning and microtome was used to cut the lung tissue into sections. Paraffin casettes including lung blocks were fix into a cold region of microtome for keeping the blocks cool during cutting process. To collect the sections into the water after cutting, firstly distilled water was added into the tank of microtome. The thickness of sections might differ according to the purpose of the experiment. For staining purposes, blocks were cut into 3µm thin sections and the cut sections were moved via glass slide from tank to water bath in 10 degrees. After a few seconds, sections were removed from

the water bath and fixed into the positively charged coating glass slides followed by drying step on a heating plate at 45°C. This step enables a better adhesion of tissue into the positively charged slide. Moreover, these sections might be kept at 37°C overnight to ensure fixation and to get rid of the excess water. The tissue slides were used for further processing like immunofluorescence or immunohistochemistry stainings as mentioned above.

2.2.5.2 Histological stainings

After lung tissue sectioning, the cut slides were processed with immunohistochemistry, immunofluorescence, H&E, and masson trichrome stainings.

a) Hematoxylin and eosin (H&E) staining

The purpose of Hematoxylin and Eosin is to view cellular and tissue structures in detail. This staining demonstrates cytoplasmic, nuclear and extracellular matrix features. Hematoxylin marks nuclei of cells as blue-purple colour via nucleic acid staining. As a counterstain, eosin was followed after nuclear staining to colour eosinophilic structures as in different intensity of red.

In the beginning of staining, tissue slides were put into xylene solution (2 times for 5 mins) used as clearing agent for deparaffinization, which is removal of paraffin in the first step, and then the slides were moved into different percentage of alcohol solutions (2 times of 100% for 1 min, 1 time of 90%, 80% and lastly 70% for 1 min) to replace xylene in the last step of the process. After these ethanol washing steps, the lung slides were incubated with Mayer´s Hemalaum staining for 5 mins followed by washing the dye with running tap water to obtain blue colour. The reason we used tap water was that it has a higher pH-value than distilled water to achieve the desired shade. 0.1% HCl-Alcohol was prepared with 70% ethanol and the slides were incubated very shorthly in it to make nuclei staining more clear. This step was followed by washing with tap water for 8 mins and then the slides were quickly dipped into distilled water. As a counterstain, 0.5% eosin solution was prepared and slides were incubated with this solution for 8 mins to stain the plasma. This step was followed by washing the slides with ethanol solutions with different percentages. Firstly, the slides were rinsed with 70%, 80%, 90% for few seconds and then they were incubated in 100% ethanol for 2

mins. Last step was repeated again. After ethanol steps, the slides were again put into xylene solution for 5 mins and this step was done two times. As a last step, 24 x 50 mm cover glasses were utilized to immobilize the tissue sections using entellan to conserve the samples. Other alternative options for entellan were DePeX, Eukitt or Euparal. After covering the samples, it is better to leave them under the hood overnight to harden and to store them protected from light.

b) Immunohistochemistry staining

The first steps of IHC staining were quite similar to H&E staining. As mentioned above, 3µm lung sections were deparaffinized in xylene solution followed by rehydration using ethanol gradient solutions. After this step, endogenous peroxidase was blocked with H_2O_2 solution (1.8%). For staining, epitope retrieval step is very important and the buffer and temperature suitable for epitope retrieval are highly dependent on antibody type. For our study, the most suitable way of retrieval was using HIER citrate buffer with pH 6.0. The slides were inserted into this buffer and placed into a rice cooking chamber for 30 mins at 125°C and 10 min at 90°C. When the program was over, the slides were removed from the cooker and incubated at room temperature for 30 mins to cool down. This step was followed by washing the slides in Tris-Wash Buffer B from Zytomed Systems for 2 mins and this step was repeated three times. To inhibit nonspecific binding, sections were blocked using rodent blocking buffer from Biocare Medical for 30 mins or more. The slides were incubated with primary antibody against Galectin 3 overnight at 4°C. The next day was followed by washing steps. Secondary antibody which was merged with an alkaline phosphatase was applied onto the tissue sections for 1 hour at room temperature. To amplify the signal, Vulcan fast red substrate was added after secondary antibody. Vulcan fast red solution should be prepared each time freshly by adding one drop of Vulcan fast red into its buffer in 2.5 ml since it is not very stable. This step is quite critical to understand the staining develops well therefore the time of incubation depends on the specific antibody. For Galectin 3 staining, 6 mins of Vulcan fast red incubation was enough to observe the staining well. Last step of the staining was counterstaining of slides with hematoxylin. This step is also dependent on antibody. If counterstain is too long, the staining might have a background and might prevent differentiation of real staining. Therefore, we

waited only 3 seconds with hematoxylin staining and immediately the slides were washed with water to get rid of the excessive staining. This step was followed by washing the slides in washing Tris buffer for 5 mins. Lastly, the lung sections were dehydrated in 96% ethanol for 1 min, 100% for 2 mins for two times and xylene for 5 mins for two times as well and immediately mounted with Entellan (Merck).

c) Immunofluorescence staining

For immunofluorescence staining, mouse and human lung samples were utilized. As mentioned in IHC staining, 3µm sections from paraffin embedded lung sections were deparaffinized and rehydrated through Xylol and ethonal gradient steps in a same way. The slides were incubated with 3% of H_20_2 (50ml) for 20 mins followed by washing twice in Tris Wash Buffer B for 10 mins (or three times for 5 mins is also fine). Again as a retrieval method, HIER citrate buffer with pH 6.0 was preferred in a rice cooking machine with the same protocol as decribed in IHC staining part. Sections were blocked with 100µl of 5% BSA (diluted in PBS) for 30 mins or more in a chamber followed by incubation of 50µl of primary antibodies, which were diluted in 1% or 5% BSA depending on antibody, overnight at 4°C. Next day started with washing steps and followed by incubation of 100µl of secondary antibody for 1 hour at room temperature. The most commonly used secondary antibodies were “anti-mouse Alexa Fluor 488 and anti-rabbit Alexa Fluor 568” from Life Technologies in our study. It is very important to keep the slides in the dark chamber after secondary antibody step since the secondary antibodies were conjugated to fluorophore. DAPI in a ratio of 1:2000 was utilized to counterstain the nuclei. As a last step, the slides were fixed with coverslips with the help of fluorescent mounting medium from Dako. Images were captured using Axioimager with an M2 microscope from Zeiss. Primary antibodies used in this study were listed detailly with the concentrations in material section Table 2.7.

d) Masson Trichrome Staining

Masson Trichrome staining is mainly used to determine the collagen fibers in the lung sections. 3µm tissue sections from paraffin embedded lung were heated for 10 mins at 60°C. Sections were deparaffinized in the Xylol for 5 mins (2x) followed by 100% ethanol for 2 mins (2x). They were rinsed in running tap water for 4 mins followed by shorthly dipping them into

the distilled water. For nuclear staining, the slides were stained with Hemalun for 8 mins and quickly rinsed with tap water followed by distilled water washing. The slides were put into the ethanol (70%) + HCl (0.1%) mix and immediately incubated with tap water for washing for 5 mins. The slides were kept in Ponceau Fuschin staining for 6 mins and rinsed first with tap water and then with distilled water. After washing steps, the slides were stained in Phosphomolybdic acid for 5 mins followed by Light Green staining for 5 mins as well. Light Green staining is for extracellular matrix staining since it binds collagen components. To get rid of the staining, the slides were washed with 100% ethanol for 3 times quickly. Before mounting, the slides were put in ethanol 100% for 1 min (2x), xylol for 1 min (2x) for clearance. 24mmx50mm cover slides were prepared and the tissues were mounted with eukitt glue. Lastly, bubbles were removed not to prevent a clear view of the whole tissue.

2.2.5.3 Quantitative morphometry

In this study, mean chord length (MLI) and macrophage numbers were determined in the stained lung tissues using stereology. Moreover, collagen quantification is also done with the help of masson trichrome staining. This method was described previously in (John-Schuster et al., 2014a). For this purpose, a computer-assisted stereological toolbox (CAST) software was utilized for quantifications together with Olympus BX51 light microscope.

Firstly, mean chord length was evaluated to quantify the air space enlargement to understand the disease severity. For this purpose, 30 random fields were selected by the CAST program unbiasedly throughout the several sections of the lung tissue. To calculate the mean chord length, the formula MLI = $\sum P_{air}$ x L(p) / $\sum I_{septa}$ x 0.5 was used. In this formula, P_{air} represents the points of the grid hitting air spaces, L(p) represents the line length per point, 99.3 µm as we measured, and lastly, I_{septa} represents the sum of intercepts of alveolar septa with grid lines. Overall, this calculation demonstrated us the differences in alveolar surface area between the lungs of FA or CS-subjected mice.

Moreover, to determine the number of galectin 3 expressing macrophages across the lung with CAST system, same principle was used as in mean chord length determination. This time, 20 random fields were choicen by the software along the lung sections and 40x objective was

set up to take the images and Galectin 3 positive macrophages were counted across these 20 random fields per lung. The mean values per lung were used as a representative number/20 fields.

To quantify collagen deposition in the lung sections, newCAST system was used again after masson trichrome staining. The same random selection was used for collagen quantification as well. Intercepts of lines crossing with airways and vessels were counted to calculate collagen ($\mu m^3/\mu m^2$) = $\sum P_{fibrotic\ area}$ x L(p)/ $\sum I_{intercept(A+V)}$. In this formula, $P_{fibrotic\ area}$ refers to the points of the grid hitting fibrotic area which were stained as green by masson trichrome staining, L(p) represents the line length per point, 9.79 µm as we measured and I_{septa} is defined as the sum of intercepts of airways and vessels to normalize the collagen deposition.

2.2.6 Flow cytometry analysis

Flow cytometry is a specialized method to analyse the cell populations according to a gating strategy in terms of their size and their granularity. Moreover, flow cytometry can also detect the levels of protein expression either on the surface of the cell or intracellularly expressed ones in the cells. In our study, either whole lung cell suspension cells or cell lines were stained for flow cytometric analysis. 10^6 cells were counted, transferred into FACS tubes and washed first with FACS buffer and spun down at 300 x g for 5 mins at 4°C. Supernatants were removed carefully and the pellets were dissolved using 500 µl FACS buffer (PBS+ 0.5 % FCS) and vortexed. After washing steps, cells were blocked with 50µl of FcR blocking antibody, CD16/CD32 in 1:100 dilutions (clone 93, eBioscience, Thermo Fisher Scientific) for 30 mins on ice to prevent unspecific antibody binding. Then, 500 µl of FACS buffer was added and the cells were undergone centrifugation step at rate of 1500 rpm for 5 minutes at 4°C. This step was followed by incubation of several antibody coctails for 30 mins on ice. The list of antibodies and their dilutions used in flow cytometry is shown in Table 2.6. The antibody incubation step was followed by washing steps and samples were run into BD FACSCanto II flow cytometer from BD Biosciences. FACS staining protocol is same for the cells in the culture but if the cells are growing as attached to the plates, trypsinisation step was added to deattach and count the cells for staining. The analysis on the FACS machine was similar using BD FACSDiva software.

2.2.7 Isolation of primary monocytes from mouse

Isolation of monocytes consists of three different parts including sample preparation, magnetic labelling and magnetic separation. Firstly, murine bone marrow cells from femur and tibias by flushing the shaft with RPMI-1640 medium using a syringe and a 26G needle. The flushed cells were then strained through 30µm nylon mesh to prevent cell clumps formation. Afterwards, the cells were placed into centrifuge for 10 mins at 4°C at the rate of 300 x g and washed once by adding MACS buffer. The cells were dissolved in buffer and counted with hematocytometer. Second part is magnetic labelling. After determining the cell number, the pellet was collected as a result of the centrifugation step. All calculations were done according to the cell number. According to the protocol from Miltenyl isolation kit, 175µl of buffer per $5x10^7$ total cells was added to resuspend the cell pellet and this was followed by addition of 25µl of FcR blocking reagent into the cell suspension. The cell suspension was gently mixed and 50µl of monocyte biotin antibody cocktail was added per $5x10^7$ total cells and it was kept in the fridge for 5 mins. Cells were washed by adding 10ml of buffer per $5x10^7$ total cells and centrifuged at 300 x g for 10 mins. Cell pellet was dissolved in 400µl of buffer per $5x10^7$ total cells and 100µl of anti-biotin microbeads were added per $5x10^7$ total cells. Incubation for 10 mins in the fridge was done after mixing well. Next step was proceeding to magnetic separation. LS columns were inserted carefully into magnetic field of a suitable MACS separator from Miltenyi and columns were washed with 3 ml of buffer and flow through was discarded. The mixture of cell suspension with antibody and beads was applied into LS columns and flow-through containing unlabelled cells, representing the enriched monocytes, was collected into falcon. To collect the remaining monocytes, 3 ml of buffer was run into columns for 3 times and this flow through was merged with first flow-through containing enriched monocytes. The flow-through was centrifuged to get rid of buffer and monocytes were used for several experimental purposes.

2.2.8 Stimulation of mouse primary monocytes

Isolated monocytes were counted and plated into 24 well plates with RPMI-1640 medium containing 10% FBS, 50µM β-mercaptoethanol and 100 U/ml penicillin and streptomycin. The

seeded cell number per well was around $4x10^5$ in 500µl medium. The monocytes were then pretreated with 1µM of BAY11-7082, NFKB inhibitor, and 20µM of JSH-23, RELA translocation inhibitor, separately for 1h at 37°C, 5% CO_2. After 1h pretreatment, 100ng/ml LPS was placed into plates to stimulate the cells for 6h and 24h. Control plates received DMSO instead of inhibitors in a same amount. The treatment was stopped by adding RNA lysis buffer into the plates for RNA isolation and RIPA buffer for protein isolation.

2.2.9 Isolation of primary human monocytes from blood

As a first step, human PBMCs were separated via ficoll density gradient from blood. Blood was diluted with 2 fold PBS and carefully replaced into falcons filled already with pancoll (density 1.077g/ml, Pan Bitech, P04-60500) without mixing blood and pancoll. Samples were undergone centrifugation step at 800 x g for 20 mins at 20°C with no brake and low acceleration. Upper layer of plasma and platelets were removed and discarded while PBMC band above the pancoll layer was collected and transferred into a new falcon. 3 volumes of PBS were added into PBMCs to resuspend and centrifuged again at 300 x g for 10 mins at 20°C. The cell pellet was washed with PBS and replaced with 10 ml MACS buffer followed by counting the cells. As a last step, human monocytes from PBMCs were isolated with a special kit from Miltenyi (130-096-537). The steps from the kit were magnetic labelling and magnetic separation. After determining the cell number, cell pellet was dissolved in 40µl of buffer per 10^7 total cells followed by the addition of 10µl of FcR blocking reagent per 10^7 total cells. Subsequently, 10µl of biotin-antibody cocktail was placed and cells were incubated for 5 mins in the fridge. This step is followed by addition of 30µl of buffer and 20µl of anti-biotin microbeads per 10^7 total cells. The cell suspension was gently shaked and incubated for 10 mins in the fridge. For magnetic cell separation part, LS columns (Miltenyi) were inserted into the magnetic field of a suitable MACS separator. Firstly, columns were rinsed with 3 ml of buffer and then cell suspension was applied onto the columns. Flow through from columns were collected containing unlabelled cells, which are the enriched monocytes in our case. More monocytes were picked up by washing the columns with 3x3 ml of buffer and this effluent was centrifuged and resuspended in an appropriate media for designed experiments.

2.2.10 Stimulation of human monocytes

According to the purpose of the experiment, human monocytes were counted and seeded into 24 well plates in a cell ratio of 10^6/ml in 500µl medium. The medium used was RPMI-1640 (Biochrom) with 1% FCS supplemented with 50µM β-mercaptoethanol and 100 U/ml penicillin and streptomycin (both Sigma-Aldrich). The monocytes were either stimulated with 1µg/ml LPS for 24h in 24 well plate or directly frozen for RNA isolation and further processing.

2.2.11 Primary ATII cell isolation and trans-differentiation to ATI cells

Primary ATII cells were isolated from the lungs of *Prmt7*$^{+/-}$ mice and wild-type littermate controls. Firstly, lungs were incubated with PBS solution containing dispase (BD Bioscience) for digestion over 45 mins at room temperature. Tissue was minced and filtered step wise through 100µm, 20µm and 10 µm nylon meshes (Sefar). The resultant single cell suspension was centrifuged for 10 mins at 200 x g and the pellets were dissolved in DMEM medium. To isolate the ATII cells, the cells were first incubated on petri dishes coated with anti-CD16/CD32 and anti-CD45 antibodies (BD Bioscience) for 30 mins at 37°C to separate leukocytes. Next, fibroblasts were removed by adherence after 25min to un-coated cell culture dishes. Purity of the ATII population was routinely assessed by analysis of epithelial (EpCAM, panCK and pro-SPC), mesenchymal (αSMA, CD90), endothelial (CD31) and hematopoietic cell (CD45) markers by flow cytometry. pATII cells were cultured in DMEM cell culture medium supplemented with 10% fetal bovine serum, 10mM HEPES, 2mM L-glutamine, 100 U/ml penicillin and streptomycin (Life Technologies) and 3.6mg/ml glucose (AppliChem GmbH). Cells were initially cultured for 24h to attach, medium changed and cultured at 37°C, 5% CO_2 for 5 days, changing their medium every other day. To obtain protein, cells were washed twice with PBS to remove FBS and they were lysed in T-PER lysis buffer containing Complete Protease Inhibitor Cocktail tablets. Lastly, lysates were centrifuged at 5660 x g and 4°C. Supernatants were retained for Western blot analysis.

2.2.12 Isolation of alveolar macrophages from lung

8 to 10 week old C57BL/6 WT mice subjected to CS or FA were anaesthetized with ketamine-xylazine mixture intraperitoneally, 100µl per 10g of mice. When the mice were asleep, chest

of the mice was opened and right ventricle was injected with 15 mL of PBS to get rid of circulating blood cells. This process is called perfusion. Perfusion efficiency can be understood by the colour and appearance of the lungs. When the lungs are clear and whitened, they were tracheostomized using an 18-gauge cannula. 1-mL syringe filled with PBS and complete inhibitor tablet was attached to the catheter and the buffer was slowly instilled into the lungs and after a few seconds the piston was pulled back with the lavage fluid. This step was repeated 10 times and all lavage fluid was pooled in 15 mL falcon. BAL fluid was centrifuged at 400 x g for 20 mins at at 4°C. BAL cells were suspended in complete RPMI-1640 medium supplemented with 10% FBS, 50µM β-mercaptoethanol and 100 U/ml penicillin and streptomycin. Then the cells were counted and placed into 24-well plates with 5×10^4 cells in 1ml. Cells were kept in the incubator for 1-4h to make the cells adhere and the rest of the cells which did not adhere were removed by PBS washing. Attached cells into plate were collected and they were frozen for further experiments. In our case, RNA lysis buffer was added into alveolar macrophages for RNA isolation.

2.2.13 Generation of bone marrow derived macrophages (BMDM)

Femurs and tibias were first collected from C57BL/6N and *Prmt7*$^{+/-}$ mice and they were flushed by pushing 18G needle with blank RPMI-1640 medium without any supplement to get bone marrow. Bone marrow cells were strained through 30µm or 70µm nylon filters and then they were counted in 1:20 dilution with trypan blue dye. After centrifugation at 300 x g for 10 mins at 4°C, the cells were dissolved in in comlete RPMI-1640 medium. 1-2x10^6 cells/ml were plated into 24 well plates and 20ng/mL of M-CSF was added into the medium. The cells were kept in a humidified incubator with 5% CO_2 at 37°C for 7 days to be differentiated. M-CSF were resupplied on day 2, 4 and 6 by changing half of the medium with fresh BMM+M-CSF. During this step, most of the non-adherent cells were discarded carefully. The last day of differentiation was day 7 and on that day, fresh medium supplemented with M-CSF was replaced and left overnight in the incubator. The next day adherent cells were collected, counted and seeded in 24 well plates with amount of cells of 1x10^6 cells/ml. These cells were cultured for 24h in fresh medium to obtain M0 cells. For polarization of the cells, BMDM were stimulated with 1 µg/ml LPS and 20 ng/ml of recombinant murine IFNγ to obtain M1

phenotype or with 20 ng/ml of recombinant murine IL-4 to get M2 phenotype for 24h. IL-4 and IFNγ were purchased from ImmunoTools. After stimulation was over, total RNA was isolated for microarray analysis.

2.2.14 Generation of bone marrow derived dendritic cells (BMDCs)

Femurs and tibias were first collected from C57BL/6N and *Prmt7*$^{+/-}$ mice and they were flushed by pushing 18G needle with blank RPMI-1640 medium without any supplement to get bone marrow. Bone marrow cells were strained with 40µm filters, counted and $10x10^6$ bone marrow cells were seeded in 6 well plates with 4 ml of complete RPMI medium in each well and were treated with 20 ng/ml of GM-CSF (Immunotools). On the second day after seeding, 2 ml of the medium was discarded and fresh medium containing 40ng/ml of GM-CSF was added into each well. Next day, whole medium was sucked up and fresh medium containing 20ng/ml of GM-CSF was replaced. The cells were kept in the incubator until the sixth day and then BMDCs, which were either loosely attached to the surface or non-attached at all, were collected and utilized for the starting source of material for FACS analysis and RNA isolation.

2.2.15 Gene Set Enrichment Analysis (GSEA)

In this study, to analyse the enriched genes in particular pathways, GSEA was utilized. NCBI GEO database offers plenty of files containing the enrichment of gene lists in molecular function. To process raw data from this website, GSEA software from the Broad Institute (http://www.gsea-msigdb.org/gsea/index.jsp) (Mootha et al., 2003; Subramanian et al., 2005) was utilized. To identify which genes were enriched in COPD patients, we used GEO database GSE76925 (Morrow et al., 2017) in our study. This database of GSE76925 consists of lung transcriptomics data from 111 COPD patients and 40 smoker controls. After collapsing into gene symbols, there were 24776 genes. Gene set size puts threshold to 15 and 500 as minimum and maximum values and this cut off resulted in 642 gene sets of the original 901 from the GO Molecular Function collection being used in the analysis.

2.2.16 Human lung tissue core sampling

Human lung samples used in this study were obtained from Dr. Stijn Verleden (University of Leuven, Belgium). Lung samples collected from the COPD patients during lung transplantation were provided us with ethical approval of the Leuven University and permissions were taken from all participiant patients.

For healthy controls, donor lungs were provided us under Belgian law with well controlled inspection. When the healthy and COPD lung samples arrived to our lab, lung cores were fixed with 4% of PFA to use for histological purposes whereas they were snap frozen for RNA and protein isolation purposes.

2.2.17 Cell culture experiments

2.2.17.1 Maintenance of the cell lines

In this project, 3 types of cell lines were utilized including MHS macrophage cells, SVEC4-10 endothelial cells and MLE12 ATII cells. MHS cells were sustained and cultured with RPMI-1640 medium containing 10% FCS, 50µM β-Mercaptoethanol and 100 U/ml penicillin and streptomycin. MHS cells were adherent cell type therefore they were splitted in a ratio of 1:4, two times per week in 75 cm^2 flasks at 37°C incubator. SVEC4-10 endothelial cells were also adherent and they were maintained with DMEM-F12 medium containing 10% FCS, 50µM β-Mercaptoethanol and 100 U/ml penicillin and streptomycin. They were maintained in a ratio of 1:5, two times per week. MLE12 cells were maintained with DMEM medium (Gibco) containing 10% FCS, 50µM β-Mercaptoethanol and 100 U/ml penicillin and streptomycin. These cells were adherent cell type therefore, they were also splitted and maintained in a ratio of 1:4, twice in a week in 75 cm^2 flasks at 37°C incubator.

2.2.17.2 MHS cell culture

Prmt7$^{+/+}$ and *Prmt7*^{null} MHS macrophage cells were cultured with RPMI-1640 medium containing 10% FBS, 50µM β-Mercaptoethanol and 100 U/ml penicillin and streptomycin at 37°C in 5% CO_2. RNA was isolated using the peqGOLD Total RNA Kit (Peqlab). To obtain protein, cells were washed gently with ice cold PBS and scrapped into ice-cold RIPA buffer (50

mM Tris HCl pH 7.4, 150 mM NaCl, 1% Triton X100, 0.5% sodium deoxycholate, 1mM EDTA, 0.1% SDS) with the addition of protease and phosphatase inhibitor cocktails. Then the suspension was incubated on ice for 30 mins and centrifuged for 15min at 4°C and 13000 rpm. Supernatants were retained for Western blot analysis. Additionally, *Prmt7*$^{+/+}$ and *Prmt7*^{null} clone MHS cells were placed in 6-well plates in a ratio of 4x10^5 cells per well in 2 ml medium and 24h later stimulated with 100ng/ml CCL2 (R&D Systems) or 1µg/ml LPS in complete RPMI-1640 medium with only 1% FBS instead of 10%. Reaction was halted by washing with ice-cold PBS and protein was obtained as decribed above.

2.2.17.3 Storage of cell lines

To be able to maintain the cells for further usage, cell lines were frozen in parallel with culturing them. Cell lines were kept in aliquots in liquid nitrogen tanks. To freeze the cells, 10^6 cells were taken and centrifuged to get rid of the existing medium. The cell pellet was dissolved in 1 ml of corresponding medium depending on cell type with 10% DMSO (900µl of 10% FCS medium and 100µl of DMSO). Cell suspension was put into cryotubes and these tubes were inserted into freezing container to prevent crystal formation in the samples. The box was kept at -80°C for one day and next day it was immediately transferred in liquid nitrogen tanks. It can be stored in the tanks for longer storage.

2.2.17.4 Thawing of frozen cell lines

When new cell line is needed for the experimental purposes, one aliquot of frozen cell suspension from liquid nitrogen tank was defrosted. The fastest way of thawing the cells without harming them was to warm them in waterbath with 37°C for about 2 mins until cell suspension becomes liquid. It is followed by immediate transfer of the cells into 75 cm^2 flasks including already fresh and appropriate medium for each cell line. Cells were kept in the incubator overnight in a flask to let them to attach to the surface and next day, the medium with DMSO was removed and fresh medium was placed into the flask. Since the cells are adherent, sucking the old medium and putting fresh medium does not disturb the cells. They were let to grow until the plate was confluent.

2.2.17.5 Stimulation of the cell lines

Cell lines or primary cells were plated either into 24 well plates or 6 well plates for RNA and protein isolation, respectively. Mainly for cell lines, they were firstly detached from 75cm^2 flasks and counted. The appropriate number for each cell types was seeded into plates with 10% FCS medium. Next day, this medium was replaced with 1% FCS medium for starvation conditions with cytokines depending on the purpose of the designed experiment. The stimulation was kept for 6h or 24h and the treatment was stopped by adding either RNA lysis buffer or RIPA buffer for RNA and protein isolation, respectively.

2.2.17.6 Treatment of cell lines with inhibitors

MHS cells were treated with 5% of CSE using RPMI-1640 medium containing 10% FCS, 50µM β-Mercaptoethanol and 100 U/ml penicillin and streptomycin for 24h and the plate was frozen for RNA isolation and qPCR to check the expression of gene of interests.

MHS cells were treated with commercially available 5µM PRMT7 inhibitor known as SGC3027 using the same RPMI-1640 medium for 24h and total protein was isolated for western blot analysis.

SVEC4-10 endothelial cells were maintained in DMEM medium containing 10% FBS and 100 U/ml penicillin and streptomycin in the incubator. For stimulation of SVEC4-10 cells, first 2x10^5 cells/ml were placed into 24 well plates with DMEM medium for 24h to allow them to recover. Next day, treatment with 5µM of SGC3027 drug and 100ng/ml TNF (PeproTech) was applied with DMEM medium with 1% fetal bovine serum for 24h. Reaction was stopped by adding RNA lysis buffer for further experiments.

2.2.17.7 Cigarette smoke extract (CSE) stimulation on the cell lines

To examine the effect of cigarette smoke on cell lines *in vitro*, CSE was generated by bubbling smoke into corresponding medium (No FBS). For this purpose, three cigarettes were utilized for 30 ml medium by consuming one cigarette every 5 mins. This original medium was referred as 100% CSE extract. CSE was freshly generated for each experiment and

immediately diluted to needed percentage. In our case it was 5% with culture medium depending on the purpose of the experiment.

2.2.17.8 siRNA transfection of cell lines

MLE12 (CRL-2110, ATCC) ATII cell line was maintained in DMEM/F12 medium containing 10% FBS and 100U/ml penicillin and streptomycin. For siRNA application to knock-down of *Prmt7* gene, cells were seeded in 24 well plates, $4x10^4$ cells/well in 500µl of full medium for 24h prior to transfection. 50nM FlexiTube siRNA Mm_BC006705_4 or Mm_BC006705_5 and 4,5µl HiPerFect transfection reagent from Qiagen was put into an ependerf tube with medium (No FBS) and the tube was gently vortexed. To generate the transfection complex, the tube was incubated at room temperature under the hood for 10 mins. The siRNA/HiPerfect complex was spilled onto the cells drop by drop and the plate was shaked very slowly to distribute the transfection complexes equally around the well. Cells were then cultured in full medium for 48h for an effective knockdown of Prmt7 however, the medium was replaced after 24h to remove dead cells to prevent cytotoxicity.

2.2.17.9 Wound healing assay

The wound healing assay is an important method to analyse the migration and proliferation of the adherent cells. For wound healing assays, MLE12 ATII and knockdown MLE12 ATII in *Prmt7* cells were placed at $1x10^5$ cells in each well for 24-well plates and a scratch was generated with the edge of the 200µl pipette tip after 24h of seeding. The scratching time was referred as time point 0. Afterwards, the cells were washed and cultured in full medium for 24h. Wound closure was determined at 24h using AxioVision software (Zeiss). To determine the wound healing ability of the cells, gap closure percentage was measured by AxioVision software.

2.2.17.10 Adhesion and proliferation of MHS cells

For cell adhesion assays, *Prmt7*$^{+/+}$ and *Prmt7*^{null} clone MHS cells were placed at $1x10^5$ cells per well in 24-well plates, and un-attached cells remaining in the medium at the given time point were counted using BD Trucount Tubes with flow cytometer.

For WST-1 cell proliferation assays, cells were cultured at $1x10^4$ cells per well in 96-well plates and WST-1 reagent was added at 1:10 dilution at set time periods and left for 1hr incubation before the absorbance was read at 450nm.

2.2.18 Monocyte trans-endothelial migration assay

This assay is utilized to determine the migration ability of specific cell types in response to specific chemokines or cytokines. In this study, we observed the migration capacity of mouse monocytes through CCL2 cytokine. For this assay, firstly, transwell 24 well inserts with a 5.0µm pore size were coated with 50µl of 4mg/ml collagen G (Biochrom) for 2 hours at room temperature. After coating is completed, wash the inserts with 200µl of PBS twice and suck the leftover PBS. $1x10^6$/ml SVEC4-10 (ATCC CRL-2181) endothelial cells were seeded onto the insert in 200ul DMEM High glucose plus GlutaMAX medium containing 10% FBS and 100 U/ml penicillin and streptomycin. 600ul of the same medium was placed into the lower wells and cells cultured for 48h at 37°C, 5% CO_2. Endothelial cells were then activated with 10ng/ml TNF (PeproTech) for 4h.

After 2 days, femurs and tibias of *Prmt7*$^{+/-}$ mice and wild-type littermate controls were collected and they were flushed with RPMI-1640 medium (No FBS) to obtain bone marrow. Monocytes were isolated using the Monocyte Isolation Kit (BM) from Miltenyi as described above. Medium was discarded from the inserts and wells gently, and 600ul serum free RPMI-1640 medium was added to the wells with and without 100ng/ml CCL2 (R&D Systems). Monocytes were transferred to the endothelial lined inserts at $1x10^6$/ml in 200ul serum free RPMI-1640 medium, and cultured for 4h in the incubator. The number of migrated monocytes in each well was then counted using BD Trucount Tubes with the help of flow cytometry.

In order to determine the receptor levels on monocytes from WT and *Prmt7*$^{+/-}$ mice, FACS was applied with PE-conjugated anti-CCR2. CCR2 is a specific receptor CCL2 ligand. The FACS results were analyzed with BD FACSDiva software.

2.2.19 CRISPR/Cas9 targeted knockout of cell lines

Double stranded CRISPR guide RNAs, guide A 5'-CACCGCACTCCAGGGATCCCGTGGTAGG-3' and guide B 5'-CACCGTGAACACTATGATTACCACCAGG-3' targeting exon 2 of *Prmt7* were both cloned using BbsI restriction sites into pX335-U6-Chimeric_BB-CBh-hSpCas9n (D10A) (Add gene plasmid #42335) (Cong et al., 2013). The double stranded DNA sequence 5'TGTGGCCGTGCCAATCCTACCACGGGATCCCTGGAGTGGCTGGAGGAGGATGAACACTATGATT ACCACCAGGAGATTGCCAGGTCAT-3' was cloned using EcoRV restriction sites into pARv-RFP (Add gene plasmid #60021) (Kasparek et al., 2014), to be used as a reporter plasmid to detect CRISPR/Cas9 activity in transfected cells.

The macrophage MHS cell line (CRL-2019, ATCC) was seeded at $1.2x10^5$ cells/well in 24 well plates in 500ul of complete RPMI-1640 medium containing 10% FBS, 50µM β-Mercaptoethanol and 100 U/ml penicillin and streptomycin and cultured at 37°C in 5% CO_2. Cells were then transfected with 375ng pX335.guide A, 375ng pX335.guide B and 125ng pARv-RFP with the Xfect™ Transfection Reagent (Clontech). Cells were then maintained in full medium for a further 48h with a medium change after 24h. RFP positive cells were single cell sorted into 96 well plates, along with negatively stained controls, using a BD FACS Aria III (BD Biosciences). Wells containing single colonies were expanded, genomic DNA isolated using DNeasy Blood and Tissue Kit from Qiagen and amplified using primer pair: 5'-TGCCTTCCAGACCTGAGATTG-3' and 5'-CCTAACAGAGACCTCAACTGC-3' for sequencing (Eurofins Medigenomix GmbH) and agarose gel analysis. MHS wild-type and *Prmt7*^{null} clone were maintained.

2.2.20 CHIP-qPCR

Prmt7$^{+/+}$ MHS and *Prmt7*^{null} MHS macrophage cells were used for CHIP-qPCR experiment. Firstly, these two cell lines were cultured into 5 dishes identically. The amount of the cells per one 15 cm dish was 600.000/ml in 15 ml RPMI-1640 medium containing 10% FBS, 50µM β-Mercaptoethanol and 100 U/ml penicillin and streptomycin. Cells were let to grow for 24h to reach confluency in 15 cm dishes. Next day, cells were fixed using 1% formaldehyde by mixing around 937µl of formaldehaydate 16% from Thermo Fisher Scientific into 15ml medium with

cells from previous day. The suspension plate was put on the shaker for 5 mins at room temperature followed by addition of 125mM of Glycine (Sigma) for 3 mins to neutralize the formaldehydate effect. Cells were exposed to cold PBS for washing two times. After washing steps, 3ml PBS with complete inhibitor (Roche) was prepared and placed into the dishes for scratching the cells. Scratched cell lysates were collected into 50ml falcon and 4 dishes were merged in the same falcon for CHIP analysis. The falcons including cell lysates were undergone centrifugation step at 1500 rpm for 5 mins at 4°C and the pellet was frozen in liquid nitrogen to undertake CHIP. Only one dish from MHS and one dish from *Prmt7*^{null} MHS cells were reserved for RNA isolation and protein isolation for further usage.

ChIP was undertaken by as previously described (Kebede et al., 2017; Tropberger et al., 2013). Chromatin was fragmented by sonication (target size 200-500bp) and 5 µg chromatin DNA used for each ChIP reaction. 5 µg anti-PRMT7 antibody (Cat. No. NBP2-19939, Novus Biologicals, Bio-Techne) was added for each immunoprecipitation overnight rotation at 4°C. 40 µl of Protein A and Protein G magnetic beads (Thermo Fisher 10003A/D) were utilized to bind immunocomplexes for 1h at 4°C. The bound immunocomplexes were washed twice with low-salt ChIP buffer, twice with high-salt ChIP buffer and twice with TE wash buffer at 4°C. The buffer ingredients were described in materials section 2.1.3. The beads were dissolved in 100 µl freshly prepared elution buffer and the immunocomplexes were eluted by incubation at room temperature for 20 min. The eluted samples first were removed from cross-linked and they purified with a PCR purification kit. Then the pure samples were utilized for qPCRs. Primers used for qPCRs were demonstrated in primer list table in materials part.

2.2.21 ATAC-Seq analysis

100,000 wild-type and *Prmt7*^{null} MHS macrophage cells were sent to Active Motif (Carlsbad, CA) for ATAC-Seq analysis, after cryopreserving the cells as described in the ATAC-Seq sample preparation guidelines supplied by the company. The ATAC seq Track across the TSS of *Prmt7* in WT cells was further analysed by JASPAR http://jaspar.genereg.net for TF binding sites.

2.2.22 Protein analysis experiments

2.2.22.1 Protein isolation from primary cells and cell lines

After treatment of cells in 6 well plates, cells were collected by removing the existing medium and washing the cells with cold PBS. Subsequently, plate was put on ice to prevent protein degradation and scratched with a tip of a pipette using 100µl of RIPA buffer which is a mixture of RIPA lysis buffer with 1:20 complete protease inhibitor and 1:100 of 100mM Vanadate. Cell lysates were collected in tubes and the tubes were frozen by snap-freeze technique in liquid nitrogen for 3-5 seconds. During thawing process, the tubes were vortexed occasionally and kept on ice. Subsequently, cell lysates were centrifuged for 15 mins at 13.000 rpm at 4°C. as a result of centrifugation step, supernatant containing total protein content and pellet containing cell debris were differentiated. The supernatants were transferred into new tubes to measure protein concentration. Cell supernatants were kept at -80°C.

2.2.22.2 Protein concentration measurement

To be able to perform experiments with isolated protein, the concentration of it should be known. To measure the protein concentration after protein extraction, BCA Protein Assay kit from Thermo Fischer was used. This method is based on chelation of bicinchoninic acid (BCA). BCA reacts with complexes between copper ions reduced by peptide bonds in proteins and the end product gives purple color depending on the concentration of protein in the reaction which absorbs light at 562 nm (Krohn, 2001). A standard curve is necessary for measuring the concentration of unknown proteins with the help of linear equation from the curve. This curve is prepared with the reference protein, which is Bovine Serum Albumin (BSA) in our case and absorbance was measured on a Tecan Plate Reader at 562nm.

In brief, reference protein BSA was utilized for preparation of a serial dilutions and from each diluted BSA protein, 10µl was added into 96 well plate. To reduce the error during measurements and pipetting, this step was repeated three times. Also unknown protein was also pipetted into 96 well plate next to BSA dilutions. Substrate reacting solution was prepared by mixing reagent A and reagent B in 50:1 ratio, respectively. From this solution, 200µl was pipetted into each well with protein inside to react with. The plate was incubated

at 37°C for 30 mins to 45 mins for reactions to take place. The absorbance at 562nm was measured using a microplate reader and with the help of standard curve, unknown protein concentrations were calculated.

2.2.22.3 SDS-PAGE and immunoblotting

For western blotting, first proper amounts of proteins were prepared by adding Laemmli loading buffer (4x) with β-Mercaptoethanol in a ratio of 9:1. Usually 20 µg of protein would be enough to detect the interested protein via western blotting however this concentration might be also dependent on the specificity of the antibody. The mixture of protein and loading buffer solution was bolied at 95°C for 10 minutes. In order to separate proteins on SDS-PAGE, a gel was prepared consisting of two different layers: stacking and separating. The percentage of stacking gel was around 5% whereas separating gel percentage was depending on the size of the interested protein. In our study, 10% and 15% separating gels were used. The compositions of the gels were listed in Table 2.20 and in Table 2.21 below.

Table 2.20: Composition of 10% SDS-PAGE gel

Reagent	***Separating gel***	***Stacking gel-5%***
Millipore-H2O	6.7 ml	5.8 ml
0.5 M Tris-HCl with pH 6.8	-	2.5 ml
1.5 M Tris-HCl with pH 8.8	4.2 ml	-
10 % SDS	165 µl	100 µl
Acrylamide/Bisacrylamide	5.5 ml	1.7 ml
TEMED	22 µl	20µl
10 % APS	22 µl	20µl

Table 2.21: Composition of 15% SDS-PAGE gel

Reagent	**Separating gel**	**Stacking gel-5%**
Millipore-H2O	4 ml	5.8 ml
0.5 M Tris-HCl with pH 6.8	-	2.5 ml
1.5 M Tris-HCl with pH 8.8	4.2 ml	-
10 % SDS	165µl	100 µl
Acrylamide/Bisacrylamide	8.3 ml	1.7 ml
TEMED	22µl	20µl
10 % APS	22µl	20µl

Separating gel was poured into gel casting apparatus and allowed to polymerize in the presence of isopropanol on top to have a smooth gel surface followed by pouring stacking gel

onto separating gel. The comb was placed immediately. After polymerization, comb was removed and the casted gel was inserted into running chamber, which is loaded with 1X running buffer. Samples were loaded in a 10% or 15% prepared gels and run at 100 V for 15 mins and then the voltage was elevated up to 120 V to run one more hour. Then, protein samples were transferred to a PVDF membrane which needs to be activated with methanol for 1 min before usage. The total transfer time is usually one and half hour in 1x transfer buffer at 100V but the time might change according to the size of the interested protein. After transfer, membranes were blocked with 5 % non-fat dry milk prepared in 1x PBST for at least 1h at room temperature to prevent unspecific bindings. Following blocking, the membrane was incubated with antibodies against PRMT7, mono-methylated arginine, T1-alpha, VCAM-1, RAP1A/B, phosphorylated ERK, total ERK, phosphorylated p38, H3R2me1, H3R2me2, H4R3me1 and H4R3me2. The detailed information about antibodies was listed in Table 2.4. The antibodies were diluted in 1% milk and incubated at 4°C overnight. Second day starts with washing membrane with PBS-T for 3 times for 10 minutes followed by incubation with horseradish peroxidase (HRP)-conjugated secondary antibodies for 1h at room temperature. Then, the membrane was again washed with PBS-T for 3 times for 10 minutes. The membranes were ready for developing. β-actin was used as a house keeping protein to control equal loading in our study.

2.2.22.4 Signal development and quantification

After secondary antibody binding step, membranes were ready for developing. Developing step is the most critical step of the western blotting. ECL Prime Western Blotting Detection Reagents (Super Signal West Dura and Femto Substrate, Thermo Fisher) were used to detect the signal in a ratio of 1:1. After mixing reagent A and B in equal amounts, this solution was placed onto membrane and incubated around 5 mins to let chemiluminescence reaction to occur. Chemidoc XRS machine from Bio-Rad which is a highly sensitive detection system was used to record the signal. The bands were analysed with the help of Image Lab 5.1 software. To compare the intensities of the visualized bands, densitometry analysis was done and the results were normalized to that of β-actin as a loading control. Statistical analysis and densitometry of the bands were done using Image Lab 5.1 software and imagej software.

2.2.22.5 Immunoprecipitation

To identify the interactions between proteins, immunoprecipitation (IP) method was performed in our study. The monomethylated proteins in WT MHS and *Prmt7*^{null} clone MHS cells were determined. 50ug of protein from wild-type and *Prmt7*^{null} clone MHS cells was used for each IP reaction. Firstly, 50ul pierce protein A agarose beads were crosslinked with 4µg anti-mono-methylated arginine antibody. 50 ug of protein from wild-type and *Prmt7*^{null} clone MHS cells was first mixed with pierce protein A agarose beads, then incubated with the antibody coated beads at 4°C for 18h under rotation. Beads were centrifuged at 14000 rpm for 1 min at 4°C and washed 3x with PBS.

IPs were undertaken for each cell type and subjected to liquid chromatography tandem-mass spectrometry (LC-MS/MS) analysis (Cox and Mann, 2008; Elias and Gygi, 2007), quantitative ratios were calculated and normalized by Max Quant software package. InCroMAP software (http://www.ra.cs.uni-tuebingen.de/software/InCroMAP/downloads/index) Version 1.7.0 (University of Tübingen, Germany) (Wrzodek et al., 2013) was used to analyze for KEGG pathway enrichment in the differentially pulled down proteins with less abundance in *Prmt7*^{null} compared to WT MHS cells (FC>-1.6; Data file S3). Protein information was obtained from UniProtKB (http://www.uniprot.org).

2.2.23 RNA expression analysis

2.2.23.1 RNA isolation

PeqGOLD Total RNA isolation kit was utilized for total RNA isolation from lung tissue or cell lysate according to the protocol from Peqlab. Firstly, cell lysates were obtained by addition of 400 µl of RNA lysis buffer into each well of 24 well plate. Cell lysates were applied onto a DNA Removing Column and columns were centrifuged at 12.000 x g for 1 min at RT. DNA Removing Columns were discarded and flow through (FT) of each sample were transferred into new 1.5 ml tubes. 400µl of 70% ethanol was added into FT and the tube was vortexed. A total volume of the mixture was transferred into a PerfectBind RNA-binding column and centrifuged at 10000 x g for 1 min. Flow through was discarded and RNA binding columns were placed in 2 ml fresh collection tubes. 500µl of RNA Wash buffer 1 was added into the

RNA-binding columns and they were centrifuged at 10000 x g for 15 seconds. This step was followed by the addition of 600µl of RNA Wash Buffer 2 and centrifuged for 15 seconds at 10000 x g. This last washing step was repeated one more time followed by a drying step to completely remove ethanol for 2 mins at 10000 x g. For elution of RNA, sterile RNAse-free dH_2O, which was preheated at 70°C to have more efficient elution, was added into each column. The amount of elution depends on the cell number that was plated in the beginning, in our case it was 50µl. The columns were centrifuged for 1 min at 5000 x g.

In order to check the RNA concentration and purity, the NanoDrop 1000 (Peqlab) was used. Nucleic Acid- RNA-40 setting was applied for measurements. 1 µl of RNA sample was inserted onto the machine and measured. Absorbance ratio at 260 nm and 280 nm is an indication of purity of the sample. A pure RNA sample gives the ratio of A260/A280 nm=~2. The measured RNA was either used for cDNA synthesis directly or kept at -80°C for long-term storage.

2.2.23.2 cDNA synthesis by reverse transcription

After RNA isolation and concentration measurement, next step is the conversion of RNA into cDNA. This process is known as reverse transcription. For cDNA synthesis, 500ng or 1 µg of isolated RNA was first diluted in 9 µl of dH_2O and then was heated at 70°C for 10 minutes followed by incubation on ice for 5 minutes. At the same time, master mix was prepared in 11µl including 10µl of RT buffer mix containing already dNTPs, random octamers and oligo dT-16 and 1µl of enzyme mix containing MuLV reverse transcriptase and RNase inhibitor protein. The master mix (11µl mix per sample) was then added into 9µl of RNA samples. Reverse transcription reaction was done in an Thermocycler with the following settings: 10 min at 20°C, 75 min at 43°C and then 5 min at 99°C. Finally, generated cDNA was diluted with dH_2O to reach 100µl volume at the end and cDNA samples were ready for real time quantitive PCR (qPCR). They can be stored at -20°C.

2.2.23.3 Quantitative real time polymerase chain reaction (qRT-PCR)

RT quantitative-PCR uses the dye Syber green to produce signal with fluorescence by intercalating into DNA molecules. It amplifies and simultaneously quantifies the targeted gene. Hypoxanthine-guanuine phophoribosyltransferase (*Hprt*) was used as the

housekeeping gene in our study to normalize the target gene expression. Fluorescence level is directly correlated with the amount of gene product through syber green binding. qPCR reaction mix was prepared according to the instructions in Table 2.22 for one assay.

Table 2.22: qPCR reaction mixture

Reagent	***Volume***
H_2O	2.4 µl
SYBR green I Master Mix	5 µl
Primer Mix-Forward/Reverse	0.6 µl
cDNA	2 µl
Total volume of the reaction mix	10 µl

Per reaction, 8 µl of master mix and 2µl of cDNA were pipetted into 96-well qPCR plates from Applied Biosystems. The reaction was performed using a Thermocycler StepOne according to the PCR protocol explained in Table 2.23.

Table 2.23: Standard qRT-PCR protocol

Step of cycle	***Temperature***	***Duration***
Initial denaturation	95°C	5 mins
Denaturation	95°C	5 seconds
Annealing	59°C	5 seconds
Elongation	72°C	20 seconds
Melting curve	60°C-95°C	1 min
Cooling down	4°C	On hold

The three steps including denaturation, annealing and elongation were repeated in 45 cycles. All qPCR experiments were done in duplicates to reduce the pipetting error and mRNA expression of gene of interest was normalized to housekeeping gene expression in the same plate using the same samples. As a result of normalization, mean Ct value for each sample used for further analysis. The formula $2^{-\Delta Ct}$, where $\Delta Ct = Ct_{target} - Ct_{control}$ was used to determine the relative expression of the gene of interest.

2.2.24 PRMT7 expression in human lung published data sets

The raw data from NCBI GEO database for GSE76925 (Morrow et al., 2017) and GSE27597 (Campbell et al., 2012) were downloaded and gene expression was analysed and normalized

to control groups. The Human Protein Atlas website https://www.proteinatlas.org was also accessed to examine lung tissue expression.

2.2.25 PRMT7 promoter analysis on publically available CHIP-Seq data

PRMT7 promoter analysis on publically available CHIP-Seq data was undertaken using the Cistrome Data Browser (http://cistrome.org) (Mei et al., 2016), of five crucial myeloid Transcription Factors (Sajti et al., 2020).

2.2.26 Statistical analysis

In this study, results were demonstrated as mean values ± SD. Figure legends contain the number of samples as well as number of repeats ("n" numbers) for each graph. To compare the significany between only two groups, student's unpaired t-test was performed however when comparing more than two groups in one experiment, one-way ANOVA following Bonferroni post-test was used. Significany was determined accoding to *P* value being lower than 0.05. All graphs were generated with the help of GraphPad Prism 6 software.

3. RESULTS

3.1 The contribution of PRMT7 to COPD immunopathogenesis

3.1.1 PRMT7 levels are increased in COPD patients

Cigarette smoke (CS) is described as the major cause of COPD however only 20% of smokers develop the disease (Terzikhan et al., 2016). The factors and pathways underlying disease progression are still elusive. In this respect, the first purpose of my thesis was to identify which molecular pathways are contributing to COPD pathogenesis in only a subset of smokers. For this purpose, unbiased gene set enrichment analysis (GSEA) was performed, with the help of Dr. Thomas Conlon, on a publically available transcriptomics data set (GSE76925). This transcriptomics data set was from the lungs of 111 COPD patients who were smokers and 40 control smokers without disease. GSEA of the GO Molecular function collection revealed N-methyltransferase activity was the most significantly enriched gene set of the 642 analysed in the lungs of COPD patients, with a p-value of 0.0057 (Figure 3.1A and B). In support, related pathways were also significantly enriched; transferring one carbon groups, S-adenosylmethionine dependent and protein methyltransferase (Figure 3.1A). Protein methyltransferases are crucial enzymes that catalyse the methylation of lysine and

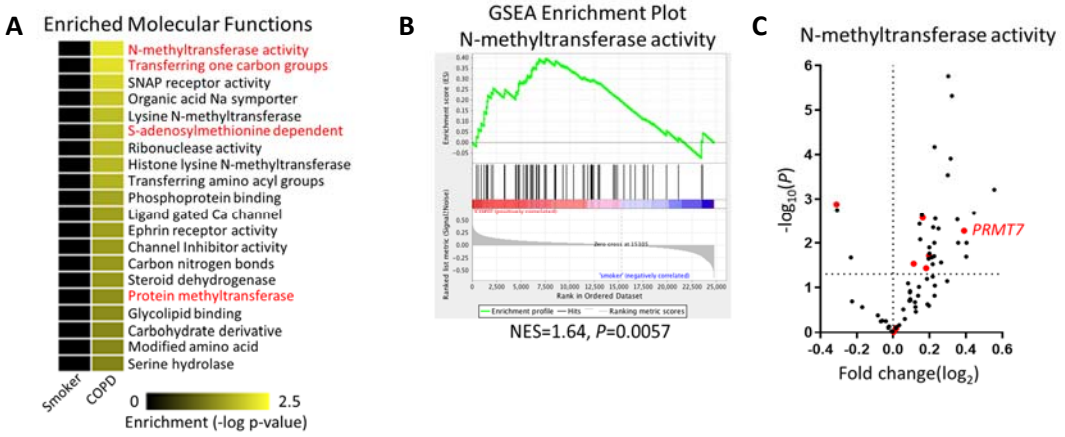

Figure 3.1 PRMT7 expression is enriched in COPD patients. (A) Heat map analysis of the most significantly enriched gene sets in the lungs of COPD patients as a result of GSEA analysis of the GO molecular function set using array data from GSE76925. Lung tissues in the analysis were from 40 healthy smoker controls and 111 COPD patients. **(B)** GSEA enrichment plot for N-methyltransferase activity with normalized enrichment score (NES) being 1.64 and p value being 0.0057 (GO:0008170). **(C)** Volcano plot of the genes involved in N-methyltransferase activity and their expression in COPD patients compared to smoker controls using the same array data from GSE76925. Red highlights represent PRMT genes.

arginine residues and play a central role in gene transcription therefore in human diseases (Kim et al., 2016). Therefore, as methyltransferase activity was the most significantly enriched gene set in COPD patients, the genes involved in methyltransferase activity were analysed. Top ten enriched gene list is shown in Table 3.1. In this list, there were mainly lysine and arginine methyltransferases including *GNMT*, *EZH2*, *SETD4*, *PNMT* and *PRMT7* as the most five enriched genes. Within the arginine methyltransferases (PRMTs) of this gene set, *PRMT7* was misregulated the highest (Figure 3.1C).

Table 3.1 GO N-methyltransferase activity gene list from the GSEA enrichment

	GENE	RANK IN GENE LIST	RANK METRIC SCORE	RUNNING ES	CORE ENRICHMENT
1	*GNMT*	467	0.245240659	0.027529905	Yes
2	*EZH2*	614	0.22739704	0.06467469	Yes
3	*SETD4*	905	0.200980946	0.090989165	Yes
4	*PNMT*	1217	0.179593578	0.112404205	Yes
5	*PRMT7*	1234	0.177996531	0.14545777	Yes
6	*WHSC1L1*	1498	0.165477723	0.16614309	Yes
7	*PRDM6*	1560	0.163096026	0.19455396	Yes
8	*MEN1*	1591	0.161792412	0.2239728	Yes
9	*RBBP5*	1966	0.147326648	0.23672844	Yes
10	*PRDM9*	2162	0.140547186	0.255446	Yes

To investigate further, from the same array of GSE76925, the expression of PRMT7 was compared to that of several well-established COPD disease markers as controls. Metalloproteinase 9 (MMP9) is involved in COPD pathogenesis by degrading matrix proteins such as elastin or collagen (Linder et al., 2015), whereas osteopontin gene (SPP1) triggers the activation of autoreactive T cells in response to cigarette smoke (Shan et al., 2012). Moreover, periostin (POSTN) is a stress response and inflammation marker in many respiratory diseases including COPD (Izuhara et al., 2016). Analysis of the publically available array data confirmed that *PRMT7* was significantly upregulated in COPD patients consistent with the altered regulation of the established COPD marker genes; *MMP9*, *SPP1* and *POSTN* (Figure 3.2).

To validate these findings, another independent cohort (GSE27597) was examined. Consistent with the previous cohort (GSE76925), *PRMT7* expression was increased in the

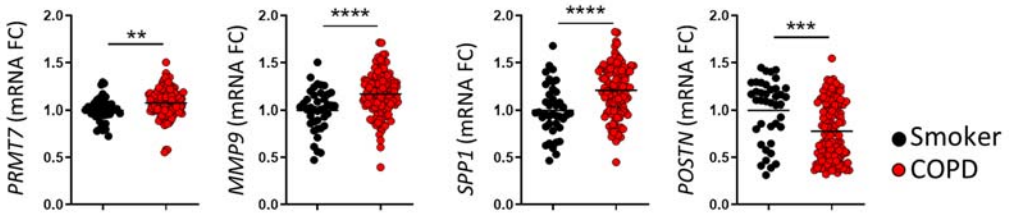

Figure 3.2 The expression of *PRMT7* and established COPD markers. Relative expression of *PRMT7*, *MMP9*, *SPP1* and *POSTN* in the lungs of COPD patients in comparison to control smokers. Each dot represents one individual from the GSE76925 data set. **P < 0.01, ***P < 0.001, and ****P < 0.0001, Mann Whitney test. FC refers to fold change.

lungs of COPD patients in comparison to smoker controls (Figure 3.3A). Crucially, the increase in *PRMT7* expression positively correlated with emphysema (airspace enlargement) development, a hallmark of COPD (Figure 3.3B).

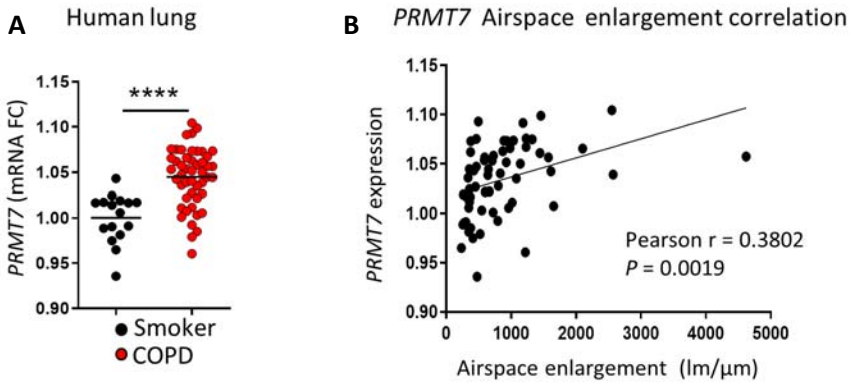

Figure 3.3 *PRMT7* expression correlates with disease severity. (A) *PRMT7* expression in COPD patients relative to healthy control smokers using analysis of GSE27597 data set. (n=16 healthy smokers and n=48 COPD patients). **(B)** Correlation of airspace enlargement, emphysema, with *PRMT7* gene expression in the same data GSE27597 having p value of 0.0019. ****P < 0.0001 Mann Whitney test. FC refers to fold change.

To further validate the findings from GSE76926 and GSE27597 transcriptomics data, PRMT7 gene and protein expression levels were examined performing qPCR and western blotting in lung core biopsies from lungs of COPD patients and healthy controls in a third independent cohort, kindly provided by Dr. Stijn Verleden with the ethical approval (University of Leuven, Belgium). The clinical features of the patients from Leuven were demonstrated in Table 3.2.

Table 3.2 : The features of COPD patients and healthy controls that were used in our study from Leuven University

	COPD	Healthy
Subjects (n)	16	11
Mean age years	57.06 ± 1.23	46 ± 4.93
Sex		
Male	7	10
Female	9	1
Height (m)	1.65 ± 0.02	1.75 ± 0.03
Weight (kg)	59.44 ± 3.18	80.45 ± 2.97
Smoking (packs/year)	39.00 ± 7.55	
FEV1 (%)	34.38 ± 5.55	
FVC (%)	82.73 ± 5.84	
FEV1/FVC (%)	31.01 ± 5.07	

FEV1: Forced expiratory volume in the first second
FVC: Forced vital capacity

qPCR analysis clearly demonstrated that *PRMT7* gene expression in COPD patients was significantly higher compared to controls (Figure 3.4A). Increased expression of *TNF* was used as positive control (Figure 3.4A), being an established inflammatory marker in COPD disease (Yao et al., 2019). Moreover, western blot analysis confirmed the increase in gene expression by showing a remarkable upregulation of PRMT7 protein in COPD patients in comparison to healthy controls (Figure 3.4B).

Protein arginine methyltransferases (PRMTs) in mammalian cells consist of nine family members that catalyse the transfer of a methyl group from AdoMet to arginine residue (Tewary et al., 2019). Between nine enzymes; PRMT1, PRMT4 (CARM1) and PRMT5 were associated with having roles in a various of diseases particularly lung disorders. For instance; elevated levels of PRMT1 is associated with several types of lung cancer (Yoshimatsu et al., 2011) and pulmonary inflammation (Sun et al., 2012), loss of CARM1 is related to emphysema development (Sarker et al., 2015) and dysregulation of PRMT5 is related to lung

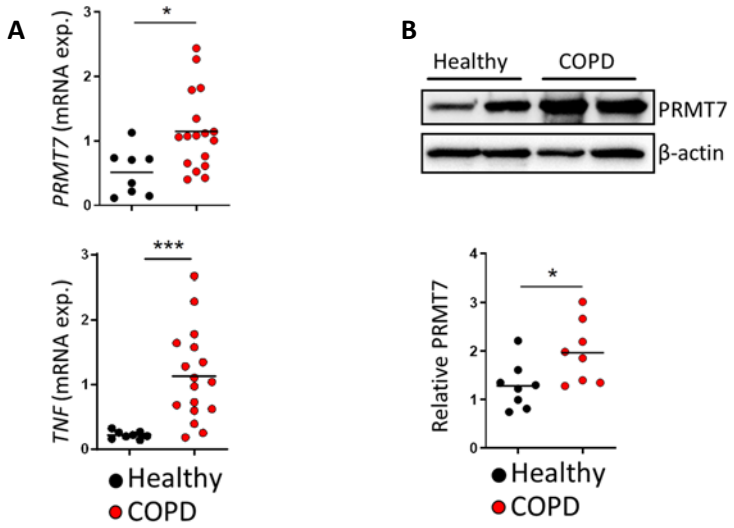

Figure 3.4 PRMT7 expression is upregulated in COPD patients. (A) The gene expression levels of *PRMT7* and *TNF* in human lung biopsies from healthy controls (n=8) and COPD patients (n=18) using qPCR analysis. **(B)** Representative picture of PRMT7 protein levels in lung core biopsies from healthy (n=2) and COPD patients (n=2) by Western blot analysis and densitometry results of 8 biological samples for healthy controls (n=8) and COPD patients (n=8). Data shown as mean ± SD, n=8-18. *P < 0.05, **P < 0.01, ***P < 0.001, and ****P < 0.0001, unpaired two-tailed Student's t test.

tumorigenesis (Wang et al., 2018a). Since their importance in lung diseases is emerging, it was important to address whether the other PRMTs might also have a role in COPD together with PRMT7. For this reason, the expression of *PRMT1*, *CARM1* and *PRMT5* was determined in COPD patients compared to healthy ones. qPCR results demonstrated that only gene expression of *PRMT5* was increased in COPD patients similar to *PRMT7,* whereas *PRMT1* and *CARM1* gene expression levels were similar between these two groups (Figure 3.5). Moreover, several chemokines and cytokines have been associated with inflammation in COPD such as IL8, IL6, CCL2 and CXCL1. Inflammatory cells including macrophages, neutrophils and T cells secrete these cytokines and chemokines in response to chronic inflammation in COPD (Barnes, 2009). Here, previous findings were confirmed, as the expression of *IL8*, *IL6*, *CCL2* and *CXCL1* chemokines were significantly increased in COPD patients in comparison to controls (Figure 3.5).

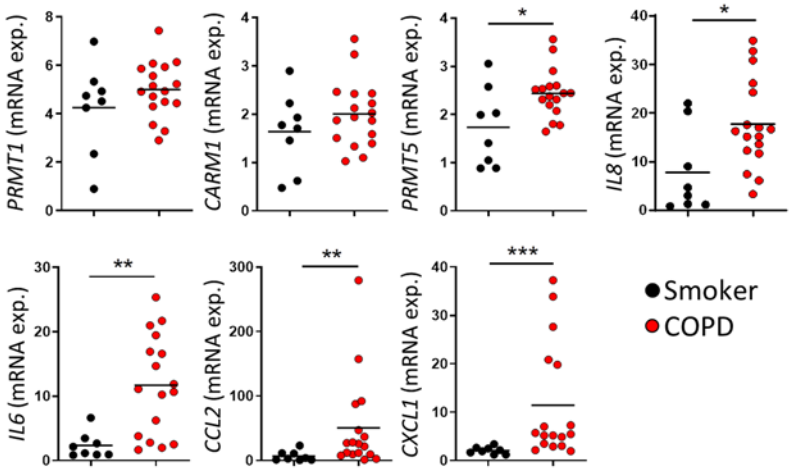

Figure 3.5 PRMT and inflammatory gene expression levels in human COPD patients. mRNA expression levels of PRMT genes including *PRMT1*, *CARM1*, *PRMT5* and inflammatory genes including *IL8*, *IL6*, *CCL2* and *CXCL1* in lung core biopsies from healthy controls (n=11) and COPD patients (n=17). mRNA expression was determined by qPCR and each dot represents and individual patient. Data shown as mean ± SD, *P < 0.05, **P < 0.01 and ***P < 0.001, Mann Whitney test.

3.1.2 PRMT7 mainly localizes to macrophages in mouse and human lungs

Since PRMT7 expression was upregulated in the lungs of COPD patients, the next question was to understand which cells in the lung express PRMT7. In the lung, there are many diverse populations of resident cells, in the respiratory tract like airway epithelial cells (e.g. Club cells), alveolar epithelial cells (e.g. ATII cells), blood cells (e.g. endothelial cells) and inflammatory cells (e.g. macrophages) (Whitsett and Alenghat, 2015). To determine where PRMT7 is predominantly expressed in the lung, the human protein atlas website (https://www.proteinatlas.org/) was examined first. In this website, PRMT7 was shown to be

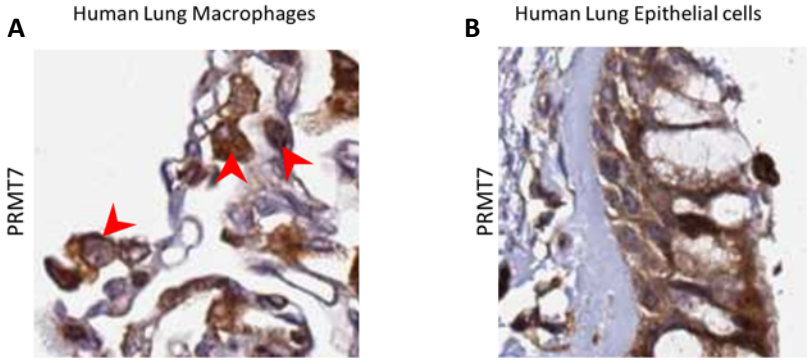

Figure 3.6 Localization of PRMT7 in lung macrophages from human lung atlas website. (A) The expression of PRMT7 in human lung macrophages using immunohistochemistry staining. Red arrows show stained macrophages for PRMT7. **(B)** the expression of PRMT7 in human bronchus epithelial cells using immunohistochemistry staining. Images were taken from the human protein atlas (https://www.proteinatlas.org/).

primarily localized to the lung macrophages following immunohistochemistry staining of human lung sections (Figure 3.6A). Another cell type expressing PRMT7 was bronchial epithelial cells but at lower levels than macrophages in human lungs (Figure 3.6B).

Therefore, considering the preliminary data from the human protein atlas, immunofluorescence analysis of lung tissue sections of human (healthy and COPD patients) and mouse (Filtered air and cigarette smoke exposed) was performed. Co-localization of PRMT7 and Galectin 3, which is a carbohydrate-binding lectin present on macrophages (Liu et al., 1995), demonstrated that PRMT7 was predominantly expressed by macrophages in the lungs of both healthy controls and COPD patients, with more double positive cells found in COPD patients (Figure 3.7A). Moreover, mouse lungs exposed to FA and CS also demonstrated that PRMT7 expression was mainly localized to lung macrophages (Figure 3.7B).

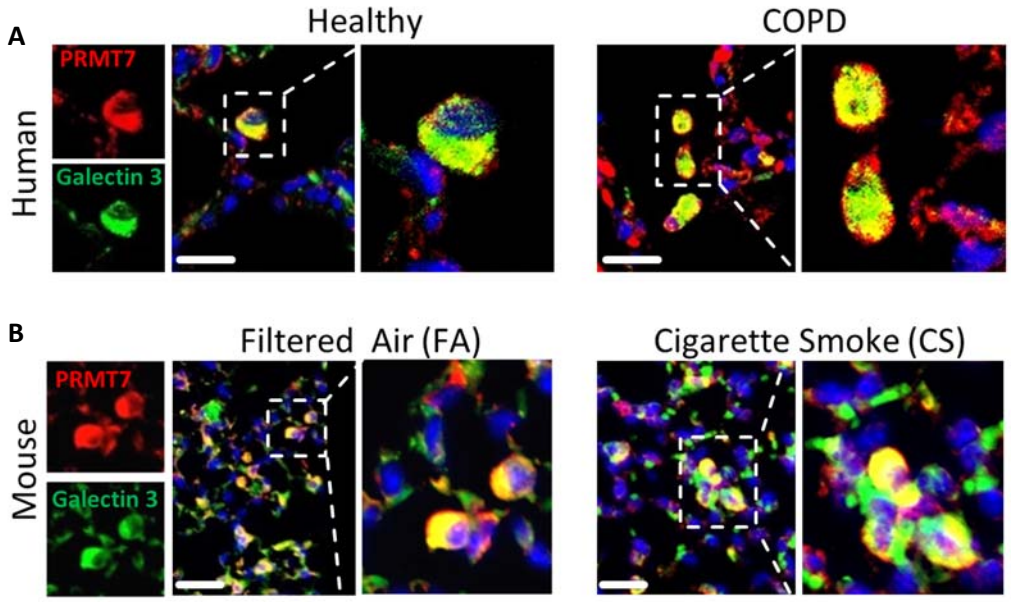

Figure 3.7 PRMT7 expression is mainly localized to macrophages. (A) Representative pictures of immunofluorescence analysis for co-localization (shown in yellow) of PRMT7 (Red) and the macrophage marker Galectin 3 (Green) in the lung core biopsy sections of healthy and COPD patients (n=5), (scale bar 20µm). **(B)** Representative pictures of immunofluorescence analysis for co-localization (shown in yellow) of PRMT7 (Red) and Galectin 3 (Green) in the sections from FA exposed and CS exposed mouse lungs (n=4), (scale bar 25µm).

Besides macrophages, the human protein atlas revealed that pneumocytes also express PRMT7 in human lungs. Further, single cell transcriptomic analysis of lung tissue (Angelidis et

al., 2019) revealed that Club cells and alveolar type II epithelial cells also express PRMT7 in the lung. Taking this finding into consideration, immunofluorescence staining for CC10 positive club cells and Pro-SPC positive alveolar type II (ATII) cells in the lungs was undertaken to examine for co-localization with PRMT7. This revealed that some of the club cells expressing CC10 (Figure 3.8A) and ATII cells expressing Pro-SPC (Figure 3.8B) also expressed PRMT7 in mouse lung tissue.

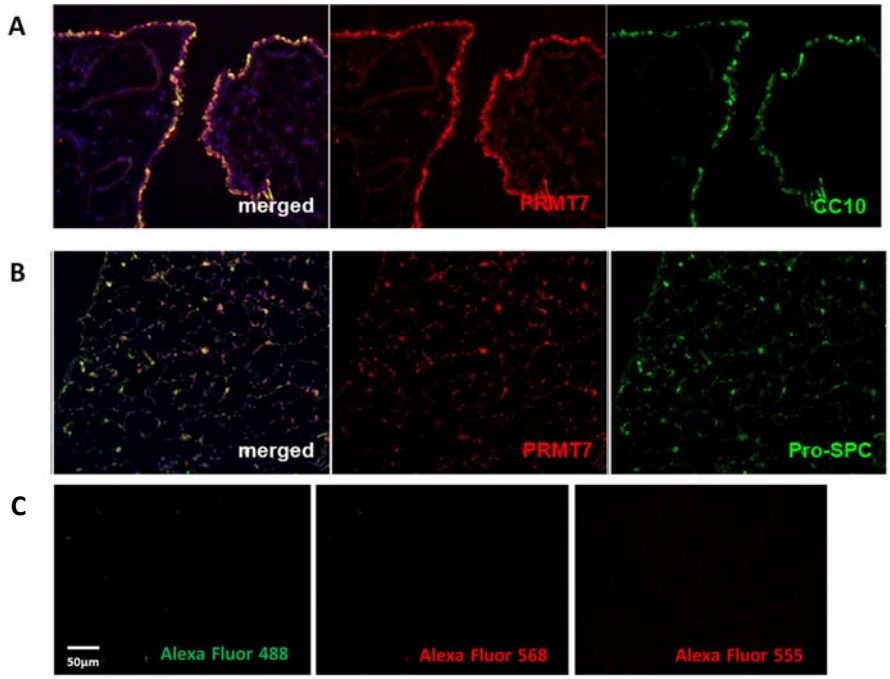

Figure 3.8 PRMT7 is also expressed in club cells and ATII cells in mouse lung. (A) Representative images of immunofluorescence analysis for co-localization (yellow) of PRMT7 (Red) and the club cell marker CC10 (Green) in sections from mouse lung (n=3, scale bar 50µm). **(B)** Representative images of immunofluorescence analysis for co-localization (yellow) of PRMT7 (Red) and alveolar type II cell marker Pro-SPC (Green) in sections from mouse lung (n=3, scale bar 50 µm). **(C)** Representative pictures of negative controls with only secondary antibodies included into stainings of the sections (scale bar 50µm). Alexa Fluor 488 shown in green whereas Alexa Fluor 568 and 555 shown in red.

3.1.3 PRMT7 increases in monocytes and macrophages upon cigarette smoke exposure

Finding that PRMT7 was mainly expressed in lung macrophages, the next objective of the study was to determine the expression levels of PRMT7 specifically in macrophages during COPD pathogenesis. To better understand and to investigate the factors and pathways involved in disease progression, the well-established CS-induced COPD mouse model was utilized (Heckman and Dalbey, 1982). Considering CS-exposure to be the main causing factor

for the development of COPD, exposing mice to CS generates inflammation and mimics the disease characteristics of COPD resulting in the development of emphysema and impaired lung function (Conlon et al., 2020; Jia et al., 2018; John-Schuster et al., 2014a). Wild type mice were first exposed to CS for 3 days and they were compared to filtered air (FA) exposed control mice. After 3 days of CS exposure alveolar macrophages were isolated from the lungs of both CS-exposed and FA control mice. Interestingly, alveolar macrophages isolated from the lungs of CS-exposed mice significantly upregulated *Prmt7* gene expression level as determined by qPCR (Figure 3.9A). Increased *Tnf* gene expression confirms a pro-inflammatory response in alveolar macrophages following CS exposure (Figure 3.9B). Similar to lung data from COPD patients, *Prmt1* and *Carm1* expression in alveolar macrophages did not differ following CS exposure (Figure 3.9C) while *Prmt5* increased similarly to *Prmt7*.

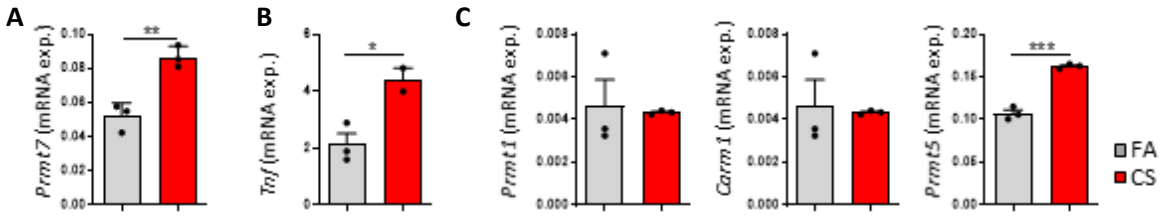

Figure 3.9 Expression of several PRMTs in alveolar macrophages from mouse lungs after cigarette smoke exposure. (A-C) mRNA expression levels of Prmt7 **(A)**, Tnfa **(B)**, Prmt1, Carm1 and Prmt5 **(C)** determined by qPCR in alveolar macrophages isolated from lungs of the mice after 3 days of cigarette smoke exposure. (n=3, one experiment). Data shown as mean ± SD, *P < 0.05, **P < 0.01 and ***P < 0.001, unpaired two-tailed Student's t test.

Furthermore, monocytes are a crucial cell type driving inflammatory responses and importantly, circulating monocytes from the blood give rise to tissue-resident and recruited macrophages in lung tissue (Shi and Pamer, 2011). Therefore, monocytes were isolated from the peripheral blood of mice exposed to CS for 3 days and the gene expression levels of *Prmt7*, *Prmt1*, *Carm1*, *Prmt5* and *Tnf* were determined. *Prmt7* expression levels increased in monocytes (Figure 3.10A) after CS exposure whereas there was no increase in *Tnf* gene expression (Figure 3.10B). Other important *Prmt* genes, including *Prmt1*, *Carm1* and *Prmt5* did not show any elevation in their transcription levels after 3 days of exposure (Figure 3.10C), suggesting that PRMT7 may be involved in monocyte mediated development of CS-induced COPD pathogenesis.

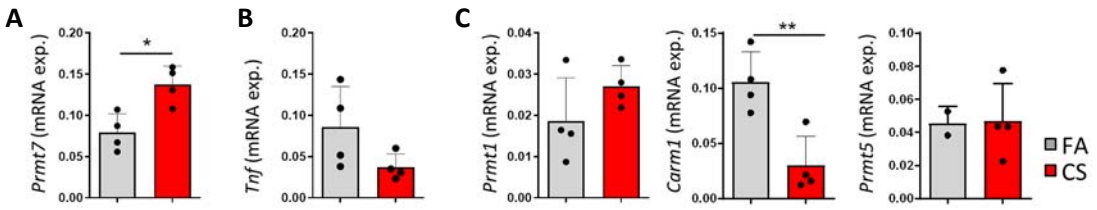

Figure 3.10 Expression of PRMTs in circulating monocytes from the blood of cigarette smoke exposed mice. (A-C) mRNA expression levels of *Prmt7* **(A)**, *Tnf* **(B),** *Prmt1*, *Carm1* and *Prmt5* **(C)** determined by qPCR in mouse monocytes isolated from the peripheral blood of mice after 3 days of cigarette smoke exposure. (n=4, one experiment). Data shown as mean ± SD, *P < 0.05, **P < 0.01 and ***P < 0.001, unpaired two-tailed student t-test.

The findings above indicated that macrophages and monocytes enhanced PRMT7 levels upon acute inflammation following 3 days of CS exposure. To confirm these findings following chronic CS-exposure, single cell RNA-Seq analysis was performed on whole lung tissue isolated from the lungs of FA and CS-exposed mice for 2 and 4 months (Kindly undertaken by the Schiller lab of the ILBD). As a result of single cell RNA-Seq analysis, it was clearly observed that *Prmt7* expression was elevated in both alveolar (Figure 3.11A) and interstitial macrophages (Figure 3.11B) following 2 and 4 months of CS exposure, consistent with the acute results. Monocytes also demonstrated increased *Prmt7* expression following chronic CS exposure (Figure 3.11C), implying that chronic CS exposure had a similar effect upon PRMT7 expression in both macrophages and monocytes as did acute CS exposure.

To support these findings in vitro, the murine lung alveolar macrophage cell line, MHS, was explored. MHS cells are a continuous cell line of murine alveolar macrophages which was created by simian virus 40 (SV40) transformation of bronchoalveolar lavage cells isolated

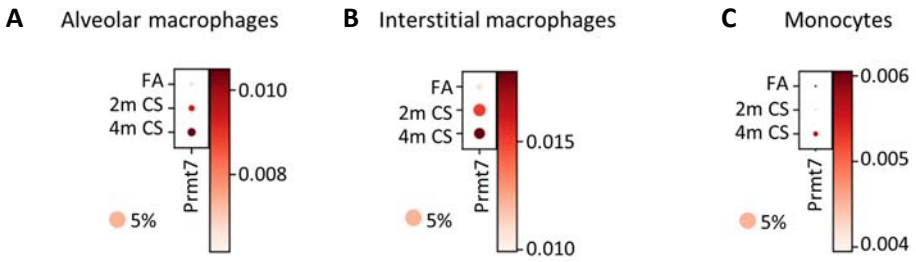

Figure 3.11 PRMT7 expression in macrophages and monocytes in single cell RNA-Seq analysis. (A-C) *Prmt7* expression in alveolar macrophages **(A)**, interstitial macrophages **(B)** and monocytes **(C)** from mouse lung single cell RNA-seq data following exposure to FA and CS for 2 and 4 months (n=3-5). Dot plot represents the cell percentage which are positive for *Prmt7* expression in each subtype. Expression scale increases from bottom to up with the colour intensity.

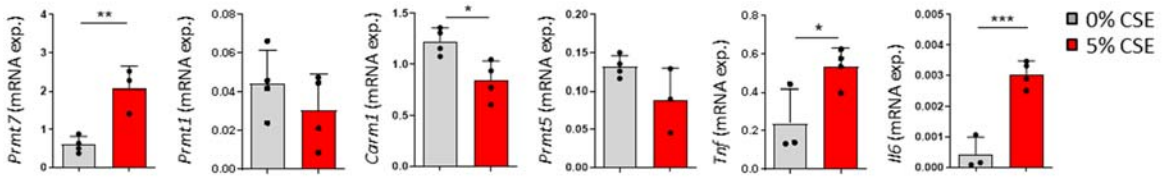

Figure 3.12 Expression of several PRMTs in MHS cells after stimulating with cigarette smoke extract (5%). The expression levels of *Prmt7*, *Prmt1*, *Carm1, Prmt5*, *Tnf* and *IL6* determined by qPCR in MHS cells with or without 5% of cigarette smoke extract (CSE) treatment for 24h (n=4, one experiment). Data shown mean ± SD, *P < 0.05, **P < 0.01 and ***P < 0.001, unpaired two-tailed student t test.

from mouse lungs (Mbawuike and Herscowitz, 1989). In this study, MHS cells were subjected to 5% of cigarette smoke extract (CSE) for 24h. MHS cells following CSE exposure significantly induced expression of *Prmt7* together with the pro-inflammatory markers *Tnf* and *IL6,* whereas *Prmt1*, *Carm1* and *Prmt5* did not show any elevation in expression levels (Figure 3.12).

To confirm the translational applicability of our murine and in vitro findings, PRMT7 expression levels in circulating human monocytes taken from the peripheral blood of individuals who have a smoking history was examined. In line with monocytes isolated from CS exposed mice, human monocytes demonstrated elevated levels of *PRMT7* in smokers compared to non-smokers (Figure 3.13). Again, similar to mice, there was no difference in the expression of *TNF* between monocytes isolated from non-smokers and smokers (Figure 3.13). Taken all together, this data suggests that PRMT7 expressed by monocytes and macrophages may potentially be contributing to CS-induced COPD pathogenesis.

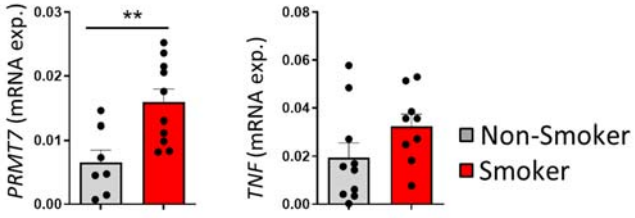

Figure 3.13 Expression of *PRMT7* and *TNF* in circulating human monocytes from the blood of non smokers and smokers. mRNA expression levels of *PRMT7* and *TNF* determined by qPCR in human monocytes isolated from the peripheral blood of non-smokers and smokers. (n=7-10 for non-smokers and n=10 for smokers). Data shown mean ± SD, *P < 0.05, **P < 0.01 and ***P < 0.001, unpaired two-tailed student t-test.

3.2 Regulation of PRMT7 in macrophages and monocytes

3.2.1 *Prmt7* gene promoter analysis

Considering that PRMT7 expression was increased in COPD patients and localized mainly to macrophages in both mouse and human lungs, elucidating how PRMT7 is regulated in these cells is essential to understand the contribution of PRMT7 to the pathogenesis of COPD. To address the mechanism underlying the upstream regulation of PRMT7 in monocytes and macrophages, promoter analysis on publically available CHIP-Seq data from the Cistrome Data Browser (Mei et al., 2016) was first undertaken. A recent study revealed that important transcriptional factors (TFs) for the function of lung macrophages included RELA, RELB, IRF1 and CEBPA (Sajti et al., 2020). CHIP-Seq analysis of the genomic binding regions of these four crucial myeloid TFs demonstrated that RELA was clustered more densely on the promoter region of *Prmt7* rather than the other TFs; RELB, IRF1 and CEBPA (Figure 3.14A). Importantly, this enrichment overlapped with H3K27ac (Zhang et al., 2020) and H3K4me3 (Guenther et al., 2007) which are described as activation marks. Moreover, the enrichment peak of RELA on the *Prmt7* promoter correlated with open chromatin as determined by the ATAC-Seq analysis of macrophages (Figure 3.14A). To support these findings, potential transcription binding

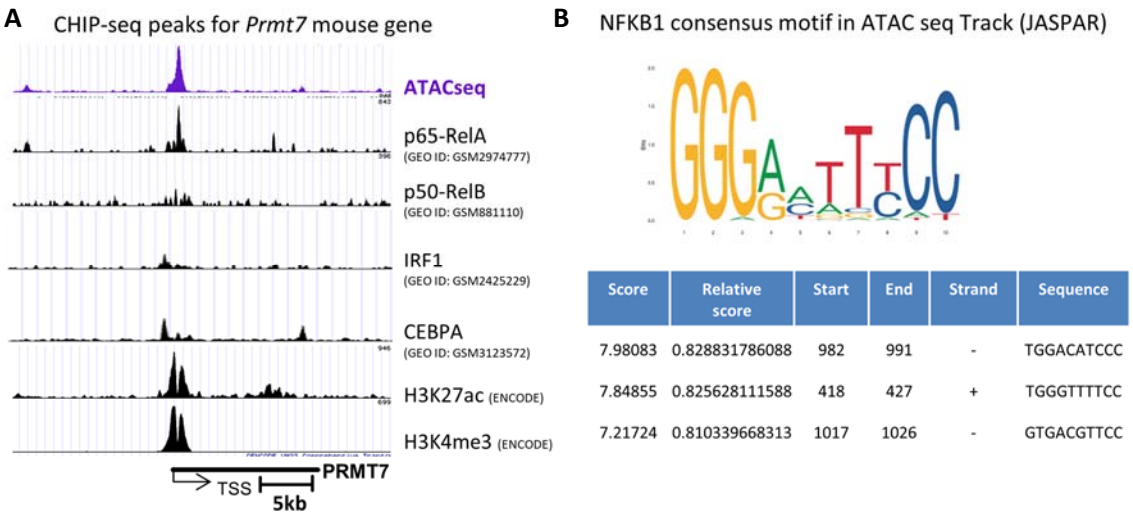

Score	Relative score	Start	End	Strand	Sequence
7.98083	0.828831786088	982	991	-	TGGACATCCC
7.84855	0.825628111588	418	427	+	TGGGTTTTCC
7.21724	0.810339668313	1017	1026	-	GTGACGTTCC

Figure 3.14 Regulation of PRMT7 expression in macrophages. (A) Enrichment peaks of transcriptional factors including p65, p50, IRF1 and CEBPA on the promoter site of mouse *Prmt7* gene by CHIP-Seq analysis using Custom tracks on the UCSC genome browser. H3K27ac and H3K4me3 represents activation marks in the genome. ATAC-Seq peak from our MHS macrophage cell line for the same region is shown in violet colour. **(B)** JASPAR analysis of the ATAC seq Track across the transcription start site (TSS) of Prmt7 showing the presence of NFKB1 consensus motifs.

sites were analysed using the JASPAR database, which is a publically available tool of high quality and matrix based transcriptional factor binding profiles (Fornes et al., 2019; Sandelin et al., 2004). As a result of JASPAR analysis across the transcriptional start site (TSS) of *Prmt7*, NFKB1 consensus motifs were found in the open ATAC seq Track (Figure 3.14B). These data together suggest that *Prmt7* transcription might be regulated via NF-κB subunits, potentially through RELA binding at the promoter.

3.2.2 PRMT7 expression is regulated via NF-κB in monocytes

RelA (referred as p65) is a subunit of the NF-κB transcription factor complex paired with NFKB1, which can be translocated into the nucleus through inflammatory TLR4 signalling to initiate the transcription of target genes (Sharif et al., 2007). Bacterial lipopolysaccharide (LPS) is a well-known ligand of TLR4 and binding of LPS to TLR4 results in translocation of NF-κB transcription factors including RelA into the nucleus (Kawai and Akira, 2010). Therefore, mouse and human primary monocytes were stimulated with LPS in order to understand whether NF-κB signaling regulates *PRMT7* transcriptional expression. As predicted from the promoter analysis, *Prmt7* gene expression in primary mouse monocytes was increased significantly following LPS stimulation, and was accompanied by the induction of the NF-κB regulated inflammatory gene *Tnf* (Figure 3.15A). To validate this finding in humans, human monocytes isolated from peripheral blood were stimulated with LPS. Similarly, *PRMT7* expression was significantly upregulated along with the inflammatory marker *TNF* (Figure 3.15B).

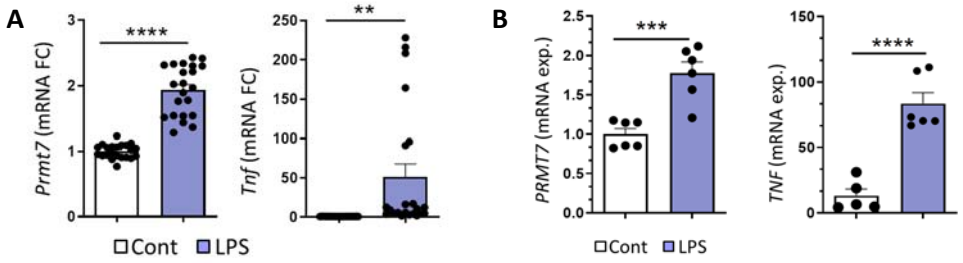

Figure 3.15 The effect of LPS stimulation on PRMT7 levels in primary mouse and human monocytes. (A) mRNA expression levels of *Prmt7* and *Tnf* determined by qPCR in primary mouse monocytes upon 100ng of LPS stimulation (n=22-25, 5 experiments). FC represents fold change. **(B)** mRNA expression levels of *PRMT7* and *TNF* determined by qPCR in primary human monocytes upon 100ng of LPS stimulation (n=5-6, one experiment). Data shown mean ± SD, *P < 0.05, **P < 0.01, ***P < 0.001 and ****P < 0.0001, unpaired two-tailed student t-test.

3.2.3 Inhibition of NF-κB pathway attenuated PRMT7 levels

PRMT7 expression increased following LPS stimulation potentially via NF-κB signaling. Therefore, it was asked whether inhibition of the NF-κB pathway could reduce the induction of *Prmt7* upon LPS stimulation. First, an irreversible inhibitor of cytokine-induced IκB-α phosphorylation, BAY11-7082, was used. BAY11-7082 inhibits the NF-κB translocation into the nucleus by preventing the release of NF-κB from the cytosolic IκB-α/NF-κB complex (Pierce et al., 1997). It is known to be a non-specific inhibitor of both canonical and non-canonical NF-κB signaling. The induction of *Prmt7* expression upon LPS treatment was reversed by using BAY11-7082 (Figure 3.16). *Tnf*, *Il6* and *Il1b* genes were also examined as they are known targets of NF-κB pathway (Liu et al., 2017; Wang et al., 2014a). As expected, their LPS-induced expression was also reduced with BAY11-7082 treatment (Figure 3.16).

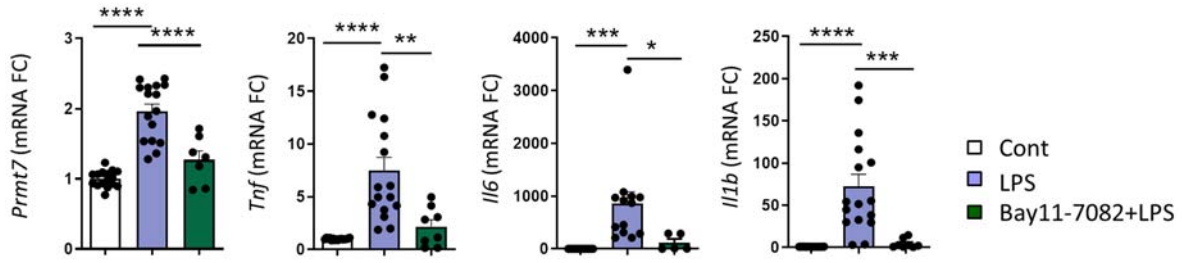

Figure 3.16 *Prmt7* expression is inhibited by BAY11-7082 NF-κB inhibitor in monocytes. mRNA expression levels of *Prmt7*, *Tnf*, *Il6* and *Il1b* determined by qPCR in primary mouse monocytes treated with 100ng LPS only or 100ng LPS combined with 1μM of BAY11-7082 compound for 24h (n=7-20, three experiments). FC refers to fold change relative to control. Data shown as mean ± SD, **P* < 0.05, ***P* < 0.01, ****P* < 0.001, and *****P* < 0.0001, one-way ANOVA Bonferroni's multiple comparisons test.

In confirmation, a more specific inhibitor of the nuclear translocation of RelA into the nucleus was utilized in LPS treated monocytes. JSH-23 is a cell permeable drug that specifically blocks the nuclear translocation of RelA/p65 without affecting upstream targets like IκB-α degradation (Shin et al., 2004). Using JSH-23 also reduced the effect of LPS stimulation on *Prmt7* expression as well as the inflammatory genes, *Tnf, Il6* and *Il1b* in primary mouse monocytes (Figure 3.17A). Consistent with gene expression levels, further western blot analysis demonstrated that JSH-23 treatment had reduced the protein level of PRMT7 upon LPS induction in primary mouse monocytes (Figure 3.17B). More importantly, the enzyme activity of PRMT7 defined by total mono-methylation levels was also diminished following

JSH-23 inhibitor treatment (Figure 3.17B). Taken together, these findings suggested that PRMT7 expression is regulated in myeloid cells by NF-κB signalling pathways predominantly via the nuclear translocation of the transcription factor RelA.

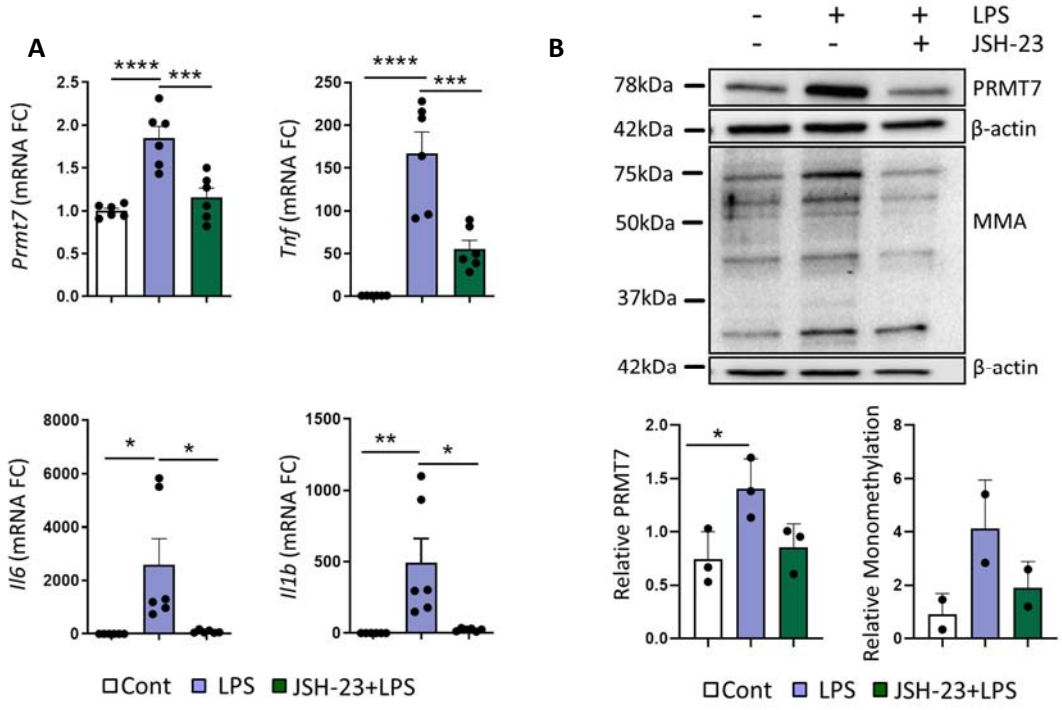

Figure 3.17 PRMT7 expression is inhibited by JSH-23 inhibitor in monocytes. (A) mRNA expression levels of *Prmt7*, *Tnf, Il6* and *Il1b* determined by qPCR in primary mouse monocytes treated with only 100ng LPS or 100ng LPS combined with 20μM of JSH-23 compound for 6h (n=6, three experiments). FC refers to fold change relative to control samples. **(B)** Representative pictures of protein levels of PRMT7 and total mono-methylation levels determined by western blot analysis in primary monocytes treated with only 100ng LPS or 100ng LPS combined with 20μM JSH-23 (n=3). Data shown as mean ± SD, **P* < 0.05, ***P* < 0.01, ****P* < 0.001, and *****P* < 0.0001, one-way ANOVA Bonferroni's multiple comparisons test. Densitometry graphs were drawn as relative to β-actin levels.

3.3 Functional consequences of altered PRMT7 levels in COPD animal models

3.3.1 Generation and validation of *Prmt7*$^{+/-}$ mouse model

To delineate the role of PRMT7 in the development of COPD, mice with a disrupted *Prmt7* allele, referred to as *Prmt7*$^{+/-}$, were used in this study. The generation of *Prmt7*$^{+/-}$ mice is explained in detail in the methods part of this thesis. The reason *Prmt7*$^{+/-}$ mice, instead of full knockout mice were used in this study, was because *Prmt7*$^{-/-}$ mice have been previously reported to die between 5-10 days of birth (Ying et al., 2015). This phenotype was also

observed by ourselves, therefore experiments were performed with *Prmt7*$^{+/-}$ animals and wild-type (WT) litter mate controls.

To validate the deficiency of PRMT7 in *Prmt7*$^{+/-}$ mice, lungs were initially isolated from WT and *Prmt7*$^{+/-}$ mice and mRNA expression levels of *Prmt7*, *Prmt1*, *Carm1* and *Prmt5* were analysed by qPCR in whole lung tissue samples. As predicted, a two-fold reduction in the levels of *Prmt7* mRNA was observed, whereas no change in the levels of *Prmt1*, *Carm1* and *Prmt5* was detectable (Figure 3.18A). Consistent with these findings, mono-methylated arginine levels of whole lung proteins were significantly decreased in *Prmt7*$^{+/-}$ mice (Figure 3.18B). Since PRMT7 is known to be the unique PRMT enzyme, which only catalyzes the mono-methylation (MMA) reaction, reduced MMA levels also proves functional deficiency of PRMT7 in whole lung. Additionally, based on the previous findings that PRMT7 was mainly expressed in macrophages in the lung, the PRMT7 levels in monocytes and alveolar macrophages from WT and *Prmt7*$^{+/-}$ mice was specifically investigated.

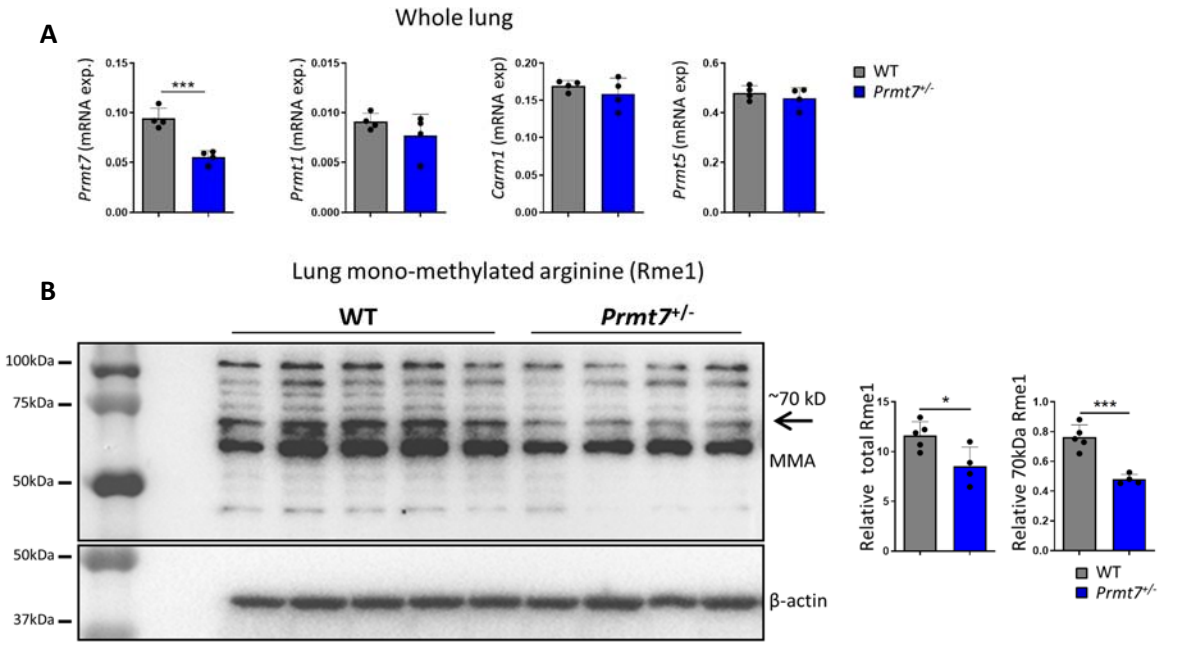

Figure 3.18 Decreased PRMT7 expression and mono-methylation levels in the lungs of *Prmt7*$^{+/-}$ mice. (A) mRNA expression levels of *Prmt7*, *Prmt1*, *Carm1* and *Prmt5* determined by qPCR in whole lung tissue of WT and *Prmt7*$^{+/-}$ mice (n=4). **(B)** Total mono-methylation levels in the lungs of WT and *Prmt7*$^{+/-}$ mice determined by western blot analysis (n=4-5). Data shown as mean ± SD, **P* < 0.05, and ****P* < 0.001 unpaired two-tailed Student's t test. Densitometry graphs were drawn as relative to β-actin levels.

Similar to whole lung tissue results, bone marrow monocytes (Figure 3.19A) and alveolar macrophages (Figure 3.19B) isolated from *Prmt7*$^{+/-}$ mice had diminished expression of *Prmt7* compared to WT mice. Importantly, mRNA expression levels of other PRMTs including *Prmt1*, *Carm1* and *Prmt5* did not show any differences between WT and *Prmt7*$^{+/-}$ mice (Figure 3.19A-B), suggesting no compensatory increase in expression.

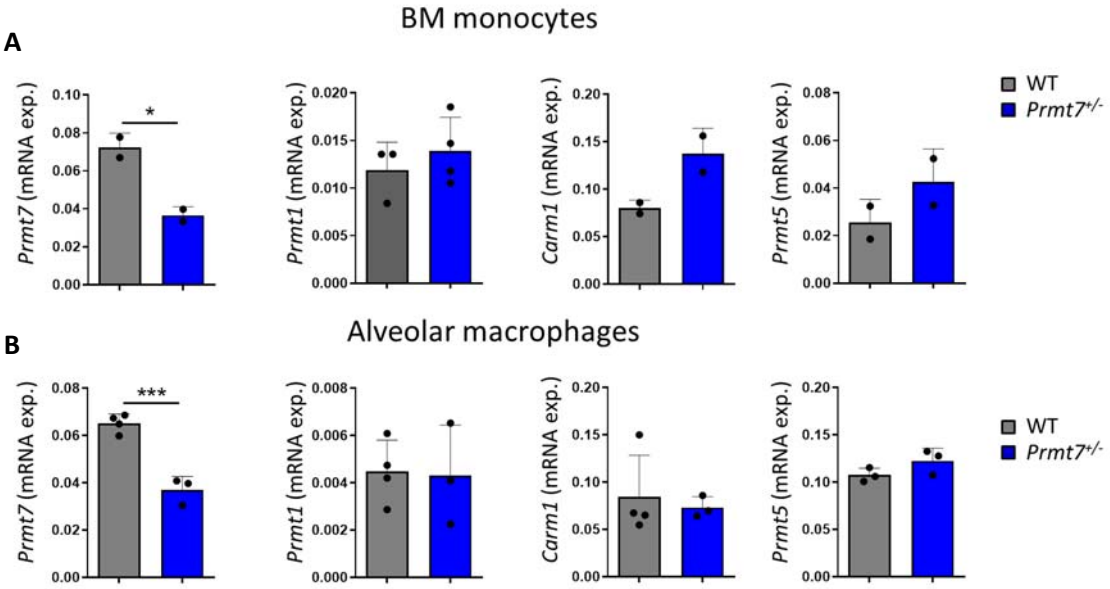

Figure 3.19 Reduced PRMT7 expression in the bone marrow monocytes and alveolar macrophages of WT and *Prmt7*$^{+/-}$ mice. (A) mRNA expression levels of *Prmt7*, *Prmt1*, *Carm1* and *Prmt5* determined by qPCR in bone marrow monocytes isolated from WT and *Prmt7*$^{+/-}$ mice (n=2-4). **(B)** mRNA expression levels of *Prmt7*, *Prmt1*, *Carm1* and *Prmt5* determined by qPCR in alveolar macrophages isolated from the lungs of WT and *Prmt7*$^{+/-}$ mice (n=4). Data shown as mean ± SD, **P* < 0.05, and ****P* < 0.001 unpaired two-tailed Student's t test.

3.3.2 Macrophage accumulation is impaired in the lungs of *Prmt7*$^{+/-}$ mice following CS exposure

To understand the function of PRMT7 in the pathogenesis of COPD, both WT and *Prmt7*$^{+/-}$ mice were subjected to CS, a well-known cause of COPD (Churg et al., 2008; Conlon et al., 2020; Jia et al., 2018; John-Schuster et al., 2014a). Following 3 days of acute CS exposure, inflammatory cell recruitment into the bronchoalveolar lavage (BAL) fluid was enhanced both in WT and *Prmt7*$^{+/-}$ mice (Figure 3.20A). However, *Prmt7*$^{+/-}$ mice demonstrated reduced amounts of total inflammatory cells in comparison to WT control mice following CS exposure (Figure 3.20A). This impaired inflammatory cell number was due to a decline in the number of macrophages, while neutrophil and lymphocyte numbers remained the same (Figure

3.20A). To validate whether macrophage numbers are less in the lungs of *Prmt7*$^{+/-}$ mice, immunohistochemistry staining of lung sections for Galectin-3 (Figure 3.20B), which is defined as a marker for macrophages (Liu et al., 1995) was undertaken. This confirmed the reduction in the number of macrophages found in the lung of *Prmt7*$^{+/-}$ mice compared to WT mice after CS exposure (Figure 3.20B and C). Quantification of macrophage number from the lung sections was assessed by computer assisted stereological toolbox (CAST) (Eriksen et al., 2017) (Figure 3.20C). To understand the reason why macrophage numbers were decreased in *Prmt7*$^{+/-}$ mice, the expression levels of *Ccl2,* the main chemokine for macrophage recruitment to the inflamed tissue (Gregory et al., 2006) was evaluated. Interestingly, expression levels of *Ccl2* increased similarly in both WT and *Prmt7*$^{+/-}$ mice after CS exposure, excluding the possibility of reduced *Ccl2* expression causing less macrophage recruitment

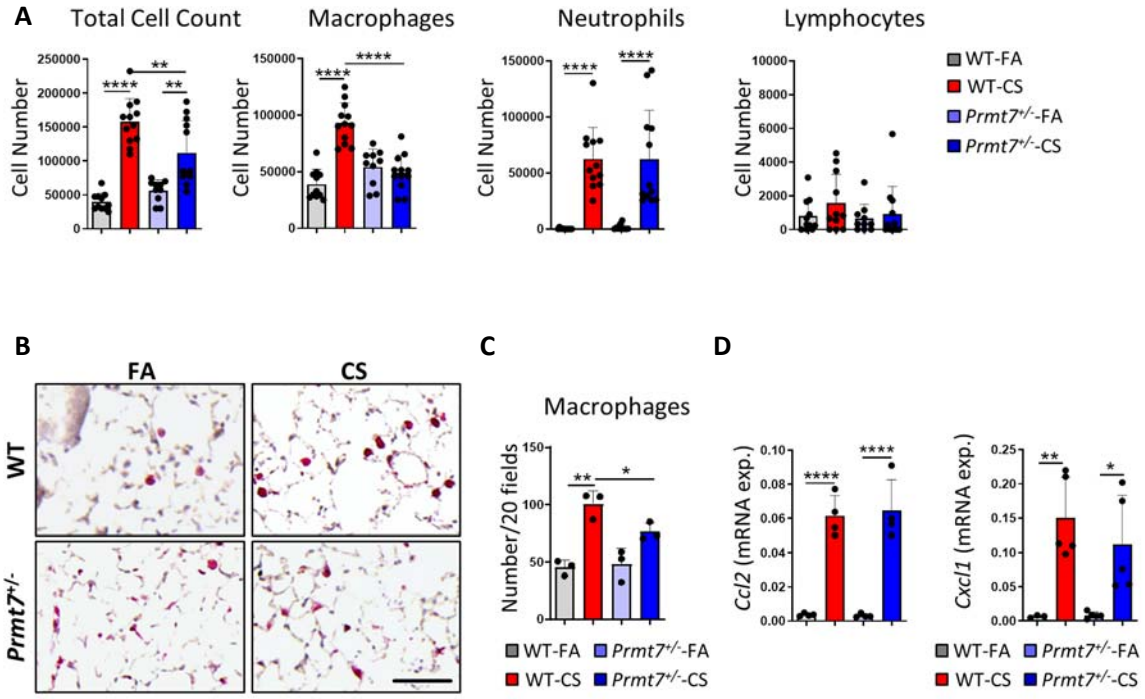

Figure 3.20 Macrophage number is reduced in the lungs of *Prmt7*$^{+/-}$ mice following acute CS exposure for 3 days. (A-D) WT and *Prmt7*$^{+/-}$ mice were exposed to filtered air (FA) or cigarette smoke (CS) for 3 days (n=4-5, three experiments). **(A)** Total inflammatory cell counts as well as macrophage, neutrophil and lymphocyte cell counts from bronchoalveolar lavage fluid (BALF). **(B)** Representative pictures of immunohistochemistry staining of lung sections for galectin-3 positive macrophages (red signal refers to galectin-3 positive macrophages). (scale bar 100µm). **(C)** Quantification of macrophage numbers from stained lung sections in each group through 20 random fields counted by CAST. **(D)** mRNA expression levels of *Ccl2* and *Cxcl1* determined by qPCR in the lungs of WT and *Prmt7*$^{+/-}$ mice with FA or CS exposure. Data shown as mean ± SD, **P* < 0.05, ***P* < 0.01, ****P* < 0.001, and *****P* < 0.0001, one-way ANOVA Bonferroni's multiple comparisons test.

(Figure 3.20D). Moreover, the expression levels of the neutrophil chemoattractant, *Cxcl1,* elevated comparably between the lungs of WT and *Prmt7*$^{+/-}$ mice post CS exposure as predicted (Figure 3.20D).

Additionally, to address if the reduction in macrophage numbers in *Prmt7*$^{+/-}$ mice after acute CS exposure for 3 days was also occurring during chronic inflammatory responses, and could potentially impact upon disease pathogenesis, mice were subjected to CS for 4 months, a well-established mouse model of COPD (Jia et al., 2018; John-Schuster et al., 2014a). Similar to what was observed after 3 days of CS exposure, quantification of immunohistochemistry staining of lung tissue sections following 4 months of chronic CS exposure for Galectin-3 demonstrated impaired macrophage numbers in *Prmt7*$^{+/-}$ mice (Figure 3.21A-B).

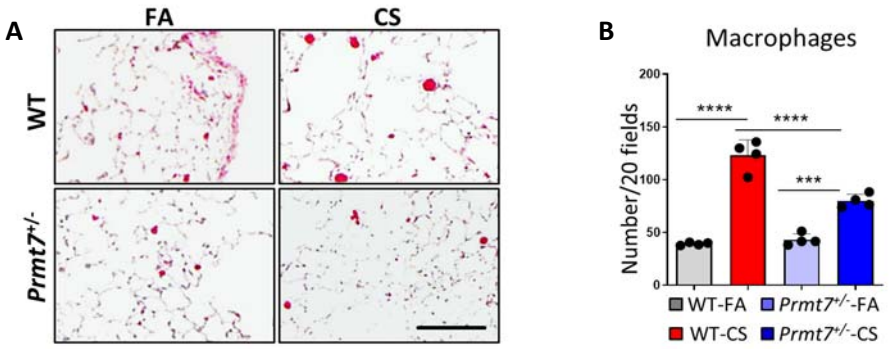

Figure 3.21 Macrophage accumulation is impaired in the lungs of *Prmt7*$^{+/-}$ mice following chronic CS exposure for 4 months. (A-B) WT and *Prmt7*$^{+/-}$ mice were exposed to filtered air (FA) or cigarette smoke (CS) for 4 months (n=4, two experiments). **(A)** Representative pictures of immunohistochemistry staining of lung sections for galectin-3 positive macrophages (red signal refers to galectin-3 positive macrophages). (scale bar 100µm). **(B)** Quantification of macrophage numbers from stained lung sections in each group through 20 random fields counted by CAST. Data shown as mean ± SD, **P* < 0.05, ***P* < 0.01, ****P* < 0.001, and *****P* < 0.0001, one-way ANOVA Bonferroni's multiple comparisons test.

Flow cytometry analysis of whole lung homogenate confirmed previous findings that total macrophages which are represented by the F480^{+} population (Dos Anjos Cassado, 2017) were reduced in *Prmt7*$^{+/-}$ mice compared to WT mice after chronic CS exposure (Figure 3.22A and B). The populations are gated according to representative plots in Figure 3.22A. Moreover, further analysis of total F480^{+} lung macrophages indicated that there was a reduction in the numbers of F480^{+}CD11b^{+} macrophages in *Prmt7*$^{+/-}$ mice in comparison to WT mice following chronic CS exposure (Figure 3.22B). CD11b helps to distinguish the monocyte-derived

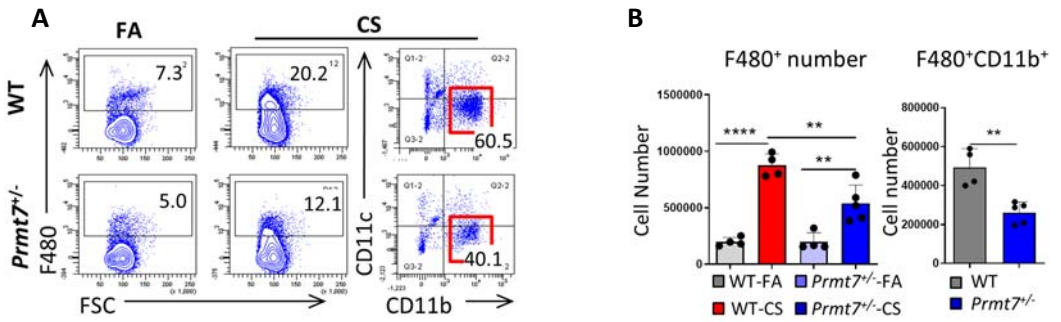

Figure 3.22 Monocyte derived macrophage number is reduced in the lungs of *Prmt7*$^{+/-}$ mice following chronic CS exposure for 4 months. (A-B) WT and *Prmt7*$^{+/-}$ mice were exposed to filtered air (FA) or cigarette smoke (CS) for 4 months (n=4, two experiments). **(A)** Representative gating strategy plots of whole lung cells. F480^{+} macrophages were gated from CD45^{+} cells and CD11b^{+} cells were gated from F480^{+} cells. **(B)** Quantification of F480^{+} macrophages as well as F480^{+} CD11b^{+} macrophages in each group from the gated populations shown in A. Data shown as mean ± SD, **P* < 0.05, ***P* < 0.01, ****P* < 0.001, and *****P* < 0.0001, one-way ANOVA Bonferroni's multiple comparisons and unpaired two-tailed Student's t test.

macrophage population from resident alveolar macrophages (Misharin et al., 2013). Therefore, these data suggested that the reduced macrophage number might originate from impaired recruitment of monocyte-derived macrophages into the lungs of *Prmt7*$^{+/-}$ mice.

To exclude that the reduction in macrophage recruitment to the lungs of *Prmt7*$^{+/-}$ mice following chronic CS exposure was caused by the lack of chemokine expression in the lungs, CCL2 and CXCL1 levels were examined. Firstly, the mRNA expression levels of *Ccl2* and *Cxcl1* were identified after chronic CS exposure by qPCR, as chemoattractants for macrophages and neutrophils, respectively. It was observed that *Ccl2* and *Cxcl1* levels were increased equally in the lungs of both WT and *Prmt7*$^{+/-}$ mice (Figure 3.23A). Moreover, since these chemoattractants are secreted into the BAL fluid, protein levels were also measured using an

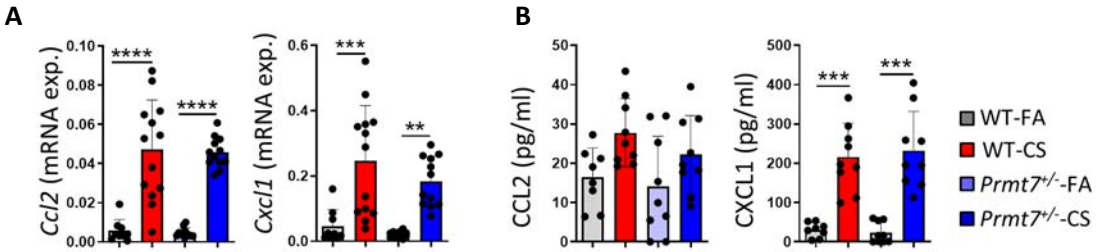

Figure 3.23 Chemokine levels are similar between the lungs of WT and *Prmt7*$^{+/-}$ mice following chronic CS exposure. (A-B) WT and *Prmt7*$^{+/-}$ mice were exposed to filtered air (FA) or cigarette smoke (CS) for 4 months (n=6-7, two experiments). **(A)** mRNA expression levels of *Ccl2* and *Cxcl1* determined by qPCR in the lungs of WT and *Prmt7*$^{+/-}$ mice. **(B)** Protein levels of CCL2 and CXCL1 determined by ELISA in the BALF of WT and *Prmt7*$^{+/-}$ mice. Data shown mean ± SD, *P < 0.05, **P < 0.01, ***P < 0.001, and ****P < 0.0001, one-way ANOVA Bonferroni's multiple comparisons test.

ELISA method. There were again similar increases in the expression of CCL2 and CXCL1 after CS exposure in both mice (Figure 3.23B). These findings indicated that the reduction of macrophage number in the lungs of *Prmt7*$^{+/-}$ mice was not derived from impaired chemoattractant levels upon chronic CS exposure.

The recruitment of immune cells including monocytes from blood vessels to tissue upon inflammatory insult also depends on adhesion molecules expressed by the endothelial cells (Ala et al., 2003). ICAM-1 and VCAM-1 are defined as two key important adhesion proteins from the immunoglobulin superfamily, which are involved in monocyte trafficking including adhesion and migration (Gerhardt and Ley, 2015). Therefore, it was next asked whether the impaired recruitment of monocyte-derived macrophages into the lungs of *Prmt7*$^{+/-}$ mice results from a deficiency in these two vital adhesion molecules. Initially, the expression levels

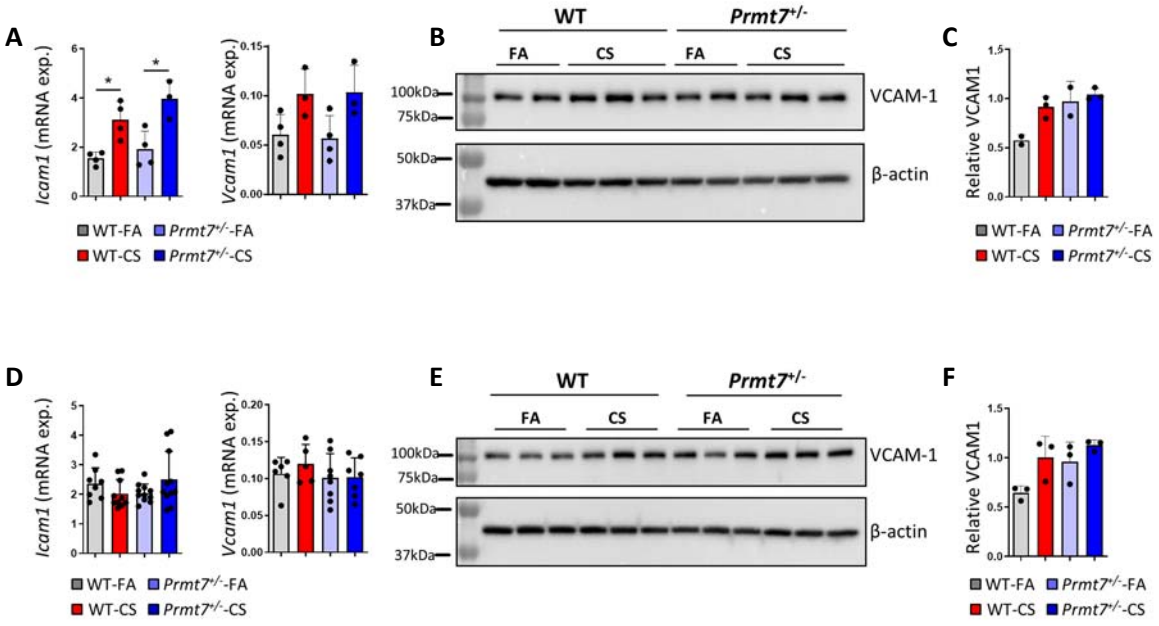

Figure 3.24 ICAM1 and VCAM1 levels are not reduced in *Prmt7*$^{+/-}$ mice following CS exposure. (A-C) WT and *Prmt7*$^{+/-}$ mice were exposed to filtered air (FA) or cigarette smoke (CS) for 3 days (n=4-5, two experiments). **(D-F)** WT and *Prmt7*$^{+/-}$ mice were exposed to filtered air (FA) or cigarette smoke (CS) for 4 months (n=6-7, two experiments). **(A)** mRNA expression levels of *Icam1* and *Vcam1* determined by qPCR in whole lungs of WT and *Prmt7*$^{+/-}$ mice upon CS exposure. **(B)** Protein levels of VCAM1 determined by Western blot analysis in the whole lungs of WT and *Prmt7*$^{+/-}$ mice upon CS exposure. **(C)** Quantification of VCAM1 levels relative to β-actin from section B. **(D)** mRNA expression levels of *Icam1* and *Vcam1* determined by qPCR in whole lungs of WT and *Prmt7*$^{+/-}$ mice upon CS exposure. **(E)** Protein levels of VCAM1 determined by Western blot analysis in the whole lungs of WT and *Prmt7*$^{+/-}$ mice upon CS exposure. **(F)** Quantification of VCAM1 levels relative to β-actin from section E. Data shown mean ± SD, *P < 0.05, **P < 0.01, ***P < 0.001, and ****P < 0.0001, one-way ANOVA Bonferroni's multiple comparisons test.

of *Icam1* and *Vcam1* were determined in the lungs of both mice when subjected to FA or CS for 3 days. Their expression did not differ between the lungs of *Prmt7*$^{+/-}$ mice compared to WT following acute CS exposure (Figure 3.24A). Similar to gene expression levels, VCAM1 protein levels were also similar in the lungs of both mice (Figure 3.24B) and western blotting quantification is performed relative to β-actin control (Figure 3.24C). Similar to what was observed in acute CS exposure, *Icam1* and *Vcam1* mRNA levels did not change between the lungs of WT and *Prmt7*$^{+/-}$ mice in response to chronic CS exposure for 4 months (Figure 3.24D). Supporting this finding, western blot analysis demonstrated that VCAM1 protein levels were also similar for WT and *Prmt7*$^{+/-}$ mice (Figure 3.24E-F).

To better understand the possible effects of PRMT7 deficiency on endothelial cell expression of ICAM1 and VCAM1, the SVEC4-10 endothelial cell line which is derived by the transformation of endothelial cells isolated from lymph node vessels with the SV40 virus (O'Connell and Edidin, 1990), were utilized in this study. SVEC4-10 cells were treated firstly with an inhibitor of PRMT7 activity, SGC3027 (Szewczyk et al., 2020) and subsequently stimulated with TNF to activate the endothelial cells. As a result of TNF stimulation, endothelial cells enhanced the expression of *Icam1* and *Vcam1* genes to a similar level regardless of PRMT7 inhibition (Figure 3.25). Considering these data suggested that the expression of key adhesion molecules including ICAM1 and VCAM1, crucial for trans-endothelial migration, did not change between WT and *Prmt7*$^{+/-}$ mice. Therefore, the reduced macrophage number in the lungs of *Prmt7*$^{+/-}$ mice following CS exposure was not caused by reduced levels of these adhesion molecules on endothelial cells or the levels of chemokines.

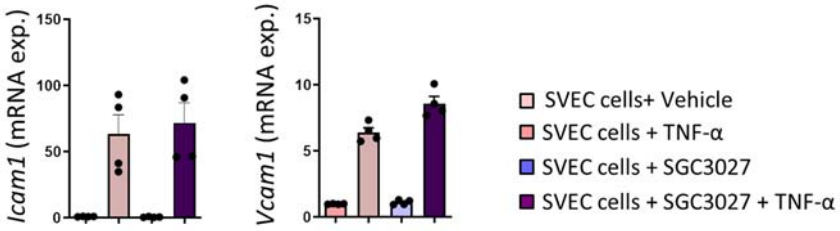

Figure 3.25 *Icam1* and *Vcam1* expression does not change with the inhibition of PRMT7 on endothelial cells. mRNA expression levels of *Icam1* and *Vcam1* determined by qPCR in endothelial cell lines, SVEC4-10, with the pretreatment of 5μM SGC3027 drug for 1h followed by 100ng TNF stimulation for 24h (n=4, two experiments).

3.3.3 *Prmt7*$^{+/-}$ mice are protected against emphysema in cigarette smoke-induced COPD model

Based on the finding that macrophage numbers in the lungs of *Prmt7*$^{+/-}$ mice were reduced following CS exposure for 4 months, it was investigated whether this reduction could affect disease development. It is well studied that chronic CS exposure in several animal models induces lung inflammation (Botelho et al., 2010) and emphysema development partly caused by macrophage derived matrix metalloproteinases and other proteases (D'Hulst et al., 2005; Jia et al., 2018; John-Schuster et al., 2014b). Considering these studies, lung damage after 4 months of CS exposure in WT and *Prmt7*$^{+/-}$ mice was examined. Hematoxylin and eosin staining of lung tissue sections showed that emphysema development was enhanced in the lungs of WT mice however, significantly CS-induced emphysema was prevented in the lungs of *Prmt7*$^{+/-}$ mice (Figure 3.26A). This observation was quantified by stereological analysis of lung tissue for airspace enlargement via the CAST system and airspace enlargement was significantly diminished in the lungs of *Prmt7*$^{+/-}$ mice post CS exposure compared to WT lungs (Figure 3.26B). Moreover, this reduction in emphysema development was supported by improved lung function. Diffusion capacity of *Prmt7*$^{+/-}$ mice did not show any impairment compared to WT mice after CS exposure (Figure 3.26C). Furthermore, small airway remodeling is also an important hallmark of COPD pathogenesis and characterized mainly by collagen deposition and fibrosis of the airways (Higham et al., 2019; James and Wenzel, 2007). Therefore, collagen deposition around small airways in the lungs of WT and *Prmt7*$^{+/-}$ mice was examined in lung tissue sections stained with Masson´s Trichrome. WT mice had increased amounts of collagen deposition whereas the lungs of *Prmt7*$^{+/-}$ mice produced significantly less collagen around the airways following CS exposure compared to WT lungs (Figure 3.26D and E). In summary, here it is clearly demonstrated that *Prmt7*$^{+/-}$ mice were protected against the development of COPD with less emphysematous and fibrotic phenotype and improved lung function.

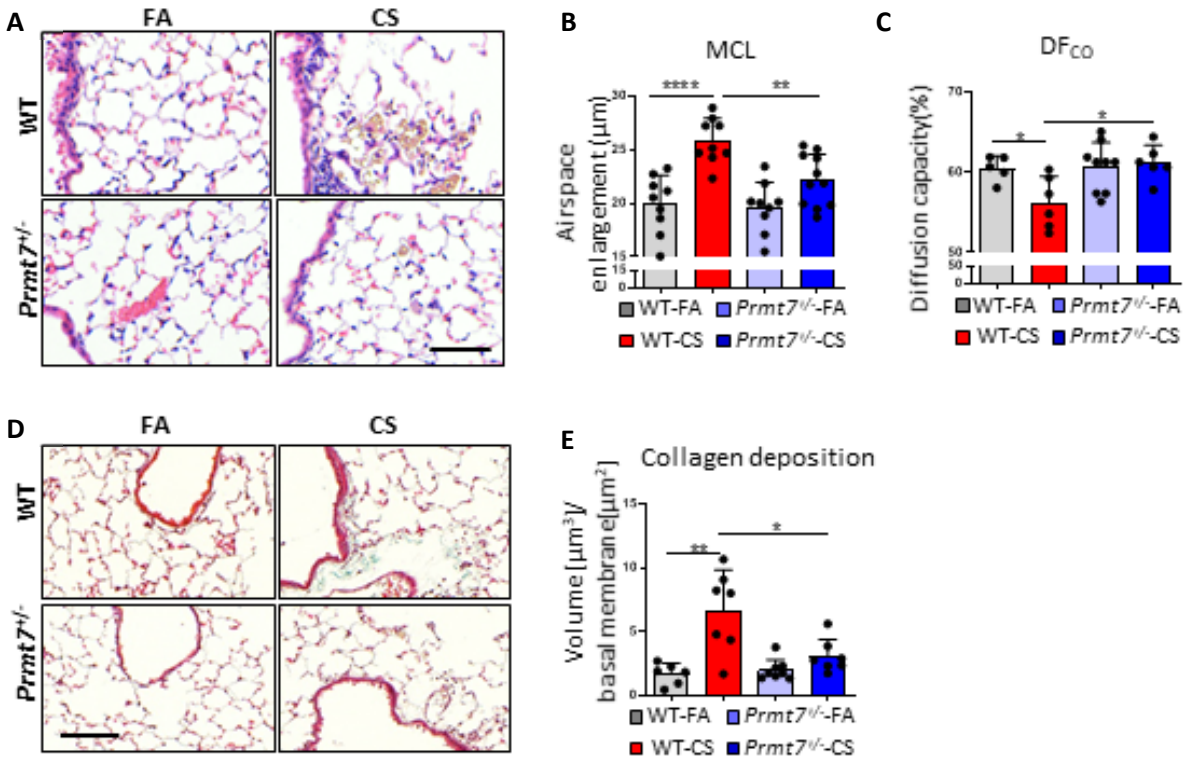

Figure 3.26 *Prmt7*$^{+/-}$ mice are protected against COPD development in response to chronic CS exposure. (A-E) WT and *Prmt7*$^{+/-}$ mice were exposed to filtered air (FA) or cigarette smoke (CS) for 4 months (n=5-10, two experiments). **(A)** Representative pictures of H&E staining of lung tissue sections from WT and *Prmt7*$^{+/-}$ mice (scale bar 50µm). **(B)** Quantification of airspace enlargement in terms of mean chord length in µm via CAST system. **(C)** Diffusion capacity measurement of carbon monoxide (CO) to determine the lung function. **(D)** Representative pictures of Masson trichrome staining of lung tissue sections from WT and *Prmt7*$^{+/-}$ mice (scale bar 50µm). **(E)** Quantification of collagen deposition volume (µm^3) per defined area (µm^2) via CAST system in lung sections of WT and *Prmt7*$^{+/-}$ mice stained with Masson´s Trichrome. Data shown as mean ± SD, **P* < 0.05, ***P* < 0.01, ****P* < 0.001, and *****P* < 0.0001, one-way ANOVA Bonferroni's multiple comparisons test.

3.3.4 Macrophage accumulation is impaired in the lungs of *Prmt7*$^{+/-}$ mice following PPE exposure

To validate the findings from the CS-induced COPD model, an independent model of emphysematous COPD, which is driven by macrophages in response to a single dose of porcine pancreatic elastase (PPE) instillation (Antunes and Rocco, 2011; Ghorani et al., 2017), was analysed. Elastase is secreted mainly by activated neutrophils in the lungs and causes damage to alveolar tissue as a proteolytic enzyme (Janoff, 1985). Therefore, the principle of elastase instillation in the mouse model is to induce an inflammatory responses resulting in lung tissue damage and the development of emphysema, mimicking what is seen in COPD

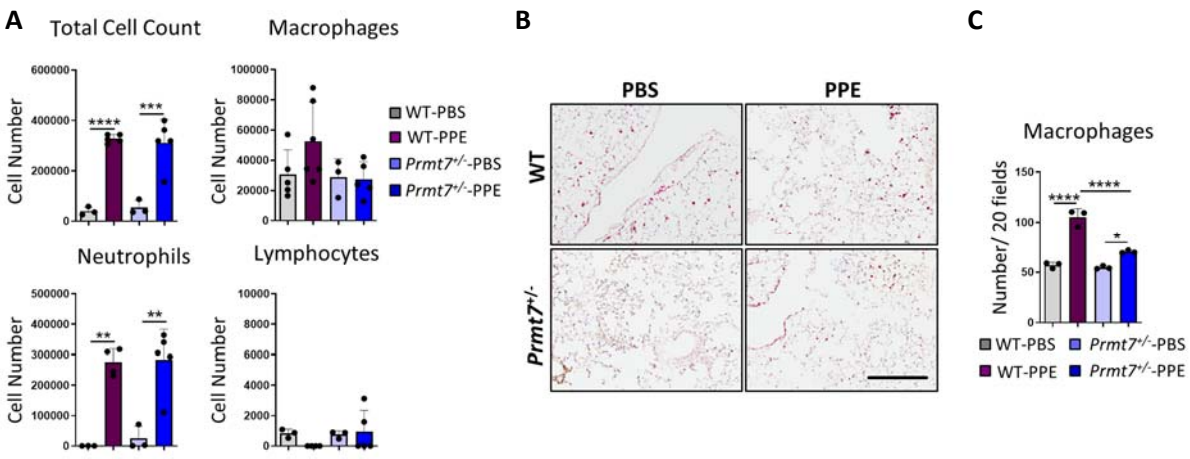

Figure 3.27 Macrophage number is reduced in the lungs of *Prmt7*$^{+/-}$ mice following acute PPE exposure for 24h. (A-C) WT and *Prmt7*$^{+/-}$ mice were treated with a single oropharyngeal application of PBS or porcine pancreatic elastase (PPE) 40U/Kg for 24h (n=3-5). **(A)** Total cell count as well as macrophage, neutrophil and lymphocyte cell counts from bronchoalveolar lavage fluid (BALF) of WT and *Prmt7*$^{+/-}$ mice after PPE or PBS instillation. **(B)** Representative pictures of immunohistochemistry stainings of lung sections with Galectin-3 antibody to stain macrophages (red signal refers Galectin-3 positive) (scale bar 200µm). **(C)** Quantification of macrophage numbers from stained lung sections in each group through 20 random fields counted by CAST. Data shown as mean ± SD, **P* < 0.05, ***P* < 0.01, ****P* < 0.001, and *****P* < 0.0001, one-way ANOVA Bonferroni's multiple comparisons test.

(Bonfield, 2012; Ghorani et al., 2017). As a result of an acute exposure to porcine pancreatic elastase (PPE) for 24h, similar findings to CS-exposure were observed in which *Prmt7*$^{+/-}$ mice had less macrophages, whereas the numbers of neutrophils and lymphocytes remained the same as the lungs of WT mice subjected to PPE (Figure 3.27A). Immunohistochemistry staining of lung sections also confirmed that the amount of Galectin-3 expressing macrophages was significantly elevated after PPE instillation following 24h in the lungs of WT mice however, this increase was clearly impaired in *Prmt7*$^{+/-}$ mice (Figure 3.27B-C). Quantification was performed using the CAST system.

To confirm these findings, WT and *Prmt7*$^{+/-}$ mice were subjected to PPE with a single dose instillation and examined after 28 days. Similar to previous results, macrophage numbers counted in the BALF from the lungs of *Prmt7*$^{+/-}$ mice were again reduced in comparison to WT controls (Figure 3.28A) and immunohistochemistry staining of lung sections against Galectin-3 confirmed this observation, by revealing that Galectin-3 positive macrophage numbers did not increase in the lungs of *Prmt7*$^{+/-}$ mice following PPE exposure (Figure 3.28B-C).

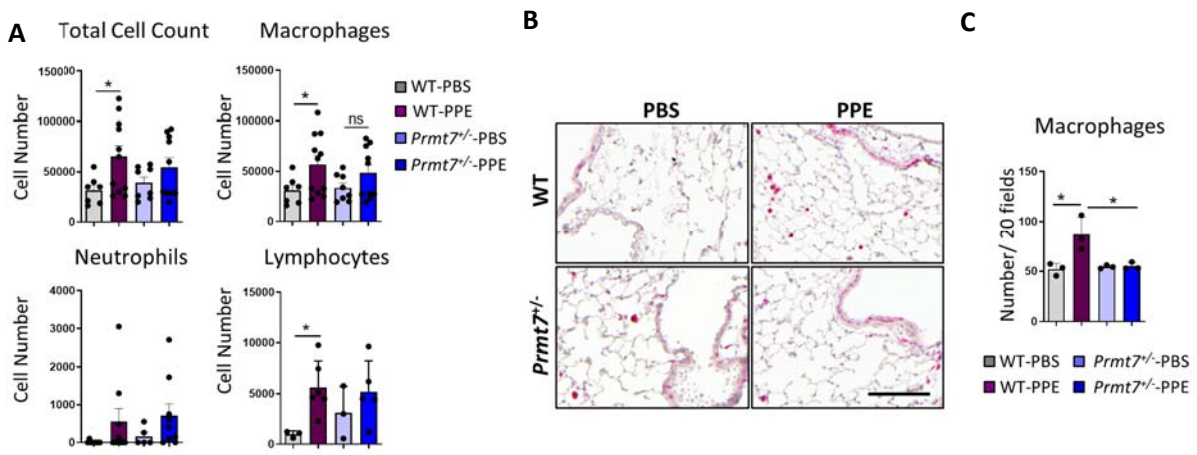

Figure 3.28 Macrophage number is reduced in the lungs of *Prmt7*$^{+/-}$ mice following chronic PPE exposure for 28 days. (A-C) WT and *Prmt7*$^{+/-}$ mice were treated with a single oropharyngeal application of PBS or porcine pancreatic elastase (PPE) 40U/Kg for 28 days (n=4-6, two experiments). **(A)** Total cell count as well as macrophage, neutrophil and lymphocyte cell counts from bronchoalveolar lavage fluid (BALF) of WT and *Prmt7*$^{+/-}$ mice after PPE or PBS instillation. **(B)** Representative pictures of immunohistochemistry stainings of lung sections with Galectin-3 antibody to stain macrophages (red signal refers Galectin-3 positive) (scale bar 200µm). **(C)** Quantification of macrophage numbers from stained lung sections in each group through 20 random fields counted by CAST. Data shown as mean ± SD, **P* < 0.05, ***P* < 0.01, ****P* < 0.001, and *****P* < 0.0001, one-way ANOVA Bonferroni's multiple comparisons test.

3.3.5 *Prmt7*$^{+/-}$ mice are protected from emphysema in the PPE-induced COPD model

To comprehend the role of PRMT7 in elastase-induced COPD progression, emphysema development was compared between WT and *Prmt7*$^{+/-}$ mice following 28 days of a single instillation of PPE. After 28 days when WT mice demonstrated clear signs of emphysema observed by destruction of alveolar structures, *Prmt7*$^{+/-}$ mice were again protected from emphysema development (Figure 3.29A). The quantification of airspace enlargement which defines the severity of emphysema development can be seen in Figure 3.29B. This observation was accompanied by improved lung function since forced vital capacity did not elevate in *Prmt7*$^{+/-}$ mice as much as it did in WT controls following PPE treatment (Figure 3.29C).

In conclusion, taking all data into consideration, these findings suggested that PRMT7 is crucial for the recruitment of macrophages into the lung following inflammatory insult. Therefore, PRMT7 plays a critical role in the progression of macrophage-driven emphysematous COPD in the lungs of both CS and PPE-exposed mice.

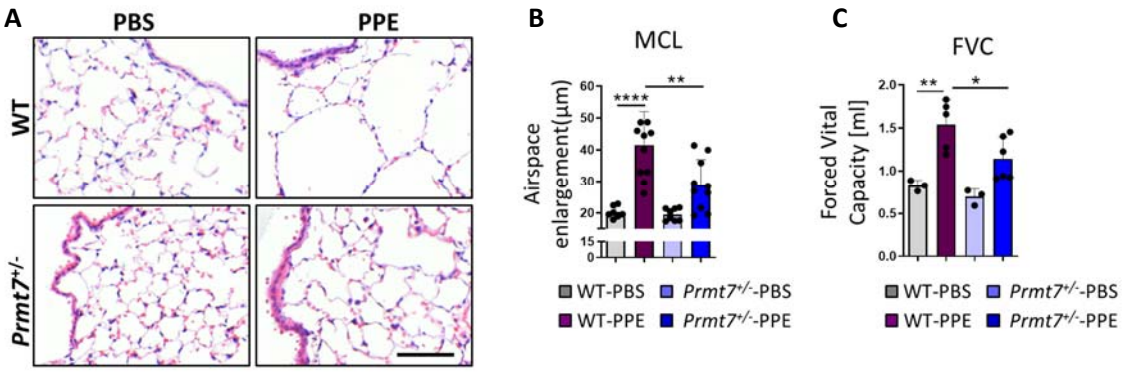

Figure 3.29 *Prmt7*$^{+/-}$ mice are protected against COPD development in response to chronic PPE exposure. (A-C) WT and *Prmt7*$^{+/-}$ mice were treated with a single oropharyngeal application of PBS or porcine pancreatic elastase (PPE) 40U/Kg for 28 days (n=4-6, two experiments). **(A)** Representative pictures of H&E stainining of lung tissue sections from WT and *Prmt7*$^{+/-}$ mice (scale bar 50µm). **(B)** Quantification of airspace enlargement in terms of mean chord length in µm via CAST system. **(C)** Forced vital capacity (FVC) measurement to determine lung function. Data shown as mean ± SD, **P* < 0.05, ***P* < 0.01, ****P* < 0.001, and *****P* < 0.0001, one-way ANOVA Bonferroni's multiple comparisons test.

3.3.6 PRMT7 regulates monocyte-derived macrophage recruitment into the lungs

Previous findings in this study already confirmed that macrophage accumulation in the lungs of *Prmt7*$^{+/-}$ mice was impaired when there is an inflammatory insult. The next question was to understand whether these macrophages were monocyte-derived, as suggested by the flow cytometry data of reduced CD11b^{+} macrophages in the lungs of *Prmt7*$^{+/-}$ mice subjected to chronic CS. To distinguish the role of monocyte-derived macrophages from resident macrophages in emphysema development, the orthotopic lung transplantation model (Smirnova et al., 2019) was used. This model is well described to comprehend immune mediated events that cause rejection after lung transplantation (Jungraithmayr et al., 2009). However, importantly for this study donor lungs retain resident alveolar macrophages during lung transplantation (Nayak et al., 2016). In this study, firstly left lungs from WT mice were transplanted into WT or *Prmt7*$^{+/-}$ recipients. All recipients were left for 3 weeks to recover from surgery and then they were exposed to a single dose of PPE. The experimental design is described in Figure 3.30A. Consistent with previous findings, macrophage recruitment was impaired in WT lungs transplanted into *Prmt7*$^{+/-}$ recipients, but not those transplanted into

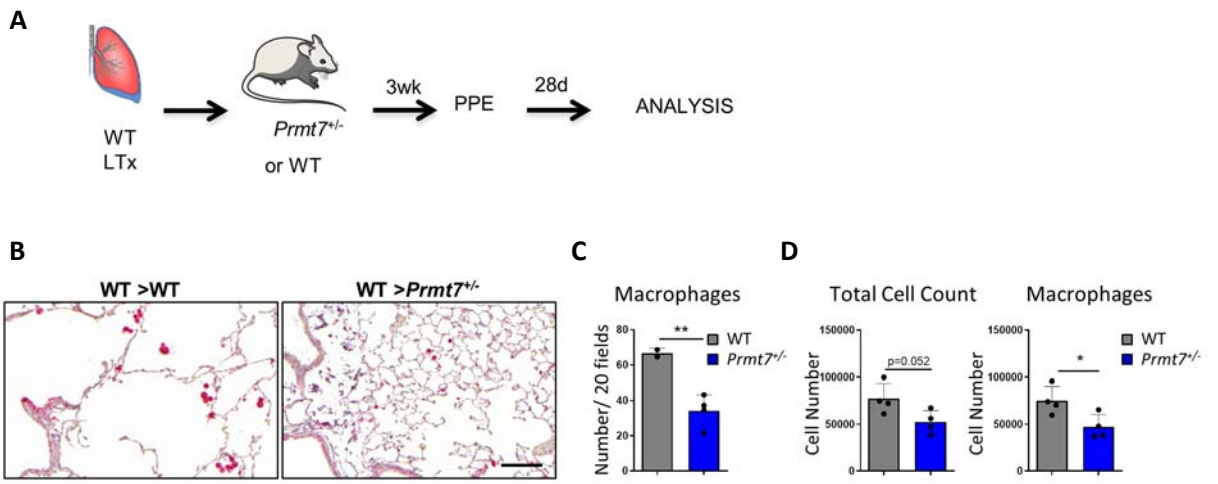

Figure 3.30 Wild-type lungs transplanted into *Prmt7*$^{+/-}$ mice had reduced macrophage recruitment. (A-D) Left lungs of WT mice were transplanted into WT or *Prmt7*$^{+/-}$ recipients and they were exposed to a single dose of PPE, 40U/K, after 3 weeks from surgery. PPE exposed mice were analysed 28 days later (n=4). **(A)** The design of the experiment. **(B)** Immunohistochemisty staining images of lung sections from transplanted lungs for Galectin-3 positive macrophages (red signal represents galectin-3 positive cells) (scale bar 100µm). **(C)** Quantification of macrophage numbers from stained sections of transplanted lungs in each group through 20 random fields counted by CAST. **(D)** Total cell count as well as macrophage cell count from bronchoalveolar lavage fluid (BALF) of WT and *Prmt7*$^{+/-}$ recipients. Data shown mean ± SD, *P < 0.05 and **P < 0.01 unpaired two-tailed Student's t test.

WT recipients (Figure 3.30B and C). Additionally, cell counts from broncoalveolar lavage fluid also confirmed that *Prmt7*$^{+/-}$ recipients had reduced numbers of macrophages (Figure 3.30D).

Crucially, reduced macrophage numbers in *Prmt7*$^{+/-}$ recipients were accompanied by protection from emphysema development (Figure 3.31A). Airspace enlargement was quantified by stereological analysis confirming that emphysema development was reduced

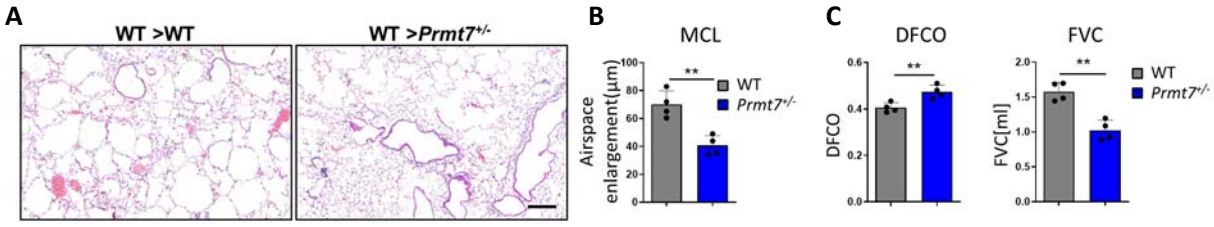

Figure 3.31 Wild-type lungs transplanted into *Prmt7*$^{+/-}$ mice are protected from elastase-induced emphysema.(A-C) Left lungs of WT mice were transplanted into WT or *Prmt7*$^{+/-}$ recipients and they were exposed to a single dose of PPE, 40U/K, after 3 weeks from surgery. PPE exposed mice were analysed 28 days later (n=4). **(A)** Hematoxylin and Eosin stained images of lung sections from transplanted lungs (scale bar 200µm). **(B)** Quantification of airspace enlargement in terms of mean chord length in µm via CAST system. **(C)** Diffusion capacity of carbon monoxide (CO) and Forced vital capacity (FVC) measuremesnt to determine lung function. Data shown as mean ± SD, *P < 0.05 and **P < 0.01 unpaired two-tailed Student's t test.

in *Prmt7*$^{+/-}$ recipients compared to WT recipients (Figure 3.31B). Diffusion capacity and forced vital capacity were also improved in *Prmt7*$^{+/-}$ recipients (Figure 3.31C). These data clearly suggested that monocyte-derived macrophages but not resident macrophages play a central role in disease pathogenesis and *Prmt7*$^{+/-}$ mice were protected against emphysema development by reduced recruitment of monocyte-derived macrophages.

To support the idea that the recruitment of monocyte-derived macrophages into the lungs of *Prmt7*$^{+/-}$ mice was impaired, trans-endothelial migration assays were performed. Primary monocytes isolated from the bone marrow of *Prmt7*$^{+/-}$ mice demonstrated impaired trans-endothelial migration compared to WT controls towards the chemokine CCL2, which is the main chemokine for macrophage recruitment (Figure 3.32A). Even though migration through CCL2 was disrupted, CCR2, the receptor of the CCL2 ligand, surface expression levels on monocytes from WT and *Prmt7*$^{+/-}$ did not differ, suggesting that the deficient migration was not caused by reduced surface levels of CCR2 (Figure 3.32B).

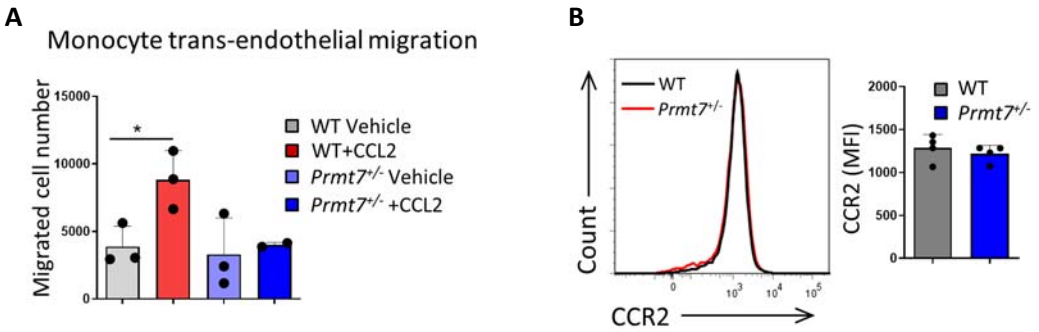

Figure 3.32 PRMT7 regulates monocyte recruitment. (A) The number of monocytes which were migrated through CCL2 ligand as a result of trans-endothelial migration assay. The monolayer was formed with SVEC endothelial cells and they were activated with 10ng/ml TNF before migration. Monocytes isolated from WT and *Prmt7*$^{+/-}$ mice were migrated through endothelial cells towards +/- 100ng/ml of CCL2 (n=3, three experiments). **(B)** Flow cytometry anaylsis of CCR2 surface expression on monocytes isolated from WT and *Prmt7*$^{+/-}$ mice. The graph shows mean fluorescent intensity of CCR2 levels in monoyctes from both mice (n=4). Data shown as mean ± SD, **P* < 0.05, ***P* < 0.01, ****P* < 0.001, and *****P* < 0.0001, one-way ANOVA Bonferroni's multiple comparisons test.

3.3.7 Macrophages from *Prmt7*$^{+/-}$ mice develop and function normally

To exclude the possibility of impaired macrophage development as a reason for reduced recruitment of macrophages into the lungs of *Prmt7*$^{+/-}$ mice following exposure to CS or PPE, the subpopulations of bone marrow derived macrophages and their polarization behavior

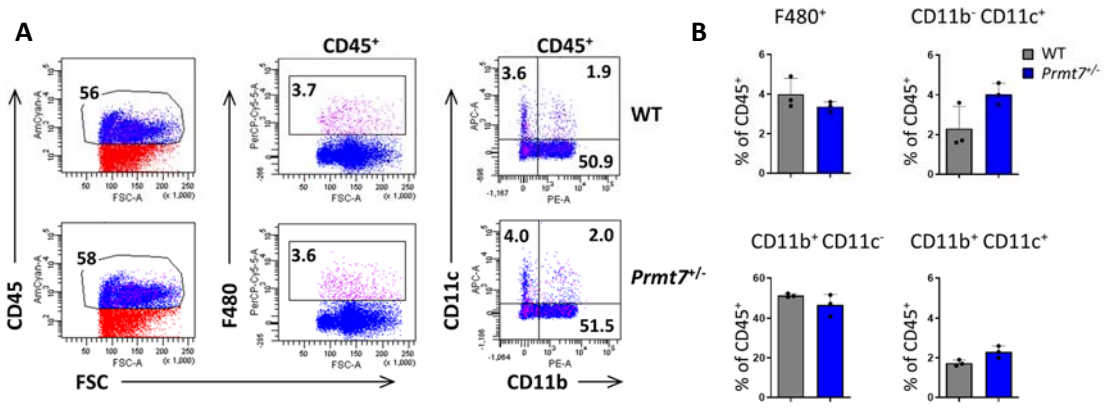

Figure 3.33 The development of macrophages from WT and *Prmt7*$^{+/-}$ mice is similar. (A-B) Flow cytometry analysis of freshly isolated bone marrow single cell suspensions from WT and *Prmt7*$^{+/-}$ mice. **(A)** Representative FACS plots showing the gates with CD45, F480, Cd11b, CD11c surface markers to evaluate different subpopulations of macrophages. **(B)** Quantification of F480^{+}, CD11b^{-}CD11c^{+}, CD11b^{+}CD11c^{-} and CD11b^{+}CD11c^{+} macrophages from A (n=3).

was examined. To do so, flow cytometric analysis using the cell surface markers CD45, F480, CD11b and CD11c was performed upon bone marrow derived macrophages (BMDMs) from WT and *Prmt7*$^{+/-}$ mice to distinguish subpopulations (Figure 3.33A). Total macrophage numbers defined by F480 did not differ between freshly isolated bone marrow of WT and *Prmt7*$^{+/-}$ mice. Moreover, the subpopulation of macrophages such as CD11b^{-}CD11c^{+}, CD11b^{+}CD11c^{-} and CD11b^{+}CD11c^{+} in freshly isolated bone marrow did not show any differences between WT and *Prmt7*$^{+/-}$ mice (Figure 3.33B).

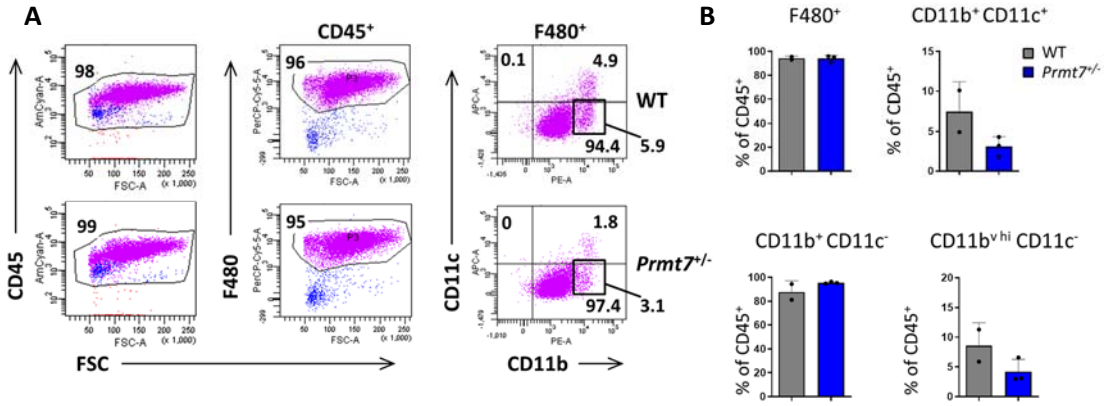

Figure 3.34 The development and differentiation of macrophages from WT and *Prmt7*$^{+/-}$ mice is similar. (A-B) Flow cytometry analysis of bone marrow derived macrophages (7-day differentiation) from WT and *Prmt7*$^{+/-}$ mice *in vitro*. **(A)** Representative FACS plots showing the gates with CD45, F480, Cd11b, CD11c surface markers to evaluate different subpopulations of macrophages. **(B)** Quantification of F480^{+}, CD11b^{-}CD11c^{+}, CD11b^{+}CD11c^{-} and CD11b^{+}CD11c^{+} macrophages from A (n=2-3).

Consistent with this finding, *in vitro* differentiation of BMDMs over 7 days did not reveal any differences in macrophage subsets across WT and *Prmt7*$^{+/-}$ mice (Figure 3.34A-B). The gating strategy and surface markers were identical to the ones in Figure 3.33. This data suggested that neither freshly isolated nor differentiated macrophages *in vitro* showed differences between WT and *Prmt7*$^{+/-}$ mice.

Since the polarization of macrophages into M1 and M2 phenotypes is crucial for their function and disease pathogenesis (Shapouri-Moghaddam et al., 2018), the next step was to analyze and compare the polarization between WT and *Prmt7*$^{+/-}$ mice. iNOS and IL1β are known as pro-M1 genes induced by classically activated macrophages whereas Fizz1 and Arg1 are reported as M2 macrophage markers (Orecchioni et al., 2019). In our study, polarization of mature BMDMs to M1 and M2 phenotypes was quite similar in WT and *Prmt7*$^{+/-}$ BMDMs (Figure 3.35).

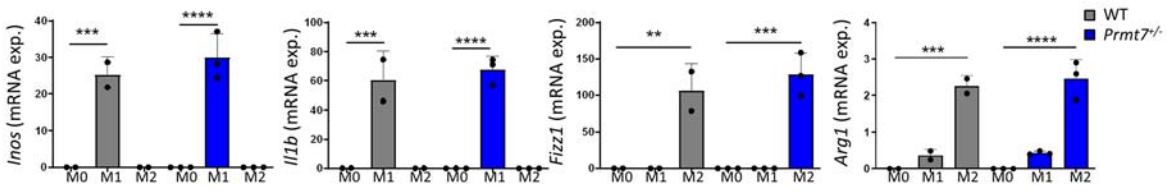

Figure 3.35 Macrophage polarization is similar in WT and *Prmt7*$^{+/-}$ mice. mRNA expression levels of *Inos*, *Il1b, Fizz1* and *Arg1* to assess M1 and M2 polarization of BMDMs isolated from WT (n=2) and *Prmt7*$^{+/-}$ mice (n=3). It is determined by qPCR. Data shown mean ± SD, $^{**}P < 0.01$, $^{***}P < 0.001$, and $^{****}P < 0.0001$, one-way ANOVA Bonferroni's multiple comparisons test.

3.3.8 Dendritic cells from *Prmt7*$^{+/-}$ mice develop and function normally

Considering the potential role of dendritic cells (DCs) as mediators of inflammation in COPD pathogenesis (Givi et al., 2012), as well as having a common bi-potent progenitor with macrophages in the bone marrow (Cheong et al., 2010; Paul et al., 2015; Schraml and Reis e Sousa, 2015), it was necessary to understand whether PRMT7 deficiency could affect DCs and their activation. The gating of bone marrow derived dendritic cells of WT and *Prmt7*$^{+/-}$ mice can be seen in Figure 3.36A. The ratio of DC populations ($CD11c^{+}$ $MHCII^{+}$ $CD11b^{lo}$) did not show any differences between WT and *Prmt7*$^{+/-}$ mice (Figure 3.36B). Moreover, there was

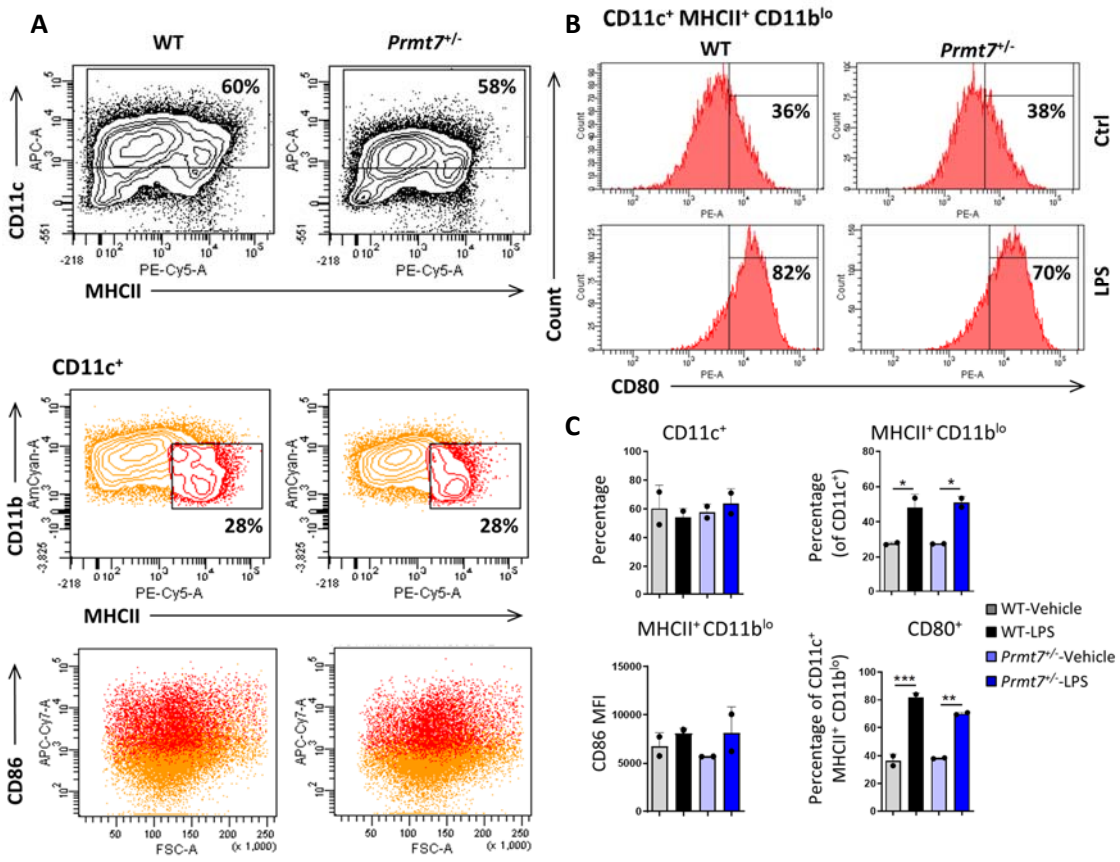

Figure 3.36 DC development and differentiation is similar in WT and *Prmt7*$^{+/-}$ mice. (A) Representative flow cytometry plots of bone marrow derived dendritic cells isolated and differentiated from WT and *Prmt7*$^{+/-}$ mice for 7 days gated with CD11c, MHCII, CD11b and CD86 markers. **(B)** Flow cytometry plot of CD80 MFI of CD11c^{+} MHCII^{+} CD11b^{lo} BMDCs stimulated with LPS**. (C)** Quantification of the percentage of CD11c^{+}, MHCII^{+} Cd11b^{lo} and CD80^{+} DCs and quantification of MFI of CD86^{+} DCs upon LPS treatment. Data shown as mean ± SD, $^{**}P < 0.01$, $^{***}P < 0.001$, and $^{****}P < 0.0001$, one-way ANOVA Bonferroni's multiple comparisons test.

also no difference in CD80 and CD86 surface activation marker levels post LPS activation in WT and *Prmt7*$^{+/-}$ mice following flow cytometric analysis (Figure 3.36C).

Consistently, upon LPS stimulation, expression levels of genes involved in DC activation including *Tnf*, *Il12p35*, *Cd86* did not exhibit any differences between WT and *Prmt7*$^{+/-}$ mice even though *Prmt7* expression was highly reduced in these DCs (Figure 3.37). As a result of these findings, one can conclude that PRMT7 deficiency does not alter the development and function of macrophages and dendritic cells.

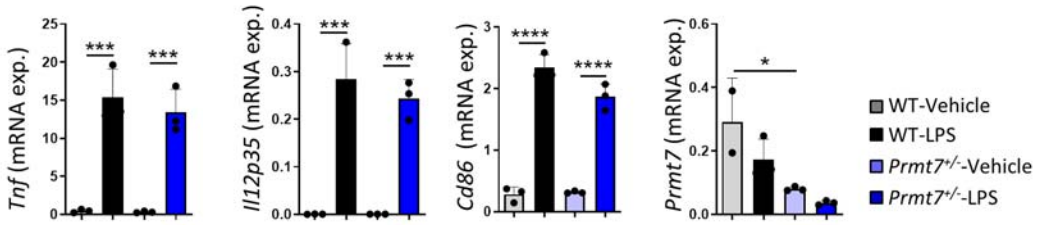

Figure 3.37 The activation of DCs is same in WT and *Prmt7*$^{+/-}$ mice. mRNA expression levels of *Tnf*, *Il12p35*, *Cd86* and *Prmt7* of DCs isolated from WT and *Prmt7*$^{+/-}$ mice. It was determined by qPCR upon LPS treatment (n=3 per group). Data shown mean ± SD, ***P* < 0.01, ****P* < 0.001, and *****P* < 0.0001, one-way ANOVA Bonferroni's multiple comparisons test.

3.3.9 The trans-differentiation of ATII cells into ATI cells is not affected by the absence of PRMT7

Earlier immunofluorescence staining results of mouse lung tissue (Figure 3.8) revealed that some Pro-SPC positive alveolar type II (ATII) cells also expressed PRMT7. This suggests that ATII cells in the lung may also be affected by PRMT7 deficiency. To support the function of PRMT7 in macrophages contributing to the pathogenesis of COPD rather than lung parenchyma, the trans-differentiation of primary ATII cells isolated from WT and *Prmt7*$^{+/-}$ mice into ATI cells was evaluated. ATII cells function as the progenitor cells for ATI cells following any damage, and play a key role in repair and regeneration processes of the lung epithelial barrier (Zhao et al., 2010). Interestingly, ATII cells from both WT and *Prmt7*$^{+/-}$ mice trans-differentiate into ATI cells similarly (Figure 3.38), as determined by western blot analysis to evaluate T1-alpha protein levels as a marker for ATI cell differentiation (Ramirez et al., 2003).

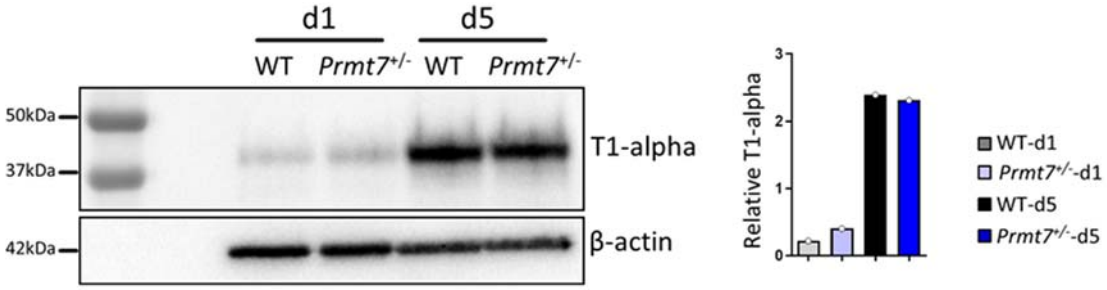

Figure 3.38 Reduced PRMT7 levels does not influence ATII cell differentiation into ATI cells. T1-alpha protein levels determined by western blot analysis at day1 and day5 after culturing alveolar type II cells isolated from WT and *Prmt7*$^{+/-}$ mice. T1-alpha is used as a marker for ATI cell differentiation. Quantification was done relative to β-actin levels (3 mice were used).

As discussed above, the trans-differentiation of ATII to ATI cells to restore alveolar structure and function is a key response to lung injury (Olajuyin et al., 2019). ATII cell activation promotes repairing and regeneration processes when lung injury occurs. In the light of this, the next step was to compare the abilities of ATII cells to repair wounds when PRMT7 expression is silenced. Therefore, siRNA knock-down of *Prmt7* in the murine ATII cell line MLE12 was performed (Figure 3.39A). However, cells did not alter their capability to repair wounds in a scratch assay following knock-down of *Prmt7* (Figure 3.39B). The wound closure was measured and calculated after 6 hours and 24 hours (Figure 3.39C). Taken together, these results suggested that the protection against emphysema observed in *Prmt7*$^{+/-}$ mice resulted from the impaired recruitment of monocyte-derived macrophages to the lungs, and not from impaired functions of lung parenchyma cells.

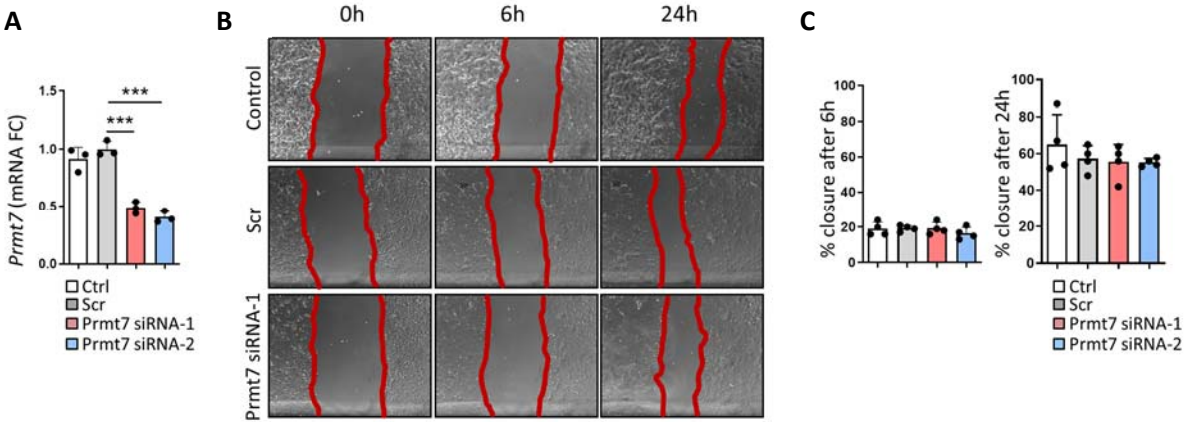

Figure 3.39 Reduced PRMT7 levels do not affect repair ability of ATII cells. (A) mRNA expression levels of *Prmt7* in the murine alveolar type II cell line, MLE12 cells, treated with scramble siRNA (Scr), two different siRNAs which target *Prmt7* gene or without any treatment (Ctrl) (n=3). **(B)** Representative images for wound healing assay using 3 different cells including control MLE12 cells, MLE12 cells treated with scrambled siRNA or treated with siRNA targetting Prmt7 gene 6h nd 24h after scratch was generated (n=4). Wound was highlighted in red. **(C)** Quantification of wound closure after 6h and 24h of scratch by measuring the wound surface area in each cell type to determine the wound closure after 6h and 24h. Data shown mean ± SD, ***$P < 0.001$ unpaired two-tailed Student's t test.

3.4 Identification of how PRMT7 mechanistically regulates macrophages in COPD

3.4.1 Generation of CRISPR/Cas9 targeted knock-out of *Prmt7* in MHS cells

To fully understand the mechanisms contributing to the impaired recruitment of macrophages into the lungs of *Prmt7*$^{+/-}$ mice, CRISPR/Cas9-mediated knockout of *Prmt7* in the MHS cell line, was undertaken in collaboration with Dr. Benoit Piavaux, to completely

abolish PRMT7 function. CRISPR/Cas9-mediated knockout of *Prmt7* was generated by targeting exon 2 of the *Prmt7* gene, using CRISPR guide A and B shown in Figure 3.40A and described in the methods, to obtain *Prmt7*^{null} cells (Figure 3.40B). A deletion of the mutation target region was confirmed by running PCR products (Figure 3.40B). The sequenced regions of *Prmt7*$^{+/+}$ MHS cells and *Prmt7*^{null} MHS cells were demonstrated in Figure 3.40C. The deleted region in *Prmt7*^{null} MHS cells are labelled in red (Figure 3.40C).

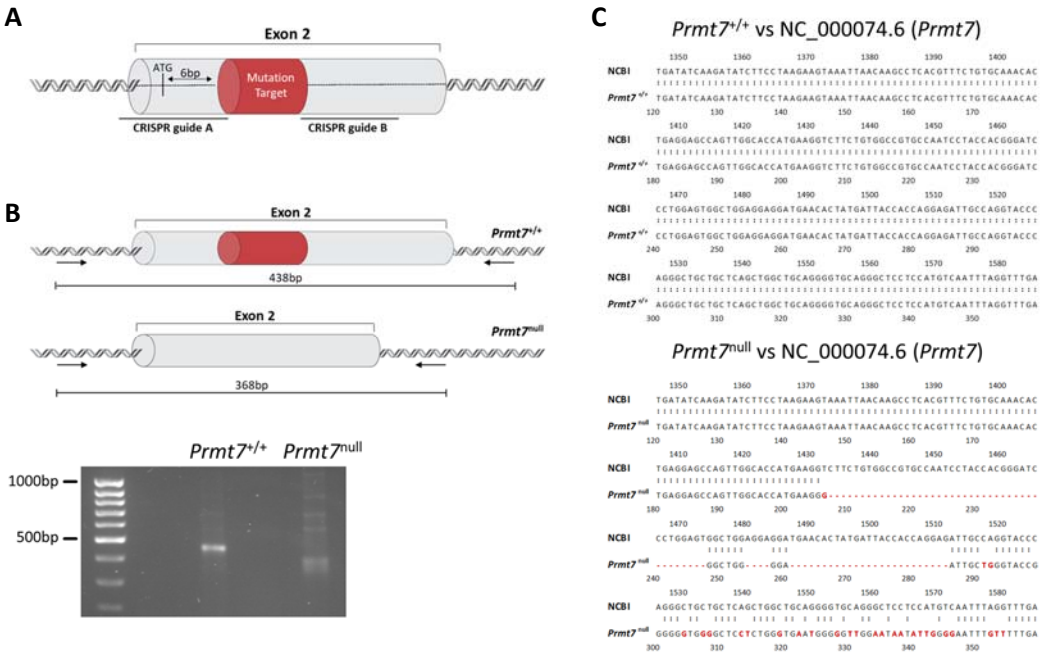

Figure 3.40 CRISPR/Cas9 knockout system targets exon 2 of *Prmt7* gene in MHS cell line. (A) Design of CRISPR guides A and B sequences targeting mutation region shown in red in exon 2 of *Prmt7* gene. **(B)** The representative DNA sequences of *Prmt7*$^{+/+}$ and *Prmt7*^{null} MHS cells with 438bp and 368bp, respectively. PCR of genomic DNA of these two cell lines. **(C)** Genomic DNAs of *Prmt7*$^{+/+}$ and *Prmt7*^{null} MHS cells confirming the deletion in exon 2. Deleted sequences shown in red.

The deficiency in PRMT7 was confirmed by qPCR revealing that *Prmt7*^{null} MHS cells depleted mRNA expression completely (Figure 3.41A). Western blot analysis showed that *Prmt7*^{null} MHS cells also lack expression of the PRMT7 protein (Figure 3.41B). Total mono-methylation (MMA) levels of proteins is a good indicator of the catalytic function of PRMT7. Therefore, mono-methylation levels in *Prmt7*$^{+/+}$ and *Prmt7*^{null} MHS cells were checked. Reduced arginine mono-methylation of multiple proteins was observed, highlighting functional impairment in these cells in the absence of PRMT7 (Figure 3.41C).

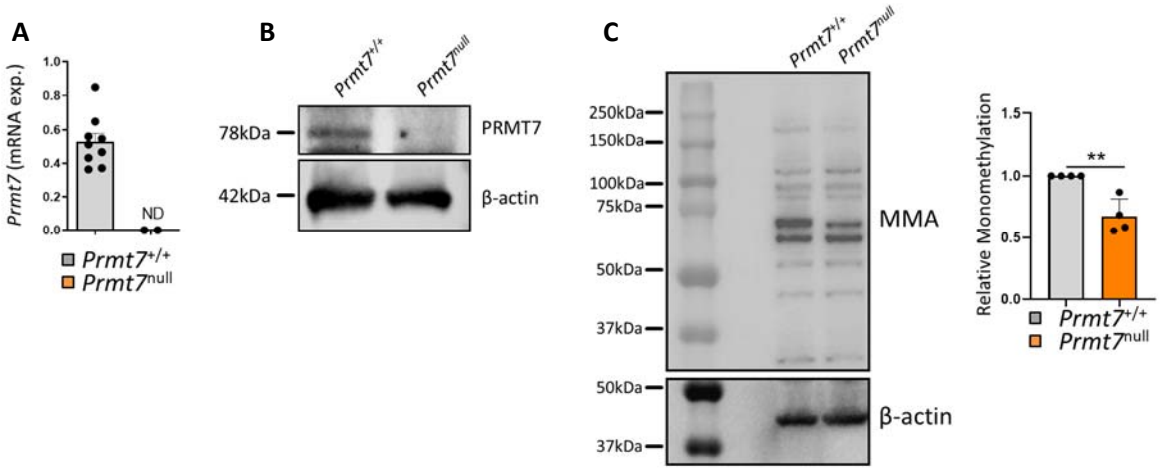

Figure 3.41 Validation of PRMT7 deficiency in MHS cell line. (A) mRNA expression level of *Prmt7* determined by qPCR in *Prmt7*$^{+/+}$ and *Prmt7*^{null} MHS cells generated by CRISPR/Cas9 (n=3, three experiments). **(B)** Western blot analysis of PRMT7 protein levels in *Prmt7*$^{+/+}$ and *Prmt7*^{null} MHS cells. **(C)** Western blot analysis of monomethylated protein levels in *Prmt7*$^{+/+}$ and *Prmt7*^{null} MHS cells. Quantification was done relative to β-actin level. Data shown as mean ± SD, **P* < 0.05, ***P* < 0.01 and ****P* < 0.001, unpaired two-tailed Student's t test.

3.4.2 PRMT7 regulates leukocyte transendothelial migration pathway

To investigate the mechanisms contributing to the impaired recruitment of macrophages into the lungs of *Prmt7*$^{+/-}$ mice, the methylation targets of PRMT7 were analyzed. To do so, proteomic analysis of proteins differentially pulled down by anti-monomethylated arginine antibody from whole-cell lysates of *Prmt7*$^{+/+}$ and *Prmt7*^{null} MHS cells was performed by our colleagues in the lab of Prof. Dr. Gunnar Dittmar of the Luxembourg Institute of Health. The design of the experiment is shown in Figure 3.42A. As validation of the approach, the levels of immunoprecipitated core histones H2B, H3 and H4, which are known histone targets of PRMT7 (Jain and Clarke, 2019), were initially examined. As expected, the levels of immunoprecipitated core histones H2B, H3 and H4 were reduced in *Prmt7*^{null} compared to *Prmt7*$^{+/+}$ MHS cells, whereas the pull down levels of H1.2 and H1.5 linker proteins did not differ between these two cell types (Figure 3.42B). This data confirmed that PRMT7 monomethylates the core histone proteins H2B, H3 and H4 in macrophages and validates the methodological approach.

InCroMAP enrichment analysis (Wrzodek et al., 2013) of the differentially regulated immunoprecipitated proteins highlighted the most dysregulated KEGG pathways under Immune Signaling, Cell Community and Signal Transduction to be leukocyte transendothelial

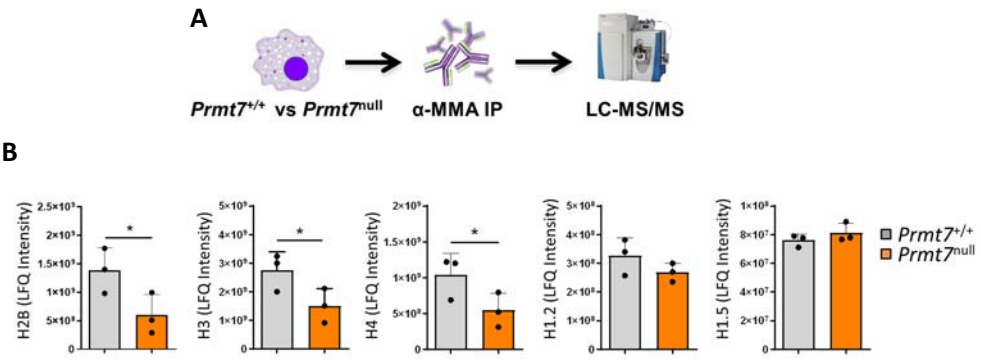

Figure 3.42 Mass spectrometry analysis confirms the methylation of core histones by PRMT7. (A) The design of experiment. Immunoprecipitation of monomethylated proteins using MMA antibody from cell lysates of *Prmt7*$^{+/+}$ and *Prmt7*^{null} MHS cells. Analysis was performed by LC-MS/MS (n=3). **(B)** The intensity of immunoprecipitation in H2B, H3, H4 and H1 histone proteins for *Prmt7*$^{+/+}$ and *Prmt7*^{null} MHS cells. Data shown mean ± SD, $^{**}P < 0.01$, $^{***}P < 0.001$, and $^{****}P < 0.0001$, unpaired two-tailed Student's t test.

migration, focal adhesion and MAPK signaling respectively (Figure 3.43A). Observing that leukocyte transendothelial migration is impaired in *Prmt7*^{null} MHS cells confirmed the previous *in vivo* and *ex vivo* findings. To further investigate the migration ability of *Prmt7*^{null} MHS cells, transwell migration assays were performed. Similar to primary monocytes from *Prmt7*$^{+/-}$ mice, *Prmt7*^{null} MHS cells had a deficiency in their ability to migrate towards CCL2 compared to *Prmt7*$^{+/+}$ MHS cells (Figure 3.43B). Moreover, wound healing assays confirmed

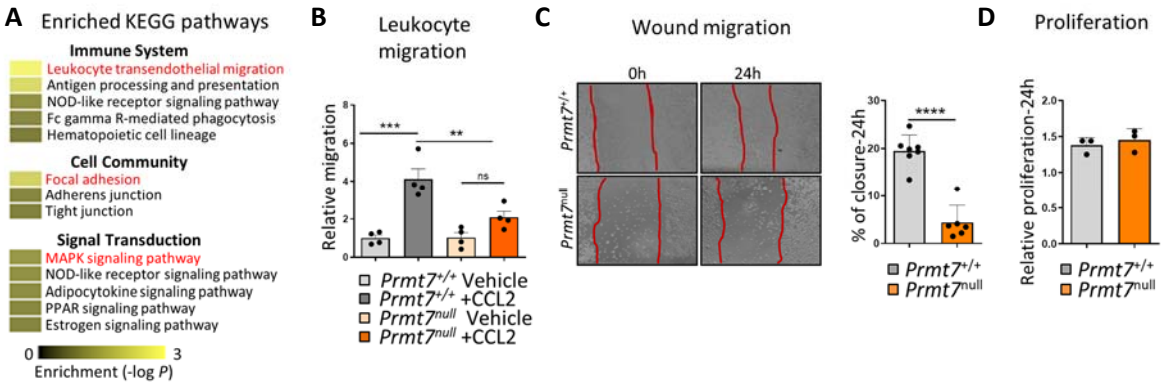

Figure 3.43 Loss of PRMT7 results in impaired transendothelial migration in MHS cells. (A) InCroMAP analysis of less pulled down proteins in *Prmt7*^{null} MHS cells using MMA antibody. Top enriched ones are indicated under KEGG pathways of immune system, cell community and signal transduction (FC<-1.6). **(B)** Migration of *Prmt7*$^{+/+}$ and *Prmt7*^{null} MHS cells towards 100ng/ml of CCL2 for 24 hours. The migration fold change was relative to *Prmt7*$^{+/+}$ control MHS cells (n=2, two experiments). **(C)** Wound migration assay of *Prmt7*$^{+/+}$ and *Prmt7*^{null} MHS cells in 24 hours after scratching. Representative images were taken at 0h and 24h post scratch and wound closure was measured by the wound area at 0h and 24h time points (n=3, two experiments). **(D)** Proliferation determined by WST assay for *Prmt7*$^{+/+}$ and *Prmt7*^{null} MHS cells at 24h post seeding (n=2, two experiments). Data shown mean ± SD, $^{**}P < 0.01$, $^{***}P < 0.001$, and $^{****}P < 0.0001$, one-way ANOVA Bonferroni's multiple comparisons test (B), unpaired two-tailed Student's t test (C).

that wound closure in *Prmt7*^{null} MHS cells was significantly reduced after 24h (Figure 3.43C), implying that migration was impaired in *Prmt7*^{null} cells. Since wound healing might be influenced not only by migration but also proliferation, proliferation of *Prmt7*$^{+/+}$ and *Prmt7*^{null} MHS cells was measured by WST assay. Proliferation of these two cell types did not show any difference between them (Figure 3.43D). In summary, these data suggested that the loss of PRMT7 contributes to an impaired migration in MHS cells.

3.4.3 PRMT7 mediates focal adhesion

Another pathway highlighted by enrichment analysis of reduced monomethylated proteins was focal adhesion of the KEGG cell community (Figure 3.44A). To understand better, a simple cell attachment experiment with *Prmt7*$^{+/+}$ and *Prmt7*^{null} MHS cells was performed. Both cell types were seeded at the same time and the unattached cells floating to the surface were quantified and compared over time. A clear difference between *Prmt7*$^{+/+}$ and *Prmt7*^{null} MHS cells in terms of their adhesion abilities was observed (Figure 3.44B). Adhesion and migration of monocytes and macrophages depends on the expression of integrins which mediate

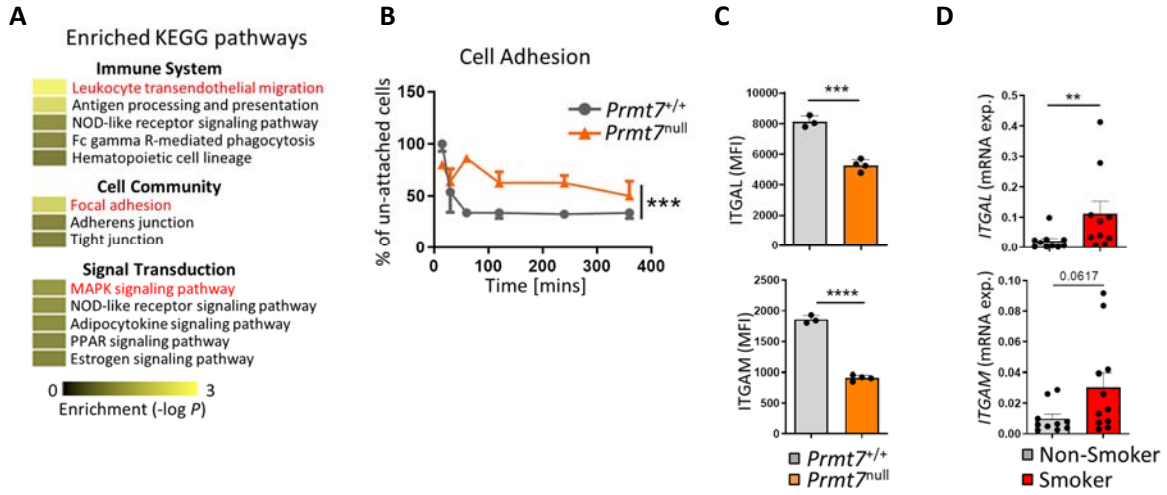

Figure 3.44 Adhesion of MHS cells is impaired in the absence of PRMT7. (A) InCroMAP analysis of less pulled down proteins in *Prmt7*^{null} MHS cells using MMA antibody. Top enriched ones are indicated under KEGG pathways of immune system, cell community and signal transduction (FC<-1.6). **(B)** Quantification of un-attached *Prmt7*$^{+/+}$ and *Prmt7*^{null} MHS cells as percentage by time when they were seeded at the same time (n=2, two experiments). **(C)** Mean fluorescence intensity (MFI) of ITGAL and ITGAM surface levels on *Prmt7*$^{+/+}$ and *Prmt7*^{null} MHS cells determined by FACS (n=3-4). **(D)** mRNA expression of *ITGAL* and *ITGAM* levels determined by qPCR in the monocytes isolated from human smokers vs non-smokers (n=10-11). Data shown mean ± SD, $^{**}P < 0.01$, $^{***}P < 0.001$, and $^{****}P < 0.0001$, unpaired two-tailed Student's t test.

interactions with endothelial cells (Meerschaert and Furie, 1995). CD11a (ITGAL) and CD11b (ITGAM) are important integrins on monocytes and their expression and activation play key roles in adhesion and transmigration (Gerhardt and Ley, 2015). The surface levels of these two key integrins on *Prmt7*$^{+/+}$ and *Prmt7*^{null} MHS cells were therefore examined by flow cytometry. ITGAL and ITGAM surface expression was significantly diminished in PRMT7 deficient MHS cells (Figure 3.44C). Consistently, the mRNA expression of these two integrins was enhanced in monocytes isolated from human smokers compared to non-smokers (Figure 3.44D) similar to *PRMT7* expression (Figure 3.4), confirming that inflammation promotes integrin expression to induce adhesion and migration of immune cells including monocytes.

In order to support these findings, the SAM-competitive PRMT7 inhibitor, SGC3027, which is a cell permeable prodrug (Szewczyk et al., 2020) was used on MHS cells. It was demonstrated that the SGC3027 PRMT7 inhibitor reduced mono-methylation levels in the mouse myoblast cell line, C2C12 (Szewczyk et al., 2020). Firstly, to confirm that the drug also functions on MHS cells, mono-methylation (MMA) levels were examined. As a result of treatment with the drug, total MMA levels in MHS cells in comparison to non-treated control MHS cells was reduced (Figure 3.45A). Consistent with previous findings, MHS cells treated with the PRMT7 inhibitor displayed attenuated surface expression of the two key integrins, ITGAL (CD11a) and ITGAM

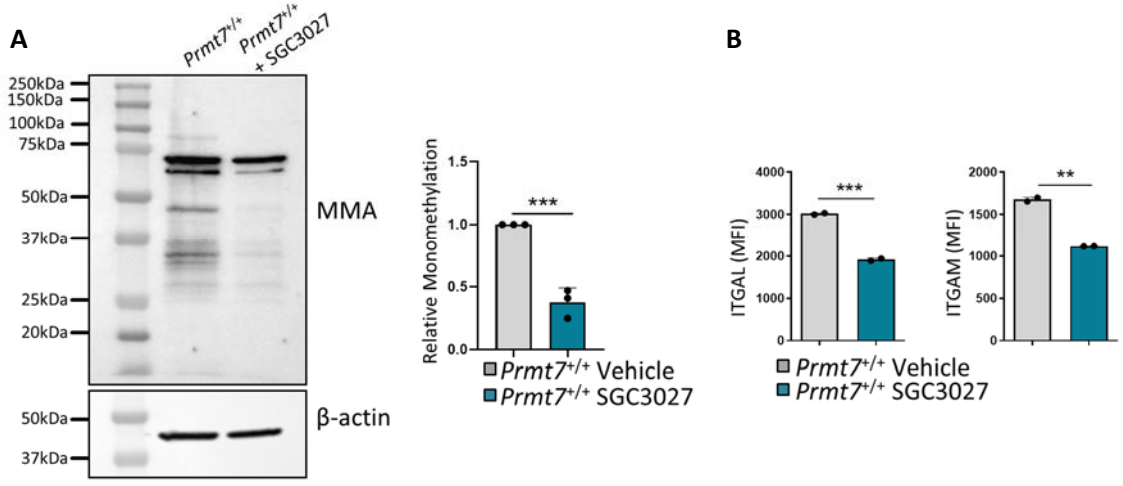

Figure 3.45 PRMT7 inhibitor, SGC3027, reduced the expression of adhesion molecules on MHS cells. (A) Total mono-methylation (MMA) levels, determined by western blot, of MHS cells treated with and without 5μM of SGC3027 inhibitor for 24h (n=3). Quantification was relative to β-actin. **(B)** Mean fluorescence intensity (MFI) of ITGAL and ITGAM surface expression determined by FACS anaylsis on MHS cells treated with and without 5μM of SGC3027 inhibitor for 24h (n=2). Data shown mean ± SD, $^{**}P < 0.01$, $^{***}P < 0.001$, and $^{****}P < 0.0001$, unpaired two-tailed Student's t test.

(CD11b) following flow cytometry analysis (Figure 3.45B). Considering the results, these data suggested that PRMT7 regulates adhesion in macrophages.

3.4.4 PRMT7 regulates MAPK signalling pathway

The same enrichment analysis using InCroMAP software of the immunoprecipitated proteins revealed that the MAPK signaling pathway was also one of the most significantly regulated KEGG pathways in *Prmt7*^{null} cells (Figure 3.46A). The importance of mitogen-activated protein kinases (MAPKs) in immune cells especially in monocytes and macrophages has been very well established (Pearson et al., 2001). So far, MAPKs have been associated with survival, proliferation, differentiation, activation and cytokine production of monocytes and macrophages (Kasper et al., 2007; Rao, 2001; Valledor et al., 2008). MAPK cascades predominantly extracellular signal-regulated kinase (ERK) and p38MAPK are activated by G-protein-coupled receptors (GPCRs) which are proteins on the cell surface responsible for signal transmission when they bind to external ligands (Marinissen and Gutkind, 2001; Naor et al., 2000). As CCR2 is a G protein-coupled receptor and activates MAPK signaling following interaction with its ligand CCL2 (Fang et al., 2012), *Prmt7*$^{+/+}$ and *Prmt7*^{null} MHS cells were stimulated with CCL2, to confirm MAPK signaling pathway is impaired in *Prmt7*^{null} MHS cells. Confirming the enrichment analysis, reduced levels of phosphorylated ERK and p38 was observed in *Prmt7*^{null} cells compared to *Prmt7*$^{+/+}$ cells (Figure 3.46B). Densitometric quantification also confirmed this observation (Figure 3.46D). To support these findings, an alternative ligand to trigger MAPK signaling in MHS cells was also used. Stimulating MHS cells with TLR4 agonist LPS, demonstrated that the phosphorylation levels of ERK and p38 was clearly diminished in *Prmt7*^{null} cells (Figure 3.46C). Quantification of western blots validated this finding (Figure 3.46D and E). Moreover, to understand whether this reduced phosphorylation in *Prmt7*^{null} cells is caused by impaired CCR2 receptor levels, FACS analysis was performed. When CCR2 surface levels on *Prmt7*$^{+/+}$ and *Prmt7*^{null} MHS cells were compared, no differences were observed, implying that reduced CCR2 was not the reason for impaired MAPK signaling in *Prmt7*^{null} cells (Figure 3.46F). All in all, these results suggested that PRMT7 regulates transendothelial migration together with adhesion and MAPK signaling in macrophages.

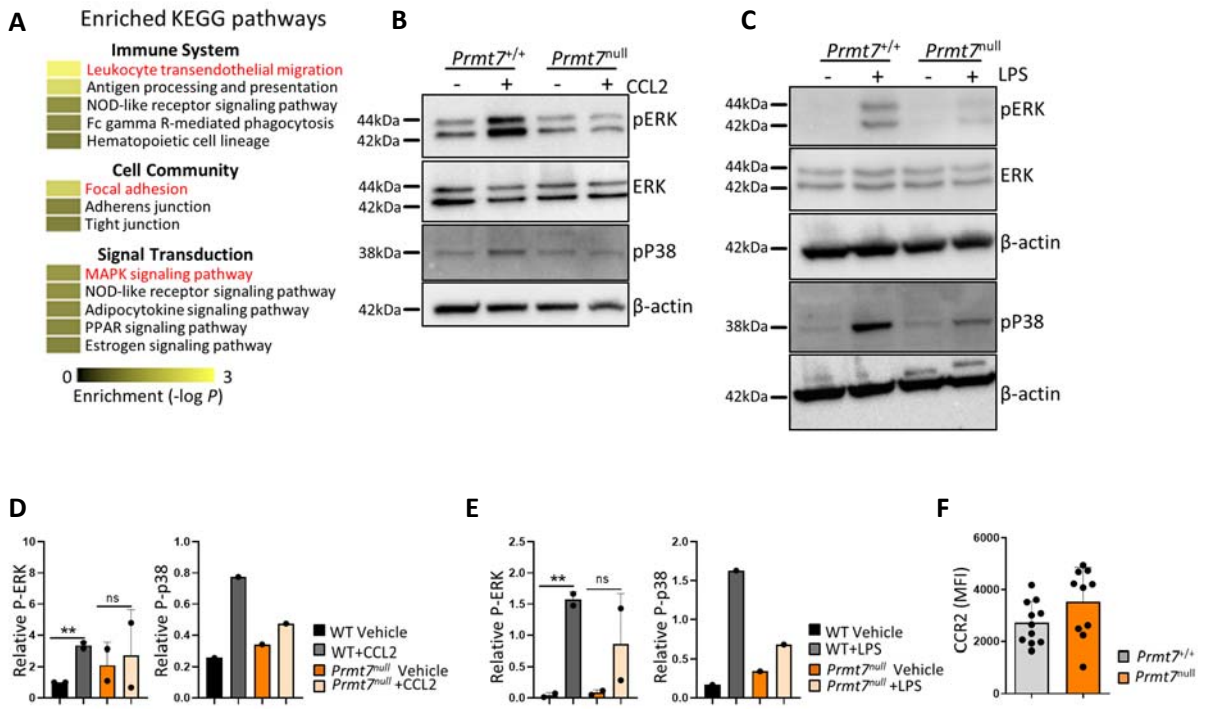

Figure 3.46 Absence of PRMT7 results in impaired MAPK signalling in MHS cells. (A) InCroMAP analysis of less pulled down proteins in *Prmt7*^{null} MHS cells using MMA antibody. Top enriched ones are indicated under KEGG pathways of immune system, cell community and signal transduction (FC<-1.6). **(B)** Analysis of phosphorylated ERK and p38 in *Prmt7*$^{+/+}$ and *Prmt7*^{null} MHS cells by western blot after incubating with 100ng/ml CCL2 for 30 mins (n=2). **(C)** Analysis of phosphorylated ERK and p38 in *Prmt7*$^{+/+}$ and *Prmt7*^{null} MHS cells by western blot after incubating with 1µg/ml LPS for 15 mins (n=2). **(D-E)** Densitometry analysis of western blots from B and C relative to β-actin, respectively. **(F)** MFI of CCR2 surface expression levels on *Prmt7*$^{+/+}$ and *Prmt7*^{null} MHS cells determined by flow cytometry (n=11). Data shown mean ± SD, $^{**}P < 0.01$, $^{***}P < 0.001$, and $^{****}P < 0.0001$, unpaired two-tailed Students t test.

3.4.5 PRMT7 regulates the expression of RAP1 via histone methylation

The findings so far have demonstrated that PRMT7 has a role in migration and MAPK signaling in macrophages. However, how PRMT7 regulates these processes is still not clear. To understand the mechanisms between these biological events and the involvement of PRMT7, a comparison of proteins across the three dysregulated pathways was undertaken. As a result of overlapping the migration, adhesion and MAPK signaling pathways, interestingly one protein known as RAP1A/B, which is a small G protein in the Ras superfamily, was revealed in common between the three pathways, which were impaired in *Prmt7*^{null} MHS cells (Figure 3.47A). Ras-associated protein-1 (RAP1A/B) has been implicated in the regulation of important cellular processes, especially integrin-mediated cellular adhesion and migration (Bos et al., 2003) as well as MAPK activation (Stork, 2003; Wu et al., 2015). For example; in

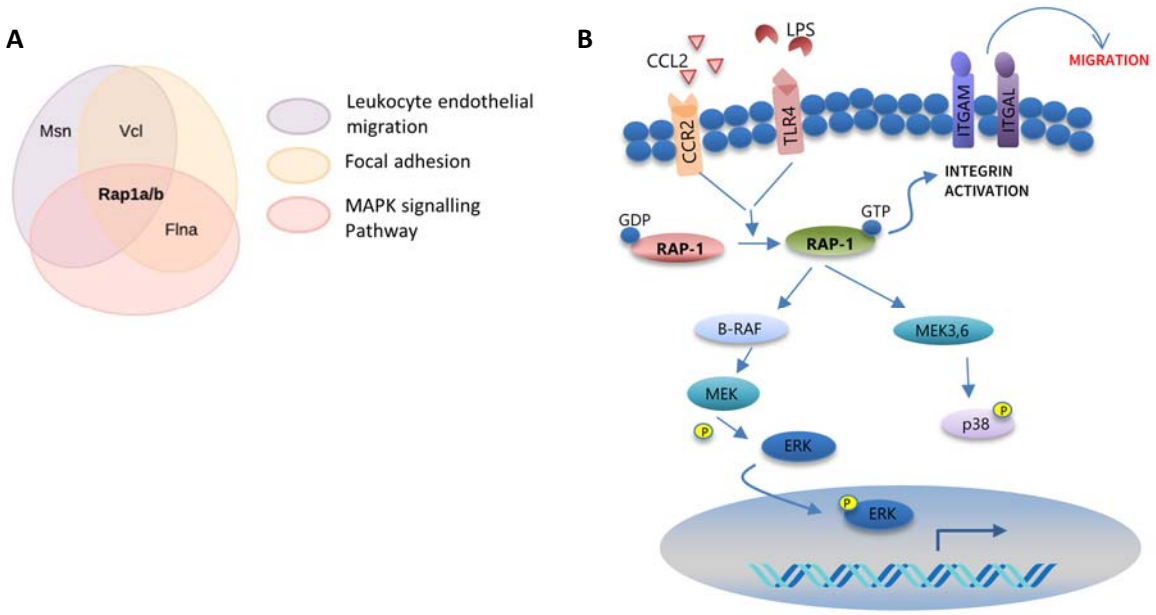

Figure 3.47 RAP1A/B is a common protein found in all three dysregulated pathways in and *Prmt7*^{null} MHS cells. (A) Venn diagram analysis of three dysregulated pathways including transendothelial migration, focal adhesion and MAPK signaling in *Prmt7*^{null} MHS cells. **(B)** Representative of RAP1A/B downstream signaling pathway targets including MAPK and integrin activation.

cancer cells, RAP1A/B was shown to promote tumorigenesis and metastasis by regulating MAPK signaling and integrin activation (Gao et al., 2006). Moreover, more specifically, *Rap1a*$^{-/-}$ mice demonstrated that cell adhesion and migration towards chemokines were adversely affected in macrophages, despite the development of macrophages remained the same (Li et al., 2007). Figure 3.47B summarizes the role of RAP1 in the cell following activation by GTP binding, and its role as an upstream regulator of MAPK signaling including ERK and p38 as well as integrin activation. In the light of these findings it is possible that RAP1 is be regulated by PRMT7.

Circumstantially supporting this hypothesis, *Rap1a* expression levels were enhanced in monocytes isolated from the lungs of chronic CS exposed mice as determined by single cell RNA-Seq (Figure 3.48A). Moreover, mRNA expression of *RAP1A* was elevated in circulating monocytes from the peripheral blood of smokers compared to non-smokers (Figure 3.48B). These data were consistent with the previous findings that PRMT7 expression was also increased in monocytes from CS exposed mice (Figure 3.11) as well as from patients with a smoking history (Figure 3.13).

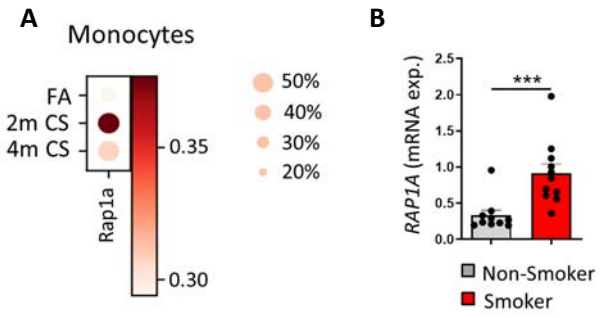

Figure 3.48 RAP1A expression is increased in monocytes from CS exposed mice and in monocytes from smokers. (A) *Rap1a* expression representation via dot plot (log transformed, normalized UMI counts) in monocytes from the lungs of CS exposed mice for 2 and 4 months determined by single cell RNA-seq data. FA control was used as comparison (n=3 for FA and n=5 for CS). **(B)** mRNA expression levels of *RAP1A* in the human monocytes isolated from the blood of smokers (n=10) and non-smokers (n=11). The data was determined by qPCR. Data shown mean ± SD, **P* < 0.05, ***P* < 0.01 and ****P* < 0.001, unpaired two-tailed Student's t test.

To understand whether RAP1 deficiency gives similar results to PRMT7 deficient MHS cells, the activity of RAP1 was first inhibited by using GGTI-298, a drug that inhibits GTP binding therefore impairing RAP1 activation (McGuire et al., 1996). Consistently, RAP1 inhibition via GGTI-298 on MHS cells decreased the surface expression levels of ITGAM and ITGAL (Figure 3.49A), which are key molecules for adhesion and migration, similar to what had been observed in *Prmt7*^{null} MHS cells (Figure 3.44C). Moreover, MHS cells inhibited with GGTI-298 demonstrated impaired phosphorylation of ERK following stimulation with LPS (Figure 3.49B). This finding was comparable to what was observed in *Prmt7*^{null} MHS cells (Figure 3.46B-C).

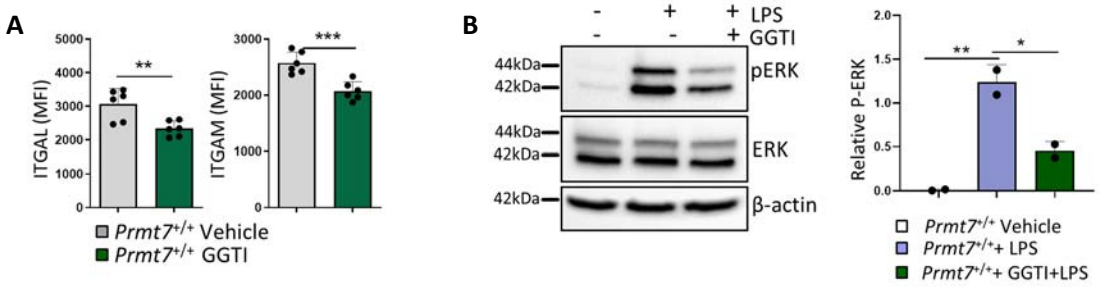

Figure 3.49 Inhibition of RAP1 activity reduced the levels of adhesion molecules and MAPK activity. (A) Mean fluorescence intensity (MFI) of ITGAL and ITGAM surface expression determined by FACS analysis on MHS cells pretreated with and without 20μM of GGTI-298 RAP1 inhibitor for 2h and analysed 6h later (n=2, three experiments). **(B)** Analysis of phosphorylated ERK in *Prmt7*$^{+/+}$ MHS cells pretreated with and without 20μM of GGTI-298 RAP1 inhibitor for 2h followed by 15 mins 1μg/ml LPS stimulation (n=2). The data was determined by western blot and quantification was relative to β-actin. Data shown as mean ± SD, **P* < 0.05, ***P* < 0.01 and ****P* < 0.001, unpaired two-tailed Student's t test.

All things considered, this data suggests that there may be a potential link between RAP1 and PRMT7. As RAP1 is an upstream regulator of leukocyte migration and MAPK signaling, its expression levels in *Prmt7*^{null} MHS cells was investigated. Interestingly, western blot analysis demonstrated that RAP1A/B protein levels were reduced in whole lysates from *Prmt7*^{null} MHS cells (Figure 3.50A). The western blot results referred to total RAP1A/B protein levels because the antibody could not distinguish between RAP1A or RAP1B protein. Therefore, mRNA expression levels of *Rap1a* and *Rap1b* was examined separately in these cell lines. qPCR revealed that *Rap1a* expression was significantly decreased in *Prmt7*^{null} MHS cells in comparison to *Prmt7*$^{+/+}$ cells (Figure 3.50B). However, there was no difference in *Rap1b* mRNA expression in the absence of PRMT7 (Figure 3.50B).

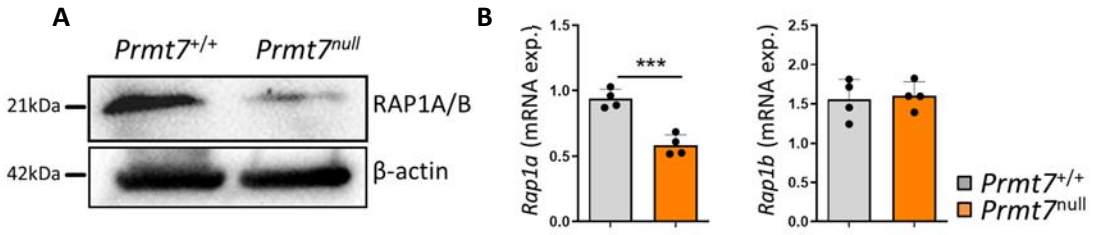

Figure 3.50 *Rap1a* expression is reduced in the absence of PRMT7 on MHS cells. (A) Western blot analysis of RAP1A/B protein levels in whole lysates from *Prmt7*$^{+/+}$ and *Prmt7*^{null} MHS cells. **(B)** mRNA expression levels of *Rap1a* and *Rap1b* in *Prmt7*$^{+/+}$ and *Prmt7*^{null} MHS cells (n=2, two experiments). The data was determined by qPCR. Data shown mean ± SD, **P* < 0.05, ***P* < 0.01 and ****P* < 0.001, unpaired two-tailed Student's t test.

To fully understand the mechanism underlying how RAP1 is potentially regulated by PRMT7, ATAC-Seq analysis was undertaken (by the company Active Motif), which is a very fast and sensitive method to examine chromatin accessibility genome-wide (Buenrostro et al., 2015). A peak correlation scatter plot of read counts across the entire genome of *Prmt7*$^{+/+}$ and *Prmt7*^{null} MHS cells did not reveal major global changes in chromatin accessibility (Figure 3.51A). Further, regions of the genome that were enriched in ATAC-Seq signal were mapped to genomic features to determine their distribution. As a result, peaks relative to genomic location between *Prmt7*$^{+/+}$ and *Prmt7*^{null} MHS cells were quite similar (Figure 3.51B). Examination of the ATAC-Seq signal enrichment around the transcription start sites (TSSs) across the two groups did not reveal any differences either (Figure 3.51C).

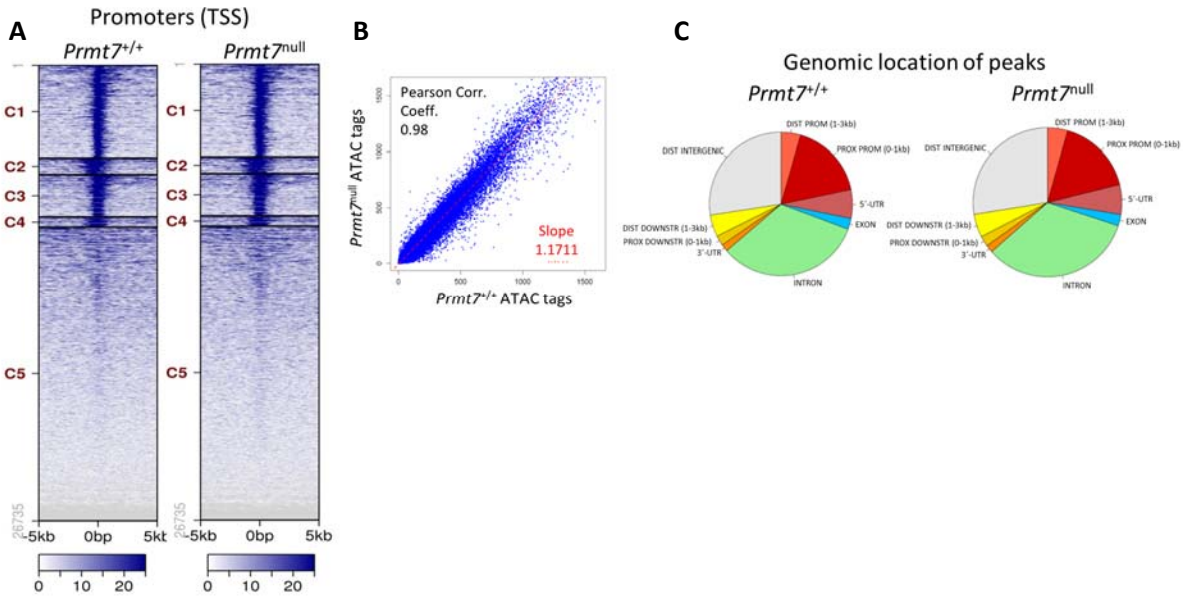

Figure 3.51 Chromatin accessibility does not differ in the whole genome between *Prmt7*$^{+/+}$ and *Prmt7*^{null} MHS cells. (A-C) ATAC-Seq anaylsis of *Prmt7*$^{+/+}$ and *Prmt7*^{null} MHS cells **(A)** Heat map of tag distributions across promoters (TSS) of *Prmt7*$^{+/+}$ and *Prmt7*^{null} MHS cells. **(B)** Peak correlation scatter plot for *Prmt7*$^{+/+}$ and *Prmt7*^{null} MHS cells with pearson correlation coefficiency 0.98 and slope 1.17. **(C)** Representative pie chart demonstrating the genomic distribution of accessible regions in *Prmt7*$^{+/+}$ and *Prmt7*^{null} MHS cells. Data and plots generated by Active Motive.

Although there was no significant difference between the two different cell types in terms of total promoter site peaks analysis, when transcription start site enrichment was analyzed specifically on *Rap1a*, the accessibility at the *Rap1a* gene was decreased in 5 different regions in *Prmt7*^{null} MHS cells compared to *Prmt7*$^{+/+}$ cells (Figure 3.52).

To investigate further how PRMT7 may transcriptionally regulate *Rap1a*, ChIP-qPCR on chromatin isolated from *Prmt7*$^{+/+}$ and *Prmt7*^{null} MHS cells was performed. Chromatin

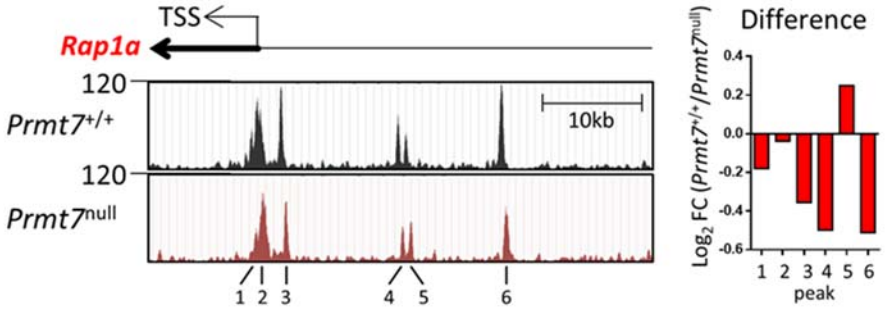

Figure 3.52 Chromatin accessibility at the Rap1a gene is reduced in the absence of PRMT7 in MHS cells. ATAC-Seq anaylsis of *Prmt7*$^{+/+}$ and *Prmt7*^{null} MHS cells. In each cell line, enrichment peaks around the transcription start site (TSS) of the *Rap1a* gene was shown. The graph on the right side shows the differences in peak height across *Prmt7*$^{+/+}$ and *Prmt7*^{null} MHS cells.

Immunoprecipitation (ChIP) is a common technique to study protein-DNA interactions in cells. When it is combined with quantitative PCR, target protein and DNA interactions at specific genomic binding sites can be also evaluated (Kim and Dekker, 2018; Lacazette, 2017). In this study, the aim was to examine whether the PRMT7 protein is enriched at the *Rap1a* gene region. Therefore, the primers in an area upstream of exon 1 that was a putative enhancer for *Rap1a* in BMDMs as determined by enrichment of H3K4me1 and H3K27a (Primer pair I) and a pair outside of this area as a control (Primer pair II) were designed (Figure 3.53A). Interestingly, ChIP-qPCR analysis demonstrated that PRMT7 was enriched at the *Rap1a* gene with primer pair I compared to the *Gapdh* locus (Figure 3.53B). As predicted, this enrichment was lost in *Prmt7*^{null} MHS cells (Figure 3.53B). Additionally, H3R2me1 and the activator mark H3R2me2s were also enriched in the same region and this enrichment was decreased in *Prmt7*^{null} MHS cells (Figure 3.53C). Consistent with these findings, PRMT7 has

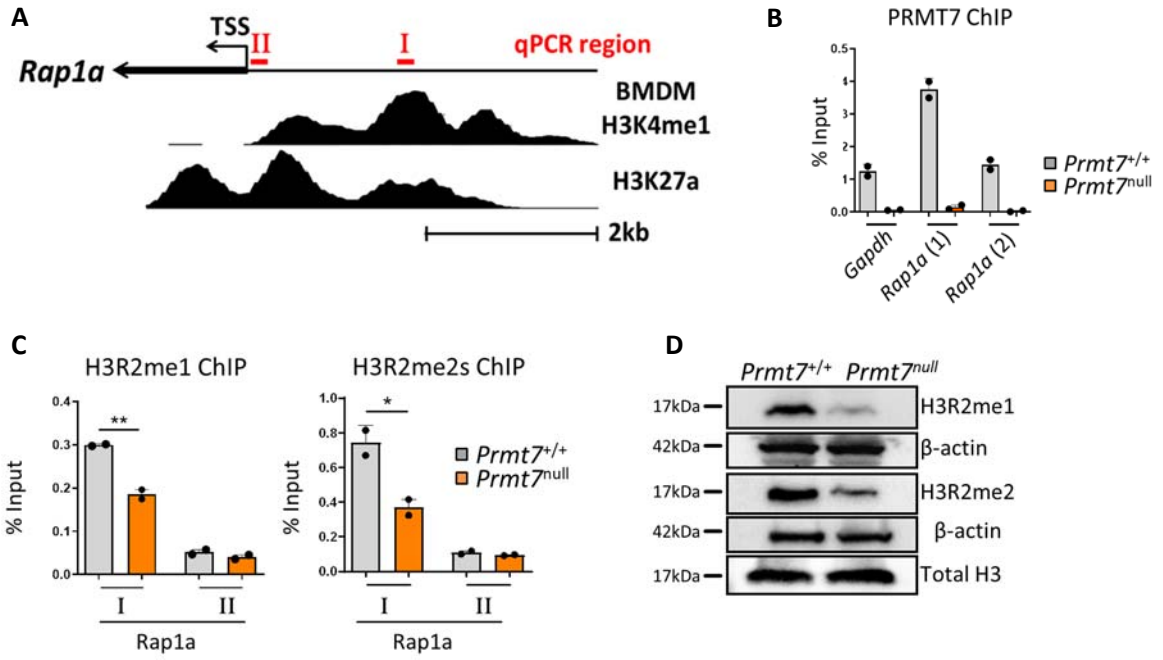

Figure 3.53 PRMT7 regulates RAP1A expression via histone methylation. (A) The primers designed for ChIP-qPCR around *Rap1a* region. H3K4me1 and H3K27a enrichment analysis in BMDMs were taken from UCSC genome browser Track accessions: wgEncodeEM002658 and wgEncodeEM002657. **(B)** ChIP-qPCR analysis with anti-PRMT7 antibody on chromatin isolated from *Prmt7*$^{+/+}$ and *Prmt7*^{null} MHS cells and primers specific for genomic regions of *Gapdh* and *Rap1a* (n=2). **(C)** ChIP-qPCR analysis with anti-H3R2me1 and anti-H3R2me2s on chromatin isolated from *Prmt7*$^{+/+}$ and *Prmt7*^{null} MHS cells and primers specific for genomic regions of *Rap1a* (n=2). **(D)** Western blot analysis of H3R2me1 and H3R2me2 as well as H3 in *Prmt7*$^{+/+}$ and *Prmt7*^{null} MHS cells. B-actin was used as loading control. Data shown as mean ± SD, **P* < 0.05, ***P* < 0.01 and ****P* < 0.001, unpaired two-tailed Student's t test.

been reported to both monomethylate arginine residues and regulate H3R2me1 and H3R2me2 marks either directly or potentially indirectly via other PRMTs (Jain et al., 2017; Yang and Bedford, 2013). Moreover, H3R2me2s and H3R2me2 marks can function as activators of transcription (Blanc et al., 2016; Migliori et al., 2012). In parallel with these previous studies, reduced levels of H3R2 mono and dimethylation was detected in *Prmt7*^{null} MHS cells compared to *Prmt7*$^{+/+}$ MHS cells, with total H3 levels similar in both cell lines (Figure 3.53D). All in all, these findings suggested that *Rap1a* is transcriptionally regulated by PRMT7 through H3R2 methylation at the regulatory regions of the *Rap1a* gene. Furthermore, reduced expression of RAP1 in PRMT7 deficient macrophages impaired adhesion and migration abilities as well as attenuated MAPK signaling.

3.5 The effect of PRMT7 deficiency specifically in macrophages in different disease models

3.5.1 Macrophage recruitment is impaired into the lungs of *Lyz2-Cre Prmt7*$^{fl/fl}$ mice upon bleomycin exposure

So far, in this study it has been demonstrated that *Prmt7*$^{+/-}$ mice had impaired migration of monocyte-derived macrophages into the lungs through the regulation of RAP1. These mice were protected against emphysema progression and to have improved lung function in two different COPD disease models including CS-induced and elastase-induced. Considering these findings, the next step was to understand whether PRMT7 regulates monocyte migration only in COPD or the effect of PRMT7 on monocyte migration is crucial for other diseases. If it is, it would make PRMT7 a great therapeutic target against multiple inflammatory diseases. For this reason, several other disease models where monocyte-derived macrophages play a central role in the pathogenesis of the disease were evaluated using conditional knock out mice, *Lyz2-Cre Prmt7*$^{fl/fl}$. These mice have a deficiency of PRMT7 expression only in myeloid cells so it is a useful model to assess the role of PRMT7 specifically in monocytes and macrophages.

The first disease model using *Lyz2-Cre Prmt7*$^{fl/fl}$ mice was bleomycin-induced lung fibrosis. Instillation of bleomycin intratracheally is a very common experimental model of lung fibrosis, however the mechanism of lung injury in response to bleomycin exposure is not yet clear (Reinert et al., 2013). Potential mechanisms might include oxidative damage, genetic susceptibility and increase in inflammatory cytokines to recruit immune cells (Sleijfer, 2001). WT and mice with a conditional knockout of Prmt7 in Lyz2 expressing cells (*Lyz2-Cre Prmt7*$^{fl/fl}$) were exposed to bleomycin or PBS and examined 14 days later. A time point at which macrophage numbers were already shown to be increased in the lungs of mice subjected to bleomycin (Izbicki et al., 2002). Immunohistochemistry staining against Galectin 3 revealed that the number of macrophages in the lungs of *Lyz2-Cre Prmt7*$^{fl/fl}$ mice post bleomycin instillation was significantly reduced compared to the lungs of WT controls (Figure 3.54A). Quantification of lung sections after IHC staining confirmed the reduction in macrophage numbers in the lungs of *Lyz2-Cre Prmt7*$^{fl/fl}$ mice using CAST (Figure 3.54B). This result was quite comparable to the COPD models.

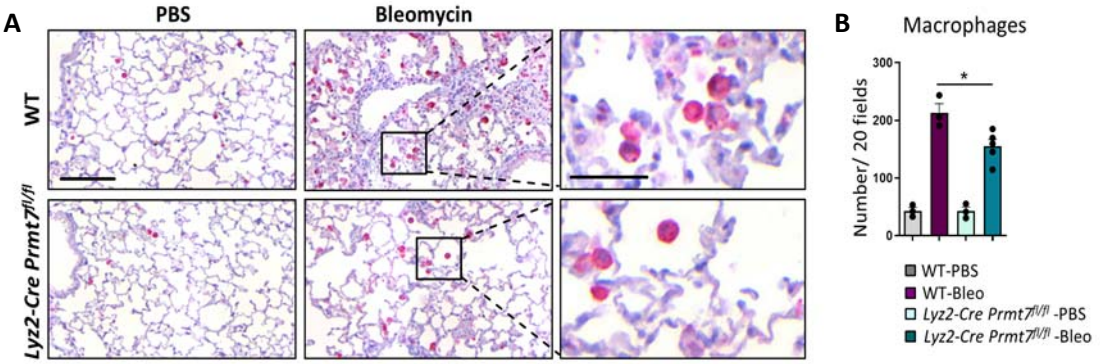

Figure 3.54 Macrophage numbers are reduced in the lungs of *Lyz2-Cre Prmt7*$^{fl/fl}$ mice upon bleomycin exposure. (A-B) WT and *Lyz2-Cre Prmt7*$^{fl/fl}$ mice were instilled with 2U/Kg bleomycin or PBS and analysed after 14 days (n=3-5). **(A)** Representative pictures of immunohistochemistry staining of lung sections for galectin-3 positive macrophages (red signal refers to galectin-3 positive macrophages). (scale bar 100µm). **(B)** Quantification of macrophage numbers from stained lung sections in each group through 20 random fields counted by CAST. Data shown as mean ± SD, **P* < 0.05, ***P* < 0.01, ****P* < 0.001, and *****P* < 0.0001, one-way ANOVA Bonferroni's multiple comparisons test.

3.5.2 *Lyz2-Cre Prmt7*$^{fl/fl}$ mice are protected against collagen deposition

To understand if the reduction in macrophage numbers in the lungs of *Lyz2-Cre Prmt7*$^{fl/fl}$ mice after bleomycin instillation influences lung fibrosis development, collagen deposition, which is a hallmark of the fibrosis (Laurent, 1985), was quantified. Masson´s trichrome staining of

lung sections demonstrated an attenuated collagen deposition in the lungs of *Lyz2-Cre Prmt7*$^{fl/fl}$ mice in comparison to WT ones (Figure 3.55A). Quantification of the volume of collagen deposition per area confirmed a significant decrease in the lungs of *Lyz2-Cre Prmt7*$^{fl/fl}$ mice compared to WT controls (Figure 3.55B). These results offer further evidence that PRMT7 is essential for the migration of monocytes and macrophages in bleomycin-induced lung fibrosis and that this contributes to collagen deposition.

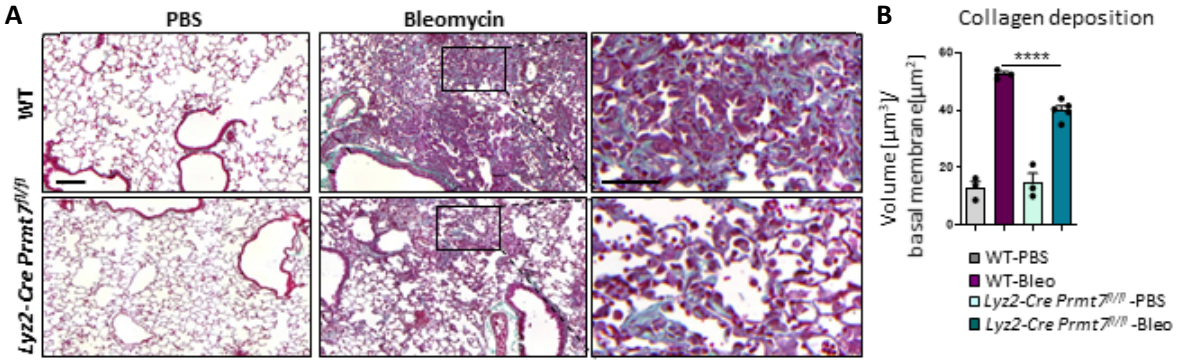

Figure 3.55 Collagen deposition is reduced in the lungs of *Lyz2-Cre Prmt7*$^{fl/fl}$ mice. (A-B) WT and *Lyz2-Cre Prmt7*$^{fl/fl}$ mice were instilled with 2U/Kg bleomycin or PBS and analysed after 14 days (n=3-5). **(A)** Representative pictures of masson´s trichrome staining of lung sections from WT and *Lyz2-Cre Prmt7*$^{fl/fl}$ mice to observe collagen formation (green; collagen, red; cytoplasm, dark brown to black; cell nuclei) (Scale bar 100µm). (B) Quantification of collagen deposition from stained lung sections in each group through 30 random fields counted by CAST. Data shown as mean ± SD, **P* < 0.05, ***P* < 0.01, ****P* < 0.001, and *****P* < 0.0001, one-way ANOVA Bonferroni's multiple comparisons test.

3.5.3 Injured skin of *Lyz2-Cre Prmt7*$^{fl/fl}$ mice recruits less macrophages than WT mice

Moreover, an independent skin injury model where macrophage recruitment plays an important role in scar formation was utilized (by the kind assistance of Dr. Dongsheng Jiang) to support the previous findings. Macrophages are key cells during each step of the wound healing process including inflammation, proliferation and remodeling (Krzyszczyk et al., 2018). Many studies implied that monocyte-derived macrophages with an M1 pro-inflammatory phenotype contributed to the inflammation in scar tissue by secreting pro-inflammatory cytokines (Delavary et al., 2011; Kreimendahl et al., 2019). When macrophage recruitment into the injured skin of WT and *Lyz2-Cre Prmt7*$^{fl/fl}$ mice was assessed, it was observed that macrophage numbers were significantly reduced in the skin of *Lyz2-Cre Prmt7*$^{fl/fl}$ mice after 3 days post-injury compared to WT mice (Figure 3.56A). Quantification of

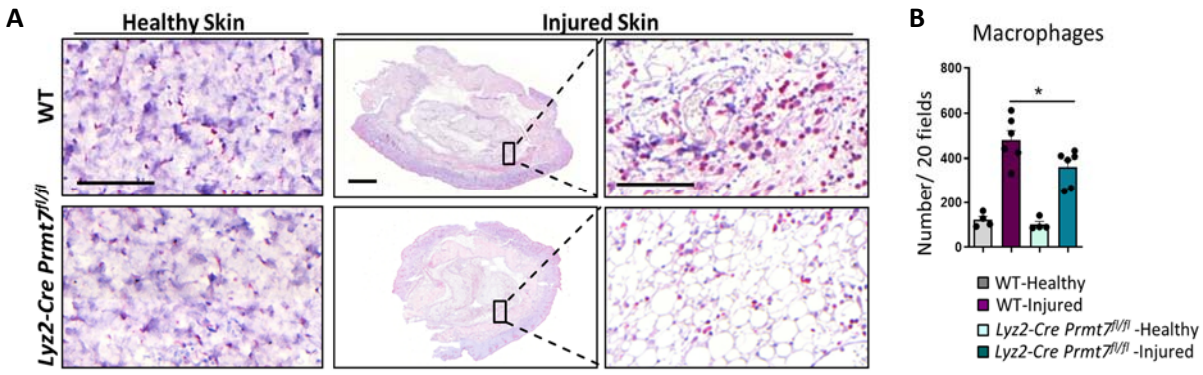

Figure 3.56 Macrophage recruitment into the injured skin of *Lyz2-Cre Prmt7*$^{fl/fl}$ mice is impaired. (A-B) WT and *Lyz2-Cre Prmt7*$^{fl/fl}$ mice were exposed to 5mm splinted full-thickness excisional dorsal wounds and they were analysed after 3 days. Healthy skin was taken from neighboring skin which are not injured as control. **(A)** Representative pictures of immunohistochemistry staining of skin sections for galectin-3 positive macrophages (red signal refers to galectin-3 positive macrophages). (scale bar 100µm). **(B)** Quantification of macrophage numbers from stained lung sections in each group through 20 random fields counted by CAST. Data shown as mean ± SD, **P* < 0.05, ***P* < 0.01, ****P* < 0.001, and *****P* < 0.0001, one-way ANOVA Bonferroni's multiple comparisons test.

Galectin-3 positive macrophages via the CAST system confirmed that *Lyz2-Cre Prmt7*$^{fl/fl}$ mice had impaired recruitment of macrophages into the injured tissue (Figure 3.56B). Taken all together this data highlights that PRMT7 regulated recruitment of monocyte derived macrophages plays a key role in multiple monocyte driven inflammatory responses in several disease models.

4. DISCUSSION

In this study, the main goal was to comprehend the potential role of PRMT7 in the pathogenesis of COPD. Here, it was demonstrated that PRMT7-driven mono-methylation of histone proteins in monocytes and macrophages is required for their accumulation in the lungs in response to inflammation, and this drives the pathogenesis of COPD and other chronic inflammatory diseases like fibrosis. The first crucial finding of this research project was that mice with a reduced expression of PRMT7, *Prmt7*$^{+/-}$ mice, were protected against emphysema progression after 4 months of CS exposure or 28 days of elastase exposure. This protection was found to be associated with impaired recruitment of pro-inflammatory monocyte derived macrophages into the lung. These findings were supported in primary monocytes that were isolated from *Prmt7*$^{+/-}$ mice, as they displayed impaired trans-endothelial migratory ability towards the main chemokine CCL2. Moreover, in this study, it was also identified mechanistically how PRMT7 mediated mono-methylation in macrophages affects their adhesion and migration abilities into the lungs. *Prmt7*^{null} macrophages had impaired transendothelial migration, focal adhesion and MAPK signalling pathways and it was further elucidated that PRMT7 induced mono-methylation of H3 histone protein in macrophages regulates *Rap1a* expression, which is a common mediator of these three pathways. Taken all together, these findings have significant indications to fully understand the monocyte trans-endothelial migration into several target organs including both lung and skin in response to inflammatory insult. Moreover, the link between migration of macrophages into these target organs and disease pathogenesis is confirmed. Collectively, these data suggest that PRMT7 might be a potential novel target for therapeutic interventions.

4.1 The function of PRMT7 in the pathogenesis of COPD

COPD recently became the third leading cause of death worldwide and COPD patients mainly suffer from an irreversible decline in lung function due to chronic exposure to toxic gases and particles especially CS (Vijayan, 2013). Inflammatory response caused by innate immune cells, predominantly macrophages and neutrophils, as well as adaptive B and T cells following CS

exposure leads to hallmarks of COPD including the destruction of alveolar tissue - emphysema, small airway remodelling and airway obstruction (Hogg et al., 2004). Even though COPD is a deadly disease with known symptoms, the precise molecular mechanisms underlying these responses remain to be elusive. Since not all cigarette smokers develop the disease (Terzikhan et al., 2016), there must be other important factors which play central roles in the development of the disease in COPD patients. The first objective in this study was to identify these intrinsic factors in COPD pathogenesis. Transcriptomics data obtained from the lungs of 111 COPD patients with smoking history and 40 control smokers (Morrow et al., 2017) was compared, COPD patients demonstrated enrichment for methyltransferase activity upon GSEA analysis (Figure 3.1). In this pathway, the most mis-regulated protein arginine methyltransferase (PRMT) gene was *PRMT7* (Figure 3.1C), thus implying a possible role in disease development. This finding was supported by the upregulation of *PRMT7* gene and protein levels in the lungs of an independent cohort of COPD patients compared to healthy controls (Figure 3.4). Consistently, this upregulation was correlated with disease severity (Figure 3.3). It was crucial to understand which cells predominantly express PRMT7 in the lungs of COPD patients and contributes to disease development. In this regard, it was clearly demonstrated for the first time that PRMT7 is mainly localized to macrophages in the lungs of COPD patients as well as in the lungs of healthy controls (Figure 3.6 and Figure 3.7) suggesting that PRMT7 exerts its function in macrophages. In support, a recent study investigating the gene expression profile of chromatin modifying enzymes showed that there was no change in the expression of PRMT7 after cigarette smoke extract exposure on human epithelial cells (Sundar and Rahman, 2016). To confirm the hypothesis that PRMT7 has a functional role in macrophages in the lung, the alveolar macrophage cell line (MHS) was subjected to cigarette smoke extract (CSE) and unsurprisingly *Prmt7* expression was highly upregulated in these macrophages upon CSE (Figure 3.12). To support these findings in primary cells as well, alveolar macrophages and blood monocytes freshly isolated from CS exposed mice for 3 days displayed similar levels of *Prmt7* upregulation (Figure 3.9 and Figure 3.10). Moreover, when the other PRMTs like PRMT1, PRMT4 and PRMT5 were analysed in MHS cells, there was no significant differences following CSE exposure unlike PRMT7 (Figure

3.12). Primary monocytes isolated from acute CS exposed mice also showed similar results (Figure 3.9). However, alveolar macrophages isolated from acute CS exposed mice demonstrated significant upregulation in *Prmt5* expression levels similar to *Prmt7* (Figure 3.10). This result is perhaps not so surprising when one considers that PRMT7 and PRMT5 are mentioned in the same biological processes together, including cancer metastasis and tumorigenesis (Shailesh et al., 2018; Yao et al., 2014) as well as RNA splicing (Gonsalvez et al., 2007a). Additionally, their functions are dependent on each other enzymatically since PRMT7 allosterically regulates the function of PRMT5 (Jain et al., 2017; Smil et al., 2015). This cooperative work might explain the increase in *Prmt5* expression in alveolar macrophages in this study. Considering these findings, it is highly suggestive that PRMT7 may have a potential role in the pathogenesis of COPD through monocytes and macrophages in the lungs.

4.2 Regulation of PRMT7 in primary monocytes through NF-κB pathway

Considering the upregulation of PRMT7 in macrophages and its potential role in disease pathogenesis, the next objective was to identify the upstream regulation of PRMT7 in macrophages. There are plenty of molecular signaling pathways that are activated in macrophages in response to inflammatory insult. Significantly, nuclear factor kappa B (NF-κB) has been highly associated with CS induced airway inflammation (Barnes, 2016; Schuliga, 2015; Zhou et al., 2018) in COPD and it plays an active role in enhancing the expression of pro-inflammatory cytokines in activated macrophages (Wang et al., 2014a). Considering the crucial involvement of NF-κB pathway in COPD, primary monocytes freshly isolated from mouse and the peripheral blood of humans were stimulated with LPS which can directly activate the NF-κB pathway via interacting with Toll Like Receptor 4 (TLR4) (Dorrington and Fraser, 2019). As a result, it was observed that primary monocytes isolated from mouse and human upregulated *Prmt7* expression upon LPS stimulation, which was suggestive that the NF-κB pathway is an upstream regulator of the *Prmt7* gene (Figure 3.15). This finding was validated by using specific NF-κB pathway inhibitors, BAY11-7082 and JSH-23 (Kumar et al., 2011; Mori et al., 2002) (Figure 3.16 and Figure 3.17). Moreover, it is relevant given the

importance of the involvement of NF-κB signaling not only in COPD but also in several other pulmonary diseases such as asthma (Gagliardo et al., 2003) (Edwards et al., 2009) and fibrosis (Hou et al., 2018; Luedde and Schwabe, 2011). Taken together, it was suggestive that PRMT7 expression is regulated via NF-κB/RELA pathway in monocytes and macrophages.

4.3 Targeting PRMT7 in COPD animal models

Next, the question how PRMT7 influenced macrophage contribution to the development of COPD was addressed. To identify the role of PRMT7 in this aspect, mice with reduced expression of PRMT7, *Prmt7*$^{+/-}$ mice were used. *Prmt7*$^{+/-}$ mice rather than homozygous mice were used because *Prmt7*$^{-/-}$ mice have been previously reported to die between 5-10 days of birth (Ying et al., 2015). Interestingly, *Prmt7*$^{+/-}$ mice did not accumulate macrophages in their lungs following acute CS for 3 days (Figure 3.20) and chronic CS for 4 months (Figure 3.21). This finding was supported by exposure to elastase (Figure 3.27 and Figure 3.28). This reduction of macrophages in the lungs of *Prmt7*$^{+/-}$ mice led to protection against emphysema development, one of the main hallmarks of COPD (Figure 3.26 and Figure 3.29). Considering that macrophages are a great source of cytokine production and proteolytic enzyme secretion like elastase (Smith et al., 1998), this result was consistent with previous findings. When macrophages were depleted after tissue injury, inflammation was significantly reduced (Duffield et al., 2013). It has also been known for some time that macrophage elastase deficient mice are protected from emphysema development following chronic CS exposure (Hautamaki et al., 1997). Supporting this finding, the deletion of alveolar macrophages in the lungs with alendronate administration inhibited airspace enlargement in an elastase-induced mouse model of COPD (Ueno et al., 2015a). Therefore, less macrophage recruitment in the lungs of *Prmt7*$^{+/-}$ mice, resulting in impaired emphysema development in COPD animal models has precedent. In support of this, endogenous monocyte derived macrophages from *Prmt7*$^{+/-}$ mice were not recruited into wild-type lungs that had been transplanted into the *Prmt7*$^{+/-}$ mice (Figure 3.30), confirming an inability of the recruitment of monocyte-derived macrophages in *Prmt7*$^{+/-}$ mice. As expected, these lungs with less macrophages were protected from emphysema development, unlike wild-type lungs grafted into wild-type

recipients (Figure 3.31). These findings were also validated by *in vivo* trans-endothelial migration assay using primary monocytes. Consistently, primary monocytes from *Prmt7*$^{+/-}$ mice displayed impaired trans-endothelial migratory ability towards CCL2 (Figure 3.32).

Monocyte-derived macrophages are recruited into inflamed tissue via CCL2, which is the main chemokine for macrophage recruitment (Mak and Uetrecht, 2019). One possible reason for impaired recruitment and accumulation of macrophages in the lungs of *Prmt7*$^{+/-}$ mice could be CCL2 deficiency. However, CCL2 was expressed similarly in the lungs and BALF of wild-type and *Prmt7*$^{+/-}$ mice after acute (Figure 3.20) and chronic CS exposure (Figure 3.23), suggesting an intrinsic defect in the macrophages of *Prmt7*$^{+/-}$ animals. Both *Prmt7*^{null} MHS cells generated by CRISPR/Cas9-targeted mutation and monocytes isolated from *Prmt7*$^{+/-}$ mice expressed CCR2 levels on their surface comparable to their wild-type counterparts. This finding highlighted that PRMT7 did not affect cytokine levels nor receptor levels. Therefore, it may be critical for the regulation of downstream receptor signaling.

The levels of two main adhesion molecules, VCAM1 and ICAM1, which play a critical role in the adhesion and migration of monocytes from blood vessels to targeted tissue (Sans et al., 1999), was also examined. The expression of these adhesion molecules did not vary between the lungs of *Prmt7*$^{+/-}$ and WT mice (Figure 3.24 and Figure 3.25), suggesting that a deficiency of VCAM1 and ICAM1 was not the cause of less macrophage recruitment in *Prmt7*$^{+/-}$ mice.

Furthermore, given the importance of macrophage involvement in the pathogenesis of COPD, the altered differentiation of macrophages, dysregulated polarization and activation all play a potential role in promoting lung tissue damage (Cornwell et al., 2018; Shaykhiev et al., 2009). It was crucial their development and differentiation in the absence of PRMT7 should also be considered carefully. However, in this study it was clearly demonstrated that macrophages isolated from *Prmt7*$^{+/-}$ mice did not have any impairments in terms of their development and differentiation (Figure 3.33, Figure 3.34 and Figure 3.35). Besides macrophages, dendritic cells (DCs) which are sharing a common progenitor with macrophages (Xiao et al., 2017) play a significant role in inflammation during COPD pathogenesis (Givi et al., 2012). For this reason, the effects of PRMT7 deficiency on the

development and activation of DCs was examined. As a result, dendritic cell development and activation was not adversely affected by the reduction of PRMT7 (Figure 3.36). All in all, these findings highly proposed that PRMT7 is crucial for the recruitment of monocyte-derived macrophages into the lungs following inflammatory insult in multiple COPD models.

4.4 Underlying molecular mechanisms of impaired macrophage recruitment into lungs in the absence of PRMT7

Prmt7$^{+/-}$ mice had impaired monocyte-derived macrophage recruitment into their lungs as a result of CS and elastase exposure. A further objective was to elucidate the underlying molecular mechanisms of this phenomenon. For this purpose, proteomic analysis of immunoprecipitated monomethylated arginine containing proteins from *Prmt7*^{null} MHS cells, which were CRISPR-Cas9 generated, was undertaken. Validation of this approach was confirmed by less monomethylated core histone proteins being detected, including H2B, H3 and H4 in *Prmt7*^{null} compared to *Prmt7*$^{+/+}$ MHS cells (Figure 3.42). This was expected as PRMT7 was already shown to target these specific histones for methylation (Feng et al., 2013). As a result of KEGG pathway analysis, three main pathways were identified to be potentially regulated by PRMT7. These were leukocyte transendothelial migration, focal adhesion as well as MAPK signaling pathways (Figure 3.43). These results were quite consistent with the previous findings of this study. Interestingly, these three different pathways have one common protein, RAP1A/B. RAP1A and RAP1B are two separate isoforms which share 95% identical sequence (Wittchen et al., 2011), therefore the peptides generated after tryptic digestion could not distinguish between RAP1A or RAP1B. Western blot results demonstrated a significant reduction of RAP1A/B protein levels in *Prmt7*^{null} MHS cells compared to *Prmt7*$^{+/+}$ MHS cells (Figure 3.50). The western blot antibody also was not able to distinguish the two different isoforms. However, qPCR analysis revealed that mRNA expression levels of *Rap1a* was reduced in *Prmt7*^{null} MHS cells compared to *Prmt7*$^{+/+}$ cells while *Rap1b* expression remained the same across the two cell lines (Figure 3.50).

RAP1 are small G proteins in the Ras superfamily and they are activated by GTP binding (Bos et al., 2001). More interestingly, RAP1 has been implicated to be associated with many

cellular events particularly adhesion related (Caron, 2003). Consistent with findings in this study, RAP1 controls cellular adhesion and migration via inducing integrin activation (Kooistra et al., 2007; Zhang et al., 2014) and modulating MAPK signaling activity (Gao et al., 2006; Stork and Dillon, 2005). In keeping, B and T cells isolated from the spleen of Rap1a deficient mice showed impaired integrin-mediated cell adhesion (Duchniewicz et al., 2006). More relevant to this study, macrophages isolated from *Rap1a*$^{-/-}$ mice demonstrated decreased adhesion ability and impaired migration towards chemokines (Li et al., 2007), similar to what was observed here with *Prmt7*^{null} MHS cells (Figure 3.43 and Figure 3.44). Considering the role of RAP1A in adhesion and migration, it was perhaps not surprising that *Prmt7*^{null} MHS cells had reduced surface expression of the integrins ITGAM and ITGAL (Figure 3.44) and impaired migration towards CCL2 (Figure 3.43). RAP1 is an upstream regulator of MAPK signaling (Zhang and Liu, 2002) and its activity is increased with the binding of LPS to TLR4 (Caron et al., 2000). Next purpose of this study was to understand whether MAPK signaling cascade was affected adversely in the absence of PRMT7, since *Rap1a* levels were significantly reduced in *Prmt7*^{null} MHS cells. As predicted, reduced phosphorylation of ERK and p38 following LPS stimulation in *Prmt7*^{null} MHS cells in comparison to *Prmt7*$^{+/+}$ cells was seen (Figure 3.46). Similarly, *Prmt7*^{null} MHS cells stimulated by CCL2 as an alternative ligand for G coupled receptor signaling demonstrated reduced phosphorylation of ERK and p38, implying impaired G protein coupled receptor signaling in PRMT7 deficient macrophages potentially due to reduced RAP1A expression.

To confirm, blocking the activity of RAP1 with GGTI-298 inhibitor (Ke et al., 2019; Li et al., 2010) in MHS cells also displayed an impairment in the phosphorylation of ERK, similar to *Prmt7*^{null} MHS cells following LPS stimulation (Figure 3.49). Moreover, GGTI-298 inhibition of RAP1 (Ke et al., 2019) also reduced the surface expression of the adhesion molecules ITGAL (CD11a) and ITGAM (CD11b) that was consistent with reduced surface expression levels observed in *Prmt7*^{null} cells (Figure 3.49). This finding was supported by using a novel PRMT7 inhibitor, SGC2037, targeting the enzyme activity of PRMT7 (Szewczyk et al., 2020). Treatment of MHS cells with the inhibitor of PRMT7 resulted in decreased surface expression levels of the key adhesion molecules ITGAL (CD11a) and ITGAM (CD11b) (Figure 3.45). These

two integrins were found to be critical for the adhesion of circulating leukocytes including monocytes to activated endothelium (Gerhardt and Ley, 2015). It was therefore not surprising that reduced expression of adhesion molecules was accompanied by impaired transendothelial migration in the absence of PRMT7 (Figure 3.43). These findings were in keeping with the proteome analysis revealing that focal adhesion and migration was impaired in *Prmt7*^{null} MHS cells compared to *Prmt7*$^{+/+}$ cells. Taken all together, this data suggests that PRMT7 may regulate RAP1A expression and subsequent downstream processes including adhesion, migration as well as MAPK signaling.

Crucial was to identify how PRMT7 regulates *Rap1a* gene expression in macrophages. PRMTs in general are known to be responsible for modulating gene expression epigenetically via histone methylations (Di Lorenzo and Bedford, 2011; Litt et al., 2009). PRMT7 has been linked to regulate two important activating marks of transcription, which are H4R3me2a and H3R2me2s (Blanc and Richard, 2017). In the same direction, lack of PRMT7 has been reported to decrease symmetrical methylation of H4R3 at gene promoters (Blanc et al., 2016). Moreover, the amount of H3R2me2s mark has been shown to be diminished in PRMT7-deficient cells (Migliori et al., 2012). So far, the function of PRMT7 in relation to its ability to monomethylate target proteins at arginine residues has been discussed. However, in many studies PRMT7 has been described to regulate dimethylation in cells, yet biochemically can only undertake mono-methylation (Zurita-Lopez et al., 2012). The explanation for this dilemma was that PRMT7 mono-methylation allosterically modulates the activity of PRMT5 to di-methylate the same substrate. These two enzymes function in conjunction to symmetrically di-methylate histone substrates including H3R2 and H4R3 (Jain et al., 2017; Smil et al., 2015). These studies suggest a potential explanation for the lack of dimethylation found following the disruption of PRMT7 here and in other studies. In terms of *RAP1A* transcriptional regulation, ChIP-Seq analysis of human CD4 T cells demonstrated that H3R2me1 and H3R2me2 were enriched upstream of the transcriptional start site of the *RAP1A* gene (Barski et al., 2007). Taking this into consideration, it is explicitly shown here that *Prmt7*^{null} MHS cells had reduced H3R2me1 and H3R2me2s marks upstream of the transcriptional start site (TSS) of *Rap1a* in comparison to *Prmt7*$^{+/+}$ cells. Consistently, PRMT7

was also enriched at the same site on the *Rap1a* gene compared to the promoter of *Gapdh*, which was completely lost in *Prmt7*^{null} MHS cells (Figure 3.53). Between two different primer pairs used to amplify the genomic region upstream of the *Rap1a* TSS, primer I resulted in the strongest enrichment. When overlaying the primer regions with UCSC/ENCODE H3K4me1 and H3K27a ChIP-Seq tracks of the *Rap1a* region taken from BMDM cells, Accession: wgEncodeEM002658 and wgEncodeEM002657 respectively, the results suggested that primer I region could be an enhancer (Heintzman et al., 2009; Shen et al., 2012). There were studies showing that PRMTs might localize at the enhancers and regulate transcription of target genes. For example; PRMT5 dependent H4R3me2s was decreased in the absence of PRMT5 and resulted in modulation of target gene transcription (Zhao et al., 2009). Moreover, another study elegantly demonstrated that localization of PRMT6 at enhancers can regulate transcription of associated genes (Bouchard et al., 2018). Consistent with these findings, PRMT7 appears to target histone H3 at active enhancer regions upstream of *Rap1a* in macrophages to regulate *Rap1a* expression.

Even though PRMT7 methylates histone proteins to regulate the transcription of potential genes, it has been also shown to target non-histone proteins. One of the direct targets of PRMT7 was reported to be dishevelled 3 protein, which plays a key role in WNT signaling (Bikkavilli et al., 2012). In that study, the methylation of dishevelled 3 by PRMT7 together with PRMT1 affected the translocation of dishevelled 3 into the membrane and regulated WNT signaling. Methylation deficient dishevelled 3 localized in the membrane and led to continuous activation of WNT signaling (Bikkavilli et al., 2012). Considering these previous findings in which PRMT7 has a crucial role in WNT signaling, it was crucial to understand if PRMT7 reduction in *Prmt7*$^{+/-}$ mice could cause less emphysema formation as a result of CS and elastase exposure through modulation of WNT signaling. WNT signaling plays a central role in the pathogenesis of lung diseases like COPD and fibrosis, particularly in repair and regeneration mechanisms of alveolar epithelial cells following inflammatory insults damaging the lung (Konigshoff and Eickelberg, 2010; Shi et al., 2017). Therefore, the trans-differentiation of ATII cells into ATI cells isolated from *Prmt7*$^{+/-}$ and WT mice was examined, as this trans-differentiation is controlled by WNT signaling. ATII cells are defined as progenitor

cells for ATI cells and this transition is a crucial step in repair and regeneration following lung injury (Aspal and Zemans, 2020). However, there was no difference in terms of the differentiation marker, T1-alpha in between cells isolated from *Prmt7*$^{+/-}$ and WT mice. Aside from trans-differentiation, wound healing ability of ATII cells with silenced PRMT7 expression remained the same when compared to control ATII cells (Figure 3.38 and Figure 3.39). Further evidence that deficiency in lung parenchyma was not the reason for the impaired emphysema development, was observed in the transplantation experiment. It was demonstrated that wild-type lungs grafted into *Prmt7*$^{+/-}$ mice were also protected from emphysema (Figure 3.31).

4.5 Contribution of PRMT7 in other disease models

In this study, it has been highlighted that *Prmt7*$^{+/-}$ mice with reduced expression and enzymatic activity of PRMT7 were protected against emphysema development, which is a main hallmark of COPD pathogenesis. The findings suggest that this protection arose from having less monocyte-derived macrophage recruitment into the lungs of *Prmt7*$^{+/-}$ mice. A further purpose of this study was to examine if macrophage expressed PRMT7 may play a key role in the progression of other diseases driven by macrophage recruitment. To address this *Lyz2-Cre Prmt7*$^{fl/fl}$ mice which do not express PRMT7 specifically in myeloid cells were generated. First these mice were used to investigate the potential role of macrophage expressed PRMT7 in the bleomycin-induced pulmonary fibrosis disease model, which is a common experimental study model of human lung fibrosis (Shi et al., 2014). This model was targeted because it has previously been demonstrated that the development of pulmonary fibrosis, which is bleomycin induced, is dependent on monocyte-derived macrophage recruitment to the lung and mice lacking macrophages had reduced fibrosis (Gibbons et al., 2011). Therefore, WT and *Lyz2-Cre Prmt7*$^{fl/fl}$ mice were exposed to bleomycin for 14 days. In supporting of previous findings in this study, *Lyz2-Cre Prmt7*$^{fl/fl}$ mice displayed less macrophage recruitment into the lungs following bleomycin instillation (Figure 3.54). To understand if this reduction in macrophage numbers in *Lyz2-Cre Prmt7*$^{fl/fl}$ mice after bleomycin instillation influences lung fibrosis development, collagen deposition, which is a

hallmark of fibrosis, was quantified. Consistently, the reduced macrophage number was accompanied by reduced collagen deposition in the lungs of *Lyz2-Cre Prmt7*$^{fl/fl}$ mice in comparison to WT mice (Figure 3.55). To further support and validate these findings, an independent skin injury model was utilized, where macrophage recruitment following skin injury is key for inflammation, scar formation and wound healing (Krzyszczyk et al., 2018). Therefore, macrophage numbers were quantified after 3 days of skin injury in *Lyz2-Cre Prmt7*$^{fl/fl}$ and WT mice. *Lyz2-Cre Prmt7*$^{fl/fl}$ mice demonstrated reduced numbers of macrophages in injured skin after 3 days compared to control mice (Figure 3.56). Furthermore, multiple sclerosis disease has the same pattern, where macrophage recruitment is considered to be harmful by initiating the demyelination of axons (Yamasaki et al., 2014). Our preliminary data in a multiple sclerosis model demonstrated that *Lyz2-Cre Prmt7*$^{fl/fl}$ mice delayed the disease onset and severity compared to WT controls after MOG injection in the EAE model (Data not shown). Further investigation is required for this experiment to quantify macrophage number in the spinal cord and correlate with disease severity. Taken all together PRMT7 is essential for the migration of monocytes and macrophages in several disease models including COPD, fibrosis, skin injury and potentially multiple sclerosis.

4.6 Conclusions and future directions

To conclude, here it has been shown that PRMT7 regulates the recruitment of monocyte-derived macrophages into tissue such as lung or skin following injury or inflammatory insult. The recruitment of macrophages into tissue is a critical step in the pathogenesis of several diseases including COPD. Translationally, methyltransferase activity accompanied by increased PRMT7 expression was enriched in COPD patients. PRMT7 expression in monocytes was found to be regulated via the NF-κB/RelA signaling pathway. Mechanistically, monomethylated histones, specifically H3, at enhancer regions via PRMT7 could regulate *Rap1a* expression in macrophages. RAP1A expression and activation play a key role in MAPK signaling as well as adhesion and migration of macrophages via integrin-mediated regulation. The schematic summary of these findings are demonstrated in (Figure 4.1).

Taking all results from this study into account, PRMT7 is revealed as an important determinant of monocyte driven inflammatory responses in lung disease and beyond. Thus targeting PRMT7 offers novel therapeutic potential against COPD and other chronic inflammatory conditions driven by monocyte recruitment.

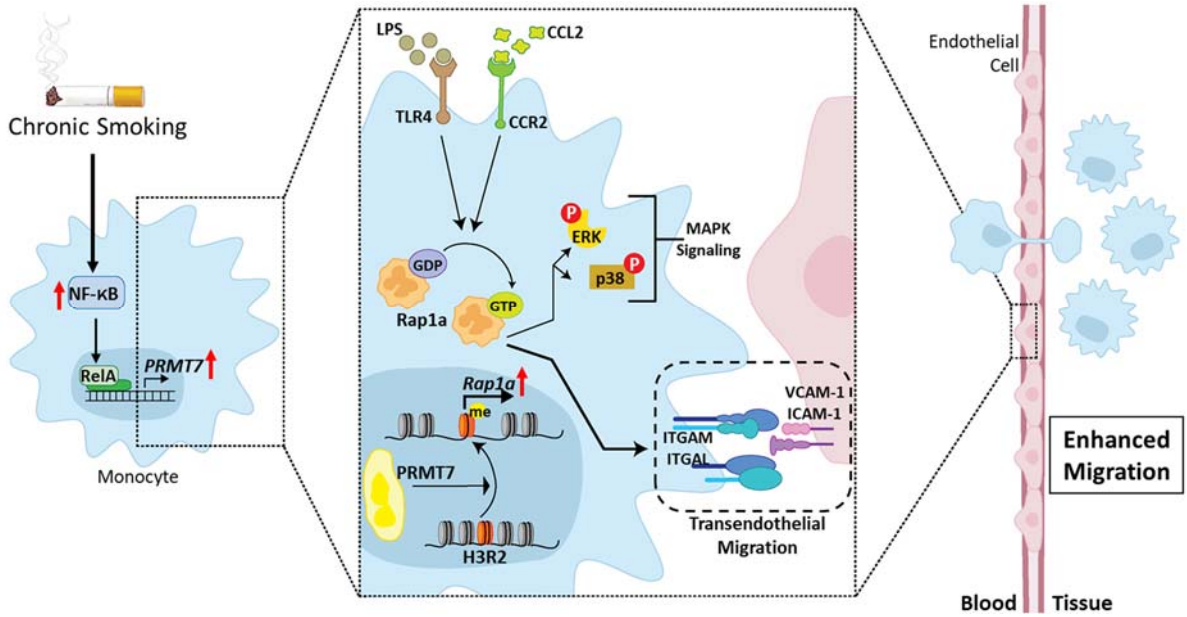

Figure 4.1 Schematic representation of PRMT7 mediated migration of macrophages into the tissue of injury. Inflammatory insults like CS exposure triggers NF-κB signaling and leads to transcriptional expression of *PRMT7* in monocytes. PRMT7 functions on histone proteins like H3 to monomethylate and monomethylated H3 enhances *Rap1a* expression. RAP1A after activation by GTP binding regulates MAPK signaling, integrin activation and therefore transendothelial migration of monocytes from blood to tissue of injury. Scheme drawing was supported by Zeynep Ertüz.

5. REFERENCES

Abboud, R.T., and Vimalanathan, S. (2008). Pathogenesis of COPD. Part I. The role of protease-antiprotease imbalance in emphysema. Int J Tuberc Lung Dis *12*, 361-367.

Abe, M., Kurosawa, M., Ishikawa, O., and Miyachi, Y. (2000). Effect of mast cell-derived mediators and mast cell-related neutral proteases on human dermal fibroblast proliferation and type I collagen production. J Allergy Clin Immunol *106*, S78-84.

Abel, A.M., Yang, C., Thakar, M.S., and Malarkannan, S. (2018). Natural Killer Cells: Development, Maturation, and Clinical Utilization. Frontiers in Immunology *9*.

Absher, M. (1973). CHAPTER 1 - Hemocytometer Counting. In Tissue Culture, P.F. Kruse, and M.K. Patterson, eds. (Academic Press), pp. 395-397.

Agolini, E., Dentici, M.L., Bellacchio, E., Alesi, V., Radio, F.C., Torella, A., Musacchia, F., Tartaglia, M., Dallapiccola, B., Nigro, V.*, et al.* (2018). Expanding the clinical and molecular spectrum of PRMT7 mutations: 3 additional patients and review. Clin Genet *93*, 675-681.

Ahsan, F., Rivas, I.P., Khan, M.A., and Torres Suarez, A.I. (2002). Targeting to macrophages: role of physicochemical properties of particulate carriers--liposomes and microspheres--on the phagocytosis by macrophages. J Control Release *79*, 29-40.

Ala, A., Dhillon, A.P., and Hodgson, H.J. (2003). Role of cell adhesion molecules in leukocyte recruitment in the liver and gut. Int J Exp Pathol *84*, 1-16.

Angelidis, I., Simon, L.M., Fernandez, I.E., Strunz, M., Mayr, C.H., Greiffo, F.R., Tsitsiridis, G., Ansari, M., Graf, E., Strom, T.-M.*, et al.* (2019). An atlas of the aging lung mapped by single cell transcriptomics and deep tissue proteomics. Nature Communications *10*, 963.

Antony, V.B., and Thannickal, V.J. (2018). Cellular Senescence in Chronic Obstructive Pulmonary Disease: Multifaceted and Multifunctional. Am J Respir Cell Mol Biol *59*, 135-136.

Antunes, M.A., and Rocco, P.R. (2011). Elastase-induced pulmonary emphysema: insights from experimental models. An Acad Bras Cienc *83*, 1385-1396.

Aspal, M., and Zemans, R. (2020). Mechanisms of ATII-to-ATI Cell Differentiation during Lung Regeneration. International Journal of Molecular Sciences *21*.

Auclair, Y., and Richard, S. (2013). The role of arginine methylation in the DNA damage response. DNA Repair (Amst) *12*, 459-465.

Auffray, C., Fogg, D., Garfa, M., Elain, G., Join-Lambert, O., Kayal, S., Sarnacki, S., Cumano, A., Lauvau, G., and Geissmann, F. (2007). Monitoring of blood vessels and tissues by a population of monocytes with patrolling behavior. Science *317*, 666-670.

Aziz, F., Penupolu, S., Xu, X., and He, J. (2010). Lung transplant in end-staged chronic obstructive pulmonary disease (COPD) patients: a concise review. J Thorac Dis *2*, 111-116.

Bagdonas, E., Raudoniute, J., Bruzauskaite, I., and Aldonyte, R. (2015). Novel aspects of pathogenesis and regeneration mechanisms in COPD. Int J Chron Obstruct Pulmon Dis *10*, 995-1013.

Balasubramanian, A., MacIntyre, N.R., Henderson, R.J., Jensen, R.L., Kinney, G., Stringer, W.W., Hersh, C.P., Bowler, R.P., Casaburi, R., Han, M.K.*, et al.* (2019). Diffusing Capacity of Carbon Monoxide in Assessment of COPD. Chest *156*, 1111-1119.

Baldwin, R.M., Haghandish, N., Daneshmand, M., Amin, S., Paris, G., Falls, T.J., Bell, J.C., Islam, S., and Côté, J. (2015). Protein arginine methyltransferase 7 promotes breast cancer cell invasion through the induction of MMP9 expression. Oncotarget *6*, 3013-3032.

Banchereau, J., Briere, F., Caux, C., Davoust, J., Lebecque, S., Liu, Y.J., Pulendran, B., and Palucka, K. (2000). Immunobiology of dendritic cells. Annu Rev Immunol *18*, 767-811.

Bao, X., Zhao, S., Liu, T., Liu, Y., Liu, Y., and Yang, X. (2013). Overexpression of PRMT5 promotes tumor cell growth and is associated with poor disease prognosis in epithelial ovarian cancer. J Histochem Cytochem *61*, 206-217.

Barnes, P.J. (2004). Alveolar macrophages in chronic obstructive pulmonary disease (COPD). Cell Mol Biol (Noisy-le-grand) *50 Online Pub*, Ol627-637.

Barnes, P.J. (2006). How corticosteroids control inflammation: Quintiles Prize Lecture 2005. Br J Pharmacol *148*, 245-254.

Barnes, P.J. (2008). Immunology of asthma and chronic obstructive pulmonary disease. Nat Rev Immunol *8*, 183-192.

Barnes, P.J. (2009). The cytokine network in chronic obstructive pulmonary disease. Am J Respir Cell Mol Biol *41*, 631-638.

Barnes, P.J. (2011). Similarities and differences in inflammatory mechanisms of asthma and COPD. Breathe *7*, 229-238.

Barnes, P.J. (2013). New anti-inflammatory targets for chronic obstructive pulmonary disease. Nat Rev Drug Discov *12*, 543-559.

Barnes, P.J. (2016). Inflammatory mechanisms in patients with chronic obstructive pulmonary disease. J Allergy Clin Immunol *138*, 16-27.

Barnes, P.J. (2017a). Cellular and molecular mechanisms of asthma and COPD. Clin Sci (Lond) *131*, 1541-1558.

Barnes, P.J. (2017b). Senescence in COPD and Its Comorbidities. Annu Rev Physiol *79*, 517-539.

Barnes, P.J., Baker, J., and Donnelly, L.E. (2019). Cellular Senescence as a Mechanism and Target in Chronic Lung Diseases. Am J Respir Crit Care Med *200*, 556-564.

Barski, A., Cuddapah, S., Cui, K., Roh, T.Y., Schones, D.E., Wang, Z., Wei, G., Chepelev, I., and Zhao, K. (2007). High-resolution profiling of histone methylations in the human genome. Cell *129*, 823-837.

Bedford, M.T., and Clarke, S.G. (2009). Protein arginine methylation in mammals: who, what, and why. Molecular cell *33*, 1-13.

Bedford, M.T., and Richard, S. (2005). Arginine methylation an emerging regulator of protein function. Mol Cell *18*, 263-272.

Belvisi, M.G., and Bottomley, K.M. (2003). The role of matrix metalloproteinases (MMPs) in the pathophysiology of chronic obstructive pulmonary disease (COPD): a therapeutic role for inhibitors of MMPs? Inflamm Res *52*, 95-100.

Bhat, T.A., Panzica, L., Kalathil, S.G., and Thanavala, Y. (2015). Immune Dysfunction in Patients with Chronic Obstructive Pulmonary Disease. Ann Am Thorac Soc *12 Suppl 2*, S169-175.

Bikkavilli, R.K., Avasarala, S., Vanscoyk, M., Sechler, M., Kelley, N., Malbon, C.C., and Winn, R.A. (2012). Dishevelled3 is a novel arginine methyl transferase substrate. Scientific reports *2*, 805-805.

Bikkavilli, R.K., and Malbon, C.C. (2012). Wnt3a-stimulated LRP6 phosphorylation is dependent upon arginine methylation of G3BP2. J Cell Sci *125*, 2446-2456.

Birnbaum, R., Yosha-Orpaz, N., Yanoov-Sharav, M., Kidron, D., Gur, H., Yosovich, K., Lerman-Sagie, T., Malinger, G., and Lev, D. (2019). Prenatal and postnatal presentation of PRMT7 related syndrome: Expanding the phenotypic manifestations. Am J Med Genet A *179*, 78-84.

Blanc, R.S., and Richard, S. (2017). Arginine Methylation: The Coming of Age. Mol Cell *65*, 8-24.

Blanc, R.S., Vogel, G., Chen, T., Crist, C., and Richard, S. (2016). PRMT7 Preserves Satellite Cell Regenerative Capacity. Cell Rep *14*, 1528-1539.

Boisvert, F.M., Déry, U., Masson, J.Y., and Richard, S. (2005). Arginine methylation of MRE11 by PRMT1 is required for DNA damage checkpoint control. Genes Dev *19*, 671-676.

Bonfield, T. (2012). In Vivo Models of Lung Disease.

Bonnardel, E., Prevel, R., Campagnac, M., Dubreuil, M., Marthan, R., Berger, P., and Dupin, I. (2019). Determination of reliable lung function parameters in intubated mice. Respir Res *20*, 211.

Bos, J.L., de Bruyn, K., Enserink, J., Kuiperij, B., Rangarajan, S., Rehmann, H., Riedl, J., de Rooij, J., van Mansfeld, F., and Zwartkruis, F. (2003). The role of Rap1 in integrin-mediated cell adhesion. Biochem Soc Trans *31*, 83-86.

Bos, J.L., de Rooij, J., and Reedquist, K.A. (2001). Rap1 signalling: adhering to new models. Nature Reviews Molecular Cell Biology *2*, 369-377.

Botelho, F.M., Gaschler, G.J., Kianpour, S., Zavitz, C.C., Trimble, N.J., Nikota, J.K., Bauer, C.M., and Stämpfli, M.R. (2010). Innate immune processes are sufficient for driving cigarette smoke-induced inflammation in mice. Am J Respir Cell Mol Biol *42*, 394-403.

Bouchard, C., Sahu, P., Meixner, M., Nötzold, R.R., Rust, M.B., Kremmer, E., Feederle, R., Hart-Smith, G., Finkernagel, F., Bartkuhn, M*., et al.* (2018). Genomic Location of PRMT6-Dependent H3R2 Methylation Is Linked to the Transcriptional Outcome of Associated Genes. Cell Rep *24*, 3339-3352.

Bowler, R.P., Barnes, P.J., and Crapo, J.D. (2004). The Role of Oxidative Stress in Chronic Obstructive Pulmonary Disease. COPD: Journal of Chronic Obstructive Pulmonary Disease *1*, 255-277.

Brandsma, C.-A., Hylkema, M.N., Geerlings, M., van Geffen, W.H., Postma, D.S., Timens, W., and Kerstjens, H.A.M. (2009). Increased levels of (class switched) memory B cells in peripheral blood of current smokers. Respir Res *10*, 108-108.

Brill, S.E., and Wedzicha, J.A. (2014). Oxygen therapy in acute exacerbations of chronic obstructive pulmonary disease. Int J Chron Obstruct Pulmon Dis *9*, 1241-1252.

Brusselle, G.G., Demoor, T., Bracke, K.R., Brandsma, C.-A., and Timens, W. (2009a). Lymphoid follicles in (very) severe COPD: beneficial or harmful? European Respiratory Journal *34*, 219-230.

Brusselle, G.G., Demoor, T., Bracke, K.R., Brandsma, C.A., and Timens, W. (2009b). Lymphoid follicles in (very) severe COPD: beneficial or harmful? Eur Respir J *34*, 219-230.

Brusselle, G.G., Joos, G.F., and Bracke, K.R. (2011). New insights into the immunology of chronic obstructive pulmonary disease. Lancet *378*, 1015-1026.

Buenrostro, J.D., Wu, B., Chang, H.Y., and Greenleaf, W.J. (2015). ATAC-seq: A Method for Assaying Chromatin Accessibility Genome-Wide. Curr Protoc Mol Biol *109*, 21.29.21-21.29.29.

Buhr, N., Carapito, C., Schaeffer, C., Kieffer, E., Van Dorsselaer, A., and Viville, S. (2008). Nuclear proteome analysis of undifferentiated mouse embryonic stem and germ cells. ELECTROPHORESIS *29*, 2381-2390.

Burgel, P.R., and Nadel, J.A. (2004). Roles of epidermal growth factor receptor activation in epithelial cell repair and mucin production in airway epithelium. Thorax *59*, 992-996.

Butler, J.S., Zurita-Lopez, C.I., Clarke, S.G., Bedford, M.T., and Dent, S.Y. (2011). Protein-arginine methyltransferase 1 (PRMT1) methylates Ash2L, a shared component of mammalian histone H3K4 methyltransferase complexes. J Biol Chem *286*, 12234-12244.

Caceres, T.B., Thakur, A., Price, O.M., Ippolito, N., Li, J., Qu, J., Acevedo, O., and Hevel, J.M. (2018). Phe71 in Type III Trypanosomal Protein Arginine Methyltransferase 7 (TbPRMT7) Restricts the Enzyme to Monomethylation. Biochemistry *57*, 1349-1359.

Campbell, J.D., McDonough, J.E., Zeskind, J.E., Hackett, T.L., Pechkovsky, D.V., Brandsma, C.-A., Suzuki, M., Gosselink, J.V., Liu, G., Alekseyev, Y.O*., et al.* (2012). A gene expression signature of emphysema-related lung destruction and its reversal by the tripeptide GHK. Genome Medicine *4*, 67.

Caramori, G., Casolari, P., Barczyk, A., Durham, A.L., Di Stefano, A., and Adcock, I. (2016). COPD immunopathology. Semin Immunopathol *38*, 497-515.

Caron, E. (2003). Cellular functions of the Rap1 GTP-binding protein: a pattern emerges. Journal of Cell Science *116*, 435-440.

Caron, E., Self, A.J., and Hall, A. (2000). The GTPase Rap1 controls functional activation of macrophage integrin alphaMbeta2 by LPS and other inflammatory mediators. Curr Biol *10*, 974-978.

Cazzola, M., Page, C.P., Calzetta, L., and Matera, M.G. (2012). Emerging anti-inflammatory strategies for COPD. European Respiratory Journal *40*, 724-741.

Chen, G., Zhou, M., Chen, L., Meng, Z.-J., Xiong, X.-Z., Liu, H.-J., Xin, J.-B., and Zhang, J.-C. (2016). Cigarette Smoke Disturbs the Survival of CD8+ Tc/Tregs Partially through Muscarinic Receptors-Dependent Mechanisms in Chronic Obstructive Pulmonary Disease. PloS one *11*, e0147232-e0147232.

Chen, T.-Y., Lee, S.-H., Dhar, S.S., and Lee, M.G. (2018). Protein arginine methyltransferase 7-mediated microRNA-221 repression maintains Oct4, Nanog, and Sox2 levels in mouse embryonic stem cells. The Journal of biological chemistry *293*, 3925-3936.

Cheng, D., Côté, J., Shaaban, S., and Bedford, M.T. (2007). The arginine methyltransferase CARM1 regulates the coupling of transcription and mRNA processing. Mol Cell *25*, 71-83.

Cheng, D., He, Z., Zheng, L., Xie, D., Dong, S., and Zhang, P. (2018). PRMT7 contributes to the metastasis phenotype in human non-small-cell lung cancer cells possibly through the interaction with HSPA5 and EEF2. Onco Targets Ther *11*, 4869-4876.

Cheng, X., Collins, R.E., and Zhang, X. (2005). Structural and sequence motifs of protein (histone) methylation enzymes. Annu Rev Biophys Biomol Struct *34*, 267-294.

Cheong, C., Matos, I., Choi, J.H., Dandamudi, D.B., Shrestha, E., Longhi, M.P., Jeffrey, K.L., Anthony, R.M., Kluger, C., Nchinda, G.*, et al.* (2010). Microbial stimulation fully differentiates monocytes to DC-SIGN/CD209(+) dendritic cells for immune T cell areas. Cell *143*, 416-429.

Cho, E.-C., Zheng, S., Munro, S., Liu, G., Carr, S., Moehlenbrink, J., Lu, Y.-C., Stimson, L., Khan, O., Konietzny, R.*, et al.* (2012). Arginine methylation controls growth regulation by E2F-1. The EMBO journal *31*, 1785-1797.

Chung, J., Karkhanis, V., Baiocchi, R.A., and Sif, S. (2019). Protein arginine methyltransferase 5 (PRMT5) promotes survival of lymphoma cells via activation of WNT/β-catenin and AKT/GSK3β proliferative signaling. J Biol Chem *294*, 7692-7710.

Churg, A., Cosio, M., and Wright, J.L. (2008). Mechanisms of cigarette smoke-induced COPD: insights from animal models. American Journal of Physiology-Lung Cellular and Molecular Physiology *294*, L612-L631.

Churg, A., Zhou, S., and Wright, J.L. (2012). Matrix metalloproteinases in COPD. European Respiratory Journal *39*, 197-209.

Ciccia, A., and Elledge, S.J. (2010). The DNA damage response: making it safe to play with knives. Mol Cell *40*, 179-204.

Clini, E.M., and Ambrosino, N. (2008). Nonpharmacological treatment and relief of symptoms in COPD. European Respiratory Journal *32*, 218-228.

Cong, L., Ran, F.A., Cox, D., Lin, S., Barretto, R., Habib, N., Hsu, P.D., Wu, X., Jiang, W., Marraffini, L.A.*, et al.* (2013). Multiplex genome engineering using CRISPR/Cas systems. Science *339*, 819-823.

Conlon, T.M., John-Schuster, G., Heide, D., Pfister, D., Lehmann, M., Hu, Y., Ertüz, Z., Lopez, M.A., Ansari, M., Strunz, M.*, et al.* (2020). Inhibition of LTβR signalling activates WNT-induced regeneration in lung. Nature.

Cornwell, W.D., Kim, V., Fan, X., Vega, M.E., Ramsey, F.V., Criner, G.J., and Rogers, T.J. (2018). Activation and polarization of circulating monocytes in severe chronic obstructive pulmonary disease. BMC pulmonary medicine *18*, 101.

Cosio, M.G., Saetta, M., and Agusti, A. (2009). Immunologic Aspects of Chronic Obstructive Pulmonary Disease. New England Journal of Medicine *360*, 2445-2454.

Cosio Piqueras, M.G., and Cosio, M.G. (2001). Disease of the airways in chronic obstructive pulmonary disease. European Respiratory Journal *18*, 41s-49s.

Covic, M., Hassa, P.O., Saccani, S., Buerki, C., Meier, N.I., Lombardi, C., Imhof, R., Bedford, M.T., Natoli, G., and Hottiger, M.O. (2005). Arginine methyltransferase CARM1 is a promoter-specific regulator of NF-kappaB-dependent gene expression. EMBO J *24*, 85-96.

Cox, J., and Mann, M. (2008). MaxQuant enables high peptide identification rates, individualized p.p.b.-range mass accuracies and proteome-wide protein quantification. Nature biotechnology *26*, 1367-1372.

Craig, J.M., Scott, A.L., and Mitzner, W. (2017). Immune-mediated inflammation in the pathogenesis of emphysema: insights from mouse models. Cell Tissue Res *367*, 591-605.

Craig, T.J., and Henao, M.P. (2018). Advances in managing COPD related to α(1) -antitrypsin deficiency: An under-recognized genetic disorder. Allergy *73*, 2110-2121.

Culpitt, S.V., Rogers, D.F., Shah, P., De Matos, C., Russell, R.E., Donnelly, L.E., and Barnes, P.J. (2003). Impaired inhibition by dexamethasone of cytokine release by alveolar macrophages from patients with chronic obstructive pulmonary disease. Am J Respir Crit Care Med *167*, 24-31.

Curtis, J.L., Freeman, C.M., and Hogg, J.C. (2007). The immunopathogenesis of chronic obstructive pulmonary disease: insights from recent research. Proceedings of the American Thoracic Society *4*, 512-521.

Cyster, J.G., Dang, E.V., Reboldi, A., and Yi, T. (2014). 25-Hydroxycholesterols in innate and adaptive immunity. Nature Reviews Immunology *14*, 731-743.

D'Hulst, A.I., Maes, T., Bracke, K.R., Demedts, I.K., Tournoy, K.G., Joos, G.F., and Brusselle, G.G. (2005). Cigarette smoke-induced pulmonary emphysema in scid-mice. Is the acquired immune system required? Respir Res *6*, 147-147.

da Silva, E.Z., Jamur, M.C., and Oliver, C. (2014). Mast cell function: a new vision of an old cell. J Histochem Cytochem *62*, 698-738.

Decramer, M., Janssens, W., and Miravitlles, M. (2012). Chronic obstructive pulmonary disease. Lancet (London, England) *379*, 1341-1351.

Delavary, B.M., van der Veer, W.M., van Egmond, M., Niessen, F.B., and Beelen, R.H.J. (2011). Macrophages in skin injury and repair. Immunobiology *216*, 753-762.

Deribe, Y.L., Pawson, T., and Dikic, I. (2010). Post-translational modifications in signal integration. Nat Struct Mol Biol *17*, 666-672.

Desch, A.N., Gibbings, S.L., Goyal, R., Kolde, R., Bednarek, J., Bruno, T., Slansky, J.E., Jacobelli, J., Mason, R., Ito, Y.*, et al.* (2016). Flow Cytometric Analysis of Mononuclear Phagocytes in Nondiseased Human Lung and Lung-Draining Lymph Nodes. Am J Respir Crit Care Med *193*, 614-626.

Deshmane, S.L., Kremlev, S., Amini, S., and Sawaya, B.E. (2009). Monocyte chemoattractant protein-1 (MCP-1): an overview. J Interferon Cytokine Res *29*, 313-326.

Dhar, S.S., Lee, S.H., Kan, P.Y., Voigt, P., Ma, L., Shi, X., Reinberg, D., and Lee, M.G. (2012). Trans-tail regulation of MLL4-catalyzed H3K4 methylation by H4R3 symmetric dimethylation is mediated by a tandem PHD of MLL4. Genes Dev *26*, 2749-2762.

Di Lorenzo, A., and Bedford, M.T. (2011). Histone arginine methylation. FEBS Lett *585*, 2024-2031.

Di Stefano, A., Capelli, A., Lusuardi, M., Balbo, P., Vecchio, C., Maestrelli, P., Mapp, C.E., Fabbri, L.M., Donner, C.F., and Saetta, M. (1998). Severity of airflow limitation is associated with severity of airway inflammation in smokers. Am J Respir Crit Care Med *158*, 1277-1285.

Di Stefano, A., Maestrelli, P., Roggeri, A., Turato, G., Calabro, S., Potena, A., Mapp, C.E., Ciaccia, A., Covacev, L., Fabbri, L.M.*, et al.* (1994). Upregulation of adhesion molecules in the bronchial mucosa of subjects with chronic obstructive bronchitis. Am J Respir Crit Care Med *149*, 803-810.

Diaz, P.T., Bruns, A.S., Ezzie, M.E., Marchetti, N., and Thomashow, B.M. (2008). Optimizing bronchodilator therapy in emphysema. Proceedings of the American Thoracic Society *5*, 501-505.

Disease, G.B.D., Injury, I., and Prevalence, C. (2018). Global, regional, and national incidence, prevalence, and years lived with disability for 354 diseases and injuries for 195 countries and territories, 1990-2017: a systematic analysis for the Global Burden of Disease Study 2017. Lancet *392*, 1789-1858.

Dolezal, E., Infantino, S., Drepper, F., Börsig, T., Singh, A., Wossning, T., Fiala, G.J., Minguet, S., Warscheid, B., Tarlinton, D.M.*, et al.* (2017). The BTG2-PRMT1 module limits pre-B cell expansion by regulating the CDK4-Cyclin-D3 complex. Nature Immunology *18*, 911-920.

Dorrington, M.G., and Fraser, I.D.C. (2019). NF-κB Signaling in Macrophages: Dynamics, Crosstalk, and Signal Integration. Frontiers in Immunology *10*.

Dos Anjos Cassado, A. (2017). F4/80 as a Major Macrophage Marker: The Case of the Peritoneum and Spleen. Results Probl Cell Differ *62*, 161-179.

Duchniewicz, M., Zemojtel, T., Kolanczyk, M., Grossmann, S., Scheele, J.S., and Zwartkruis, F.J.T. (2006). Rap1A-Deficient T and B Cells Show Impaired Integrin-Mediated Cell Adhesion. Molecular and Cellular Biology *26*, 643-653.

Duffield, J.S., Lupher, M., Thannickal, V.J., and Wynn, T.A. (2013). Host responses in tissue repair and fibrosis. Annu Rev Pathol *8*, 241-276.

Eapen, M.S., Hansbro, P.M., McAlinden, K., Kim, R.Y., Ward, C., Hackett, T.-L., Walters, E.H., and Sohal, S.S. (2017). Abnormal M1/M2 macrophage phenotype profiles in the small airway wall and lumen in smokers and chronic obstructive pulmonary disease (COPD). Scientific reports *7*, 13392-13392.

Ebert, R.V., and Terracio, M.J. (1975). The bronchiolar epithelium in cigarette smokers. Observations with the scanning electron microscope. Am Rev Respir Dis *111*, 4-11.

Edwards, M.R., Bartlett, N.W., Clarke, D., Birrell, M., Belvisi, M., and Johnston, S.L. (2009). Targeting the NF-kappaB pathway in asthma and chronic obstructive pulmonary disease. Pharmacol Ther *121*, 1-13.

Elias, J.E., and Gygi, S.P. (2007). Target-decoy search strategy for increased confidence in large-scale protein identifications by mass spectrometry. Nature methods *4*, 207-214.

Elliot, J.G., Jensen, C.M., Mutavdzic, S., Lamb, J.P., Carroll, N.G., and James, A.L. (2004). Aggregations of lymphoid cells in the airways of nonsmokers, smokers, and subjects with asthma. Am J Respir Crit Care Med *169*, 712-718.

Eriksen, A.C., Andersen, J.B., Kristensson, M., dePont Christensen, R., Hansen, T.F., Kjær-Frifeldt, S., and Sørensen, F.B. (2017). Computer-assisted stereology and automated image analysis for quantification of tumor infiltrating lymphocytes in colon cancer. Diagn Pathol *12*, 65.

Ernst, P., Saad, N., and Suissa, S. (2015). Inhaled corticosteroids in COPD: the clinical evidence. European Respiratory Journal *45*, 525-537.

Fahy, J.V., and Dickey, B.F. (2010). Airway mucus function and dysfunction. N Engl J Med *363*, 2233-2247.

Falk, J.A., Minai, O.A., and Mosenifar, Z. (2008). Inhaled and systemic corticosteroids in chronic obstructive pulmonary disease. Proceedings of the American Thoracic Society *5*, 506-512.

Fang, W.B., Jokar, I., Zou, A., Lambert, D., Dendukuri, P., and Cheng, N. (2012). CCL2/CCR2 chemokine signaling coordinates survival and motility of breast cancer cells through Smad3 protein- and p42/44 mitogen-activated protein kinase (MAPK)-dependent mechanisms. The Journal of biological chemistry *287*, 36593-36608.

Feenstra, T.L., van Genugten, M.L., Hoogenveen, R.T., Wouters, E.F., and Rutten-van Molken, M.P. (2001). The impact of aging and smoking on the future burden of chronic obstructive pulmonary disease: a model analysis in the Netherlands. Am J Respir Crit Care Med *164*, 590-596.

Feng, Y., Maity, R., Whitelegge, J.P., Hadjikyriacou, A., Li, Z., Zurita-Lopez, C., Al-Hadid, Q., Clark, A.T., Bedford, M.T., Masson, J.Y., *et al.* (2013). Mammalian protein arginine methyltransferase 7 (PRMT7) specifically targets RXR sites in lysine- and arginine-rich regions. J Biol Chem *288*, 37010-37025.

Ferkol, T., and Schraufnagel, D. (2014). The global burden of respiratory disease. Ann Am Thorac Soc *11*, 404-406.

Fischer, B.M., Pavlisko, E., and Voynow, J.A. (2011). Pathogenic triad in COPD: oxidative stress, protease-antiprotease imbalance, and inflammation. Int J Chron Obstruct Pulmon Dis *6*, 413-421.

Fornes, O., Castro-Mondragon, J.A., Khan, A., van der Lee, R., Zhang, X., Richmond, P.A., Modi, B.P., Correard, S., Gheorghe, M., Baranašić, D., *et al.* (2019). JASPAR 2020: update of the open-access database of transcription factor binding profiles. Nucleic Acids Res *48*, D87-D92.

Fuhrmann, J., and Thompson, P.R. (2016). Protein Arginine Methylation and Citrullination in Epigenetic Regulation. ACS Chem Biol *11*, 654-668.

Fulton, M.D., Brown, T., and Zheng, Y.G. (2019). The Biological Axis of Protein Arginine Methylation and Asymmetric Dimethylarginine. International journal of molecular sciences *20*, 3322.

Gagliardo, R., Chanez, P., Mathieu, M., Bruno, A., Costanzo, G., Gougat, C., Vachier, I., Bousquet, J., Bonsignore, G., and Vignola, A.M. (2003). Persistent activation of nuclear factor-kappaB signaling pathway in severe uncontrolled asthma. Am J Respir Crit Care Med *168*, 1190-1198.

Gao, L., Feng, Y., Bowers, R., Becker-Hapak, M., Gardner, J., Council, L., Linette, G., Zhao, H., and Cornelius, L.A. (2006). Ras-Associated Protein-1 Regulates Extracellular Signal-Regulated Kinase Activation and Migration in Melanoma Cells: Two Processes Important to Melanoma Tumorigenesis and Metastasis. Cancer Research *66*, 7880-7888.

Garbuzenko, E., Nagler, A., Pickholtz, D., Gillery, P., Reich, R., Maquart, F.X., and Levi-Schaffer, F. (2002). Human mast cells stimulate fibroblast proliferation, collagen synthesis and lattice contraction: a direct role for mast cells in skin fibrosis. Clin Exp Allergy *32*, 237-246.

Gary, J.D., and Clarke, S. (1998). RNA and protein interactions modulated by protein arginine methylation. Prog Nucleic Acid Res Mol Biol *61*, 65-131.

Geng, P., Zhang, Y., Liu, X., Zhang, N., Liu, Y., Liu, X., Lin, C., Yan, X., Li, Z., Wang, G., *et al.* (2017). Automethylation of protein arginine methyltransferase 7 and its impact on breast cancer progression. The FASEB Journal *31*, 2287-2300.

Gerhardt, T., and Ley, K. (2015). Monocyte trafficking across the vessel wall. Cardiovasc Res *107*, 321-330.

Gharib, S.A., Manicone, A.M., and Parks, W.C. (2018). Matrix metalloproteinases in emphysema. Matrix Biol *73*, 34-51.

Ghorani, V., Boskabady, M.H., Khazdair, M.R., and Kianmeher, M. (2017). Experimental animal models for COPD: a methodological review. Tob Induc Dis *15*, 25-25.

Gibbons, M.A., MacKinnon, A.C., Ramachandran, P., Dhaliwal, K., Duffin, R., Phythian-Adams, A.T., van Rooijen, N., Haslett, C., Howie, S.E., Simpson, A.J.*, et al.* (2011). Ly6Chi monocytes direct alternatively activated profibrotic macrophage regulation of lung fibrosis. Am J Respir Crit Care Med *184*, 569-581.

Ginhoux, F., and Jung, S. (2014). Monocytes and macrophages: developmental pathways and tissue homeostasis. Nat Rev Immunol *14*, 392-404.

Givi, M.E., Redegeld, F.A., Folkerts, G., and Mortaz, E. (2012). Dendritic cells in pathogenesis of COPD. Curr Pharm Des *18*, 2329-2335.

Gogebakan, B., Bayraktar, R., Ulaslı, M., Oztuzcu, S., Tasdemir, D., and Bayram, H. (2014). The role of bronchial epithelial cell apoptosis in the pathogenesis of COPD. Molecular Biology Reports *41*, 5321-5327.

Gomis-Rüth, F.X., Maskos, K., Betz, M., Bergner, A., Huber, R., Suzuki, K., Yoshida, N., Nagase, H., Brew, K., Bourenkov, G.P.*, et al.* (1997). Mechanism of inhibition of the human matrix metalloproteinase stromelysin-1 by TIMP-1. Nature *389*, 77-81.

Gonsalvez, G., Ospina, J., Boisvert, F.-M., Lamond, A., and Matera, A.G. (2007a). Two distinct arginine methyltransferases are required for biogenesis of Sm-class ribonucleoproteins. The Journal of cell biology *178*, 733-740.

Gonsalvez, G.B., Tian, L., Ospina, J.K., Boisvert, F.M., Lamond, A.I., and Matera, A.G. (2007b). Two distinct arginine methyltransferases are required for biogenesis of Sm-class ribonucleoproteins. J Cell Biol *178*, 733-740.

Goven, D., Boutten, A., Leçon-Malas, V., Marchal-Sommé, J., Amara, N., Crestani, B., Fournier, M., Lesèche, G., Soler, P., Boczkowski, J.*, et al.* (2008). Altered Nrf2/Keap1-Bach1 equilibrium in pulmonary emphysema. Thorax *63*, 916-924.

Grashoff, W.F., Sont, J.K., Sterk, P.J., Hiemstra, P.S., de Boer, W.I., Stolk, J., Han, J., and van Krieken, J.M. (1997). Chronic obstructive pulmonary disease: role of bronchiolar mast cells and macrophages. Am J Pathol *151*, 1785-1790.

Greenblatt, S.M., Liu, F., and Nimer, S.D. (2016). Arginine methyltransferases in normal and malignant hematopoiesis. Exp Hematol *44*, 435-441.

Gregory, J.L., Morand, E.F., McKeown, S.J., Ralph, J.A., Hall, P., Yang, Y.H., McColl, S.R., and Hickey, M.J. (2006). Macrophage Migration Inhibitory Factor Induces Macrophage Recruitment via CC Chemokine Ligand 2. The Journal of Immunology *177*, 8072-8079.

Grzela, K., Litwiniuk, M., Zagorska, W., and Grzela, T. (2016). Airway Remodeling in Chronic Obstructive Pulmonary Disease and Asthma: the Role of Matrix Metalloproteinase-9. Arch Immunol Ther Exp (Warsz) *64*, 47-55.

Guccione, E., and Richard, S. (2019). The regulation, functions and clinical relevance of arginine methylation. Nature Reviews Molecular Cell Biology *20*, 642-657.

Guendel, I., Carpio, L., Pedati, C., Schwartz, A., Teal, C., Kashanchi, F., and Kehn-Hall, K. (2010). Methylation of the tumor suppressor protein, BRCA1, influences its transcriptional cofactor function. PLoS One *5*, e11379.

Guenther, M.G., Levine, S.S., Boyer, L.A., Jaenisch, R., and Young, R.A. (2007). A chromatin landmark and transcription initiation at most promoters in human cells. Cell *130*, 77-88.

Guo, Z., Zheng, L., Xu, H., Dai, H., Zhou, M., Pascua, M.R., Chen, Q.M., and Shen, B. (2010). Methylation of FEN1 suppresses nearby phosphorylation and facilitates PCNA binding. Nat Chem Biol *6*, 766-773.

Haghandish, N., Baldwin, R.M., Morettin, A., Dawit, H.T., Adhikary, H., Masson, J.-Y., Mazroui, R., Trinkle-Mulcahy, L., and Côté, J. (2019). PRMT7 methylates eukaryotic translation initiation factor 2α and regulates its role in stress granule formation. Mol Biol Cell *30*, 778-793.

Halpin, D.M., Miravitlles, M., Metzdorf, N., and Celli, B. (2017). Impact and prevention of severe exacerbations of COPD: a review of the evidence. Int J Chron Obstruct Pulmon Dis *12*, 2891-2908.

Hamard, P.J., Santiago, G.E., Liu, F., Karl, D.L., Martinez, C., Man, N., Mookhtiar, A.K., Duffort, S., Greenblatt, S., Verdun, R.E*., et al.* (2018). PRMT5 Regulates DNA Repair by Controlling the Alternative Splicing of Histone-Modifying Enzymes. Cell Rep *24*, 2643-2657.

Hannedouche, S., Zhang, J., Yi, T., Shen, W., Nguyen, D., Pereira, J.P., Guerini, D., Baumgarten, B.U., Roggo, S., Wen, B*., et al.* (2011). Oxysterols direct immune cell migration via EBI2. Nature *475*, 524-527.

Hartman, J.E., Ten Hacken, N.H., Klooster, K., Boezen, H.M., de Greef, M.H., and Slebos, D.J. (2012). The minimal important difference for residual volume in patients with severe emphysema. Eur Respir J *40*, 1137-1141.

Hasegawa, M., Toma-Fukai, S., Kim, J.D., Fukamizu, A., and Shimizu, T. (2014). Protein arginine methyltransferase 7 has a novel homodimer-like structure formed by tandem repeats. FEBS Lett *588*, 1942-1948.

Hautamaki, R.D., Kobayashi, D.K., Senior, R.M., and Shapiro, S.D. (1997). Requirement for macrophage elastase for cigarette smoke-induced emphysema in mice. Science *277*, 2002-2004.

He, W., Ma, X., Yang, X., Zhao, Y., Qiu, J., and Hang, H. (2011). A role for the arginine methylation of Rad9 in checkpoint control and cellular sensitivity to DNA damage. Nucleic Acids Res *39*, 4719-4727.

Heckman, C.A., and Dalbey, W.E. (1982). Pathogenesis of lesions induced in rat lung by chronic tobacco smoke inhalation. J Natl Cancer Inst *69*, 117-129.

Heintzman, N.D., Hon, G.C., Hawkins, R.D., Kheradpour, P., Stark, A., Harp, L.F., Ye, Z., Lee, L.K., Stuart, R.K., Ching, C.W*., et al.* (2009). Histone modifications at human enhancers reflect global cell-type-specific gene expression. Nature *459*, 108-112.

Henson, P.M., Vandivier, R.W., and Douglas, I.S. (2006). Cell death, remodeling, and repair in chronic obstructive pulmonary disease? Proc Am Thorac Soc *3*, 713-717.

Hernández, M., García, G., Falco, J., García, A.R., Martín, V., Ibarrola, M., and Quadrelli, S. (2018). Impact of using the new GOLD classification on the distribution of COPD severity in clinical practice. Int J Chron Obstruct Pulmon Dis *13*, 351-356.

Herrmann, F., Bossert, M., Schwander, A., Akgün, E., and Fackelmayer, F.O. (2004). Arginine methylation of scaffold attachment factor A by heterogeneous nuclear ribonucleoprotein particle-associated PRMT1. J Biol Chem *279*, 48774-48779.

Herrmann, F., Pably, P., Eckerich, C., Bedford, M.T., and Fackelmayer, F.O. (2009). Human protein arginine methyltransferases in vivo – distinct properties of eight canonical members of the PRMT family. Journal of Cell Science *122*, 667-677.

Hibbs, M.S., Hasty, K.A., Seyer, J.M., Kang, A.H., and Mainardi, C.L. (1985). Biochemical and immunological characterization of the secreted forms of human neutrophil gelatinase. J Biol Chem *260*, 2493-2500.

Higham, A., Quinn, A.M., Cançado, J.E.D., and Singh, D. (2019). The pathology of small airways disease in COPD: historical aspects and future directions. Respir Res *20*, 49.

Hikichi, M., Mizumura, K., Maruoka, S., and Gon, Y. (2019). Pathogenesis of chronic obstructive pulmonary disease (COPD) induced by cigarette smoke. J Thorac Dis *11*, S2129-S2140.

Hodge, S., Hodge, G., Holmes, M., and Reynolds, P.N. (2005). Increased airway epithelial and T-cell apoptosis in COPD remains despite smoking cessation. Eur Respir J *25*, 447-454.

Hodge, S., Hodge, G., Scicchitano, R., Reynolds, P.N., and Holmes, M. (2003). Alveolar macrophages from subjects with chronic obstructive pulmonary disease are deficient in their ability to phagocytose apoptotic airway epithelial cells. Immunol Cell Biol *81*, 289-296.

Hogg, J.C., Chu, F., Utokaparch, S., Woods, R., Elliott, W.M., Buzatu, L., Cherniack, R.M., Rogers, R.M., Sciurba, F.C., Coxson, H.O*., et al.* (2004). The Nature of Small-Airway Obstruction in Chronic Obstructive Pulmonary Disease. New England Journal of Medicine *350*, 2645-2653.

Holtzman, M.J., Tyner, J.W., Kim, E.Y., Lo, M.S., Patel, A.C., Shornick, L.P., Agapov, E., and Zhang, Y. (2005). Acute and chronic airway responses to viral infection: implications for asthma and chronic obstructive pulmonary disease. Proc Am Thorac Soc *2*, 132-140.

Hou, J., Ma, T., Cao, H., Chen, Y., Wang, C., Chen, X., Xiang, Z., and Han, X. (2018). TNF-α-induced NF-κB activation promotes myofibroblast differentiation of LR-MSCs and exacerbates bleomycin-induced pulmonary fibrosis. Journal of Cellular Physiology *233*, 2409-2419.

Hsu, W.Y., Chao, Y.W., Tsai, Y.L., Lien, C.C., Chang, C.F., Deng, M.C., Ho, L.T., Kwok, C.F., and Juan, C.C. (2011). Resistin induces monocyte-endothelial cell adhesion by increasing ICAM-1 and VCAM-1 expression in endothelial cells via p38MAPK-dependent pathway. J Cell Physiol *226*, 2181-2188.

Huang, S., Litt, M., and Felsenfeld, G. (2005). Methylation of histone H4 by arginine methyltransferase PRMT1 is essential in vivo for many subsequent histone modifications. Genes Dev *19*, 1885-1893.

Hwang, J.Y., Randall, T.D., and Silva-Sanchez, A. (2016). Inducible Bronchus-Associated Lymphoid Tissue: Taming Inflammation in the Lung. Frontiers in immunology *7*, 258-258.

Ishii, T., Itoh, K., Takahashi, S., Sato, H., Yanagawa, T., Katoh, Y., Bannai, S., and Yamamoto, M. (2000). Transcription factor Nrf2 coordinately regulates a group of oxidative stress-inducible genes in macrophages. J Biol Chem *275*, 16023-16029.

Izbicki, G., Segel, M.J., Christensen, T.G., Conner, M.W., and Breuer, R. (2002). Time course of bleomycin-induced lung fibrosis. Int J Exp Pathol *83*, 111-119.

Izuhara, K., Conway, S.J., Moore, B.B., Matsumoto, H., Holweg, C.T.J., Matthews, J.G., and Arron, J.R. (2016). Roles of Periostin in Respiratory Disorders. American journal of respiratory and critical care medicine *193*, 949-956.

Jain, K., and Clarke, S.G. (2019). PRMT7 as a unique member of the protein arginine methyltransferase family: A review. Arch Biochem Biophys *665*, 36-45.

Jain, K., Jin, C.Y., and Clarke, S.G. (2017). Epigenetic control via allosteric regulation of mammalian protein arginine methyltransferases. Proceedings of the National Academy of Sciences *114*, 10101-10106.

James, A.L., and Wenzel, S. (2007). Clinical relevance of airway remodelling in airway diseases. European Respiratory Journal *30*, 134-155.

Janeway, C.A., Jr., and Bottomly, K. (1994). Signals and signs for lymphocyte responses. Cell *76*, 275-285.

Jang, Y.J., Son, H.J., Choi, Y.M., Ahn, J., Jung, C.H., and Ha, T.Y. (2017). Apigenin enhances skeletal muscle hypertrophy and myoblast differentiation by regulating Prmt7. Oncotarget *8*, 78300-78311.

Janoff, A. (1985). Elastases and emphysema. Current assessment of the protease-antiprotease hypothesis. Am Rev Respir Dis *132*, 417-433.

Jansson, M., Durant, S.T., Cho, E.C., Sheahan, S., Edelmann, M., Kessler, B., and La Thangue, N.B. (2008). Arginine methylation regulates the p53 response. Nat Cell Biol *10*, 1431-1439.

Jeong, H.-J., Lee, H.-J., Vuong, T.A., Choi, K.-S., Choi, D., Koo, S.-H., Cho, S.C., Cho, H., and Kang, J.-S. (2016). Prmt7 Deficiency Causes Reduced Skeletal Muscle Oxidative Metabolism and Age-Related Obesity. Diabetes *65*, 1868-1882.

Jia, J., Conlon, T.M., Sarker, R.S., Tasdemir, D., Smirnova, N.F., Srivastava, B., Verleden, S.E., Gunes, G., Wu, X., Prehn, C*., et al.* (2018). Cholesterol metabolism promotes B-cell positioning during immune pathogenesis of chronic obstructive pulmonary disease. EMBO Mol Med *10*.

Jiang, H., Zhu, Y., Zhou, Z., Xu, J., Jin, S., Xu, K., Zhang, H., Sun, Q., Wang, J., and Xu, J. (2018). PRMT5 promotes cell proliferation by inhibiting BTG2 expression via the ERK signaling pathway in hepatocellular carcinoma. Cancer Med *7*, 869-882.

Johannessen, A., Lehmann, S., Omenaas, E.R., Eide, G.E., Bakke, P.S., and Gulsvik, A. (2006). Post-bronchodilator spirometry reference values in adults and implications for disease management. Am J Respir Crit Care Med *173*, 1316-1325.

John-Schuster, G., Hager, K., Conlon, T., Irmler, M., Beckers, J., Eickelberg, O., and Yildirim, A.Ö. (2014a). Cigarette smoke-induced iBALT mediates macrophage activation in a B cell-dependent manner in COPD. European Respiratory Journal *44*, 4857.

John-Schuster, G., Hager, K., Conlon, T.M., Irmler, M., Beckers, J., Eickelberg, O., and Yildirim, A.O. (2014b). Cigarette smoke-induced iBALT mediates macrophage activation in a B cell-dependent manner in COPD. Am J Physiol Lung Cell Mol Physiol *307*, L692-706.

Johnson, D.C. (2000). Importance of adjusting carbon monoxide diffusing capacity (DLCO) and carbon monoxide transfer coefficient (KCO) for alveolar volume. Respir Med *94*, 28-37.

Jungraithmayr, W.M., Korom, S., Hillinger, S., and Weder, W. (2009). A mouse model of orthotopic, single-lung transplantation. J Thorac Cardiovasc Surg *137*, 486-491.

Kaku, Y., Imaoka, H., Morimatu, Y., Matsuoka, M., Natori, H., Suetomo, M., Kawayama, T., and Hoshino, T. (2014). M2 macrophage marker CD163, CD204 and CD206 expression on alveolar macrophages in the lung of patients with chronic obstructive pulmonary. European Respiratory Journal *44*, P1481.

Kamata, H., Honda, S., Maeda, S., Chang, L., Hirata, H., and Karin, M. (2005). Reactive oxygen species promote TNFalpha-induced death and sustained JNK activation by inhibiting MAP kinase phosphatases. Cell *120*, 649-661.

Karkhanis, V., Wang, L., Tae, S., Hu, Y.-J., Imbalzano, A.N., and Sif, S. (2012). Protein arginine methyltransferase 7 regulates cellular response to DNA damage by methylating promoter histones H2A and H4 of the polymerase δ catalytic subunit gene, POLD1. The Journal of biological chemistry *287*, 29801-29814.

Kasparek, P., Krausova, M., Haneckova, R., Kriz, V., Zbodakova, O., Korinek, V., and Sedlacek, R. (2014). Efficient gene targeting of the Rosa26 locus in mouse zygotes using TALE nucleases. FEBS letters *588*, 3982-3988.

Kasper, B., Brandt, E., Brandau, S., and Petersen, F. (2007). Platelet factor 4 (CXC chemokine ligand 4) differentially regulates respiratory burst, survival, and cytokine expression of human monocytes by using distinct signaling pathways. J Immunol *179*, 2584-2591.

Katsuno, Y., Qin, J., Oses-Prieto, J., Wang, H., Jackson-Weaver, O., Zhang, T., Lamouille, S., Wu, J., Burlingame, A., Xu, J*., et al.* (2018). Arginine methylation of SMAD7 by PRMT1 in TGF-β-induced epithelial-mesenchymal transition and epithelial stem-cell generation. J Biol Chem *293*, 13059-13072.

Katz, J.E., Dlakić, M., and Clarke, S. (2003). Automated identification of putative methyltransferases from genomic open reading frames. Mol Cell Proteomics *2*, 525-540.

Kawai, T., and Akira, S. (2010). The role of pattern-recognition receptors in innate immunity: update on Toll-like receptors. Nature Immunology *11*, 373-384.

Ke, Y., Karki, P., Zhang, C., Li, Y., Nguyen, T., Birukov, K.G., and Birukova, A.A. (2019). Mechanosensitive Rap1 activation promotes barrier function of lung vascular endothelium under cyclic stretch. Mol Biol Cell *30*, 959-974.

Kebede, A.F., Nieborak, A., Shahidian, L.Z., Le Gras, S., Richter, F., Gomez, D.A., Baltissen, M.P., Meszaros, G., Magliarelli, H.F., Taudt, A*., et al.* (2017). Histone propionylation is a mark of active chromatin. Nature structural & molecular biology *24*, 1048-1056.

Kernohan, K.D., McBride, A., Xi, Y., Martin, N., Schwartzentruber, J., Dyment, D.A., Majewski, J., Blaser, S., Care4Rare Canada, C., Boycott, K.M*., et al.* (2017). Loss of the arginine methyltranserase PRMT7 causes syndromic intellectual disability with microcephaly and brachydactyly. Clin Genet *91*, 708-716.

Kim, C., Lim, Y., Yoo, B.C., Won, N.H., Kim, S., and Kim, G. (2010). Regulation of post-translational protein arginine methylation during HeLa cell cycle. Biochim Biophys Acta *1800*, 977-985.

Kim, J.H., Yoo, B.C., Yang, W.S., Kim, E., Hong, S., and Cho, J.Y. (2016). The Role of Protein Arginine Methyltransferases in Inflammatory Responses. Mediators of Inflammation *2016*, 4028353.

Kim, T.H., and Dekker, J. (2018). ChIP-Quantitative Polymerase Chain Reaction (ChIP-qPCR). Cold Spring Harb Protoc *2018*.

Kim, V., and Criner, G.J. (2013). Chronic bronchitis and chronic obstructive pulmonary disease. Am J Respir Crit Care Med *187*, 228-237.

Kim, V., and Criner, G.J. (2015). The chronic bronchitis phenotype in chronic obstructive pulmonary disease: features and implications. Curr Opin Pulm Med *21*, 133-141.

Kolodziej, M., de Veer, M.J., Cholewa, M., Egan, G.F., and Thompson, B.R. (2017). Lung function imaging methods in Cystic Fibrosis pulmonary disease. Respir Res *18*, 96.

Konigshoff, M., and Eickelberg, O. (2010). WNT signaling in lung disease: a failure or a regeneration signal? Am J Respir Cell Mol Biol *42*, 21-31.

Kooistra, M.R.H., Dubé, N., and Bos, J.L. (2007). Rap1: a key regulator in cell-cell junction formation. Journal of Cell Science *120*, 17-22.

Kreimendahl, F., Marquardt, Y., Apel, C., Bartneck, M., Zwadlo-Klarwasser, G., Hepp, J., Jockenhoevel, S., and Baron, J.M. (2019). Macrophages significantly enhance wound healing in a vascularized skin model. J Biomed Mater Res A *107*, 1340-1350.

Krohn, R.I. (2001). The Colorimetric Detection and Quantitation of Total Protein. Current Protocols in Food Analytical Chemistry *00*, B1.1.1-B1.1.28.

Krzyszczyk, P., Schloss, R., Palmer, A., and Berthiaume, F. (2018). The Role of Macrophages in Acute and Chronic Wound Healing and Interventions to Promote Pro-wound Healing Phenotypes. Front Physiol *9*, 419-419.

Kumar, A., Negi, G., and Sharma, S.S. (2011). JSH-23 targets nuclear factor-kappa B and reverses various deficits in experimental diabetic neuropathy: effect on neuroinflammation and antioxidant defence. Diabetes Obes Metab *13*, 750-758.

Lacazette, E. (2017). A laboratory practical illustrating the use of the ChIP-qPCR method in a robust model: Estrogen receptor alpha immunoprecipitation using Mcf-7 culture cells. Biochemistry and Molecular Biology Education *45*, 152-160.

Lahzami, S., Bridevaux, P.O., Soccal, P.M., Wellinger, J., Robert, J.H., Ris, H.B., and Aubert, J.D. (2010). Survival impact of lung transplantation for COPD. European Respiratory Journal *36*, 74-80.

Lakshmi, S.P., Reddy, A.T., and Reddy, R.C. (2017). Emerging pharmaceutical therapies for COPD. Int J Chron Obstruct Pulmon Dis *12*, 2141-2156.

Lamberth, C. (2016). Naturally occurring amino acid derivatives with herbicidal, fungicidal or insecticidal activity. Amino Acids *48*, 929-940.

Lambrecht, B.N., Prins, J.B., and Hoogsteden, H.C. (2001). Lung dendritic cells and host immunity to infection. Eur Respir J *18*, 692-704.

Laurent, G.J. (1985). Biochemical pathways leading to collagen deposition in pulmonary fibrosis. Ciba Found Symp *114*, 222-233.

Lee, S.J., Lee, H.R., Lee, T.W., Ju, S., Lim, S., Go, S.I., You, J.W., Cho, Y.J., Lee, G.W., Jeong, Y.Y.*, et al.* (2016). Usefulness of neutrophil to lymphocyte ratio in patients with chronic obstructive pulmonary disease: a prospective observational study. Korean J Intern Med *31*, 891-898.

Lee, W.H., Loo, C.Y., Traini, D., and Young, P.M. (2015). Nano- and micro-based inhaled drug delivery systems for targeting alveolar macrophages. Expert Opin Drug Deliv *12*, 1009-1026.

Leem, Y.-E., Bae, J.-H., Jeong, H.-J., and Kang, J.-S. (2019). PRMT7 deficiency enhances adipogenesis through modulation of C/EBP-β. Biochemical and Biophysical Research Communications *517*, 484-490.

Li, L., Wang, S., Jezierski, A., Moalim-Nour, L., Mohib, K., Parks, R.J., Retta, S.F., and Wang, L. (2010). A unique interplay between Rap1 and E-cadherin in the endocytic pathway regulates self-renewal of human embryonic stem cells. Stem Cells *28*, 247-257.

Li, Y., Yan, J., De, P., Chang, H.C., Yamauchi, A., Christopherson, K.W., 2nd, Paranavitana, N.C., Peng, X., Kim, C., Munugalavadla, V.*, et al.* (2007). Rap1a null mice have altered myeloid cell functions suggesting distinct roles for the closely related Rap1a and 1b proteins. Journal of immunology *179*, 8322-8331.

Lim, S.K., Jeong, Y.W., Kim, D.I., Park, M.J., Choi, J.H., Kim, S.U., Kang, S.S., Han, H.J., and Park, S.H. (2013). Activation of PRMT1 and PRMT5 mediates hypoxia- and ischemia-induced apoptosis in human lung epithelial cells and the lung of miniature pigs: the role of p38 and JNK mitogen-activated protein kinases. Biochem Biophys Res Commun *440*, 707-713.

Lin, W.J., Gary, J.D., Yang, M.C., Clarke, S., and Herschman, H.R. (1996). The mammalian immediate-early TIS21 protein and the leukemia-associated BTG1 protein interact with a protein-arginine N-methyltransferase. J Biol Chem *271*, 15034-15044.

Linder, R., Rönmark, E., Pourazar, J., Behndig, A., Blomberg, A., and Lindberg, A. (2015). Serum metalloproteinase-9 is related to COPD severity and symptoms - cross-sectional data from a population based cohort-study. Respir Res *16*, 28-28.

Litt, M., Qiu, Y., and Huang, S. (2009). Histone arginine methylations: their roles in chromatin dynamics and transcriptional regulation. Biosci Rep *29*, 131-141.

Liu, F., Wan, L., Zou, H., Pan, Z., Zhou, W., and Lu, X. (2020). PRMT7 promotes the growth of renal cell carcinoma through modulating the β-catenin/C-MYC axis. The International Journal of Biochemistry & Cell Biology *120*, 105686.

Liu, F.T., Hsu, D.K., Zuberi, R.I., Kuwabara, I., Chi, E.Y., and Henderson, W.R., Jr. (1995). Expression and function of galectin-3, a beta-galactoside-binding lectin, in human monocytes and macrophages. Am J Pathol *147*, 1016-1028.

Liu, Q., and Dreyfuss, G. (1995). In vivo and in vitro arginine methylation of RNA-binding proteins. Molecular and cellular biology *15*, 2800-2808.

Liu, T., Zhang, L., Joo, D., and Sun, S.-C. (2017). NF-κB signaling in inflammation. Signal Transduct Target Ther *2*, 17023.

Liu, Y.C., Zou, X.B., Chai, Y.F., and Yao, Y.M. (2014). Macrophage polarization in inflammatory diseases. Int J Biol Sci *10*, 520-529.

Lomas, D.A. (2016). Does Protease-Antiprotease Imbalance Explain Chronic Obstructive Pulmonary Disease? Ann Am Thorac Soc *13 Suppl 2*, S130-137.

Loukides, S., Bartziokas, K., Vestbo, J., and Singh, D. (2013). Novel anti-inflammatory agents in COPD: targeting lung and systemic inflammation. Curr Drug Targets *14*, 235-245.

Luedde, T., and Schwabe, R.F. (2011). NF-κB in the liver--linking injury, fibrosis and hepatocellular carcinoma. Nat Rev Gastroenterol Hepatol *8*, 108-118.

MacNee, W. (2005). Pathogenesis of chronic obstructive pulmonary disease. Proceedings of the American Thoracic Society *2*, 258-291.

MacNee, W., and Tuder, R.M. (2009). New paradigms in the pathogenesis of chronic obstructive pulmonary disease I. Proc Am Thorac Soc *6*, 527-531.

Macosko, E.Z., Basu, A., Satija, R., Nemesh, J., Shekhar, K., Goldman, M., Tirosh, I., Bialas, A.R., Kamitaki, N., Martersteck, E.M*., et al.* (2015). Highly Parallel Genome-wide Expression Profiling of Individual Cells Using Nanoliter Droplets. Cell *161*, 1202-1214.

Mak, A., and Uetrecht, J. (2019). Involvement of CCL2/CCR2 macrophage recruitment in amodiaquine-induced liver injury. J Immunotoxicol *16*, 28-33.

Mannino, D.M., Doherty, D.E., and Sonia Buist, A. (2006). Global Initiative on Obstructive Lung Disease (GOLD) classification of lung disease and mortality: findings from the Atherosclerosis Risk in Communities (ARIC) study. Respir Med *100*, 115-122.

Mannino, D.M., and Kiriz, V.A. (2006). Changing the burden of COPD mortality. Int J Chron Obstruct Pulmon Dis *1*, 219-233.

Mantovani, A., Sica, A., Sozzani, S., Allavena, P., Vecchi, A., and Locati, M. (2004). The chemokine system in diverse forms of macrophage activation and polarization. Trends Immunol *25*, 677-686.

Marinissen, M.J., and Gutkind, J.S. (2001). G-protein-coupled receptors and signaling networks: emerging paradigms. Trends in Pharmacological Sciences *22*, 368-376.

Martin, C., Frija-Masson, J., and Burgel, P.R. (2014). Targeting mucus hypersecretion: new therapeutic opportunities for COPD? Drugs *74*, 1073-1089.

Mbawuike, I.N., and Herscowitz, H.B. (1989). MH-S, a murine alveolar macrophage cell line: morphological, cytochemical, and functional characteristics. J Leukoc Biol *46*, 119-127.

McGuinness, A.J.A., and Sapey, E. (2017). Oxidative Stress in COPD: Sources, Markers, and Potential Mechanisms. J Clin Med *6*, 21.

McGuire, T.F., Qian, Y., Vogt, A., Hamilton, A.D., and Sebti, S.M. (1996). Platelet-derived growth factor receptor tyrosine phosphorylation requires protein geranylgeranylation but not farnesylation. J Biol Chem *271*, 27402-27407.

Meerschaert, J., and Furie, M.B. (1995). The adhesion molecules used by monocytes for migration across endothelium include CD11a/CD18, CD11b/CD18, and VLA-4 on monocytes and ICAM-1, VCAM-1, and other ligands on endothelium. The Journal of Immunology *154*, 4099-4112.

Mei, S., Qin, Q., Wu, Q., Sun, H., Zheng, R., Zang, C., Zhu, M., Wu, J., Shi, X., Taing, L*., et al.* (2016). Cistrome Data Browser: a data portal for ChIP-Seq and chromatin accessibility data in human and mouse. Nucleic Acids Res *45*, D658-D662.

Meister, G., Eggert, C., Bühler, D., Brahms, H., Kambach, C., and Fischer, U. (2001). Methylation of Sm proteins by a complex containing PRMT5 and the putative U snRNP assembly factor pICln. Curr Biol *11*, 1990-1994.

Meister, G., and Fischer, U. (2002). Assisted RNP assembly: SMN and PRMT5 complexes cooperate in the formation of spliceosomal UsnRNPs. The EMBO journal *21*, 5853-5863.

Mercado, N., Ito, K., and Barnes, P.J. (2015). Accelerated ageing of the lung in COPD: new concepts. Thorax *70*, 482-489.

Mestas, J., and Ley, K. (2008). Monocyte-endothelial cell interactions in the development of atherosclerosis. Trends Cardiovasc Med *18*, 228-232.

Migliori, V., Muller, J., Phalke, S., Low, D., Bezzi, M., Mok, W.C., Sahu, S.K., Gunaratne, J., Capasso, P., Bassi, C.*, et al.* (2012). Symmetric dimethylation of H3R2 is a newly identified histone mark that supports euchromatin maintenance. Nat Struct Mol Biol *19*, 136-144.

Min, J.K., Kim, Y.M., Kim, S.W., Kwon, M.C., Kong, Y.Y., Hwang, I.K., Won, M.H., Rho, J., and Kwon, Y.G. (2005). TNF-related activation-induced cytokine enhances leukocyte adhesiveness: induction of ICAM-1 and VCAM-1 via TNF receptor-associated factor and protein kinase C-dependent NF-kappaB activation in endothelial cells. J Immunol *175*, 531-540.

Miranda, T.B., Miranda, M., Frankel, A., and Clarke, S. (2004). PRMT7 is a member of the protein arginine methyltransferase family with a distinct substrate specificity. J Biol Chem *279*, 22902-22907.

Misharin, A.V., Morales-Nebreda, L., Mutlu, G.M., Budinger, G.R.S., and Perlman, H. (2013). Flow cytometric analysis of macrophages and dendritic cell subsets in the mouse lung. American journal of respiratory cell and molecular biology *49*, 503-510.

Mootha, V.K., Lindgren, C.M., Eriksson, K.F., Subramanian, A., Sihag, S., Lehar, J., Puigserver, P., Carlsson, E., Ridderstrale, M., Laurila, E.*, et al.* (2003). PGC-1alpha-responsive genes involved in oxidative phosphorylation are coordinately downregulated in human diabetes. Nature genetics *34*, 267-273.

Morales-Nebreda, L., Misharin, A.V., Perlman, H., and Budinger, G.R. (2015). The heterogeneity of lung macrophages in the susceptibility to disease. Eur Respir Rev *24*, 505-509.

Morales, Y., Caceres, T., May, K., and Hevel, J.M. (2016). Biochemistry and regulation of the protein arginine methyltransferases (PRMTs). Arch Biochem Biophys *590*, 138-152.

Mori, N., Yamada, Y., Ikeda, S., Yamasaki, Y., Tsukasaki, K., Tanaka, Y., Tomonaga, M., Yamamoto, N., and Fujii, M. (2002). Bay 11-7082 inhibits transcription factor NF-kappaB and induces apoptosis of HTLV-I-infected T-cell lines and primary adult T-cell leukemia cells. Blood *100*, 1828-1834.

Morrow, J.D., Zhou, X., Lao, T., Jiang, Z., DeMeo, D.L., Cho, M.H., Qiu, W., Cloonan, S., Pinto-Plata, V., Celli, B.*, et al.* (2017). Functional interactors of three genome-wide association study genes are differentially expressed in severe chronic obstructive pulmonary disease lung tissue. Sci Rep *7*, 44232.

Mortaz, E., Folkerts, G., and Redegeld, F. (2011). Mast cells and COPD. Pulm Pharmacol Ther *24*, 367-372.

Motz, G.T., Eppert, B.L., Wortham, B.W., Amos-Kroohs, R.M., Flury, J.L., Wesselkamper, S.C., and Borchers, M.T. (2010). Chronic cigarette smoke exposure primes NK cell activation in a mouse model of chronic obstructive pulmonary disease. J Immunol *184*, 4460-4469.

Murakami, H., Suzuki, T., Tsuchiya, K., Gatanaga, H., Taura, M., Kudo, E., Okada, S., Takei, M., Kuroda, K., Yamamoto, T.*, et al.* (2020). Protein Arginine N-methyltransferases 5 and 7 Promote HIV-1 Production. Viruses *12*.

Najbauer, J., Johnson, B.A., Young, A.L., and Aswad, D.W. (1993). Peptides with sequences similar to glycine, arginine-rich motifs in proteins interacting with RNA are efficiently recognized by methyltransferase(s) modifying arginine in numerous proteins. J Biol Chem *268*, 10501-10509.

Nakai, K., Xia, W., Liao, H.W., Saito, M., Hung, M.C., and Yamaguchi, H. (2018). The role of PRMT1 in EGFR methylation and signaling in MDA-MB-468 triple-negative breast cancer cells. Breast Cancer *25*, 74-80.

Nakajima, T., Nakamura, H., Owen, C.A., Yoshida, S., Tsuduki, K., Chubachi, S., Shirahata, T., Mashimo, S., Nakamura, M., Takahashi, S.*, et al.* (2016). Plasma Cathepsin S and Cathepsin S/Cystatin C Ratios Are Potential Biomarkers for COPD. Dis Markers *2016*, 4093870.

Naor, Z., Benard, O., and Seger, R. (2000). Activation of MAPK Cascades by G-protein-coupled Receptors: The Case of Gonadotropin-releasing Hormone Receptor. Trends in Endocrinology & Metabolism *11*, 91-99.

Nayak, D.K., Zhou, F., Xu, M., Huang, J., Tsuji, M., Hachem, R., and Mohanakumar, T. (2016). Long-Term Persistence of Donor Alveolar Macrophages in Human Lung Transplant Recipients That Influences Donor-Specific Immune Responses. Am J Transplant *16*, 2300-2311.

Ni, L., and Dong, C. (2018). Roles of Myeloid and Lymphoid Cells in the Pathogenesis of Chronic Obstructive Pulmonary Disease. Front Immunol *9*, 1431.

Niu, H., Xiao, J., Ma, Z., and Chen, L. (2020). Prmt4-mediated methylation of NF-κB is critical for neural differentiation of embryonic stem cells. Biochem Biophys Res Commun.

Norbury, C., and Nurse, P. (1992). Animal cell cycles and their control. Annu Rev Biochem *61*, 441-470.

Nurwidya, F., Damayanti, T., and Yunus, F. (2016). The Role of Innate and Adaptive Immune Cells in the Immunopathogenesis of Chronic Obstructive Pulmonary Disease. Tuberc Respir Dis (Seoul) *79*, 5-13.

O'Brien, K.B., Alberich-Jordà, M., Yadav, N., Kocher, O., Diruscio, A., Ebralidze, A., Levantini, E., Sng, N.J., Bhasin, M., Caron, T.*, et al.* (2010). CARM1 is required for proper control of proliferation and differentiation of pulmonary epithelial cells. Development *137*, 2147-2156.

O'Connell, K.A., and Edidin, M. (1990). A mouse lymphoid endothelial cell line immortalized by simian virus 40 binds lymphocytes and retains functional characteristics of normal endothelial cells. The Journal of Immunology *144*, 521-525.

O'Donnell, R., Breen, D., Wilson, S., and Djukanovic, R. (2006). Inflammatory cells in the airways in COPD. Thorax *61*, 448-454.

Olajuyin, A.M., Zhang, X., and Ji, H.-L. (2019). Alveolar type 2 progenitor cells for lung injury repair. Cell Death Discovery *5*, 63.

Orecchioni, M., Ghosheh, Y., Pramod, A.B., and Ley, K. (2019). Macrophage Polarization: Different Gene Signatures in M1(LPS+) vs. Classically and M2(LPS–) vs. Alternatively Activated Macrophages. Frontiers in Immunology *10*.

Osterburg, A.R., Lach, L., Panos, R.J., and Borchers, M.T. (2020). Unique natural killer cell subpopulations are associated with exacerbation risk in chronic obstructive pulmonary disease. Sci Rep *10*, 1238.

Ou, C.Y., LaBonte, M.J., Manegold, P.C., So, A.Y., Ianculescu, I., Gerke, D.S., Yamamoto, K.R., Ladner, R.D., Kahn, M., Kim, J.H.*, et al.* (2011). A coactivator role of CARM1 in the dysregulation of β-catenin activity in colorectal cancer cell growth and gene expression. Mol Cancer Res *9*, 660-670.

Pal, S., Vishwanath, S.N., Erdjument-Bromage, H., Tempst, P., and Sif, S. (2004). Human SWI/SNF-associated PRMT5 methylates histone H3 arginine 8 and negatively regulates expression of ST7 and NM23 tumor suppressor genes. Mol Cell Biol *24*, 9630-9645.

Pandey, K.C., De, S., and Mishra, P.K. (2017). Role of Proteases in Chronic Obstructive Pulmonary Disease. Frontiers in pharmacology *8*, 512-512.

Paul, F., Arkin, Y., Giladi, A., Jaitin, D.A., Kenigsberg, E., Keren-Shaul, H., Winter, D., Lara-Astiaso, D., Gury, M., Weiner, A.*, et al.* (2015). Transcriptional Heterogeneity and Lineage Commitment in Myeloid Progenitors. Cell *163*, 1663-1677.

Paul, S., and Lal, G. (2017). The Molecular Mechanism of Natural Killer Cells Function and Its Importance in Cancer Immunotherapy. Frontiers in Immunology *8*.

Pearson, G., Robinson, F., Beers Gibson, T., Xu, B.-e., Karandikar, M., Berman, K., and Cobb, M.H. (2001). Mitogen-Activated Protein (MAP) Kinase Pathways: Regulation and Physiological Functions*. Endocrine Reviews *22*, 153-183.

Pellegrino, R., Viegi, G., Brusasco, V., Crapo, R.O., Burgos, F., Casaburi, R., Coates, A., van der Grinten, C.P.M., Gustafsson, P., Hankinson, J.*, et al.* (2005). Interpretative strategies for lung function tests. European Respiratory Journal *26*, 948-968.

Pierce, J.W., Schoenleber, R., Jesmok, G., Best, J., Moore, S.A., Collins, T., and Gerritsen, M.E. (1997). Novel inhibitors of cytokine-induced IkappaBalpha phosphorylation and endothelial cell adhesion molecule expression show anti-inflammatory effects in vivo. J Biol Chem *272*, 21096-21103.

Plataki, M., Tzortzaki, E., Rytila, P., Demosthenes, M., Koutsopoulos, A., and Siafakas, N.M. (2006). Apoptotic mechanisms in the pathogenesis of COPD. Int J Chron Obstruct Pulmon Dis *1*, 161-171.

Polverino, F., Cosio, B.G., Pons, J., Laucho-Contreras, M., Tejera, P., Iglesias, A., Rios, A., Jahn, A., Sauleda, J., Divo, M.*, et al.* (2015). B Cell-Activating Factor. An Orchestrator of Lymphoid Follicles in Severe Chronic Obstructive Pulmonary Disease. Am J Respir Crit Care Med *192*, 695-705.

Ponzoni, M., Pastorino, F., Di Paolo, D., Perri, P., and Brignole, C. (2018). Targeting Macrophages as a Potential Therapeutic Intervention: Impact on Inflammatory Diseases and Cancer. International journal of molecular sciences *19*, 1953.

Poulard, C., Corbo, L., and Le Romancer, M. (2016). Protein arginine methylation/demethylation and cancer. Oncotarget *7*, 67532-67550.

Qin, Y., Hu, Q., Xu, J., Ji, S., Dai, W., Liu, W., Xu, W., Sun, Q., Zhang, Z., Ni, Q.*, et al.* (2019). PRMT5 enhances tumorigenicity and glycolysis in pancreatic cancer via the FBW7/cMyc axis. Cell Commun Signal *17*, 30.

Qiu, S.L., Kuang, L.J., Tang, Q.Y., Duan, M.C., Bai, J., He, Z.Y., Zhang, J.Q., Li, M.H., Deng, J.M., Liu, G.N.*, et al.* (2018). Enhanced activation of circulating plasmacytoid dendritic cells in patients with Chronic Obstructive Pulmonary Disease and experimental smoking-induced emphysema. Clin Immunol *195*, 107-118.

Quaderi, S.A., and Hurst, J.R. (2018). The unmet global burden of COPD. Glob Health Epidemiol Genom *3*, e4-e4.

Ra, H.-J., and Parks, W.C. (2007). Control of matrix metalloproteinase catalytic activity. Matrix Biol *26*, 587-596.

Rahman, I., and Adcock, I.M. (2006). Oxidative stress and redox regulation of lung inflammation in COPD. European Respiratory Journal *28*, 219-242.

Rahman, I., and MacNee, W. (1996). Role of oxidants/antioxidants in smoking-induced lung diseases. Free Radic Biol Med *21*, 669-681.

Rahman, I., and MacNee, W. (1998). Role of transcription factors in inflammatory lung diseases. Thorax *53*, 601-612.

Ramirez, M.I., Millien, G., Hinds, A., Cao, Y., Seldin, D.C., and Williams, M.C. (2003). T1α, a lung type I cell differentiation gene, is required for normal lung cell proliferation and alveolus formation at birth. Developmental Biology *256*, 62-73.

Rao, K.M.K. (2001). MAP kinase activation in macrophages. Journal of Leukocyte Biology *69*, 3-10.

Raposo, A.E., and Piller, S.C. (2018). Protein arginine methylation: an emerging regulator of the cell cycle. Cell Div *13*, 3.

Rashid, K., Sundar, I.K., Gerloff, J., Li, D., and Rahman, I. (2018). Lung cellular senescence is independent of aging in a mouse model of COPD/emphysema. Scientific Reports *8*, 9023.

Reinert, T., Baldotto, C.S.d.R., Nunes, F.A.P., and Scheliga, A.A.d.S. (2013). Bleomycin-Induced Lung Injury. Journal of Cancer Research *2013*, 480608.

Rennard, S.I., Togo, S., and Holz, O. (2006). Cigarette smoke inhibits alveolar repair: a mechanism for the development of emphysema. Proc Am Thorac Soc *3*, 703-708.

Rogers, A.V., Adelroth, E., Hattotuwa, K., Dewar, A., and Jeffery, P.K. (2008). Bronchial mucosal dendritic cells in smokers and ex-smokers with COPD: an electron microscopic study. Thorax *63*, 108-114.

Rosseau, S., Selhorst, J., Wiechmann, K., Leissner, K., Maus, U., Mayer, K., Grimminger, F., Seeger, W., and Lohmeyer, J. (2000). Monocyte migration through the alveolar epithelial barrier: adhesion molecule mechanisms and impact of chemokines. J Immunol *164*, 427-435.

Rovina, N., Koutsoukou, A., and Koulouris, N.G. (2013). Inflammation and immune response in COPD: where do we stand? Mediators Inflamm *2013*, 413735.

Russell, R.E., Culpitt, S.V., DeMatos, C., Donnelly, L., Smith, M., Wiggins, J., and Barnes, P.J. (2002). Release and activity of matrix metalloproteinase-9 and tissue inhibitor of metalloproteinase-1 by alveolar macrophages from patients with chronic obstructive pulmonary disease. Am J Respir Cell Mol Biol *26*, 602-609.

Saetta, M. (1999). Airway inflammation in chronic obstructive pulmonary disease. Am J Respir Crit Care Med *160*, S17-20.

Saetta, M., Turato, G., Facchini, F.M., Corbino, L., Lucchini, R.E., Casoni, G., Maestrelli, P., Mapp, C.E., Ciaccia, A., and Fabbri, L.M. (1997). Inflammatory cells in the bronchial glands of smokers with chronic bronchitis. Am J Respir Crit Care Med *156*, 1633-1639.

Sajti, E., Link, V.M., Ouyang, Z., Spann, N.J., Westin, E., Romanoski, C.E., Fonseca, G.J., Prince, L.S., and Glass, C.K. (2020). Transcriptomic and epigenetic mechanisms underlying myeloid diversity in the lung. Nature Immunology *21*, 221-231.

Sandelin, A., Alkema, W., Engström, P., Wasserman, W.W., and Lenhard, B. (2004). JASPAR: an open-access database for eukaryotic transcription factor binding profiles. Nucleic Acids Res *32*, D91-94.

Sans, M., Panes, J., Ardite, E., Elizalde, J.I., Arce, Y., Elena, M., Palacin, A., Fernandez-Checa, J.C., Anderson, D.C., Lobb, R.*, et al.* (1999). VCAM-1 and ICAM-1 mediate leukocyte-endothelial cell adhesion in rat experimental colitis. Gastroenterology *116*, 874-883.

Saqib, U., Sarkar, S., Suk, K., Mohammad, O., Baig, M.S., and Savai, R. (2018). Phytochemicals as modulators of M1-M2 macrophages in inflammation. Oncotarget *9*, 17937-17950.

Sarker, R., John-Schuster, G., Bohla, A., Mutze, K., Burgstaller, G., Bedford, M., Königshoff, M., Eickelberg, O., and Yildirim, A. (2015). CARM1 Regulates Alveolar Epithelial Senescence and Elastase-induced Emphysema Susceptibility. American journal of respiratory cell and molecular biology *53*.

Sarker, R.S.J., Conlon, T.M., Morrone, C., Srivastava, B., Konyalilar, N., Verleden, S.E., Bayram, H., Fehrenbach, H., and Yildirim, A.Ö. (2019). CARM1 regulates senescence during airway epithelial cell injury in COPD pathogenesis. American Journal of Physiology-Lung Cellular and Molecular Physiology *317*, L602-L614.

Schenkel, A.R., Mamdouh, Z., and Muller, W.A. (2004). Locomotion of monocytes on endothelium is a critical step during extravasation. Nature Immunology *5*, 393-400.

Schraml, B.U., and Reis e Sousa, C. (2015). Defining dendritic cells. Curr Opin Immunol *32*, 13-20.

Schuliga, M. (2015). NF-kappaB Signaling in Chronic Inflammatory Airway Disease. Biomolecules *5*, 1266-1283.

Seys, L.J., Verhamme, F.M., Schinwald, A., Hammad, H., Cunoosamy, D.M., Bantsimba-Malanda, C., Sabirsh, A., McCall, E., Flavell, L., Herbst, R.*, et al.* (2015). Role of B Cell-Activating Factor in Chronic Obstructive Pulmonary Disease. Am J Respir Crit Care Med *192*, 706-718.

Shafazand, S. (2013). ACP Journal Club. Review: inhaled medications vary substantively in their effects on mortality in COPD. Ann Intern Med *158*, Jc2.

Shailesh, H., Zakaria, Z.Z., Baiocchi, R., and Sif, S. (2018). Protein arginine methyltransferase 5 (PRMT5) dysregulation in cancer. Oncotarget *9*, 36705-36718.

Shan, M., Yuan, X., Song, L.Z., Roberts, L., Zarinkamar, N., Seryshev, A., Zhang, Y., Hilsenbeck, S., Chang, S.H., Dong, C.*, et al.* (2012). Cigarette smoke induction of osteopontin (SPP1) mediates T(H)17 inflammation in human and experimental emphysema. Sci Transl Med *4*, 117ra119.

Shapiro, S.D., Goldstein, N.M., Houghton, A.M., Kobayashi, D.K., Kelley, D., and Belaaouaj, A. (2003). Neutrophil elastase contributes to cigarette smoke-induced emphysema in mice. The American journal of pathology *163*, 2329-2335.

Shapouri-Moghaddam, A., Mohammadian, S., Vazini, H., Taghadosi, M., Esmaeili, S.-A., Mardani, F., Seifi, B., Mohammadi, A., Afshari, J.T., and Sahebkar, A. (2018). Macrophage plasticity, polarization, and function in health and disease. Journal of Cellular Physiology *233*, 6425-6440.

Sharif, O., Bolshakov, V.N., Raines, S., Newham, P., and Perkins, N.D. (2007). Transcriptional profiling of the LPS induced NF-κB response in macrophages. BMC Immunology *8*, 1.

Shaykhiev, R., Krause, A., Salit, J., Strulovici-Barel, Y., Harvey, B.G., O'Connor, T.P., and Crystal, R.G. (2009). Smoking-dependent reprogramming of alveolar macrophage polarization: implication for pathogenesis of chronic obstructive pulmonary disease. Journal of immunology *183*, 2867-2883.

Shen, Y., Yue, F., McCleary, D.F., Ye, Z., Edsall, L., Kuan, S., Wagner, U., Dixon, J., Lee, L., Lobanenkov, V.V*., et al.* (2012). A map of the cis-regulatory sequences in the mouse genome. Nature *488*, 116-120.

Shi, C., and Pamer, E.G. (2011). Monocyte recruitment during infection and inflammation. Nat Rev Immunol *11*, 762-774.

Shi, J., Li, F., Luo, M., Wei, J., and Liu, X. (2017). Distinct Roles of Wnt/β-Catenin Signaling in the Pathogenesis of Chronic Obstructive Pulmonary Disease and Idiopathic Pulmonary Fibrosis. Mediators of inflammation *2017*, 3520581-3520581.

Shi, K., Jiang, J., Ma, T., Xie, J., Duan, L., Chen, R., Song, P., Yu, Z., Liu, C., Zhu, Q*., et al.* (2014). Pathogenesis pathways of idiopathic pulmonary fibrosis in bleomycin-induced lung injury model in mice. Respiratory Physiology & Neurobiology *190*, 113-117.

Shin, H.M., Kim, M.H., Kim, B.H., Jung, S.H., Kim, Y.S., Park, H.J., Hong, J.T., Min, K.R., and Kim, Y. (2004). Inhibitory action of novel aromatic diamine compound on lipopolysaccharide-induced nuclear translocation of NF-kappaB without affecting IkappaB degradation. FEBS Lett *571*, 50-54.

Siddiqi, A., and Sethi, S. (2008). Optimizing antibiotic selection in treating COPD exacerbations. Int J Chron Obstruct Pulmon Dis *3*, 31-44.

Siddiqui, F.M., and Diamond, J.M. (2018). Lung transplantation for chronic obstructive pulmonary disease: past, present, and future directions. Curr Opin Pulm Med *24*, 199-204.

Siddiqui, S., Hollins, F., Saha, S., and Brightling, C.E. (2007). Inflammatory cell microlocalisation and airway dysfunction: cause and effect? Eur Respir J *30*, 1043-1056.

Sleijfer, S. (2001). Bleomycin-induced pneumonitis. Chest *120*, 617-624.

Smil, D., Eram, M.S., Li, F., Kennedy, S., Szewczyk, M.M., Brown, P.J., Barsyte-Lovejoy, D., Arrowsmith, C.H., Vedadi, M., and Schapira, M. (2015). Discovery of a Dual PRMT5-PRMT7 Inhibitor. ACS Med Chem Lett *6*, 408-412.

Smirnova, N.F., Conlon, T.M., Morrone, C., Dorfmuller, P., Humbert, M., Stathopoulos, G.T., Umkehrer, S., Pfeiffer, F., Yildirim, A.O., and Eickelberg, O. (2019). Inhibition of B cell-dependent lymphoid follicle formation prevents lymphocytic bronchiolitis after lung transplantation. JCI Insight *4*.

Smith, E., Zhou, W., Shindiapina, P., Sif, S., Li, C., and Baiocchi, R.A. (2018). Recent advances in targeting protein arginine methyltransferase enzymes in cancer therapy. Expert Opinion on Therapeutic Targets *22*, 527-545.

Smith, J.J., Rücknagel, K.P., Schierhorn, A., Tang, J., Nemeth, A., Linder, M., Herschman, H.R., and Wahle, E. (1999). Unusual sites of arginine methylation in Poly(A)-binding protein II and in vitro methylation by protein arginine methyltransferases PRMT1 and PRMT3. J Biol Chem *274*, 13229-13234.

Smith, M.E., van der Maesen, K., and Somera, F.P. (1998). Macrophage and microglial responses to cytokines in vitro: phagocytic activity, proteolytic enzyme release, and free radical production. J Neurosci Res *54*, 68-78.

Stockley, R.A. (1999). Neutrophils and protease/antiprotease imbalance. Am J Respir Crit Care Med *160*, S49-52.

Stork, P.J. (2003). Does Rap1 deserve a bad Rap? Trends Biochem Sci *28*, 267-275.

Stork, P.J., and Dillon, T.J. (2005). Multiple roles of Rap1 in hematopoietic cells: complementary versus antagonistic functions. Blood *106*, 2952-2961.

Subramanian, A., Tamayo, P., Mootha, V.K., Mukherjee, S., Ebert, B.L., Gillette, M.A., Paulovich, A., Pomeroy, S.L., Golub, T.R., Lander, E.S*., et al.* (2005). Gene set enrichment analysis: a knowledge-based approach for interpreting genome-wide expression profiles. Proceedings of the National Academy of Sciences of the United States of America *102*, 15545-15550.

Sue, D.Y. (2013). Measurement of lung volumes in patients with obstructive lung disease. A matter of time (constants). Ann Am Thorac Soc *10*, 525-530.

Sun, Q., Yang, X., Zhong, B., Jiao, F., Li, C., Li, D., Lan, X., Sun, J., and Lu, S. (2012). Upregulated Protein Arginine Methyltransferase 1 by IL-4 Increases Eotaxin-1 Expression in Airway Epithelial Cells and Participates in Antigen-Induced Pulmonary Inflammation in Rats. The Journal of Immunology *188*, 3506-3512.

Sundar, I.K., and Rahman, I. (2016). Gene expression profiling of epigenetic chromatin modification enzymes and histone marks by cigarette smoke: implications for COPD and lung cancer. Am J Physiol Lung Cell Mol Physiol *311*, L1245-L1258.

Szewczyk, M.M., Ishikawa, Y., Organ, S., Sakai, N., Li, F., Halabelian, L., Ackloo, S., Couzens, A.L., Eram, M., Dilworth, D.*, et al.* (2020). Pharmacological inhibition of PRMT7 links arginine monomethylation to the cellular stress response. Nature Communications *11*, 2396.

Szewczyk, M.M., Ishikawa, Y., Organ, S., Sakai, N., Li, F., Halabelian, L., Ackloo, S., Eram, M., Dilworth, D., Fukushi, H.*, et al.* (2019). Pharmacological inhibition of PRMT7 links arginine monomethylation to the cellular stress response. bioRxiv, 503136.

Tan, H.-X., Esterbauer, R., Vanderven, H.A., Juno, J.A., Kent, S.J., and Wheatley, A.K. (2019). Inducible Bronchus-Associated Lymphoid Tissues (iBALT) Serve as Sites of B Cell Selection and Maturation Following Influenza Infection in Mice. Frontiers in immunology *10*, 611-611.

Tang, Y., Zhang, M., Feng, Y., and Liang, B. (2016). The measurement of lung volumes using body plethysmography and helium dilution methods in COPD patients: a correlation and diagnosis analysis. Sci Rep *6*, 37550.

Tashkin, D.P., and Strange, C. (2018). Inhaled corticosteroids for chronic obstructive pulmonary disease: what is their role in therapy? Int J Chron Obstruct Pulmon Dis *13*, 2587-2601.

Taylor, A.E., Finney-Hayward, T.K., Quint, J.K., Thomas, C.M., Tudhope, S.J., Wedzicha, J.A., Barnes, P.J., and Donnelly, L.E. (2010). Defective macrophage phagocytosis of bacteria in COPD. Eur Respir J *35*, 1039-1047.

Terzikhan, N., Verhamme, K.M.C., Hofman, A., Stricker, B.H., Brusselle, G.G., and Lahousse, L. (2016). Prevalence and incidence of COPD in smokers and non-smokers: the Rotterdam Study. Eur J Epidemiol *31*, 785-792.

Tetley, T.D. (2002). Macrophages and the pathogenesis of COPD. Chest *121*, 156s-159s.

Tetley, T.D. (2005). Inflammatory cells and chronic obstructive pulmonary disease. Curr Drug Targets Inflamm Allergy *4*, 607-618.

Tewary, S.K., Zheng, Y.G., and Ho, M.-C. (2019). Protein arginine methyltransferases: insights into the enzyme structure and mechanism at the atomic level. Cell Mol Life Sci *76*, 2917-2932.

Thiery, J., Keefe, D., Boulant, S., Boucrot, E., Walch, M., Martinvalet, D., Goping, I.S., Bleackley, R.C., Kirchhausen, T., and Lieberman, J. (2011). Perforin pores in the endosomal membrane trigger the release of endocytosed granzyme B into the cytosol of target cells. Nature immunology *12*, 770-777.

Thomassen, M., Tan, Q., and Kruse, T.A. (2009). Gene expression meta-analysis identifies chromosomal regions and candidate genes involved in breast cancer metastasis. Breast Cancer Research and Treatment *113*, 239-249.

Tian, P.-W., and Wen, F.-Q. (2015). Clinical significance of airway mucus hypersecretion in chronic obstructive pulmonary disease. J Transl Int Med *3*, 89-92.

Tinkelman, D.G., Price, D., Nordyke, R.J., and Halbert, R.J. (2007). COPD screening efforts in primary care: what is the yield? Prim Care Respir J *16*, 41-48.

Traves, S.L., Culpitt, S.V., Russell, R.E.K., Barnes, P.J., and Donnelly, L.E. (2002). Increased levels of the chemokines GROalpha and MCP-1 in sputum samples from patients with COPD. Thorax *57*, 590-595.

Traves, S.L., Smith, S.J., Barnes, P.J., and Donnelly, L.E. (2004). Specific CXC but not CC chemokines cause elevated monocyte migration in COPD: a role for CXCR2. J Leukoc Biol *76*, 441-450.

Trombetta, A.C., Soldano, S., Contini, P., Tomatis, V., Ruaro, B., Paolino, S., Brizzolara, R., Montagna, P., Sulli, A., Pizzorni, C*., et al.* (2018). A circulating cell population showing both M1 and M2 monocyte/macrophage surface markers characterizes systemic sclerosis patients with lung involvement. Respir Res *19*, 186-186.

Tropberger, P., Pott, S., Keller, C., Kamieniarz-Gdula, K., Caron, M., Richter, F., Li, G., Mittler, G., Liu, E.T., Buhler, M*., et al.* (2013). Regulation of transcription through acetylation of H3K122 on the lateral surface of the histone octamer. Cell *152*, 859-872.

Tsai, Y.F., and Hwang, T.L. (2015). Neutrophil elastase inhibitors: a patent review and potential applications for inflammatory lung diseases (2010 - 2014). Expert Opin Ther Pat *25*, 1145-1158.

Tuder, R.M., and Petrache, I. (2012). Pathogenesis of chronic obstructive pulmonary disease. J Clin Invest *122*, 2749-2755.

Tuder, R.M., Petrache, I., Elias, J.A., Voelkel, N.F., and Henson, P.M. (2003). Apoptosis and emphysema: the missing link. Am J Respir Cell Mol Biol *28*, 551-554.

Turato, G., Zuin, R., Miniati, M., Baraldo, S., Rea, F., Beghé, B., Monti, S., Formichi, B., Boschetto, P., Harari, S*., et al.* (2002). Airway inflammation in severe chronic obstructive pulmonary disease: relationship with lung function and radiologic emphysema. Am J Respir Crit Care Med *166*, 105-110.

Ueno, M., Maeno, T., Nishimura, S., Ogata, F., Masubuchi, H., Hara, K., Yamaguchi, K., Aoki, F., Suga, T., Nagai, R*., et al.* (2015a). Alendronate inhalation ameliorates elastase-induced pulmonary emphysema in mice by induction of apoptosis of alveolar macrophages. Nat Commun *6*, 6332.

Ueno, M., Maeno, T., Nishimura, S., Ogata, F., Masubuchi, H., Hara, K., Yamaguchi, K., Aoki, F., Suga, T., Nagai, R.*, et al.* (2015b). Alendronate inhalation ameliorates elastase-induced pulmonary emphysema in mice by induction of apoptosis of alveolar macrophages. Nature communications *6*, 6332.

Upham, J.W., and Xi, Y. (2017). Dendritic Cells in Human Lung Disease: Recent Advances. Chest *151*, 668-673.

Vadnais, C., Chen, R., Fraszczak, J., Yu, Z., Boulais, J., Pinder, J., Frank, D., Khandanpour, C., Hébert, J., Dellaire, G.*, et al.* (2018). GFI1 facilitates efficient DNA repair by regulating PRMT1 dependent methylation of MRE11 and 53BP1. Nat Commun *9*, 1418.

Valenzuela, I., Segura-Puimedon, M., Rodriguez-Santiago, B., Fernandez-Alvarez, P., Vendrell, T., Armengol, L., and Tizzano, E. (2019). Further delineation of the phenotype caused by loss of function mutations in PRMT7. Eur J Med Genet *62*, 182-185.

Valledor, A.F., Sánchez-Tilló, E., Arpa, L., Park, J.M., Caelles, C., Lloberas, J., and Celada, A. (2008). Selective Roles of MAPKs during the Macrophage Response to IFN-γ. The Journal of Immunology *180*, 4523-4529.

van Furth, R., Cohn, Z.A., Hirsch, J.G., Humphrey, J.H., Spector, W.G., and Langevoort, H.L. (1972). The mononuclear phagocyte system: a new classification of macrophages, monocytes, and their precursor cells. Bull World Health Organ *46*, 845-852.

van oud Alblas, A.B., and van Furth, R. (1979). Origin, Kinetics, and characteristics of pulmonary macrophages in the normal steady state. J Exp Med *149*, 1504-1518.

Vanoirbeek, J.A., Rinaldi, M., De Vooght, V., Haenen, S., Bobic, S., Gayan-Ramirez, G., Hoet, P.H., Verbeken, E., Decramer, M., Nemery, B.*, et al.* (2010). Noninvasive and invasive pulmonary function in mouse models of obstructive and restrictive respiratory diseases. American journal of respiratory cell and molecular biology *42*, 96-104.

Varmaghani, M., Dehghani, M., Heidari, E., Sharifi, F., Saeedi Moghaddam, S., and Farzadfar, F. (2019). Global prevalence of chronic obstructive pulmonary disease: systematic review and meta-analysis. Eastern Mediterranean health journal = La revue de santé de la Méditerranée orientale = al-Majallah al-ṣiḥḥīyah li-sharq al-mutawassiṭ *25*, 1-2019.

Vaz Fragoso, C.A., Concato, J., McAvay, G., Van Ness, P.H., Rochester, C.L., Yaggi, H.K., and Gill, T.M. (2010). The ratio of FEV1 to FVC as a basis for establishing chronic obstructive pulmonary disease. American journal of respiratory and critical care medicine *181*, 446-451.

Vermaelen, K., and Pauwels, R. (2005). Pulmonary dendritic cells. Am J Respir Crit Care Med *172*, 530-551.

Viegi, G., Paoletti, P., Prediletto, R., Di Pede, F., Carrozzi, L., Carmignani, G., Mammini, U., Lebowitz, M.D., and Giuntini, C. (1990). Carbon monoxide diffusing capacity, other indices of

lung function, and respiratory symptoms in a general population sample. Am Rev Respir Dis *141*, 1033-1039.

Vijayan, V.K. (2013). Chronic obstructive pulmonary disease. Indian J Med Res *137*, 251-269.

Vlahos, R., and Bozinovski, S. (2014). Role of alveolar macrophages in chronic obstructive pulmonary disease. Frontiers in immunology *5*, 435-435.

Vleeming, W., Rambali, B., and Opperhuizen, A. (2002). The role of nitric oxide in cigarette smoking and nicotine addiction. Nicotine Tob Res *4*, 341-348.

Vogelmeier, C.F., Criner, G.J., Martinez, F.J., Anzueto, A., Barnes, P.J., Bourbeau, J., Celli, B.R., Chen, R., Decramer, M., Fabbri, L.M.*, et al.* (2017). Global Strategy for the Diagnosis, Management, and Prevention of Chronic Obstructive Lung Disease 2017 Report: GOLD Executive Summary. Arch Bronconeumol *53*, 128-149.

Walters, J.A., Walters, E.H., and Wood-Baker, R. (2005). Oral corticosteroids for stable chronic obstructive pulmonary disease. Cochrane Database Syst Rev, Cd005374.

Walton, G.M., Stockley, J.A., Griffiths, D., Sadhra, C.S., Purvis, T., and Sapey, E. (2016). Repurposing Treatments to Enhance Innate Immunity. Can Statins Improve Neutrophil Functions and Clinical Outcomes in COPD? J Clin Med *5*.

Wang, J., Urbanowicz, R., Tighe, P., Todd, I., Corne, J., and Fairclough, L. (2013). Differential Activation of Killer Cells in the Circulation and the Lung: A Study of Current Smoking Status and Chronic Obstructive Pulmonary Disease (COPD). PloS one *8*, e58556.

Wang, N., Liang, H., and Zen, K. (2014a). Molecular mechanisms that influence the macrophage m1-m2 polarization balance. Frontiers in immunology *5*, 614-614.

Wang, Q., Xu, J., Li, Y., Huang, J., Jiang, Z., Wang, Y., Liu, L., Leung, E.L.H., and Yao, X. (2018a). Identification of a Novel Protein Arginine Methyltransferase 5 Inhibitor in Non-small Cell Lung Cancer by Structure-Based Virtual Screening. Frontiers in Pharmacology *9*.

Wang, X., Huang, Y., Zhao, J., Zhang, Y., Lu, J., and Huang, B. (2012). Suppression of PRMT6-mediated arginine methylation of p16 protein potentiates its ability to arrest A549 cell proliferation. Int J Biochem Cell Biol *44*, 2333-2341.

Wang, X., Zhang, C., Huang, G., Han, D., Guo, Y., Meng, X., and Kan, C. (2015). Resveratrol inhibits dysfunction of dendritic cells from chronic obstructive pulmonary disease patients through promoting miR-34. Int J Clin Exp Pathol *8*, 5145-5152.

Wang, Y.-C., Peterson, S.E., and Loring, J.F. (2014b). Protein post-translational modifications and regulation of pluripotency in human stem cells. Cell Research *24*, 143-160.

Wang, Y., Xu, J., Meng, Y., Adcock, I.M., and Yao, X. (2018b). Role of inflammatory cells in airway remodeling in COPD. Int J Chron Obstruct Pulmon Dis *13*, 3341-3348.

Wang, Y.P., Zhou, W., Wang, J., Huang, X., Zuo, Y., Wang, T.S., Gao, X., Xu, Y.Y., Zou, S.W., Liu, Y.B*., et al.* (2016). Arginine Methylation of MDH1 by CARM1 Inhibits Glutamine Metabolism and Suppresses Pancreatic Cancer. Mol Cell *64*, 673-687.

Weinreich, U.M., Thomsen, L.P., Brock, C., Karbing, D.S., and Rees, S.E. (2015). Diffusion capacity of the lung for carbon monoxide - A potential marker of impaired gas exchange or of systemic deconditioning in chronic obstructive lung disease? Chron Respir Dis *12*, 357-364.

Welte, T. (2009). Optimising treatment for COPD--new strategies for combination therapy. International journal of clinical practice *63*, 1136-1149.

Welte, T., Vogelmeier, C., and Papi, A. (2015). COPD: early diagnosis and treatment to slow disease progression. Int J Clin Pract *69*, 336-349.

Whitsett, J.A., and Alenghat, T. (2015). Respiratory epithelial cells orchestrate pulmonary innate immunity. Nature immunology *16*, 27-35.

Wittchen, E.S., Aghajanian, A., and Burridge, K. (2011). Isoform-specific differences between Rap1A and Rap1B GTPases in the formation of endothelial cell junctions. Small GTPases *2*, 65-76.

Wolf, S.S. (2009). The protein arginine methyltransferase family: an update about function, new perspectives and the physiological role in humans. Cellular and Molecular Life Sciences *66*, 2109-2121.

Wong, C.H., Heit, B., and Kubes, P. (2010). Molecular regulators of leucocyte chemotaxis during inflammation. Cardiovasc Res *86*, 183-191.

Wrzodek, C., Eichner, J., Buchel, F., and Zell, A. (2013). InCroMAP: integrated analysis of cross-platform microarray and pathway data. Bioinformatics *29*, 506-508.

Wu, Y., Zhou, J., Li, Y., Zhou, Y., Cui, Y., Yang, G., and Hong, Y. (2015). Rap1A Regulates Osteoblastic Differentiation via the ERK and p38 Mediated Signaling. PloS one *10*, e0143777-e0143777.

Xiao, Y., Palomero, J., Grabowska, J., Wang, L., de Rink, I., van Helvert, L., and Borst, J. (2017). Macrophages and osteoclasts stem from a bipotent progenitor downstream of a macrophage/osteoclast/dendritic cell progenitor. Blood Adv *1*, 1993-2006.

Yamasaki, K., and Eeden, S.F.V. (2018). Lung Macrophage Phenotypes and Functional Responses: Role in the Pathogenesis of COPD. Int J Mol Sci *19*.

Yang, Y., and Bedford, M.T. (2013). Protein arginine methyltransferases and cancer. Nat Rev Cancer *13*, 37-50.

Yang, Y., Hadjikyriacou, A., Xia, Z., Gayatri, S., Kim, D., Zurita-Lopez, C., Kelly, R., Guo, A., Li, W., Clarke, S.G*., et al.* (2015). PRMT9 is a Type II methyltransferase that methylates the splicing factor SAP145. Nature Communications *6*, 6428.

Yao, R., Jiang, H., Ma, Y., Wang, L., Wang, L., Du, J., Hou, P., Gao, Y., Zhao, L., Wang, G*., et al.* (2014). PRMT7 induces epithelial-to-mesenchymal transition and promotes metastasis in breast cancer. Cancer Res *74*, 5656-5667.

Yao, Y., Zhou, J., Diao, X., and Wang, S. (2019). Association between tumor necrosis factor-α and chronic obstructive pulmonary disease: a systematic review and meta-analysis. Therapeutic Advances in Respiratory Disease *13*, 1753466619866096.

Yildirim, A.O., Bulau, P., Zakrzewicz, D., Kitowska, K.E., Weissmann, N., Grimminger, F., Morty, R.E., and Eickelberg, O. (2006). Increased protein arginine methylation in chronic hypoxia: role of protein arginine methyltransferases. Am J Respir Cell Mol Biol *35*, 436-443.

Yildirim, A.O., Muyal, V., John, G., Muller, B., Seifart, C., Kasper, M., and Fehrenbach, H. (2010). Palifermin induces alveolar maintenance programs in emphysematous mice. American journal of respiratory and critical care medicine *181*, 705-717.

Ying, Z., Mei, M., Zhang, P., Liu, C., He, H., Gao, F., and Bao, S. (2015). Histone Arginine Methylation by PRMT7 Controls Germinal Center Formation via Regulating Bcl6 Transcription. J Immunol *195*, 1538-1547.

Yona, S., Kim, K.W., Wolf, Y., Mildner, A., Varol, D., Breker, M., Strauss-Ayali, D., Viukov, S., Guilliams, M., Misharin, A*., et al.* (2013). Fate mapping reveals origins and dynamics of monocytes and tissue macrophages under homeostasis. Immunity *38*, 79-91.

Yoshimatsu, M., Toyokawa, G., Hayami, S., Unoki, M., Tsunoda, T., Field, H.I., Kelly, J.D., Neal, D.E., Maehara, Y., Ponder, B.A*., et al.* (2011). Dysregulation of PRMT1 and PRMT6, Type I arginine methyltransferases, is involved in various types of human cancers. Int J Cancer *128*, 562-573.

Yu, Z., Chen, T., Hébert, J., Li, E., and Richard, S. (2009). A mouse PRMT1 null allele defines an essential role for arginine methylation in genome maintenance and cell proliferation. Molecular and cellular biology *29*, 2982-2996.

Zakrzewicz, D., Zakrzewicz, A., Preissner, K.T., Markart, P., and Wygrecka, M. (2012). Protein Arginine Methyltransferases (PRMTs): promising targets for the treatment of pulmonary disorders. International journal of molecular sciences *13*, 12383-12400.

Zaynagetdinov, R., Sherrill, T.P., Kendall, P.L., Segal, B.H., Weller, K.P., Tighe, R.M., and Blackwell, T.S. (2013). Identification of myeloid cell subsets in murine lungs using flow cytometry. Am J Respir Cell Mol Biol *49*, 180-189.

Zhang, H., Chang, Y.-C., Brennan, M.L., and Wu, J. (2014). The structure of Rap1 in complex with RIAM reveals specificity determinants and recruitment mechanism. J Mol Cell Biol *6*, 128-139.

Zhang, S., Ma, Y., Hu, X., Zheng, Y., and Chen, X. (2019). Targeting PRMT5/Akt signalling axis prevents human lung cancer cell growth. J Cell Mol Med *23*, 1333-1342.

Zhang, T., Zhang, Z., Dong, Q., Xiong, J., and Zhu, B. (2020). Histone H3K27 acetylation is dispensable for enhancer activity in mouse embryonic stem cells. Genome Biology *21*, 45.

Zhang, W., and Liu, H.T. (2002). MAPK signal pathways in the regulation of cell proliferation in mammalian cells. Cell Research *12*, 9-18.

Zhang, X., Zhou, L., and Cheng, X. (2000). Crystal structure of the conserved core of protein arginine methyltransferase PRMT3. The EMBO journal *19*, 3509-3519.

Zhang, X.P., Jiang, Y.B., Zhong, C.Q., Ma, N., Zhang, E.B., Zhang, F., Li, J.J., Deng, Y.Z., Wang, K., Xie, D.*, et al.* (2018). PRMT1 Promoted HCC Growth and Metastasis In Vitro and In Vivo via Activating the STAT3 Signalling Pathway. Cell Physiol Biochem *47*, 1643-1654.

Zhao, C.-z., Fang, X.-c., Wang, D., Tang, F.-d., and Wang, X.-d. (2010). Involvement of type II pneumocytes in the pathogenesis of chronic obstructive pulmonary disease. Respiratory Medicine *104*, 1391-1395.

Zhao, Q., Rank, G., Tan, Y.T., Li, H., Moritz, R.L., Simpson, R.J., Cerruti, L., Curtis, D.J., Patel, D.J., Allis, C.D.*, et al.* (2009). PRMT5-mediated methylation of histone H4R3 recruits DNMT3A, coupling histone and DNA methylation in gene silencing. Nat Struct Mol Biol *16*, 304-311.

Zheng, S., Moehlenbrink, J., Lu, Y.C., Zalmas, L.P., Sagum, C.A., Carr, S., McGouran, J.F., Alexander, L., Fedorov, O., Munro, S.*, et al.* (2013). Arginine methylation-dependent reader-writer interplay governs growth control by E2F-1. Mol Cell *52*, 37-51.

Zhou, L., Liu, Y., Chen, X., Wang, S., Liu, H., Zhang, T., Zhang, Y., Xu, Q., Han, X., Zhao, Y.*, et al.* (2018). Over-expression of nuclear factor-kappaB family genes and inflammatory molecules is related to chronic obstructive pulmonary disease. Int J Chron Obstruct Pulmon Dis *13*, 2131-2138.

Zhou, Y., Tan, X., Kuang, W., Liu, L., and Wan, L. (2012). Erythromycin ameliorates cigarette-smoke-induced emphysema and inflammation in rats. Transl Res *159*, 464-472.

Zhu, F., Guo, H., Bates, P.D., Zhang, S., Zhang, H., Nomie, K.J., Li, Y., Lu, L., Seibold, K.R., Wang, F.*, et al.* (2019). PRMT5 is upregulated by B-cell receptor signaling and forms a positive-feedback loop with PI3K/AKT in lymphoma cells. Leukemia *33*, 2898-2911.

Zhu, F., and Rui, L. (2019). PRMT5 in gene regulation and hematologic malignancies. Genes Dis *6*, 247-257.

Zhu, Y. (2018). PRMT1 mediates podocyte injury and glomerular fibrosis through phosphorylation of ERK pathway. Biochem Biophys Res Commun *495*, 828-838.

Zinellu, E., Zinellu, A., Fois, A.G., Carru, C., and Pirina, P. (2016). Circulating biomarkers of oxidative stress in chronic obstructive pulmonary disease: a systematic review. Respir Res *17*, 150.

Zurita-Lopez, C.I., Sandberg, T., Kelly, R., and Clarke, S.G. (2012). Human protein arginine methyltransferase 7 (PRMT7) is a type III enzyme forming omega-NG-monomethylated arginine residues. J Biol Chem *287*, 7859-7870.

ACKNOWLEDGEMENTS

Now I would like to thank and express my gratitude to everyone who has supported me and contributed to my PhD process.

First of all, I would like to express my deepest gratitude to my supervisor, Dr. Ali Önder Yildirim, for giving me the opportunity to work on this project in his Lab. His valuable guidance and support was always there whenever l needed. I am deeply grateful to be to meet such a nice person and a great scientist. I should say that PhD period was not always easy especially if you are working with such a dedicated and passionate scientist however his expertise in the field and his discipline truly taught me a lot; not only about my project, but also about science in general. Now when l think about all the years during my PhD, l feel extremely lucky to work with someone cheerful, supportive and always friendly. It was a great pleasure to be part of your lab family!

I would like to thank also my thesis advisory Committee supervisors, PD Dr. Med. Anne Hilgendorff and Dr. Alexander Wolf for their contribution to my project with their ideas and suggestions during our meetings. Their supportive comments about my project helped me a lot to progress further in a right direction. I am really grateful for their contribution.

I would like to thank my supervisor, Dr. Thomas Conlon, for his excellent guidance, endless help and support throughout five years including my master studies. l have learned a lot by his experiences. I would not be able to succeed if he did not encourage me always. There were some days l was completely frustrated but his positive attitude and inspirations helped me a lot to be motivated again. Thank you for always being there to discuss the ideas about the project, to answer my questions and to share your knowledge whenever l needed. And lastly thank you for being nice and friendly, smiling is like an infectious disease that affects everybody.

Furthermore, I would like to thank to all members of the lab for the warm atmosphere, l had such a great time with them. It was awesome and encouraging to discuss my project with them. Firstly, l want to thank my lab mates in this lab, Zeynep, Carolina, Aicha, Carmela and

Christine for being very helpful colleagues and great friends. We shared many scientific and non-scientific memories together during our coffee breaks. I had lots of fun with all of them and I am sure that the lab would not be the same without them. They are definitely a big part of my success!

I would like to thank all of my friends from all over the world for sharing my excitement during the project. Specifically, to my friends from Munich, “Bacolar”. I can´t find enough words to describe how valuable their support is for me. I never felt alone in this city, they were always there for me. I feel very lucky to spend the best years of my life with them. Bacolar, each of you is very unique and special, l am deeply grateful to meet you and to spend time with you.

Sevgili Nigar, Seren ve Zeynep arkadaslarima da ayrica tesekkür etmek istiyorum. Bu zor sürecte her zaman yanimda olduklari icin. Agladigimda, üzüldügümde beni kucaklayan, mutlu oldugumda benimle birlikte sevinen, ve her zaman ama her zaman yardima hazir olan Zeynep, canimsin ve iyi ki varsin. Seren ve Nigar, sizin dostlugunuz bana her zaman güc verdi. 6 yildir her animda yanimda oldugunuz icin, bana bir dosttan da öte ailem oldugunuzu hissettirdiginiz icin tesekkür ederim. Mükemmel insanlarsiniz, benim canim Top Secretimsiniz!

Tabiki sevgili esim Umut´a özel olarak tesekkür etmek istiyorum. Öncelikle her zaman ve her kosulda yanimda oldugu ve beni hep destekledigi icin. Bir hayli zorlandigim bu sürecte her gün bana katlandigin, hayatimi kolaylastirmak icin elinden gelenin en iyisini yaptigin icin sana minnettarim. Bütün planlarimizi benim deneylerime ve sunumlarima göre ayarlamak dünyanin en zor isiydi ama sen hep elinden geleni yaptin. Ben hayatimda senin kadar anlayisli, sabirli ve sevecen birini tanimadim, sen benim bu hayattaki en büyük sansimsin.

Son olarak canım ailem Nesrin Güneş ve Mehmet Güneş´e bugünlere gelmemdeki büyük paylarından dolayı ve beni her zaman koşulsuzca destekledikleri için sonsuz minnetlerimi sunarım. Bana her zaman inandığınız icin tesekkür ederim, basarılarım ve başaracaklarım sizin sayenizde! Ve tabiki de hayatta olmasa bile her zaman yanımda hissettigim babam Ali Güneş´e tesekkür ederim, kücük kızıyla gurur duyuyordur eminim cünkü ben onun kızı olmaktan hep gurur duydum ve duyacagım.

AFFIDAVIT

Affidavit

Günes Günsel, Gizem

Surname, first name

Ingolstädter Landstraße 1

Street

85764, Neuherberg, Germany

Zip code, town, country

I hereby declare, that the submitted thesis entitled:

Role of PRMT7 in the recruitment of monocyte-derived macrophages into lung tissue and COPD pathogenesis

is my own work. I have only used the sources indicated and have not made unauthorised use of services of a third party. Where the work of others has been quoted or reproduced, the source is always given.

I further declare that the submitted thesis or parts thereof have not been presented as part of an examination degree to any other university.

__Munich, 17.08.2021___ _____Gizem Güneş Günsel_____

place, date Signature doctoral candidate

LIST OF PUBLICATIONS

Conlon, T.M., John-Schuster, G., Heide, D., Pfister, D., Lehmann, M., Hu, Y., Ertüz, Z., Lopez, M.A., Ansari, M., Strunz, M., Mayr, C., Ciminieri, C., Costa, R., Kohlhepp, M., Guillot, A., **Günes, G.**, *et al.* (2020). Inhibition of LTβR signalling activates WNT-induced regeneration in lung. Nature.

Jia, J., Conlon, T.M., Sarker, R.S., Tasdemir, D., Smirnova, N.F., Srivastava, B., Verleden, S.E., **Günes, G.**, Wu, X., Prehn, C., *et al.* (2018). Cholesterol metabolism promotes B-cell positioning during immune pathogenesis of chronic obstructive pulmonary disease. EMBO Mol Med *1*